Scanning Tunneling Microscopy
of
Electrode Surfaces

by

Ian George Blackham

A thesis submitted in part fulfilment of the
requirements for the degree of **Doctor of Philosophy**
at the **University of Oxford**

St. Catherine's College
Oxford

September 1992

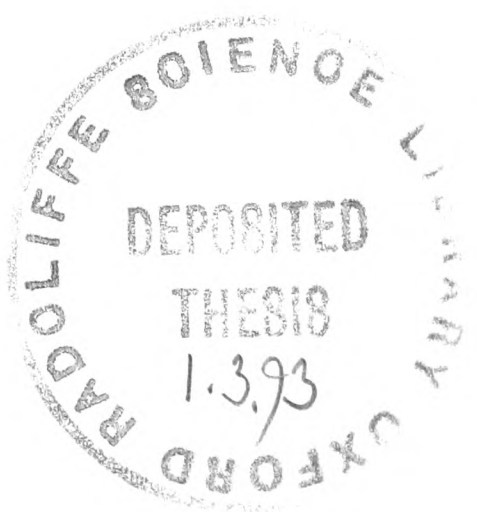

Acknowledgements

Firstly I would like to thank Professors Hirsch and Green for the provision of laboratory space and technical support for the duration of this work.

I would like to express my gratitude to Dr. Andrew Briggs and Dr. Allen Hill F.R.S. for their guidance, support and supervision throughout the project.

My thanks also to Prof. Andrew Hamnett who as a tutor and Pt.II supervisor motivated me to continue in science and has continued to advise and support since then.

Thanks also to: Dr. Paul Christensen for allowing me to play with his FT-IR spectrometer, providing ideas and general words of encouragement ('more upbeat you pillock'), Dr. Peter Trevellick for large doses of electronics expertise, design ideas and fine conversation about the merits of French auto engineering and Dr. Tommaso Cataldi for his dedication, commitment and ability to sing opera convincingly.

I would also like to acknowledge: Prof. R. J. Behm and Dr. J. Hotlos for allowing us to visit their lab in Munich, Dr. S. Myhra, the electronics and mechanical workshops of the Materials and Inorganic Chemistry Depts. (especially John Stead for the Macor machining), and C. Goodwin of the O.U. Thin Films Facility.

I would like to express my gratitude to all those in the Hamnett (Oxford and Newcastle), Hill, Briggs/Pethica and.....(extended) Mingos groups who made life far more entertaining.

Many thanks to David for proof reading, encouragement and along with Roy a fine snowball fight at C.P.H. Hi, Jane - give up smoking. Anthony, cheers for the binding. A special thanks to St. Aldates and the Bath St. Fellowship group for being there.

I am also tremendously grateful to my parents for all their support, guidance and encouragement over the years.

Abstract

Scanning tunneling microscopy of electrode surfaces

A thesis submitted by I.G.Blackham of St. Catherine's College, Oxford, in Trinity term 1992, for the degree of Doctor of Philosophy in the University of Oxford.

A scanning tunneling microscope (STM) suitable for the *in-situ* study of electrode surfaces under electrochemical control has been developed. The system consists of commercially available software and feedback electronics, with a custom-built stage and electrochemical control. The stage incorporates an automatic coarse approach mechanism for ease of operation.

Gold single crystal spheres (SCS) and gold on mica thin films have been studied as surfaces potentially suitable for samples in *in-situ* electrochemical STM experiments. Characteristic features of each surface have been identified.

High resolution *in-situ* STM imaging of the electro-oxidation of a gold surface in a sulphuric acid electrolyte has been achieved. Surface rearrangement at potentials positive of the double layer region has been observed and correlated with cyclic voltammetry. As yet unexplained features resulting from biasing the surface at potentials negative of the double layer region are reported. In phosphate electrolyte, bulk surface oxide formation and the surface resulting from reduction of the oxide have been imaged.

Some aspects of the direct electrochemistry of cytochrome *c* at 4, 4' dithiodipyridine (SSBPY) modified gold electrodes have been investigated. *In-situ* FTIR showed the potential dependent orientation of adsorbed thiopyridine species, while *ex-situ* and *in-situ* STM studies showed a novel surface pitting process to be active. It is hypothesised the STM experiment itself induces the process to take place. Features attributable to cytochrome *c* molecules have been observed.

Rearrangement of gold on mica surfaces, on exposure to certain aqueous solutions has been observed and the process is attributed to the interaction of the solutions with the original surface structure present.

Abbreviations

Note

As with all literature on scanning probe microscopy, the acronym STM represents both the technique - scanning tunneling microscopy and the instrument a scanning tunneling microscope. This convention is used for other variants e.g. AFM - atomic force microscopy.

In line with the bulk of the published literature, tunneling has been spelt in the U.S. manner.

CITS	Current Imaging Tunneling Spectroscopy
CV	Cyclic Voltammogram
ESTM	Electrochemical Scanning Tunneling Microscopy
EXAFS	Extended X-Ray Absorption Fine Structure
FT-IR	Fourier Transform Infra-Red spectroscopy
HOPG	Highly Oriented Pyrolytic Graphite
IRAS/IRRAS	Infra-Red Reflection-Absorption Spectroscopy
LDOS	Local Density Of States
LEED	Low Energy Electron Diffraction
ms	Milli-seconds i.e. 10^{-3}s
M.M.S.	Mercury/Mercurous Sulphate
nA	Nano amperes i.e. 10^{-9}A
ORC	Oxidation Reduction Cycle
SERS	Surface Enhanced Raman Spectroscopy
S.C.E.	Saturated Calomel Electrode
SECM	Scanning Electrochemical Microscopy
SICM	Scanning Ion Conductance Microscopy
STS	Scanning Tunneling Spectroscopy

SPy	4-thiopyridine
SSBPY	4,4'-dithiodipyridine
SXM/SPM	Scanning Probe Microscopy
UHV	Ultra-high Vacuum
UPD	Underpotential Deposition

Contents

Chapter One

Introduction

1.I Introduction to the study of electrode surfaces

A decade ago Binnig and Rohrer invented the scanning tunneling microscope (STM)[1]. Over the past ten years this high resolution surface study technique has rapidly achieved wide recognition[2] and some measure of the popularity of the field may be gauged by the presence, at the most recent international STM conference[3], of approximately ten companies selling 'off the shelf' STM systems.

This introduction is intended to put STM in the context of its application to electrochemical studies. In addition to attempting to evaluate STM alongside competing and complementary techniques used in the study of electrode surfaces, relevant work and new directions will be discussed. An outline of the basic principles and experimental aspects of STM is contained in Chapter Two.

Characterisation of the structure and properties of the electrode surface contributes much to the understanding of the electrode/electrolyte interface, vital in work involving electron transfer processes. The applications of such knowledge are huge, being relevant to areas including corrosion, catalysis, fuel cell technology, (bio)sensors and biological systems.

Traditional electrochemical measurements of current-voltage relationships may provide indirect, sparse and ambiguous information about the electrode/electrolyte interface and a variety of techniques that directly probe the electrode surface have been developed[4,5].

1.I.i. *Ex-* and *in-situ* techniques

If the electrode is transferred from solution to ultra-high vacuum (UHV) a battery of well known surface science techniques, such as electron microscopy and low energy electron diffraction (LEED), may be applied[6]. Thus information on morphology at the sub-micron scale, ordering of adlayers and chemical composition of the surface may be obtained. Unfortunately the short path length of electrons in condensed media mitigates against the use of such experiments in *in-situ* studies. An additional complication is that when an electrode is transferred into UHV, its environment changes substantially and this has to be borne in mind when the results of such *ex-situ* experiments are being interpreted[6].

The most common *in-situ* experiments are spectroelectrochemical, the most popular making use of vibrational spectroscopy, i.e. infra-red[7] and Raman[8]. A number of different approaches have been developed and each experiment has its own limitations. Knowledge of these limitations is crucial when applying the techniques. Infra-red (IR) methods are considered in more detail in Chapter Two. Both spectroscopies yield information on the identity, orientation, bonding and reaction dynamics of molecular species at the electrode surface. Major problems involving the absorbance of IR radiation by water and instrumental limitations have largely been overcome, making IR experiments more popular and widely applicable than those based on Raman spectroscopy.

Ellipsometry was the first optical reflection spectroscopy technique to be applied to electrode characterisation[9]. It provides information on the thickness and ordering of thin films formed on the electrode surface, by measurement of the change in polarisation of plane polarised light after reflection at the electrode surface. Interpretation of results relies on

the fitting of data to theoretical models thus making the technique's application to complex systems non-trivial. Photocurrent spectroscopy[10] (measurement of the response of an electrode during optical irradiation) and electroreflectance[11] (probing of a surface by monitoring reflectivity) are two more related techniques yielding information on the existence and ordering of individual adsorbates and films at the electrode surface.

Radiotracer experiments using radioactively labelled species were the first successful *in-situ* studies of the surfaces of solid electrodes by non-electrochemical means[12]. These studies provided information on the presence and packing (and hence orientation) of species on the electrode.

The recent availability of synchotron radiation has enabled X-ray absorption spectroscopies to be applied to *in-situ* investigations[13]. These techniques provide electronic and structural information on adsorbate layers, including bond lengths and the local environment of a particular species at the liquid-solid interface.

Rather less common techniques applied to this area include X-ray diffraction methods [13], second harmonic generation[14] and Mössbauer spectroscopy[15].

1.I.ii. STM as a probe of electrode surface structure

STM, although originally conceived as a vacuum technique, was rapidly found to be operational with comparable high resolution under liquids (several workers have imaged gold surfaces at atomic resolution[16,17,18]). The technique probes the surface electronic structure of a conducting sample by monitoring quantum mechanical tunneling between it and an ultra-fine tip, positioned approximately 5-20Å from the surface, upon application of a bias voltage (the basic configuration of an STM is shown schematically in fig. 1.1). Uniquely the technique shows the *real space* structure of a

surface as opposed to the diffraction techniques already referred to, which yield averaged information in reciprocal space. In addition to the unique ability of STM to image small local structures, certain operating modes can provide measurements of the local density of states, or an indication of the workfunction (or barrier height to tunneling) at a given position, although these experiment are usually restricted to high vacuum environments. In practice, STM is cheap and simple as compared with the cost of UHV equipment or synchotron availability.

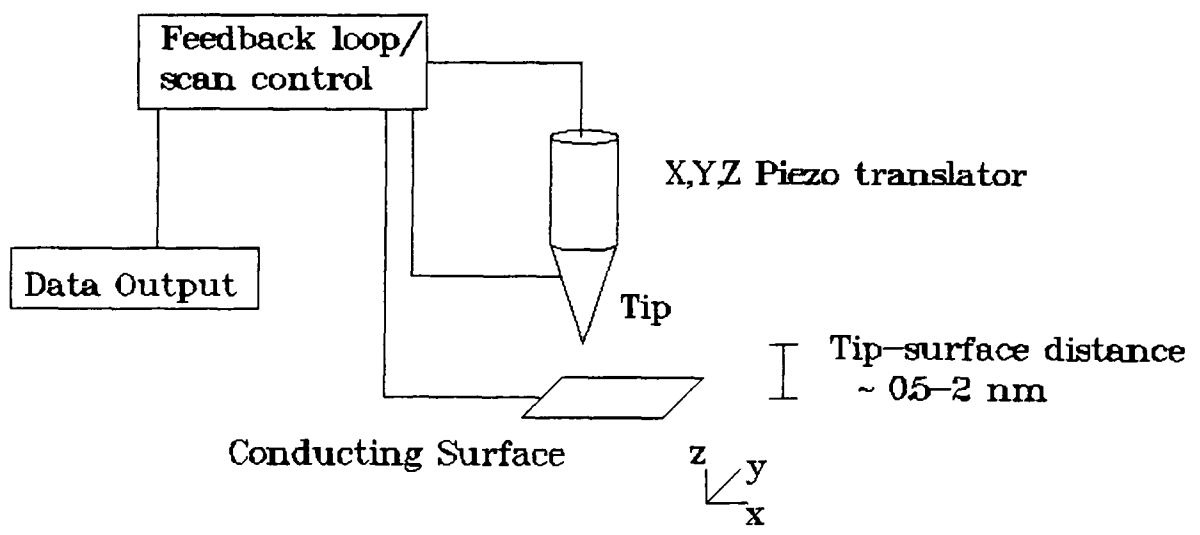

Fig. 1.1. Schematic diagram of an STM. Tip-surface bias voltage typically 10-2000 mV, tunneling current 0.5-25 nA

STM results often resemble (and may sometimes be interpreted in terms of) simple topographs of a surface, hence, despite the high spatial resolution, unequivocal identification of features is not always possible. Similarly, information on molecular species is limited.

A common theme between all these techniques has been the growing use of single crystal surfaces. For most methods this simplifies the interpretation of data, which is an average response from an area of surface. It also improves the definition of conditions under which a set of

results are obtained. Whilst use of the STM with its real space imaging ability allows investigation of amorphous surfaces, it is found that well defined single crystal surfaces can potentially yield far more information and STM will thus reinforce the trend of using these surfaces in electrochemical investigations (a point enlarged upon in later Chapters).

1.II. Introduction to STM

The potential of the STM was quickly recognised by researchers working in a diversity of fields; some idea of the breadth of applications can be gained by a glance at the proceedings from any of the more recent STM conferences[19]. An overview of the state of the art at the time is contained in the proceedings of the NATO advanced study institute on basic concepts and applications of scanning tunneling microscopy, which took place at Erice, Italy, in April 1989[20]. It is perhaps worth highlighting some of the main areas of interest.

A great deal of STM work has involved investigations of bare and adsorbate-covered metal and semiconductor surfaces under UHV conditions (atomic resolution imaging has been particularly useful in the latter case): the development of spectroscopic modes of operation for the STM has been driven by the interest in probing the local electronic structure of semiconductor surfaces. Additionally STM has been applied to studies of a diverse range of conducting or semi-conducting materials including superconductors, graphite intercalation compounds and chalcogenides exhibiting charge density wave effects[19].

Highly oriented pyrolytic graphite (HOPG), an easily cleaved material revealing clean atomically flat surfaces, has found use as a conductive support for a vast range of studies of organic compounds (ranging from

discrete molecules to conducting polymers) and biological molecules such as DNA. Much controversy has arisen in this area as researchers have discovered that the bare substrate often contains features which are extremely similar to those attributed to bio-molecules in other experiments[21,22]. Bard[23] and Everson[24] in their respective work on Nafion™ (a solid polymer electrolyte) and polypyrrole deposited on HOPG, were both careful to comment on structures due to the substrate itself. Despite these cautionary works and although the contrast mechanism giving rise to images of organic species is not clearly understood, experimental work in the area is still gathering momentum.

Not content with using the STM as a probe, many workers have used the technique to execute high resolution modification of the surface followed by imaging of the structures formed[25] (this type of 'nanolithography' had previously been carried out only by high resolution electron microscopes). In some experiments STM has been used to 'write' on a surface, e.g. by controlled transfer of material from tip to surface[26] or physically manipulating individual atoms adsorbed on a surface[27].

Apart from work in UHV, many studies (excepting semiconductors that form an insulating oxide layer on exposure to air) have been carried out under ambient conditions. Work under liquids will be covered in detail in the next sections of this Chapter. Low temperature experiments have been used for studies on superconductors and in investigations where reduced surface mobility is required. More recently STM has been applied to the observation of surface diffusion at elevated temperatures[28].

1.III. Applications of STM to the study of the liquid-solid interface

Not all *in-situ* STM work has been aimed at the study of specifically electrochemical problems: as P.K.Hansma and co-workers, at the universities of California and Virginia, pointed out in the papers that launched work in this area, the only method of maintaining a clean surface free of adventitious impurities outside a UHV environment is to submerge it under a contaminant free liquid.

Following this line of research TaS_2 was imaged under liquid N_2[29], while HOPG, GaAs and gold were observed under a variety of non-polar room temperature liquids (e.g. silicone oil and fluorocarbon grease)[30,31,32,33]. These workers also found the liquid environment allowed lithography to be carried out; while imaging gold under fluorocarbon grease, the bias voltage was pulsed to approximately 3V and depressions in the surface were created. Subsequently, organic liquids that form structured monolayers at the liquid-solid interface have been used: Foster *et al.*[34] claimed to have pinned a di(2-ethylhexyl)phthalate molecule to a HOPG support after applying a voltage pulse while tunneling onto the HOPG through a drop of the liquid phthalate. Other workers[35,36] have however produced similar results, both in the presence and absence of organic liquid, thereby casting doubt on the original conclusions. The straightforward study of molecular ordering at the organic liquid-solid interface has been attempted by a number of groups (see ref. 19).

It should be noted that much of this work has taken place on graphite substrates, where unexpected experimental observations, e.g. long range defect free periodicity, anomalous periodicity and unusually large surface corrugation, have provoked controversy about the contrast mechanism in these experiments[37,38]. One rationalisation for these effects, advanced by

Todd and Pethica, based on a tip-surface contact is illustrated in fig. 1.2. Their model proposes that tip-surface contact in such materials will induce a small area of surface to slide over the bulk solid. It was assumed an electron scattering interface, with electrical properties similar to a periodically appearing and disappearing grain boundary, is formed. Rough calculations showed that as the lattices matched and mismatched the variation in conductance through the system was sufficient to give the contrast (and enhanced corrugation) observed in atomic resolution STM images of HOPG.

The extended periodicity, coupled to uncertainties in the tunneling process in organic molecules, implies that the same caution should be applied to the interpretation of images showing molecular ordering.

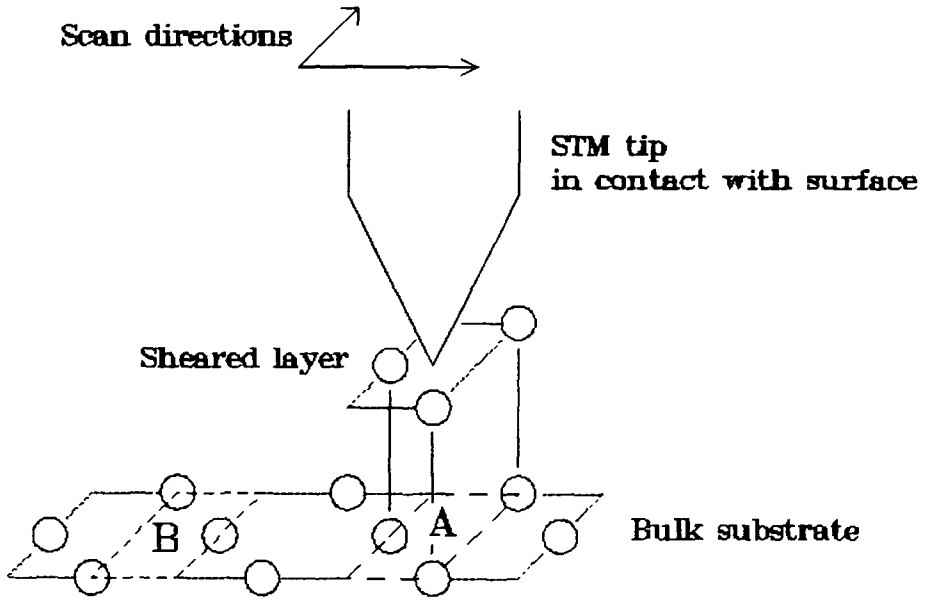

Fig. 1.2. Todd and Pethica's shear model for STM imaging[37]. At A the atomic lattice is aligned and a higher current is detected than at B. The resultant current has a periodicity equivalent to the lattice parameters of the substrate.

The precursor to the whole field of *in-situ* electrochemical STM was Sonnenfeld and Hansma's demonstration of atomic resolution on HOPG under water[39]. In the same paper they also presented an image of a gold film under a 2mM NaCl solution to showing the potential of STM for studying dilute solutions of DNA. To carry out this experiment all but the the last 50μm of the Pt-Ir tip was insulated with a glass coating to reduce spurious (and uncontrolled) electrochemically induced currents. Subsequently the corrosion of stainless steel under a chloride containing solution, both in the presence and absence of an organic corrosion inhibitor, was studied by Bard[40].

Much of the work on bio-molecules, such as various types of DNA, has been on native and metal-shadowed samples imaged in air or vacuum (e.g. references 41 and 42); *in-situ* investigations are less common and often rely on the molecular species being electrochemically deposited on the surface before imaging is attempted. DNA[43] and phosphorylase enzymes[44] have been studied by using this procedure.

Joachim and Garcia have modelled electron tunneling in organic systems in an attempt to understand the STM imaging of these bulk non-conductors (see for example the articles in ref 20), while Lindsay has proposed that the pressure caused by the tip in the tunnel gap modifies the electronic structure of molecules sufficiently to allow tunneling[45].

Yuan *et al.* have suggested an alternative method for topographically imaging non-conductive biological materials, by using the ionic flow through a thin film of water covering the sample, instead of a tunneling current of unknown origin[46].

1.IV. Applications of STM to electrochemistry

Since Arvia's discussion of the potential applications of STM to electrochemistry[47] a number of articles reviewing early work in the area have appeared, aimed at drawing the attention of electrochemists to the technique[48,49,50,51]. Since these publications the level of activity in *in-situ* electrochemical STM has increased substantially and therefore this section is intended to provide an overview of more recent developments.

1.IV.i. *Ex-situ* studies

Arvia, Baró and co-workers have carried out a number of studies on polycrystalline gold and platinum electrodes, including investigating electrofacetting[52,53], fractal deposits from electroreducing hydrous gold oxide layers[54], surface diffusion coefficients[55] and also amorphous metal electrodes for water electrolysis[56]. Siperko used STM, in conjunction with Raman spectroscopy, to examine pyrolytic graphite electrodes after applying an anodic current to the electrodes while immersed in a depleted electro-less copper plating solution[57]. Otsuka has observed the electrochemical roughening of a polycrystalline silver electrode in KCl solution by SEM and STM[58].

The utility of such *ex-situ* experiments is questionable because of the problems caused by sampling small areas. As will become clear in later Chapters, it is difficult to characterise even carefully prepared samples at the nanometre scale. For the inhomogeneous surfaces provided by a mechanically polished sample the task is almost impossible. Thus if the sample is removed from the STM, modified and replaced, the probability of the same area being scanned is negligible. Without starting with a well defined topography, differences in 'before' and 'after' topographies may be due to intrinsic differences in surface structure, rather than the

effects of any modification procedure.

The majority of investigations concerning conducting polymers have been carried out *ex-situ*. Examples of such work are provided by Yang *et al.* who have carried out morphological studies on polypyrrole and polythiophene films doped with different counter-ions[59,60]. This work used HOPG as a support (a surface thought to be well characterised, but see section 1.II.), as did Everson's examination of 8 and 40Å thick perchlorate-doped polypyrrole films[24]. Porter deposited thicker (10μm) films to mask substrate effects when using a platinum electrode for investigations of polythiophene and poly-3-bromothiophene films[61]. In related work Bonnell[62] used the spectroscopy mode of STM in an attempt to elucidate the electronic structure of a *ca.* 2000Å polyaniline film spin-coated onto a silicon wafer and imaged *in-vacuo*.

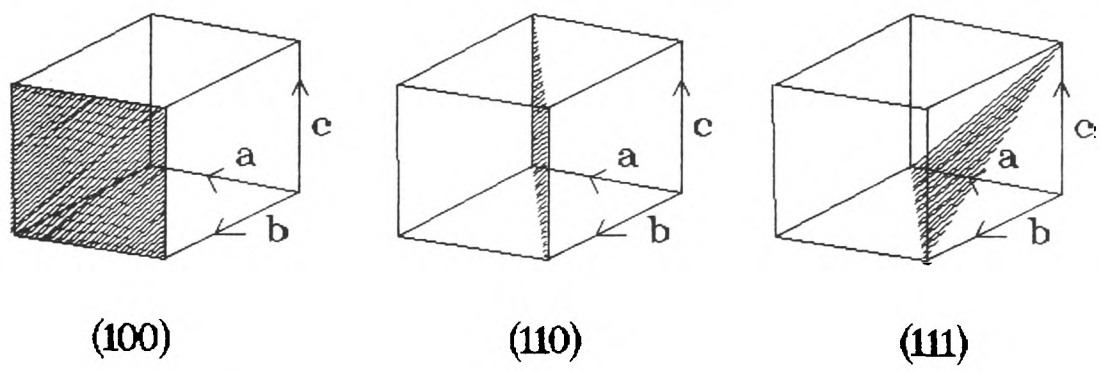

Fig. 1.3. Low index faces of a cubic crystal.

Schardt *et al.* have carried out studies of iodine adlayers on a Pt (111) surface in air[63,64], resolving different orderings depending on surface preparation (for reference, the low index faces commonly studied by surface scientists are shown in fig. 1.3). In the latter work, an attempt was made to correlate spatially-localised STM tunneling properties and the

outer sphere electron transfer kinetics of a series of cobalt complexes, for each of the adlayers. Resolution of the atomic structure of the adlayers allowed speculations to be made about geometric contributions to the measured reaction rates.

Alkane thiolate monolayers on gold surfaces have long attracted attention as model systems for the study of organic interfaces (an example of their use is outlined in Chapter 6). Porter *et al.* have resolved atomically sized features during STM[65] and AFM[66] investigations of such adlayers from which the structure of the layer has been deduced. Crooks *et al.* have attempted to derive information about defects within these layers by electrochemically depositing copper onto a surface previously exposed to the organic species[67]. The metal can only deposit on regions not covered by adsorbate and previously unidentified features on flat areas of surface were attributed to copper islands deposited at defects in the organic layer.

1.IV.ii. *In-situ* STM: Practical problems

Under a conductive liquid, the STM tip and sample act as two electrodes at different potentials. Depending on the bias voltage and electrolyte, uncontrolled processes may occur at each interface, potentially causing physical or chemical change to the metal surfaces (e.g. roughening, dissolution or passivation). In this case a Faradaic current several orders of magnitude larger than the tunneling current may flow through the system. The STM feedback loop merely responds to current flow through the tip and as the electrochemical current flow will dominate, the STM experiment becomes inoperable. To define the state of the tip and sample and prevent degradation of either, in addition to ensuring the operation of the STM experiment, electrochemical potential control of such

a system is necessary even if an electrochemical process is not being investigated.

Conventional study of an electrochemical process may be achieved by using a three electrode cell[68]; current is passed between the electrode of interest (working electrode) and a counter electrode, while a reference electrode, through which no current passes, provides a fixed point against which the potential of the working electrode may be monitored. In an *in-situ* electrochemical STM system the tip acts as a fourth electrode and must also be controlled (the system is illustrated in fig. 1.4). To control and define reactions at the interfaces of interest (sample and tip) it is necessary to employ bipotentiostatic control, whereby the sample-reference and tip-reference potentials can be set independently[68]. Just as a surface in UHV can be defined by the conditions of the system, the same applies *in-situ*: even without charge transfer the interface will have a potential dependent composition.

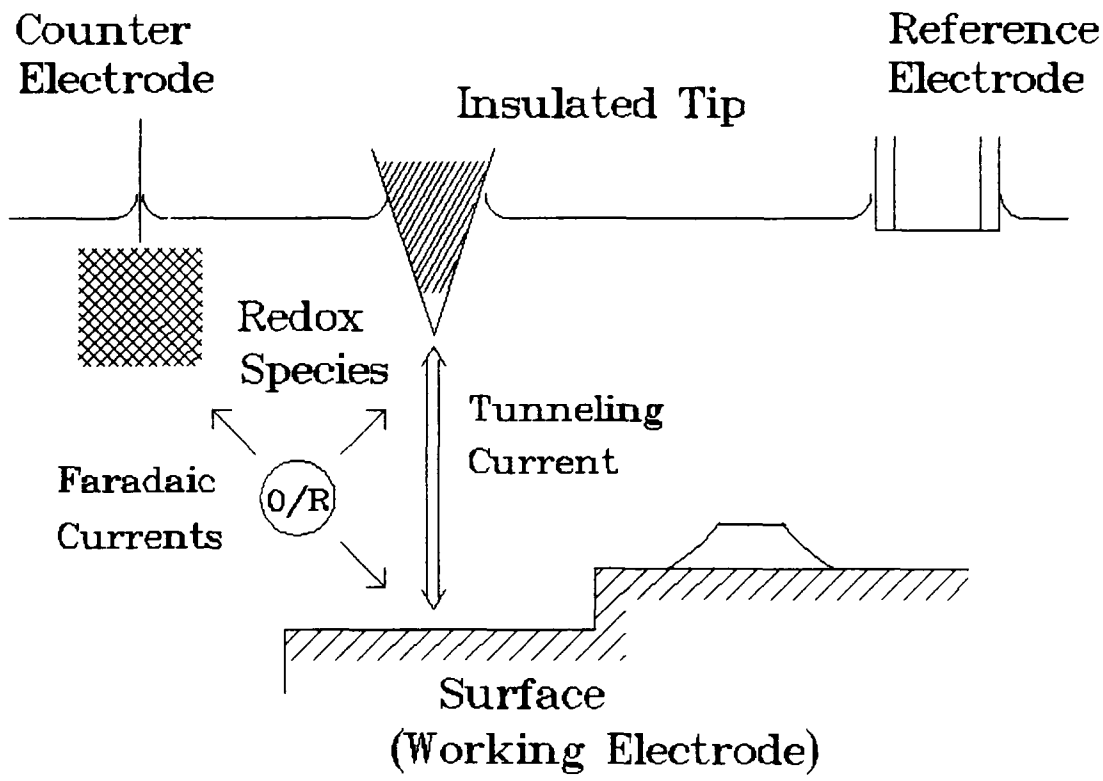

Fig. 1.4. Representation of electron transfer processes in in-situ STM.

Many of the first *in-situ* experiments utilising potential control during scanning used variations on this theme; the original demonstration, by Siegenthaler and colleagues, of STM imaging of graphite in an electrochemically defined environment made use of a current-carrying reference electrode and the tip potential was controlled relative to the sample[69].

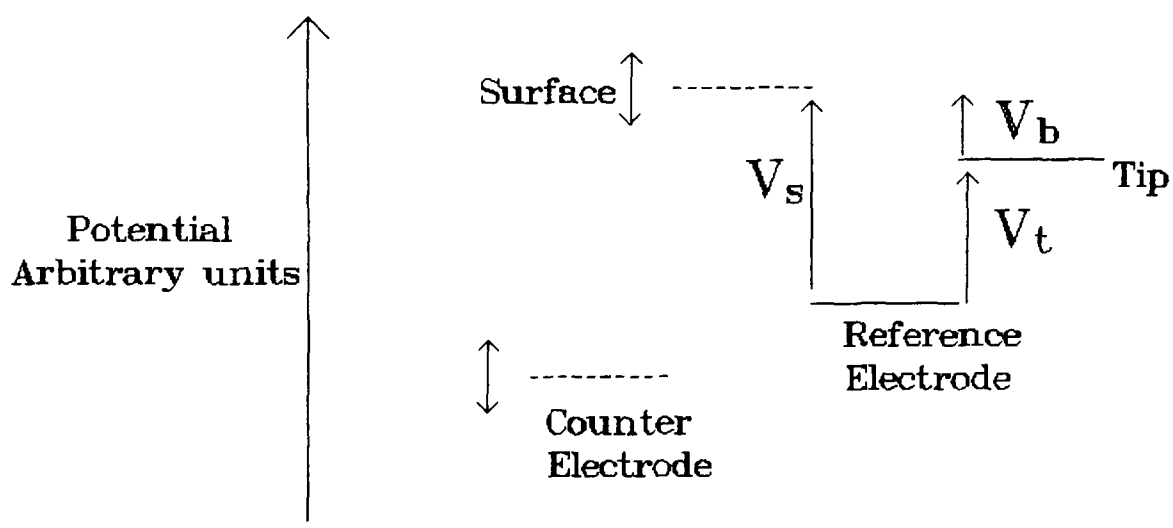

Fig. 1.5. STM potential control. V_s is the sample potential (controllable variable), V_t the tip potential (fixed) and V_b the bias voltage (variable).

One of the first examples of independent control of tip and sample potentials was shown by Behm *et al.*[70] and the experimental method developed by his group (and others at about the same time) is now widely used. The tip potential is set within a potential region where, for that system, it approximates to an ideally polarizable electrode i.e. charge transfer across the interface does not occur. In practice, this is hard to maintain and because current flow due to spurious Faradaic processes occuring at the tip, may easily be three orders of magnitude above the tunneling current, insulation of the tip is still a prerequisite. The

sample-reference potential can then be varied to allow different electrochemical reactions to take place at the surface. This does mean, however, that the bias voltage between tip and sample varies, but for commonly studied metal surfaces this has little effect. The method is summarised in fig. 1.5.

An alternative mode of working is to fix the bias voltage and vary the tunneling current, to overcome any small current flow, as the sample potential is varied, but again care is needed to prevent tip degradation[71].

There has been little theoretical work carried out on the STM experiment in the presence of electrolyte. Sass and Gimzewski[72] have considered the contribution of solvent dynamics to observed barrier height lowering under polar liquids[43,73], as part of a hypothesis that STM can act as a model system for understanding electron transfer in solution[74]. While appearing to agree, at least in part, with the former work the latter hypothesis has been rejected by Schmickler[75]. In his investigation of the possibility of measuring adsorbate density of states *in-situ*, he suggested that reorganisation of solvent (important in electron transfer theory) is far slower than electron transfer between tip and sample. Elsewhere, Merichev[76] has disagreed with Arvia's proposal that the STM could be used to investigate the double layer at an electrode[47], citing work which implies that the double layer structure oscillates faster than the STM can collect an image.

1.IV.iii. *In-situ* STM without potential control

Early *in-situ* STM investigations of electrochemical processes did not define the potentials of the tip and sample and used separate 3-electrode control of an electrochemical reaction, while the STM experiment was temporarily halted and the tip retracted from the surface.

This work predominantly involved topographical observation of electrodeposition processes including silver[77] and platinum[78] on graphite and gold on both graphite[79] and gold[80]. Itaya *et al.* observed the effect of subjecting a platinum surface to potential cycles in sulphuric acid[81] and Bard, Lev and Fan used basic potential control to prevent substrate etching when following nickel passivation in sulphuric acid[82].

1.IV.iv. *In-situ* STM with potential control

This section is sub-divided according to substrate in an attempt to make the body of work discussed here more digestible. Within each category the experiments are approached in the same order; reconstruction, oxidation/reduction processes, deposition processes and miscellaneous. A list of the literature discussed here, ordered by process, is presented in Appendix A.

Gold

The first, direct real space, *in-situ* observation of a reversible potential-induced surface reconstruction, at atomic resolution, was reported by Hamelin *et al.*[16]: an Au (100) surface was cycled in perchloric acid solution; below about -250 mV (vs saturated calomel electrode, S.C.E.) the surface exhibits a corrugated structure distinct from the (1 x 1) unreconstructed surface found at positive potentials (a brief explanation of reconstruction and adlayer nomenclature may be found in Appendix B). In a separate study the initial structure of the (100) surface was shown to depend sensitively on the sample preparation, an observation rationalising previously recorded electrochemical measurements[83].

Subsequently the same workers have also imaged reversible potential dependent phase transitions on Au (110) ((1 x 2) to (1 x 1))[84] and Au

(111) (($\sqrt{3}$ x 22) to (1 x 1))[85].

In the same area Tao and Lindsay have imaged the (22 x $\sqrt{3}$) reconstruction of the Au (111) surface under several electrolytes[86]. In contrast to the work of Hamelin *et al*, they found the reconstruction stable to *ca.* 200 mV (vs a silver quasi-reference), but above this the structure was irreversibly lost and the gold surface became covered with features 25Å high, 40Å in diameter.

Recently Behm and co-workers have claimed the first imaging of electrolyte anions, by reporting the observation of an ordered hydrogensulphate adsorbate layer on a Au (111) face under sulphuric acid (apparently no similar layer could be seen on the (110) and (100) faces)[87]. Imaging was dependent on tunneling current: above 400 nA the adlayer was lost and the underlying gold surface became visible.

Earlier, Behm's group studied larger scale potential-induced structural changes on Au (100)[88]. At positive potentials in acidic electrolyte (700-1000 mV vs S.C.E.) surface features were found to be mobile leading to self-annealing of the surface. In these experiments the ability to follow individual features on an identifiable area is essential, indicating the usefulness of STM in *in-situ* studies. Addition of small concentrations of chloride ions increased the mobility of the surface (previous work by the same group on a (111) surface had shown topographical changes in the double layer region under chloride-containing acidic electrolyte, but reported the surface was stable in the presence of acid alone[70]). At potentials leading to oxide formation, gross roughening of the surface was observed and as the features formed were 2-10Å high, it was concluded that an island growth process was taking place. The alternative layer growth mechanism for the oxide would be expected to yield regular

monatomically high (2Å) islands. Moving the potential back to lower positive potentials, causing dissolution of the oxide, revealed a pitted surface which quickly self-annealed. This supports the concept of gold-oxygen place-exchange[89] taking place during oxide formation (fig. 1.6).

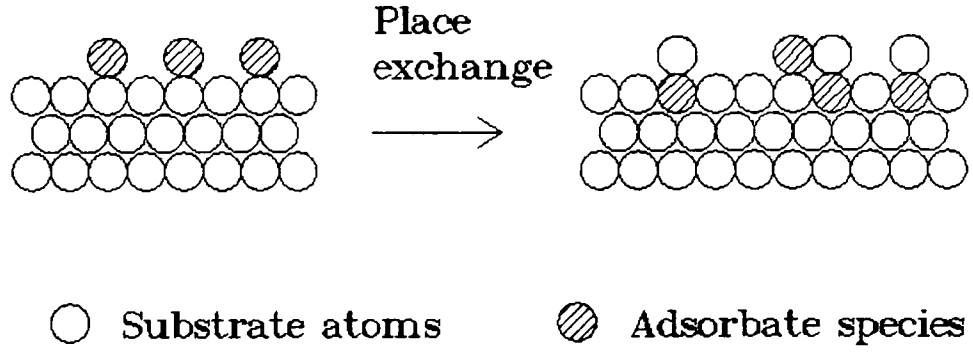

Fig. 1.6. Place exchange at a surface. Removal of the adsorbate atoms by changing potential leaves a roughened surface.

Possibly the most elegant imaging of pitting after oxide formation followed by surface annealing, with enhanced surface mobility in chloride-containing solutions, has been provided by Trevor *et al.*[90] on a Au (111) surface under perchloric acid. In a similar study, it has been proposed that the annealing process takes place by diffusion of step adatoms along step edges[91]. Attention was drawn to the behaviour of the surface varying with sample age, providing a possible explanation for the stability of features observed in Itaya's reproduction of this experiment[92].

Studies in alkaline media are less common: Brooker *et al.* examined the topographical changes associated with sweeping the potential of a polycrystalline gold electrode in hydroxide solution[93]. Prior to this, the

electrode had been electrochemically 'activated' in the solution. The large scale roughening and smoothing observed was ascribed to the influence of specifically adsorbed OH^- species.

Elsewhere the imaging of oxidative roughening of Au (111) in aqueous salt solutions (KCl, $AgNO_3$, $NaNO_3$, $AgClO_4$) has been reported by Holland-Moritz and co-workers[94]. Disconcertingly, it was stated that an unknown process, *not* shown in cyclic voltammetry of the systems used, was taking place.

The underpotential deposition of copper on single crystal gold faces provided the first atomically resolved images of adlayers in *in-situ* studies and has received attention from several groups[17,18,95,96].

Underpotential deposition (UPD) is the phenomenon whereby sub-monolayers and monolayers of foreign ad-atoms can be deposited onto an electrode surface at potentials positive of bulk deposition[68]. This arises when the interaction between the foreign ad-atom and the surface is stronger than that between the ad-atoms themselves. Study of these processes is useful as some UPD deposits are found to give surfaces with enhanced catalytic activity, while the structure of initially deposited layers influences bulk deposition.

In initial experiments, carried out in a $CuSO_4/H_2SO_4$ electrolyte, UPD on the Au (111) surface was found to yield an adlayer with a ($\sqrt{3}$ x $\sqrt{3}$) R30° structure (illustrated in fig. 1.7), in agreement with LEED and EXAFS experiments. This was found to evolve into a (5 x 5) structure not predicted by LEED[95]. Subsequent work by that group and others[18,96] has indicated that chloride contamination from the saturated calomel reference electrode used in initial studies, led to the (5 x 5) ordering. Itaya *et al.*[18] also ascribe the increased noise Behm's group found in atomic

resolution of the (111) surface to chloride impurities, as opposed to increased interactions of sulphate ions with the (111) surface, in comparison to the (100) and (110) faces, as originally suggested[95]. The influence of anions in adlayer packing is further shown by the contrast with vacuum deposition, where at sub-monolayer coverage copper forms islands of (1 x 1) structure.

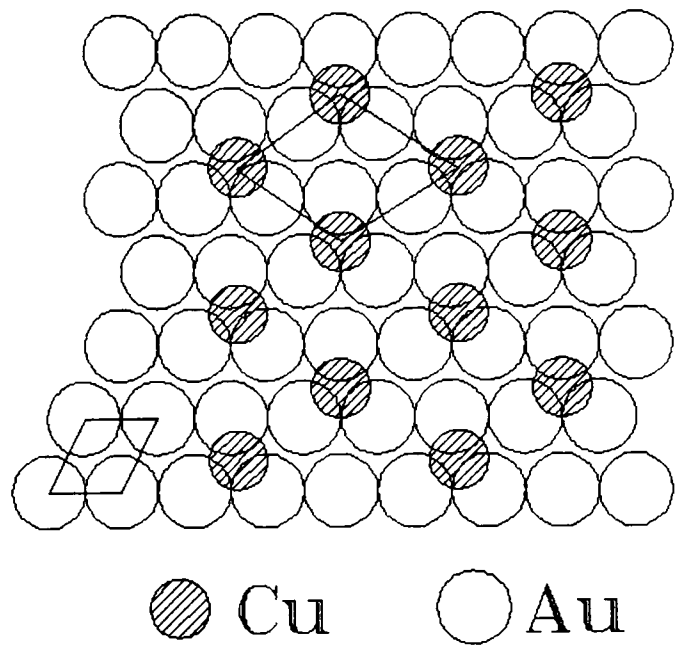

Fig. 1.7. Schematic representation of the copper ($\sqrt{3}$ x $\sqrt{3}$) R30° adlayer on gold (111). Copper adlayer and gold substrate unit cells marked.

Deposition on the (100) surface yielded less well ordered quasi-hexagonal arrays, which showed some variation with increasing copper coverage, while on the (110) surface no new superstructure could be observed as the potential was altered. There was increased corrugation in the STM image as the deposition potential was reached, and this was concluded to be due to a (1 x 1) copper adlayer. In all cases complete superstructures appeared abruptly as the potential was varied, in contrast to the continuous increase in coverage implied by current-voltage plots.

The lack of observation of adlayer islands was proposed to be due to the deposited copper atoms being mobile at low coverages. High resolution STM images, showing extended periodic structure, may be unconvincing (*cf* discussion of HOPG) but in many of the results presented with this work, the periodicity is broken up by the presence of steps in the substrate and defects within the ordered layers. Although not conclusive, these features support the interpretation of the images as being due to a tunneling process.

A study of bulk deposition[97] showed island growth preferentially at step edges and defects with lateral expansion being faster than vertical. Removal of the final traces of the copper was often at unexpectedly positive potentials, implying some alloying of the copper and gold. Further work using an organic additive appeared to indicate that the molecule (crystal violet) favoured 2D, while hindering 3D, growth of the deposit, and thus promoted development of a smoother surface.

The underpotential deposition of lead on Au (111) has gained attention from Binggeli *et al.*, for the possibilities of observing time dependent reconstruction of the surface[73] and Green *et al.* who were interested in the growth of the monolayer[98,99]. The former workers, using relatively rough electrochemically polished single crystal samples, did not monitor the growth of the adlayer, but considered the deposition and stripping process to alter the morphology of the gold surface. The work also contained barrier height measurements and an attempt to evaluate tip sample distances by point contact studies. In contrast, Green *et al.* working with gold on mica substrates exhibiting atomically flat terraces, observed development of the lead monolayer. Initial growth was at step edges, with free standing but occasionally mobile lead islands forming at more negative

potentials; lateral growth continued until the monolayer was complete. Here stripping was observed to cause minor changes in the detail of the surface but the gross morphology was undisturbed.

Atomic resolution studies of the adsorption of iodine and bromine onto an Au (111) face have shown the packing of the adlayer to be potential dependent[100], while the electro-oxidation of sulphide adlayers to S_8 species on the same face has also been observed[101].

Platinum

Itaya and co-workers have produced the most detailed studies of the behaviour of a Pt (111) surface after repeated oxidation-reduction cycles. Their more recent results[102,103] show the surface roughens, giving an island structure (of di- and tri-atomic height) which after developing over about ten cycles remains unchanged by further potential sweeps. This is reflected in the cyclic voltammetry of the surface which evolves with cycling. Unlike gold the platinum surface was not observed to show mobility leading to annealing.

Early low resolution studies of bulk copper deposition[104,105], have been superseded by the atomic resolution investigation of the UPD of copper[106] and silver[107] on a Pt (111) surface, by Itaya and co-workers. The latter study showed that, contrary to previous conclusions, the first silver adlayer is formed prior to surface oxidation. Additionally, the subtle difference between adlayer growth *in-situ* and in UHV was highlighted when, under electrolyte, the first and second monolayers form completely and consecutively before 3D growth: in UHV 3D growth follows monolayer formation (Stranski-Krastanov behaviour).

The stable adlattices formed by iodine on platinum are utilised to

protect single crystal surfaces from atmospheric contamination during transfer from preparation site to electrochemical cell. The potential dependence of the adlayer structures on (110)[108] and (100)[109] surfaces has been investigated: in the former study, appropriate choice of bias voltage allowed selective imaging of either metal surface or adlayer (a similar phenomenon was noticed in the gold based experiment[100]).

A subsequent investigation on an iodine covered (100) surface showed the substrate consisted of large (1 x 1) terraces, while replacement of the iodine by carbon monoxide (CO) caused formation of 20-40Å islands with (1 x 1) structure[110]. As the electrode potential applied to the perchloric acid electrolyte was moved to more positive values the islands were found to coalesce. *In-situ* infra-red reflection-absorption spectroscopy (IRAS) was used to investigate the change in coordination of adsorbed CO species with potential. It showed a decrease in bridging CO (thought to be present at step edges) with increasing potential, supporting the STM data.

Silver

Studies have been made of silver electrodes undergoing oxidation reduction cycles (ORC) in KCl electrolyte[111]. The process is used to prepare electrodes for surface enhanced Raman spectroscopy (SERS) type experiments. Formation of AgCl was observed to roughen the surface, which self-annealed on reduction to silver. The smoothing was faster in the first few minutes after reduction, corresponding to the known reduction in activity for SERS over this timescale.

Hottenhuis and co-workers have monitored the electrocrystallisation of silver, correlating STM images with optical observations[112]. Optically rough and smooth areas were ascribed to inactive and active growth regions

respectively; STM data implied that the inactive regions were not totally static but exhibited slow modification. Höpfner *et al.*[113] examined real and quasi-perfect single crystals, both in air and under electrolyte, primarily to investigate the typical surface topography of each, finding the step density and corrugation of the former (as prepared in this study) to be much higher than the latter. Interpretation of much data on UPD processes taking place on real single crystals is based upon the assumption that a quasi-perfect, regular atomic structure is present for the electrode surface. STM examination of such surfaces has shown this to be unrealistic because, unless very careful surface preparation is carried out, any electrode surface will exhibit an extremely rough and heterogeneous surface at the atomic level.

The first investigation of a UPD process on silver was provided by Siegenthaler and colleagues' low resolution study of lead at a chemically polished single crystal (100) face[114]. The surface topography became smoother when covered by a lead monolayer; on stripping only minor changes to the underlying substrate were detected. Deposition of an estimated 5-10 monolayers and subsequent removal led to more pronounced changes in some regions of the substrate. Later work has allowed the structure of UPD layers on (100) and (111) faces to be resolved at the atomic level[115]. For the (100) face it appears that the lead UPD monolayer reconstructs before bulk deposition occurs.

Semiconductors

In the same vein as Hansma and co-worker's early work with GaAs, both Behm and Itaya's groups have imaged Si(100) samples using an electrochemical environment as protection against atmospheric oxidation,

after removing the native oxide layer by chemical etching[116,117].

The electronic structure of semiconductors means that additional care has to be taken when attempting to image under electrolyte, however the well known photoelectrochemical properties of these materials makes the *in-situ* study of this area highly attractive. Itaya and Tomita have reported that n-type TiO_2 could be successfully imaged only at potentials negative of the flat-band potential[118] (the flat-band potential being the applied potential at which there is no potential drop within the semiconductor due to charge accumulation, either positive or negative, in a layer adjacent to the interface).

Uosaki and co-workers have imaged the decomposition of p-GaP (111) in dilute perchloric acid[119] and anodic photocorrosion of n-GaAs (100) in dilute sodium hydroxide[120] after establishing tunneling conditions for study of each system. They found for these systems there was only a small potential window, just positive of the flat-band potential within which tunneling was not possible.

To investigate the role of surface states in facilitating tunneling onto semiconductor surfaces, n-GaAs electrodes were treated with ruthenium and sulphur containing solutions[121]. The former treatment increases the density of surface states and only a small potential window not supporting tunneling was found. The sulphur treatment removes surface states and here it was found that the electrode behaved as an ideal semiconductor, no imaging was possible at potentials positive of the flat-band potential.

More generally, Lindsay and co-workers have carried out preliminary investigations of deposition processes[122] (nickel on Ge (111) and the photoelectrodeposition of gold on GaAs (100)).

Miscellaneous

The oxidation of HOPG in sulphuric acid as monitored by Bard and co-workers gave an oxide layer of amorphous structure which, on probing by barrier height measurements, was found to be more insulating than the native surface[123]. McCormick and co-workers have made a number of carbon based studies including: the effect of phenol oxidation on a glassy carbon electrode[124], the spatial variation of conductivity on a carbon paste electrode[125] and the imaging of a polypyrrole-entrapped glucose oxidase electrode[126].

The anodic dissolution of polycrystalline copper electrodes has been imaged by Zhang and Stimming[127] and Pickering and co-workers[128]. The former work investigated the possibility of using *in-situ* STM to evaluate local reaction rates, while the latter used large scale (μm) imaging to follow topographic changes. This study also followed the effect of the addition of an inhibitor to the electrolyte and the de-alloying (selective removal of copper under anodic polarisation) of a copper-gold alloy. In work on the passivation on surfaces under potential control, Bockris and co-workers have studied aluminium in sodium hydroxide solution[129] and iron in a borate buffer[130]. Similarly, Lindsay *et al.* have reported the morphological change of a tantalum foil surface being imaged under a sodium hydroxide electrolyte during scanning. the smoothing observed at negative tip bias was ascribed to oxide formation[131].

The susceptibility of experiments involving the imaging of bio-molecules to be complicated by contamination and inhomogeneity of deposition, has led some researchers to investigate the possibilities of preparing and studying the systems *in-situ* in an electrochemical environment. Work on the deposition of DNA supported in a buffered

electrolyte showed the potential of this methodology[132]. It also highlighted the need for investigation of the electrochemistry of individual components of each system, as it was suspected that there was some convolution of effects due to buffer adsorption in addition to bio-molecule deposition.

Itaya *et al.* cycled Rh (111) and Pd (111) surfaces in sulphuric acid and found both to exhibit island formation after repeated cycles, with a steady state structure forming after about ten cycles[103]. The rhodium islands appeared to be monatomic in height, while the palladium surface showed larger corrugation. It was postulated that a place exchange mechanism, assumed to be responsible for the roughening of the rhodium surface, was supplemented by anodic dissolution on the palladium electrode.

One of the more interesting studies to have been carried out in this area was the parallel STM and IRAS investigation, into the potential dependent structure of a saturated CO monolayer on a rhodium (111) face[71]. The IRAS data provided information on the bonding, coordination and orientation of the CO species which was correlated with real-space information derived from STM images. This was the first published work on the *in-situ* imaging of a CO adlayer and the exact contrast mechanism leading to the observed features is not clear (especially in view of the lack of success in imaging CO adlayers in UHV). The strength of the work lies in the complementary use of the STM and IRAS techniques to draw out structural conclusions despite unresolved imaging problems.

1.V Related work and possible new directions

The STM has given rise to a whole family of related techniques collectively known as scanning probe microscopy (SXM)[20]. In these techniques the local probe uses various interactions to gain information

about the surface under study. The most important of these is the atomic force microscope (AFM)[133] in which a tip mounted on a deflectable cantilever is tracked across a surface and is deflected by the atomic forces between tip and sample. Depending on the interatomic forces being probed, the tip and surface may be a few nm apart (attractive) or, as in most AFM work, in contact (repulsive). The field of AFM is expanding rapidly and more extensive coverage of the topic can be found in ref. 20; here only issues relevant to the rest of this Chapter are indicated.

The immediate advantage over the STM is that there is no requirement for the substrate to be conducting, and this aspect of operation has allowed applications such as the investigation of etch pits during quartz dissolution[134]. Workers wishing to image bio-molecules have also exploited this property, examples include; the imaging by Hansma and co-workers of the clotting of the protein fibrin[135] and the parallel STM and AFM studies by Edstrom *et al.* of a protein in air[136] and under water[44], where it was found vertical heights as measured by STM were 12% of those measured by AFM.

Gewirth and co-workers are currently investigating the application of AFM to electrochemistry (here, as the tip is non-conductive, a standard 3-electrode potential control system may be used). Studies of Au (111) oxidation[137] and copper UPD[138] on the same face came to the same conclusions as previous STM studies. Subsequently the same group has investigated UPD adlayers of bismuth[139], silver[140] and mercury[141] on Au (111) faces, reporting that only the silver adlayer system formed different structures depending on the electrolyte.

There is however some uncertainty in the contrast mechanism leading to such high resolution images in contact mode, as both the contact area and

forces acting at that point of interaction (with repercussions for deformation of tip and sample) are as yet unknown or ill-defined[142,143] for work in air or liquids. A recent analysis of repulsive mode imaging of organic molecules (e.g. in a Langmuir-Blodgett film) concluded the best possible resolution in air may be 20-30Å and that non-contact mode operation will grow in importance for samples (e.g. bio-molecules) that are potentially deformable[144].

Another STM related technique is the scanning electrochemical microscope (SECM) pioneered and subsequently developed by Bard's group in Texas[145]. In this *in-situ* technique an ultramicroelectrode tip (radius ≤ 10 μm) detects a Faradaic current flow due to an electroactive species in the solution. Generally, the current is controlled by reactions at the tip and sample and is influenced by the tip sample separation, conductivity and chemical properties of the sample. Although a number of applications have been reported (for example studies of conducting polymers, imaging bio-molecules and investigating enzyme kinetics)[146], the technique has as yet been little developed, possibly because the information yielded is mainly electrochemical and relies on an understanding of ultramicroelectrode electrochemistry.

A scanning ion conductance microscope (SICM), that topographically images non-conducting surfaces under electrolyte, by monitoring the substrate hindered flow of ions through a solution filled micropipette has been demonstrated[147]. Resolution of about 0.2 μm was estimated in the imaging of ion flow through a porous membrane and a proposal was made that ion transfer through bio-membranes may be followed by using an instrument with ion selective specificity. As Rohrer has pointed out, the resolution of any SXM experiment depends on the property probed and the smallest

practical probe size[148]. This is particularly appropriate here and low resolution, in addition to limited experimental applicability, has meant little more has been heard of the technique.

1.VI. Summary

Scanning tunneling microscopy is undoubtedly a major development for electrochemical investigations with the literature discussed showing the potential of the technique being realised.

The main points to come from the literature survey are:

(i) The technique has progressed from being used to image nanometre scale surface movement, via atomic resolution of, first deposited adlayers then electrode surfaces, to observation of the arrangement of adsorbed anion layers (originally thought impossible).

(ii) The need for carefully defined experiments, *cf.* the importance of co-adsorbed anions in metal adlayer structures, is being increasingly found. Correlation of STM results with cyclic voltammetry is essential and studies using complementary techniques, like infra-red, are appearing.

(iii) Bias-dependent imaging, previously acknowledged to be important in semiconductor work, is becoming important in the imaging of adlayers on metal surfaces.

(iv) Atomic force microscopy *may* replace STM for certain applications, e.g. metal adlayer imaging, because the system employs simpler three electrode control.

1.VII. Aims of research

The aims of this project may be broadly summarised as:

(i) To construct a scanning tunneling microscope for use in the *in-situ* study of electrochemical systems.

(ii) To develop sample surfaces appropriate for *in-situ* electrochemical STM studies.

(iii) To apply the STM to a well characterised electrochemical system to develop experimental procedure and show the performance and utility of the instrument.

(iv) To investigate aspects of the direct reversible electrochemistry of cytochrome *c* at SSBPY modified gold electrodes.

The long term aim of the work started here was to apply *in-situ* STM to the study of electrochemically generated or self-assembled ionic or molecular adlayers. Primarily this could provide information relevant to fundamental electrochemical studies and in addition the potential of such a system for high density data storage could be evaluated. For example if one bit were to be represented by the presence (or absence) of one copper atom in a UPD monolayer (an area of about 60Å2), information could be stored at a density of approximately 10^{14} bits per cm^2 (currently maximum density is about 10^9 bits cm^{-2}).

To extend work already under active study in Oxford the initial system chosen for investigation was the self assembled monolayer formed by the adsorption of 4,4'-dithiodipyridine (SSBPY) at gold. The surface formed has been found to promote the direct electrochemistry of the redox protein cytochrome *c* at gold electrodes and accordingly it was felt

appropriate to spend some time investigating the application of STM to the SSBPY/cytochrome *c* system.

At the start of this work the application of STM to *in-situ* studies was relatively new, therefore Chapter One has hopefully shown the growing importance of STM in electrochemical investigations by reviewing the published work in this area. Chapter Two contains relevant background theoretical information, describes the experimental procedures used, parts of the apparatus used and the sample preparations. Chapter Three describes in some detail the design of the scanning tunneling microscope. Chapter Four outlines the characterisation of the surfaces used for the studies. In Chapter Five results are presented from the *in-situ* studies of the gold/sulphuric acid and gold/phosphate buffer systems. Chapter Six describes investigations of the SSBPY/cytochrome *c* system including an *in-situ* FTIR study of the adsorption of SSBPY on a gold surface.

Chapter Two

Experimental Details

2.I. Scanning Tunneling Microscopy

This Section covers the fundamentals of STM and provides a framework for understanding work presented in later Chapters [20,149,150].

2.I.i. Theoretical aspects

The tunneling current is an indication of the degree of overlap of the electronic wavefunctions of the tip and sample. By analogy with one dimensional tunneling[1], the relationship between the tunneling current, I, and tip-sample separation, s, can be represented by:

$$I = B \exp(-Ks) \qquad (1)$$

where:

$$K = A\Phi\text{-}1/2 \qquad (2)$$

A is a constant ($1.025 Å^{-1} eV^{-1/2}$) and Φ is the effective average barrier height to tunneling. At tip sample separations of over *ca.* 20Å, the barrier height closely corresponds to the local work function of the surface; at smaller values the relationship is not so direct.

For a barrier height of 4eV, a 1Å variation in tip-sample distance causes an order of magnitude change in the tunneling current. This exponential relationship between current and distance provides the fundamental basis for the technique's ultra-high vertical resolution. This simple description implies STM images are straightforward topographs of the surface. A more rigorous treatment of the problem by Tersoff and Hamann[151] revealed, within certain approximations (e.g. weak tip-sample interaction, tip wavefunction that approximates to an *s* wave wavefunction) that the current is proportional to the surface local density of states (LDOS), at the Fermi energy (E_F), at that tip position.

The pre-exponential factor B is proportional to the local density of

states involved in tunneling and these states are selected by the bias voltage applied between tip and sample.

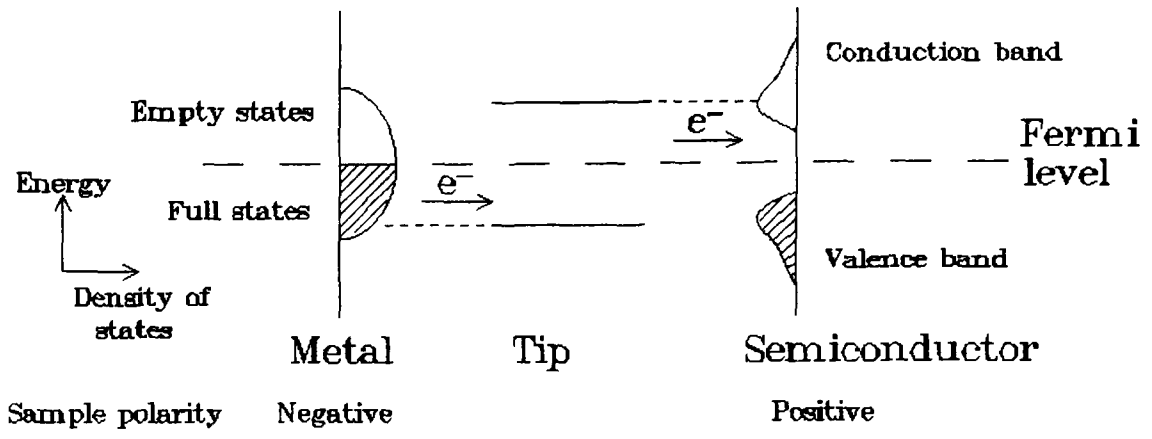

Fig. 2.1. Schematic representation of the effect of band structure and bias voltage in an STM experiment. For clarity the tip band structure has been reduced to an indication of the position of E_F at two different bias voltages.

As indicated in fig. 2.1, for metals the local density of states around the Fermi level is reasonably invariant with energy and images are not voltage dependent, hence STM results of *bare* metal surfaces are often interpreted as simple topographs. For semiconductors with full and empty valence and conduction bands respectively, reversing the bias voltage polarity has the immediate effect of changing the band involved in tunneling. As these bands have different spatial distributions in addition to internal energy related structure, STM images of these surfaces require careful interpretation. A clear example of this is illustrated by the GaAs (110) surface which only reveals one atom per unit cell at either positive or negative bias voltages[152]. If both images are obtained simultaneously the atoms are shown to occupy different positions. At positive bias,

electrons tunnel into the conduction band whose states are localised on the Ga atoms, while electrons tunneling out of the valence band at negative bias locate the As atoms.

The vertical resolution of the technique is system dependent as it relies on the mechanical stability of the tunneling gap, a variable related to the design of the instrument and the cleanliness of the tip and surface, but if the current can be kept constant to 2% then the gap will remain constant to 0.01Å[150]. Some theoretical effort has gone into estimating the lateral resolution of STM[153], a quantity that is related to the tip geometry and tip-sample separation, in addition to the electronic nature and intrinsic corrugation of the surface. In practice, although the actual mechanism for imaging is unclear, atomic resolution of low index faces of several metals (e.g. gold, aluminium and nickel) has been carried out. Two of the possible explanations advanced have been based upon tip-substrate contact[37], and the effect of *p* and *d* tip orbitals in the tunneling process[154]. High resolution STM studies require atomically sharp tips, an apparently daunting target. In practice, reliance is placed on the exponential decay of tunneling current with distance with the hope that, if the tip geometry is approximately correct, there will be a single lowest atom through which tunneling will occur.

2.I.ii. Operating modes

There are two widely used modes of operation of STM's which produce topographic images of the local density of states being probed. Both involve the tip being raster-scanned over the surface (the fast scan direction generally designated as the x - axis) while a parameter reflecting the tip-surface interaction is monitored. The ultra-fine 3D

movement required in STM is achieved by suspending the tip above the surface by a system of piezoelectric elements. Plotting the measured parameter against the lateral tip position, as provided by monitoring the voltages supplied to the piezos controlling lateral displacement, builds an image of the surface.

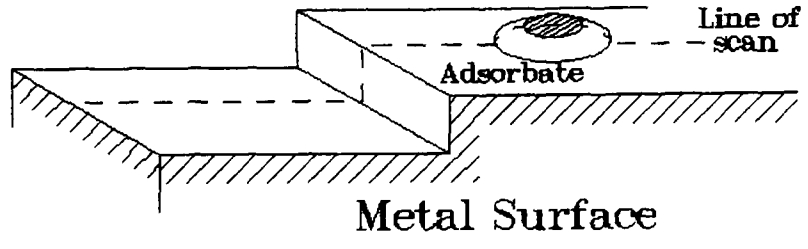

Fig. 2.2 (a). Schematic surface

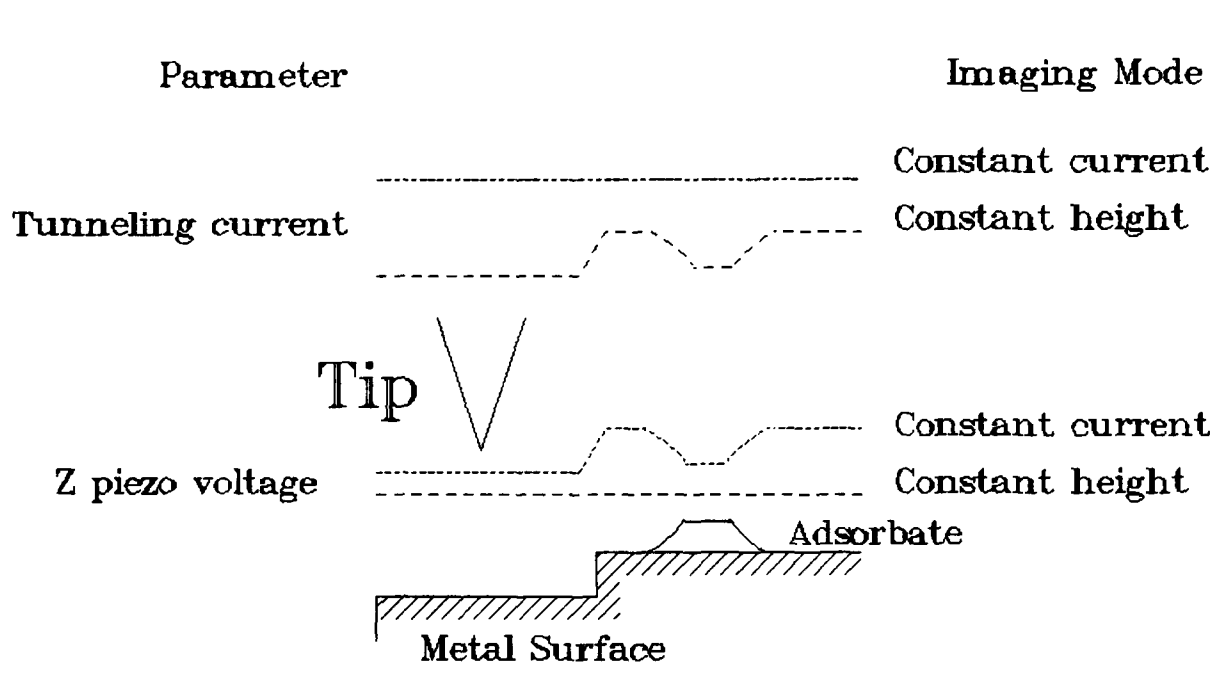

Fig. 2.2 (b) 'Topographic' STM imaging modes

Consider the surface in fig. 2.2 (a), which represents a stepped metal surface with an adsorbate present, which presents a large barrier to tunneling. In 'constant current' mode, the tunneling current is maintained at a preset value during scanning by an electronic negative feedback loop

which acts on the vertical displacement piezo, z. The parameter of interest here is the voltage applied to the z piezo. In 'constant height' mode the tip-sample distance is kept constant and the tunneling current is recorded. These modes are illustrated in fig. 2.2 (b).

In both cases, although the imaging of the exposed metal surface is topographic, the increase in barrier height at the adsorbate (causing a decrease in detected tunneling current) means the resultant linescan does not accurately reflect the physical profile of the surface. It must always be remembered that STM probes surface *electronic* structure which may be very different from the geometric structure of the surface.

Early STM images[1] were constructed simply of linescans. Nowadays sophisticated software is used to manipulate and enhance data, with images often being produced in pseudo 3D or greyscale. Examples of this are provided in subsequent chapters of this Thesis.

The constant current mode is most commonly used and is essential for imaging nanoscopically rough surfaces. The z motion should, however, have frequency components below the instrument defined mechanical resonance frequency of the tip-sample gap (e.g. 5kHz[148]), hence limiting the speed of this mode of operation. Constant height imaging is achieved by increasing the time constant of the feedback loop so that it responds only very slowly to gross changes in topography. The limiting factor now is the scan frequency and the mode gives faster data collection. This is the mode most commonly used for imaging flat surfaces at high resolution (e.g. close packed metal surfaces) but, because of the risk of tip-surface contact, is comparatively useless for areas of surface that are not atomically flat.

As pointed out in section 2.I.i. and illustrated in fig. 2.1., STM

probes the electronic states of the surface and hence intrinsically the STM yields spectroscopic information. Various modes of operation have been developed (occasionally known as scanning tunneling spectroscopy, STS) to yield explicit information on the local density of states involved in tunneling[155]. The most trivial of these, involving reversing the bias voltage to access different bands, has already been mentioned. The increasingly common current imaging tunneling spectroscopy (CITS) requires the STM to be operated in constant current mode; however at each sampling point the feedback loop is disabled and the tunneling current is recorded as a function of varying bias voltage. Spectroscopic information, a current-voltage (I-V) plot, is then available for every point on a standard image. The energy band gap for semiconductors is given directly whilst the first derivative of the plot (dI/dV), gives information on the local density of states. This data can also be used to provide measures of the barrier height to tunneling and the local work function, although this requires more detailed analysis of the tunneling process than is immediately obvious from Equation (1).

2.I.iii. The Oxford Electrochemical STM

All the STM data presented in this Thesis was produced using the Oxford electrochemical STM system (fig. 2.3). The system is a hybrid of commercial and 'home-built' components and was developed over the course of the D.Phil project.

A detailed description of the STM stage, coarse approach control and additions/modifications to the feedback electronics is contained in Chapter 3. Description and analysis of electronic negative feedback loops for controlling STM experiments may be found in, for example, references 149,156,157. The potentiostat is described in Section 2.III.ii.

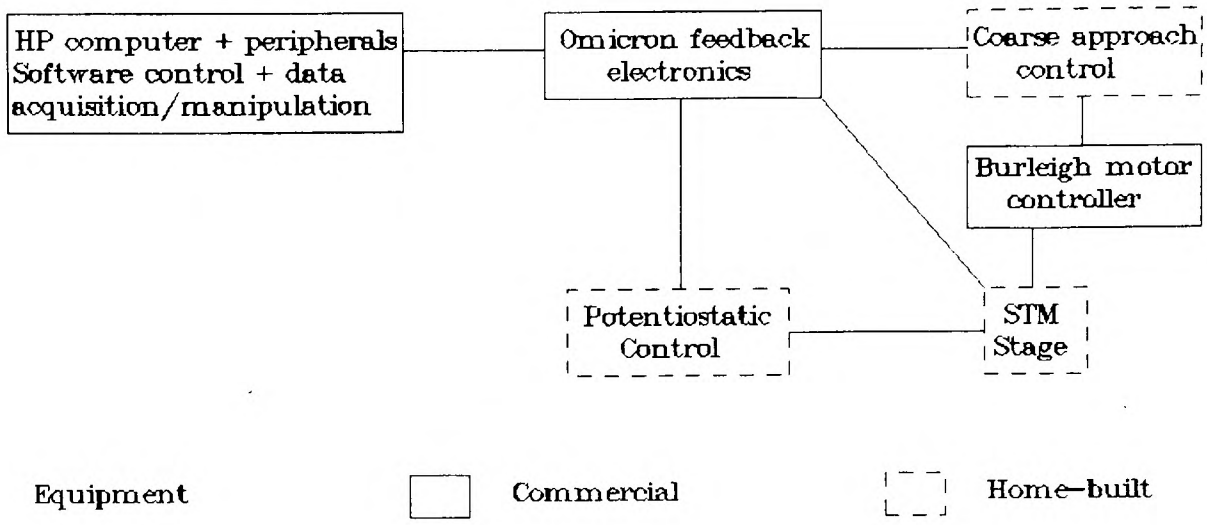

Fig. 2.3 (a). Schematic diagram of the Oxford Electrochemical STM.

Fig. 2.3 (b). Photograph of the Oxford Electrochemical STM.

The feedback electronics and software package controlling imaging, spectroscopy, data storage and data processing were supplied by Omicron Vakuumphysik[158]. The software allows full control of imaging parameters such as tunneling current, bias voltage, scan size and orientation, imaging resolution and speed. Some control of the response time of the feedback loop is allowed through the front panel of the electronics. The software is run on a Hewlett-Packard 9000 series computer equipped with dual hard disk drive, high resolution monitor and tape drive. The data processing package contains a standard range of facilities for example greyscale, colour or 3D displays, sectioning and enlarging operations, and smoothing functions to reduce noise on images. More specific information on the operation of the system is given where appropriate.

2.II. Infra-Red Spectroscopy

2.II.i. Introduction

In-situ IR studies can be made based on either internal or external reflection of the incident radiation from the electrode (transmittance IR is insensitive to study of the near electrode region)[7]. In the former experiment the electrode is a thin film coated onto an IR transparent crystal, IR radiation is passed through the crystal at an angle that forces it to undergo total internal reflection, and attenuation of the reflected signal gives information of the species at the interface.

In comparison to external reflection techniques this mode of operation requires high concentrations of adsorbing material and electrode preparation is critical. External reflectance techniques, while being more sensitive and less demanding of electrode preparation, are handicapped by

the strong absorption of IR radiation by most common solvents; water absorbs across the whole of the mid-IR range. This problem is minimised by using thin-layer cells where the working electrode is only separated by approximately 1-5 microns of solution from the IR transparent window. To improve sensitivity, several techniques using slightly different experimental systems (depending on the IR instrument and the system to be studied) have been developed. The *in-situ* IR studies presented here were made using external reflectance measurements with a commercial Fourier transform instrument.

To understand the information yielded by the technique it may be useful to consider the reflection of IR radiation from a surface (fig. 2.4). Two orthogonal components of the radiation may be distinguished; that with the electric field vector polarised *parallel* to the plane of reflection (xz plane) and that polarised *perpendicular*, E_p and E_s respectively. On reflection at the surface, components of the electric field vector *parallel to the surface* (E_s and E_{px}) have a phase change of 180°, whereas the component *perpendicular to the surface* (E_{pz}) undergoes a phase change dependent on the angle of incidence (maximum 90°). Superposition of incident and reflected electromagnetic radiation gives a standing wave; for E_s and E_{px} this has a node at the surface and thus negligible electric field strength, for E_{pz} there is an anti-node at the surface with the field strength angle dependent. The constructive superposition of waves is maximised at about 86°, although the exact angle depends on the properties of the interface[159]. As the magnitude of intensity change between reflected and incident light is dependent on the electric field strength, dipole moment changes parallel to the surface therefore contribute little to the adsorbance spectra. The *surface*

selection rule which implies only dipole moment changes with components *perpendicular* to the surface will significantly contribute to the absorbance spectrum is thus derived.

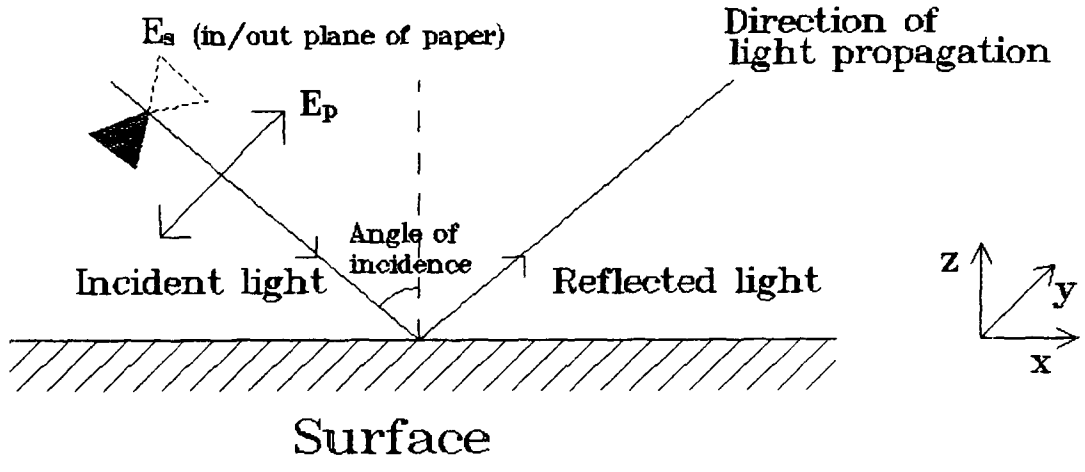

Fig. 2.4. IR radiation at a surface.

2.II.ii. *In-situ* External Reflectance FT-IR Spectroscopy

In a Fourier transform (FT) system the sample is positioned inside a Michelson interferometer arrangement, where it is illuminated by an intense broad band IR source (fig. 2.5).

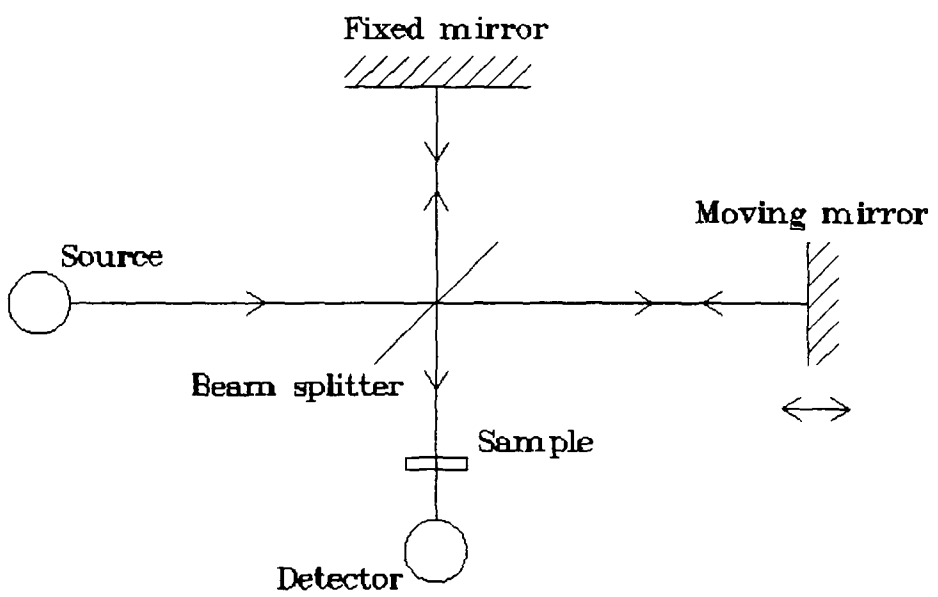

Fig 2.5. Michelson interferometer system.

As shown above the IR radiation is split into two beams of equal intensity by a beam splitter. Recombination of the beams may be constructive or destructive, depending on the exact path length of the light reflected from the moving mirror. When the mirrors are equal distances apart the detector records a maximum intensity of reflected radiation (due to constructive interference), the so-called centre-burst, but as the mirror moves destructive interference reduces the intensity of detected radiation. A plot of intensity (of reflected light) against mirror position gives an interferogram. This interferogram is a superposition of waves of a range of amplitudes, wavelengths and phases at each mirror displacement (the source is *not* monochromatic).

Therefore each point in the interferogram contains information about the wavelength dependence of the system (source, detector, sample) and this superposition of waveforms corresponds to a Fourier transformation. It can be deconvoluted into a conventional intensity vs wavelength spectrum by using a computer to record the data and carry out a Fourier transform on the interferogram.

Spectra are plotted as $\Delta R/R$ against wavenumber[160];

$$\Delta R/R = (R_2 - R_1)/R_2$$

where spectra R_n are recorded at a base potential, E_1, and a working potential, E_2. Scans at each potential are co-added, averaged (yielding a high signal to noise ratio) and those taken at E_1 are subtracted from those taken at E_2 and the result normalised. The subtraction of spectra removes the wavenumber dependent contributions from solvent absorption, source and detector envelopes, and other system invariants such as the instrument optics and cell window. This ensures features appearing on the resulting

spectra are due to potential-dependent processes occurring at the electrode-electrolyte interface. Features may arise from electroreflectance effects, where electron density changes at the electrode surface due to applied potential affect IR reflectivity, re-organisation of the double layer or changes in the quantity, orientation or IR absorbance of adsorbed species. In addition loss or generation of chromophores in the thin layer will adsorb radiation, although these changes will not be subject to the surface selection rule.

In the spectra, an upward pointing band shows the loss of an absorbance in the latter spectra relative to the base spectrum, while a downward pointing band indicates a gain. This can give rise to bipolar bands where the potential dependent IR absorption characteristics of an adsorbed species gives closely spaced loss and gain features. This is illustrated in fig. 2.6.

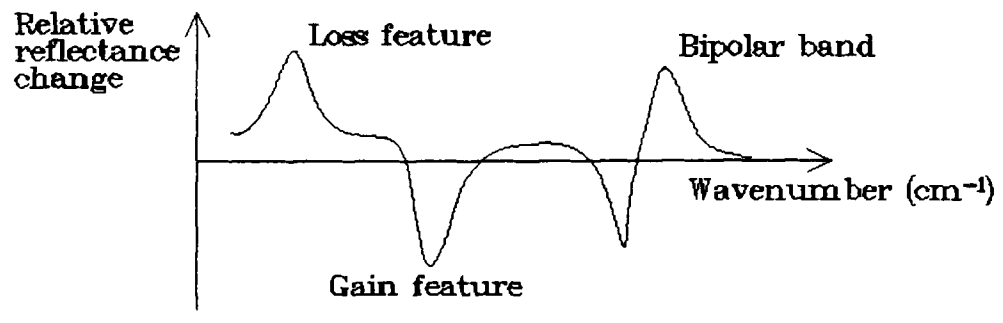

Fig. 2.6. Schematic of features of a differential IR spectra.

2.II.ii. Instrumentation

The spectrometer used was a Bio-Rad FTS-40 fitted with a narrow band mercury cadmium telluride (MCT) detector. For the *in-situ* experiments, the spectrometer and cell electrochemistry was controlled via an Oxsys Micros Electrochemical Interface[161]. This was also used for

manipulation of the IR spectra. The thin layer spectroelectrochemical cell was mounted on a modified version of the Spectra-Tech Series 500 variable angle specular reflectance attachment. Where required a KRS-5 wire grid polariser (Specac) was used. To minimise the effects of vibration the instrument was mounted on an Ealing Instruments air table. To reduce unwanted IR adsorption by atmospheric water vapour and CO_2 the sample chamber was purged with N_2 from a cryogenic boil off supply, as were all solutions prior to use. The spectroelectrochemical cell is shown in fig. 2.7. A screw arrangement is used to push the electrode against the IR transparent CaF_2 window (BDH Crystran 24mm diameter, 4mm thick plate).

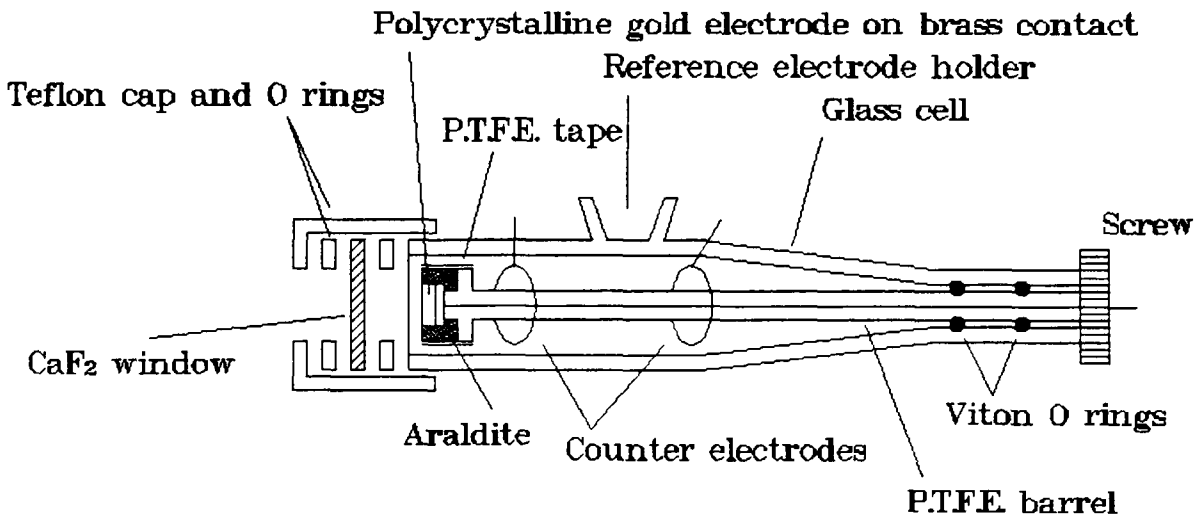

Fig. 2.7. Thin layer spectroelectrochemical cell.

The working electrode was a circular 10 mm diameter polycrystalline gold disc which was polished with 0.3 and 0.0125 μm alumina and sonicated in ultra-pure water. The reference was a saturated calomel electrode (S.C.E.). Two platinum wire counter electrodes were used (the system was controlled by a bipotentiostat) one acting conventionally, the

other was biased at -0.3V vs S.C.E. during the experiment to reduce trace O_2 (it was found in initial experiments absorptions due to species resulting from O_2 reduction at the gold electrode were obscuring the weak signal from the adsorbed species under study).

IR transmission spectra were carried out using the same instrument using germanium plates with a conventional transmittance attachment.

For both sets of experiments spectra were recorded at 8 cm^{-1} resolution. In the transmission experiment 100 scans were recorded and averaged, and in the *in-situ* experiments 250 or 500 scans were collected at each potential step.

2.III. Electrochemistry

2.III.i. Introduction[68,162]

In a three electrode cell used to investigate the electrochemical characteristics of a system, the potential of the working electrode is varied relative to a reference electrode. The reference electrode has a constant composition (no d.c. current is allowed to flow through it) and hence an invariant potential, thus all monitored potential changes in the cell are effected at the working electrode (potential changes at the counter electrode occur as a response to those imposed at the working electrode and should have no influence on the experiment). As the potential (and consequently the energy level of the electrons) of the electrode is varied, electron flow to or from species in solution may occur if vacant orbitals of a corresponding energy are available. The situation is analogous to that shown in fig. 2.1, where a molecular or atomic orbital should be substituted for the tip band structure.

The electron flow may cause a number of processes to occur e.g.

change the charge residing on a solution species, cause chemical change to a solution species or cause dissolution of, or deposition on, the electrode surface. These processes involving charge transfer across the electrode-electrolyte interface are known as Faradaic processes.

One of the most straightforward methods of characterising the electrochemistry of a system is cyclic voltammetry. In this experiment a triangular wave potential sweep is repeatedly applied to the working electrode and the current flow through the electrode is recorded as a function of applied potential, a plot known as a cyclic voltammogram (CV), as shown in fig. 2.8.

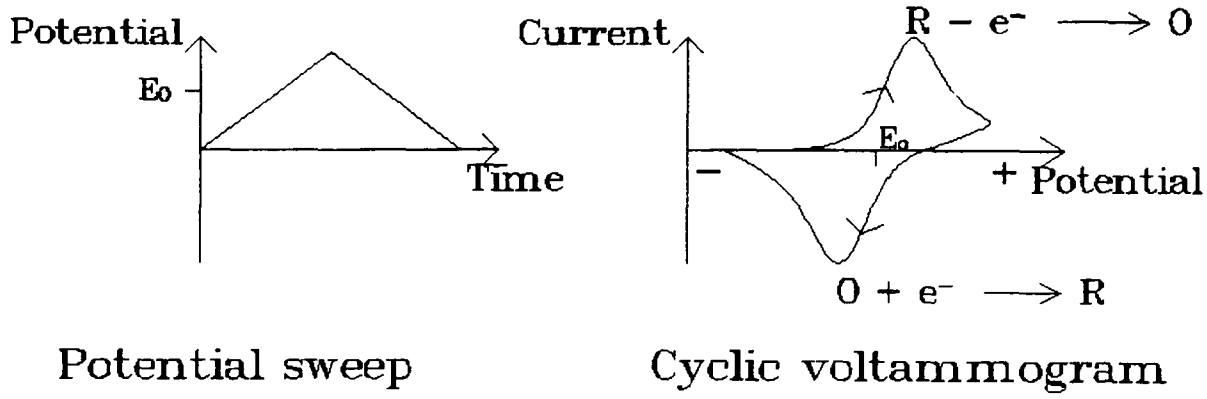

Fig 2.8. Cyclic voltammetry.

Consider a sweep across the potential region in which the reversible process;

$$O(aq) + ne^- \text{------} > R(aq)$$

occurs (see fig. 2.8). As the appropriate potential is reached reduction begins and current flows. As the potential sweep continues the surface concentration of the oxidised species decreases, consequently increasing the concentration gradient of these species to the surface, the flux of the

species at the surface and the current flow. Eventually there will be almost no oxidised species present at the surface and the current reaches a maximum. As reduction carries on, an increasing volume of solution adjacent to the electrode will have a decreasing concentration of oxidised species and the concentration gradient, and current, will fall. On reversing the direction of the potential sweep, the oxidation process will give a similar peak.

Analysis of cyclic voltammograms can give information about the reversibility of electrochemical processes[68,162] and CV's can be a useful tool in the characterisation of an electrochemical system.

The cyclic voltammetry carried out in the course of this work has been on well-known and previously characterised systems, and in the case of the STM experiments has effectively been used to check and characterise the performance of the electrochemistry *in-situ*.

2.III.ii. Instrumentation

To control the potentials of the three electrodes in a simple electrochemical experiment a potentiostat is used. The device allows control of the potential difference between working and reference electrodes, and lets the potential of the counter electrode settle at a value which supports the current flow demanded by the processes occuring at the working electrode. Standard features of a potentiostat are; the ability to combine input signals e.g. a ramp signal and an offset, to have a high impedance input for the reference electrode, to prevent current flow through it and an ability to monitor and output the current flow through the working electrode.

As pointed out in 1.IV.ii. bipotentiostatic control is needed for *in-*

situ STM where two working electrodes are present and the home-built potentiostat (designed by Dr. P.R. Trevellick) used in the STM system was constructed with this aim. A diagram of the circuit is given below.

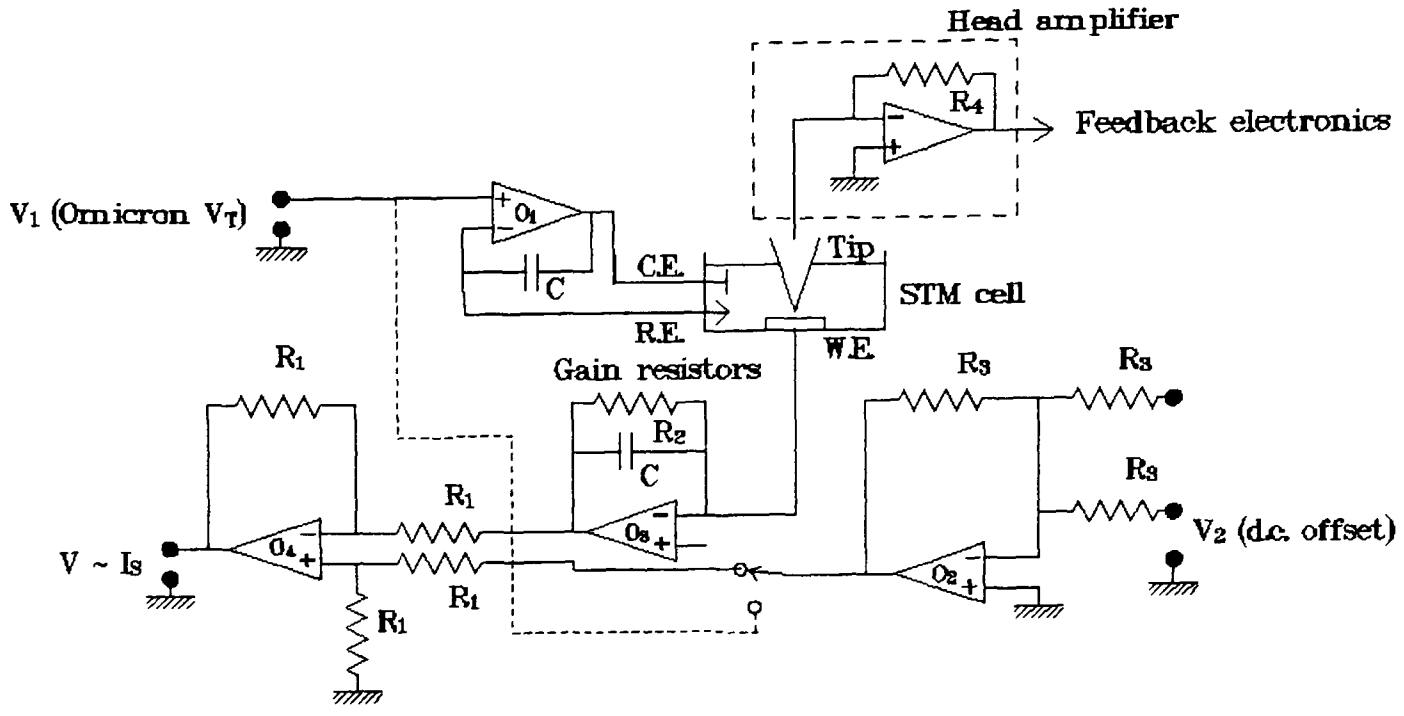

Fig. 2.9. Schematic diagram of the STM electrochemical potential control. Dotted line shows optional adder input positioning; full line shows normal connection. Electrodes can be switched out to a dummy cell when not in use.

Key: O_1, O_3: *CA3140 operational amplifiers*
O_2, O_4: *LM11 operational amplifiers*

C $0.1\mu F$
R_1 $100K\Omega$
R_2 *Gain resistors* 10Ω - $1M_\Omega$
R_3 $10K\Omega$
R_4 $100M\Omega$

W.E. *Working electrode i.e. sample*
C.E. *Counter electrode*
R.E. *Reference electrode*

In the Oxford electrochemical STM system the tip is maintained at virtual earth in both air and *in-situ* experiments. To ensure all the electrodes have the same reference point and to avoid ground loops the

potentiostat was powered from the Omicron electronics. In the following explanation of potential control reference to Chapter 1, fig. 1.5 is helpful.

The reference electrode (R.E.) is attached to the high impedance inverting input of op-amp O_1, which ensures minimal current is passed. The non-inverting input controls the potential of the reference electrode. If a potential V_1 is applied at that point the reference electrode becomes biased to V_1 vs earth and thus the *tip-reference* potential is $-V_1$. The counter electrode (C.E.) is allowed to swing to whatever potential is required due to the low impedance of the op-amp output. Potentials may be applied to the sample via the adder input, O_2, connected to the non-inverting input of the current follower, O_3. Gain resistors in the current follower and a differential amplifier stage, O_4, allow the current flow (I_S) through the sample (i.e. the working electrode, W.E.) to be monitored. Here applying a potential V_2 to the adder input will result in the sample being at a potential $-V_2$ vs earth. Correspondingly the bias voltage is $-V_2$ and the *sample-reference* potential is $(-V_2 - V_1)$.

In-situ STM experiments were carried out with the *tip-reference* potential fixed and varying *bias* voltages (see 1.IV.ii.). It was found convenient to apply the software controlled bias voltage (V_T) as V_1 while the variable sample potential, V_2, was supplied by a manually adjustable home-built d.c. supply. If the alternative mode of operation (constant bias voltage, variable tip vs reference potential) was required V_1 and V_2 would be switched.

In the configuration described the adder input appears as an unnecessary complication with the sample being manually adjusted to different potentials between images, however the overdesign was useful

when the potentiostat was used to perform cyclic voltammetry. In this case the potentiostat was operated conventionally with the sample being grounded, and the adder input switched to apply voltages to O_1 (as shown by the dotted line in fig. 2.9).

The potentiostat was constructed to be compatible with home-built electrochemical apparatus based upon the modular R.S. Components 19" rack system previously used in the Hamnett group[163]. For cyclic voltammetry a triangle wave generator in conjunction with a d.c. voltage source (to vary the midpoint of a scan) were used, with the same voltage source providing potentials for *in-situ* STM experiments. The chart recorder used was a Bryans series 60000.

The cyclic voltammetry associated with the FT-IR experiments was conducted *in-situ* in the spectroelectrochemical cell using the Oxsys Micros Electrochemical Interface.

2.III.iii. Apparatus

A small amount of cyclic voltammetry was conducted in a conventional cell, which allowed for deaeration of solution and electrochemistry under an inert atmosphere. Most cyclic voltammetry was carried out in the small cells used within the STM (fig. 2.10) to reproduce the conditions of the system during an STM experiment. For STM the working electrodes used within these cells were gold on mica. Preparation of large sheets of these substrates is described in Section 2.V.iii. For use as STM electrodes the substrates were cut into smaller pieces with the approximate dimensions 4 mm x 8 mm.

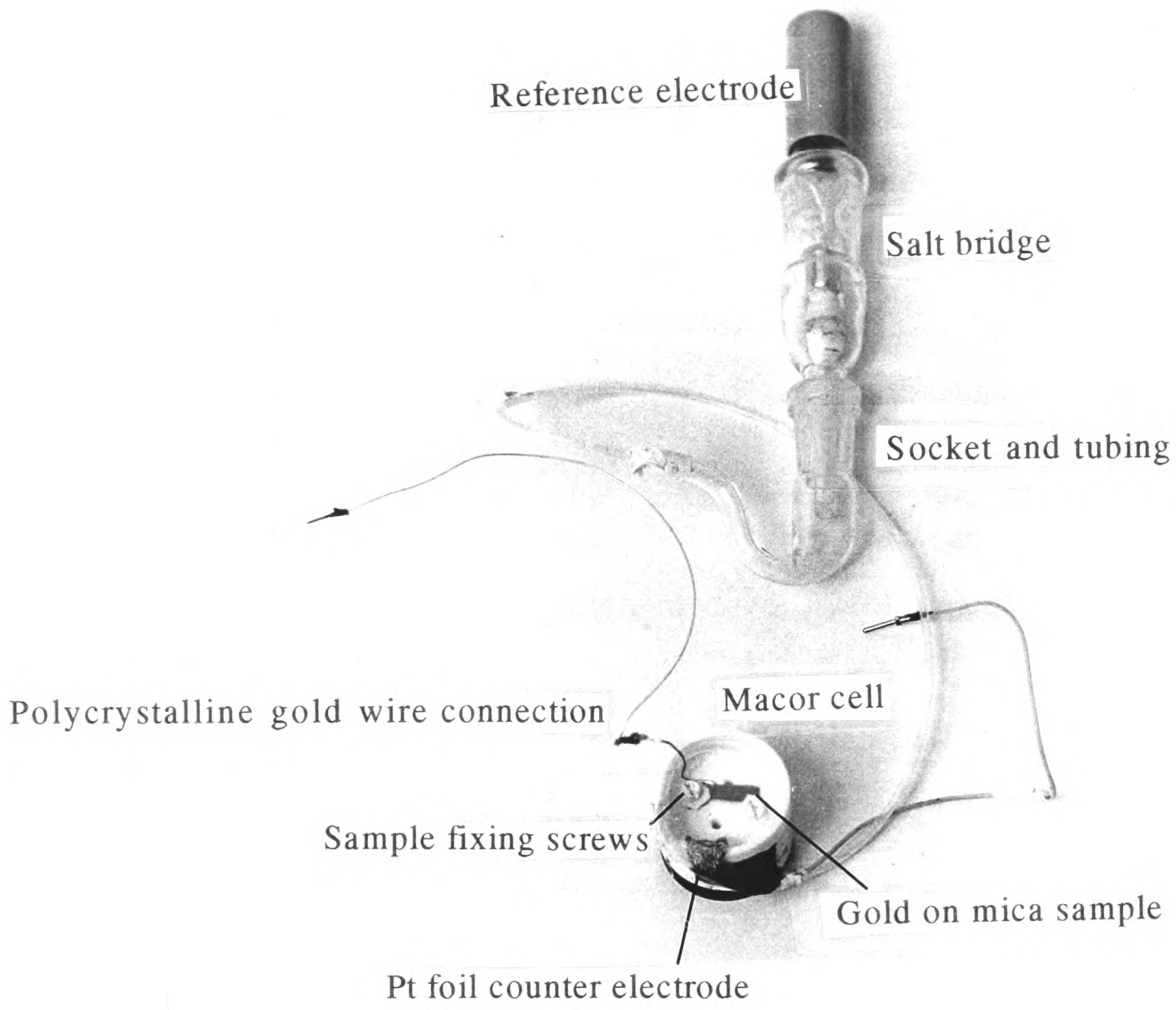

Fig. 2.10. Photograph of sample mount/reference electrode for the STM.

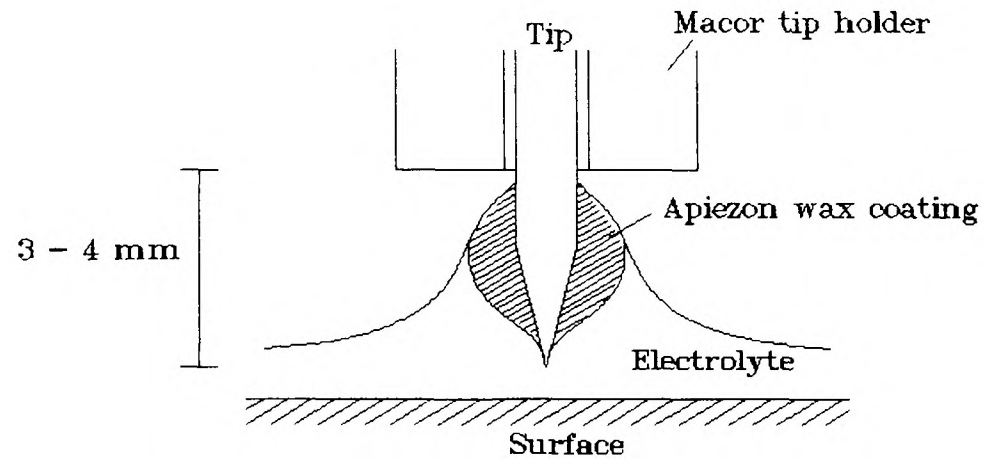

Fig. 2.11. Schematic diagram of the tip-electrolyte interaction.

As shown the cells have a small volume (*ca.* 1.5 ml) with there being no possibility for *in-situ* deaeration of electrolyte and electrochemistry was carried out in ambient conditions. One of the possible improvements to the STM system as a whole would be to include the capability of tunneling under an inert atmosphere.

The cells are made from Macor, a machinable glass ceramic[164], mounted on a brass stub (to give the correct sample height for the STM). Both for ambient and *in-situ* experiments nylon screws and teflon washers were used to position the sample rigidly and hold the gold wire (Johnson Matthey Puratronic) connection in physical contact with the sample. A platinum gauze counter electrode was used. The reference electrode, supported in a salt bridge and glass socket was connected to the cell via approximately 200 mm of 1 mm diameter polyethene tubing fixed by Araldite to the cell wall (the length of tubing being required for the STM set up). Commercial calomel (Hg/Hg_2Cl_2) and mercurous sulphate (Hg/Hg_2SO_4) reference electrodes were used[165].

Between sets of experiments aqua regia was used to clean the cell and noble metal connections, and appropriate solvents were drawn into the tubing prior to sonication to clean it. To avoid air bubbles, the system was filled by drawing liquid from the cell into the tubing by a syringe, connecting the tubing to the socket and, while maintaining liquid in the cell, using gravity to let liquid fill the socket.

In standard electrochemical cells often a luggin capillary is used to minimise the voltage drop through solution resistance between the working and the reference electrodes. For the *in-situ* set up used here this was not possible but the configuration as described gave acceptable potential control.

During *in-situ* experiments the electrolyte volume was reduced to *ca.* 1.1 ml to prevent liquid from touching the tip holder (fig. 2.11). If this occurred, current flow through exposed metal would overcome, or contribute an excessive proportion of, the desired tunneling current. Evaporation of the electrolyte was occasionally a problem, often *in-situ* experiments were checked periodically to confirm the presence of liquid. Usually aqueous electrolyte would last 1-3 hrs although because of evaporation tunneling under ethanol was difficult.

2.IV. Tip Preparation

As pointed out in a recent article[166] there are a plethora of methods available for preparing tips suitable for high resolution STM studies. The method and materials used for producing tips for the Oxford electrochemical STM are closely based upon those used by Behm's group in Munich[70] although the technique for insulating the tip with an inert coating is slightly different and was arrived at after some trial and error.

The apparatus for tip manufacture is shown in fig. 2.12. A 2.5V a.c. supply is passed between a 0.2 mm diameter tungsten wire and a platinum-iridium wire ring, through an approximately 2M sodium hydroxide solution causing etching of the tungsten wire. The wire forms a 'neck' and eventually cleaves (the influence of the wires' own weight in the final stages of etching being thought to contribute to tip effectiveness). The bottom portion is collected (the top half by remaining in contact with the etchant becomes blunted) and is then rinsed in Milli-Q water.

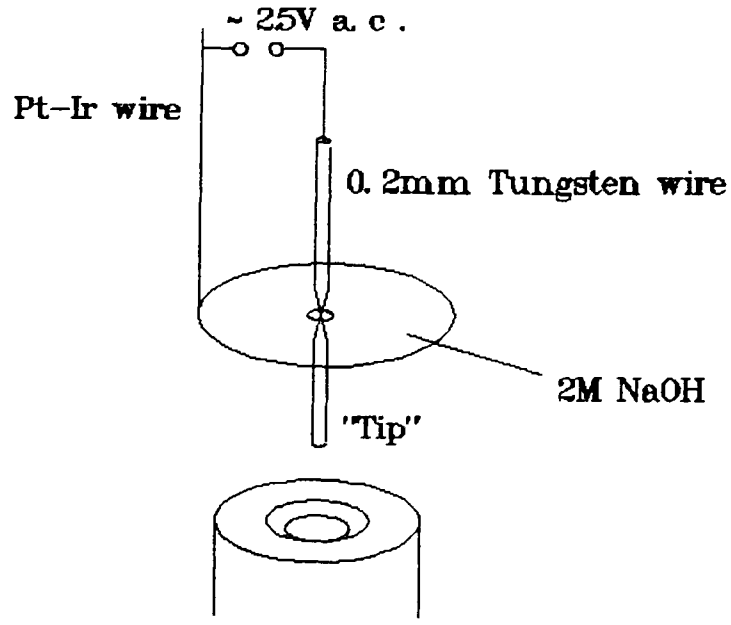

Fig. 2.12. Tip etching

Conventionally STM tips are made of material that is rigid and stable (the rearrangement of atoms at the end of a tip will cause havoc to high resolution imaging) and also easy to etch (although some workers form tips by simply cutting wire), providing some rationale behind the popularity of tungsten as a tip material. The length of a tip will affect the stability of the tunneling gap, the longer the tip the more vibration sensitive it may be, so for operation in air, tips are cut to protrude 1-2 mm from the tip holder.

The tips are insulated by dipping, point first, into molten (bubbling) Apiezon wax. The wax is supported on a porcelain dish and heated in small quantities in a fume hood. Inspection under an optical microscope reveals that the wax does not adhere to the very end of the tip, probably a surface tension effect. The thinnest coatings are obtained by using very hot, fresh wax. The performance of the wax decreases with re-use (presumably due to the loss of volatile components) and acts like colder wax in giving more globular coatings which may, due to the lack of flow of the liquid, completely cover the tip. The process is quite empirical but after some trial and error, success rates approach 90%. Due to the need to

keep liquid away from the tip holder, but maintain a workable volume (see above) insulated tips are normally covered to a length of 3-4 mm and most of this protrudes from the tip holder. As tips are held by tweezer during insertion into the tip holder, care must be taken not to clamp the insulated tip so tightly the wax is pulled off by the tweezer.

Although several groups have carried out characterisation of the exposed area of tip after insulation (e.g. refs. 167,168), neither this nor electron microscopy of uninsulated tips has been attempted; rather reliance has been placed on the performance of the tips during experiment. Optical microscopy of tips after insulation is used to check the point is exposed. Monitoring residual Faradaic current by oscilloscope, when the tip enters solution as a coarse approach to tunneling is carried out, will quickly show the effectiveness of insulation. Usually, for an appropriately biased tip, the residual current is below 0.5 nA. The exact geometry of the region of tip through which tunneling takes place is effectively uncontrollable and as with all STM, acceptable imaging may require tip modification by applying a pulse to the bias voltage or just patience!

In the area of *in-situ* STM a number of other different tip materials e.g. gold[73], tantalum[69], platinum/iridium[167,169], platinum[18] and tip insulation materials/methods e.g. Apiezon[170], poly α- methylstyrene[167], epoxy resin[168], glass[167], nail varnish[110] are being used. Attempts were made to use Pt/Ir as a tip material; etching in 2M NaOH / 6M KCN solution[167] gave on inspection good tips but due to the materials used the process was undesirable. The alternative etchant of 60% saturated $CaCl_2$, 36% water, 4% HCl[168] was never used successfully, the process yielding optically blunt and jagged points.

Poly α-methylstyrene and epoxy resin gave clear coatings from

which it was hard to observe the coating of the tip and were not used. Nail varnish was originally used to insulate tips, while fitted in the STM, but was found to be unsatisfactory as the varnish took a couple of hours to set and was unpredictable in insulating ability.

2.V. Sample Preparation

2.V.i. Graphite

The graphite samples were ZYH grade pyrolytic graphite monochromators (Union Carbide). Clean, highly oriented basal planes were exposed by removing the previous surface with adhesive tape.

2.V.ii. Gold single crystal

An Au (111) single crystal (Johnson Matthey) was mechanically polished by G. Read (Clarendon Laboratory, Oxford) using 6 and 3μm diamond paste. The crystal was then degreased and flame annealed before use. Although the surface was highly reflective, polishing scratches were visible to the naked eye.

2.V.iii. Gold on mica

Samples of gold on mica were kindly prepared by Mr. Chris Goodwin of the Thin Films Facility of Oxford University Nuclear Physics Department.

Gold (≥99.99% pure) was thermally evaporated onto air-cleaved mica (samples 1-3, mica of unknown origin, previously coated, here cleaved to reveal fresh surface, samples 4 and 5 mica as supplied from Agar scientific, sample 6 mica as supplied from Polaron) in an Edwards chamber evacuated to a pressure of approximately 10^{-5} torr. The samples were fitted into 1" x 2" jigs. Film thickness was monitored by a quartz

thickness monitor. The substrate was heated from the rear radiantly and a thermocouple mounted under mica sheet on the jig holding the substrate, was used to monitor the temperature. As the system contained only one power source the mica and gold could not be heated simultaneously, so the deposition process involved evaporation onto a slowly cooling substrate. A number of slightly different deposition methods were tried (based upon methods used by Chidsey *et al.*[171] and Lindsay *et al.*[132]) and these are detailed below:

1. Initial mica temperature of 230°C dropping to 190°C during deposition. Deposition rate 3-10Ås^{-1}. Thickness 1236Å

2. Mica temperature initially 220°C dropping to 165°C during deposition. Deposition rate 1-3Ås^{-1}. Thickness 1207Å. Substrate annealed at 250°C for 2 hours after deposition.

3. Mica heated at 240°C for 1 hour prior to deposition after which the temperature was 190°C. Deposition rate 5Ås^{-1}. Thickness approximately 1762Å.

4. As 3. except final temperature 180°. Thickness 1739Å.

5. Initial mica temperature 280°C dropping to 190°C. Deposition rate 2Ås^{-1}. Thickness 1799Å.

6. Prepared in same run as 5.

The different samples are marked in the text as Au n (n = 1-6) as appropriate. Samples were covered and stored under ambient conditions.

2.V.iv. Gold single crystal spheres[32,92,172]

Gold wire (0.5 or 1 mm diameter >99.99% pure) was melted in air in a butane flame to form a molten ball on the end of the wire. On cooling in air or quenching in distilled water, optically flat facets (required for STM purposes) were often, but not always, formed. If no suitable facets

were identifiable the bead was reheated until 2/3 of the ball was molten and cooled again, the process being repeated until successful. The bead was then mounted, in araldite, with an appropriate facet uppermost.

Chapter Three

Instrumental Details

3.I. Introduction

A considerable amount of time during the project was spent on instrumental development and in this Chapter two different microscope systems are discussed: the first was quickly discarded but gave important clues for subsequent designs. The second system was found to be far more satisfactory and subsequently the stage was replaced by a slightly improved design. Hence although three stages are referred to (Mks 1-3), the latter two belong to the same system and differ only in ease of use with no observable difference in performance.

This Chapter aims to describe the development of the Oxford Electrochemical STM. Emphasis is placed on a description of the configuration and use of the second system (all the illustrations are of the Mk. 3 stage). Evaluation of the performance of the system is described in Chapter 4.

3.II. Mechanical Aspects of STM design[149,173]

3.II.i. General guidelines

An STM stage may be sub-divided into three areas;

(i) Vibration isolation components - to aid maintenance of a stable tip-sample gap.

(ii) A piezo network - to facilitate highly accurate tip positioning during scanning.

(iii) A coarse approach mechanism - to allow the tip-sample distance to vary from several cm to less than a μm (i.e. within the range of the piezo network).

The high vertical and lateral resolution of the STM can only be achieved by controlling the relative positions of the tip and sample at a

sub-Angström level. It is therefore essential to protect the tip-sample loop from vibrations. This is achieved by using a coarse vibration isolation system to damp out low frequency vibrations arising from the physical surroundings of the instrument (buildings typically vibrate at 10 - 100 Hz) and making the stage itself as rigid as possible to maximise its resonant frequency. This requirement leads in practice to stages that are small and have a minimum of components in the tip-sample loop.

At such high resolution thermal drift may also be a problem and this can be reduced by using a symmetrical stage design. The problems of rigidity and drift need to be considered when deciding on the nature of the coarse approach mechanism. In addition to providing a long term stable support for the tip-sample loop, it must be capable of positioning the tip over the sample within the range of the Z-piezo (to an accuracy of about half the maximum extension of the piezo, often about 0.5μm) without overshoot, backlash or slip. All of which may cause tip crash on approach.

The fine positioning piezo network suffers from the having to trade off translation range against resonant frequency; the longer the piezo element (tube, beam etc.) the greater the overall movement possible but the lower the resonant frequency. Piezoelectric components in addition to having inevitable thermal drift also have undesirable hysteresis (in voltage - displacement plots) and creep (piezo displacement with no change in applied voltage) characteristics, both of which are exacerbated by subjecting the piezo to high fields.

It should be remembered that the particular use of the STM (for example UHV or electrochemical work) will place yet more constraints on the design and materials used.

3.II.ii. Practical solutions

Although nowadays commercial instruments are becoming more readily available[174] many research groups worldwide have, and possibly for economic and specific experimental aims, may continue to develop instruments. Hence the scientific literature contains a large number of examples of microscopes designed for a multitude of purposes. Binnig and Rohrer's account of the development of STM's in their own laboratory provides a good background to the area[175], while Kuk and Silverman[149] have reviewed the area prior to mid - 1988.

Some trends and common ground can be identified with the IBM 'pocket size' STM design[176] being highly influential; vibration isolation may be achieved by supporting the stage on a 'stack' of metal plates separated by rubber spacers[176]. This is then supported; in air on an optical bench, by a heavy stone on air tubes[157] by elastic from a solid support, or in UHV with small springs and possibly magnetic damping.

The piezoelectric scan elements, although originally arranged in the form of a tripod with orthogonal X,Y,Z blocks or tubes, are often now represented by a single tube scanner[177] (described in 3.IV.ii.). This design has been found to have a more favourable resonant frequency while still allowing large displacements.

The widest variation in design has come in the different implementations of coarse approach. Many designs have been based around piezoelectric 'walkers'[176] where alternate piezo expansion and electrostatic clamping is used to close the tip-sample gap. An alternative design by Demuth *et al.*[178] using a screw micrometer pushing on a reduction lever giving a more sensitive approach, with the sample holder easily 'flipped' away from the tip for access, has also proved popular.

Automated coarse approaches incorporating motorised micrometers[179] and designs based upon commercial (see refs 180,181 and section 3.IV.) and home built 'inchworm' assemblies[182] have been reported. A novel method of 'inertial translation' using a 'stick-slip' mechanism has been developed by Pohl[183].

3.II.iii. Electrochemical STM

Designing a stage for electrochemical applications adds a few constraints: trivially, gravity restricts the tip-sample configuration. Careful attention should be paid to sample mounting; while still enabling the sample (working electrode) to be firmly positioned in the stage, it must also act as an electrochemical cell, supporting reference and counter electrodes and being constructed of inert material (as pointed out in 2.III.iii. and by Dovek *et al.*[48], unless insulated the tip supporting network should also be kept clear of the electrolyte). For example while Teflon is generally regarded as inert, its easily deformable nature makes it an unsuitable component of the tip-sample loop. Glass is another commonly used cell material but does not readily lend itself to machining for a clamping arrangement. Metal spring clips used to clamp samples in other types of stage are inappropriate due to possible reactivity. One result of the requirement for a cell type arrangement may be to cause the coarse approach range to be relatively large to allow easy sample changing.

Sonnenfeld and Hansma[39] (although not a true electrochemical STM) and Dovek *et al.*[184] designed stages to be used with the sample holders immersed in a beaker of liquid. Commercial stages as used in Schardt's[71] and Trevor's[90] laboratories, have been adapted for *in-situ*

purposes by using the sample as the base of the electrochemical cell and clamping a ring of inert material on it to complete the cell. In the Oxford STM, the sample is mounted in a self contained, detachable cell in a similar manner to Behm[70] and Siegenthaler's[69] instruments.

3.III. Oxford Electrochemical STM: Mk.1

The first attempt at STM design was based upon the reduction lever type approach and is shown in figs. 3.1 (a) and (b).

The stage was divided into two main parts (see fig. 3.1). The lower contained two micrometers which adjusted the pivot point for the coarse approach, a third (differential) micrometer giving the coarse approach and the electrochemical cell. The upper part held the piezo tube for scanning. The upper plate was supported on three brass threaded rods, which rested on ball bearings fixed to the micrometer spindles. These rods allowed the adjustment of the pivot point relative to the upper plate. The 20:1 reduction of the system meant 1 μm travel of the differential micrometer translated into 500Å movement of the tip, a distance within the range of movement of the piezo tube.

The system was supported on a 'stack' on a concrete slab riding on an inflated bicycle inner tube. The stage was made from stainless steel and gravity ensured the stable positioning of top and bottom parts.

The cell was a Teflon unit encased in a stainless steel surround which was bolted into the lower part. It was envisaged that samples would be encased in Araldite on a bolt which screwed into the metal cell surround. A Viton 'O' ring was positioned to prevent leakage of electrolyte onto metal. The piezo tube was held in a Macor plate, with connections made from the LEMO socket to Macor plate via wire coils to minimise transfer of vibration through the piezo power leads to the tube.

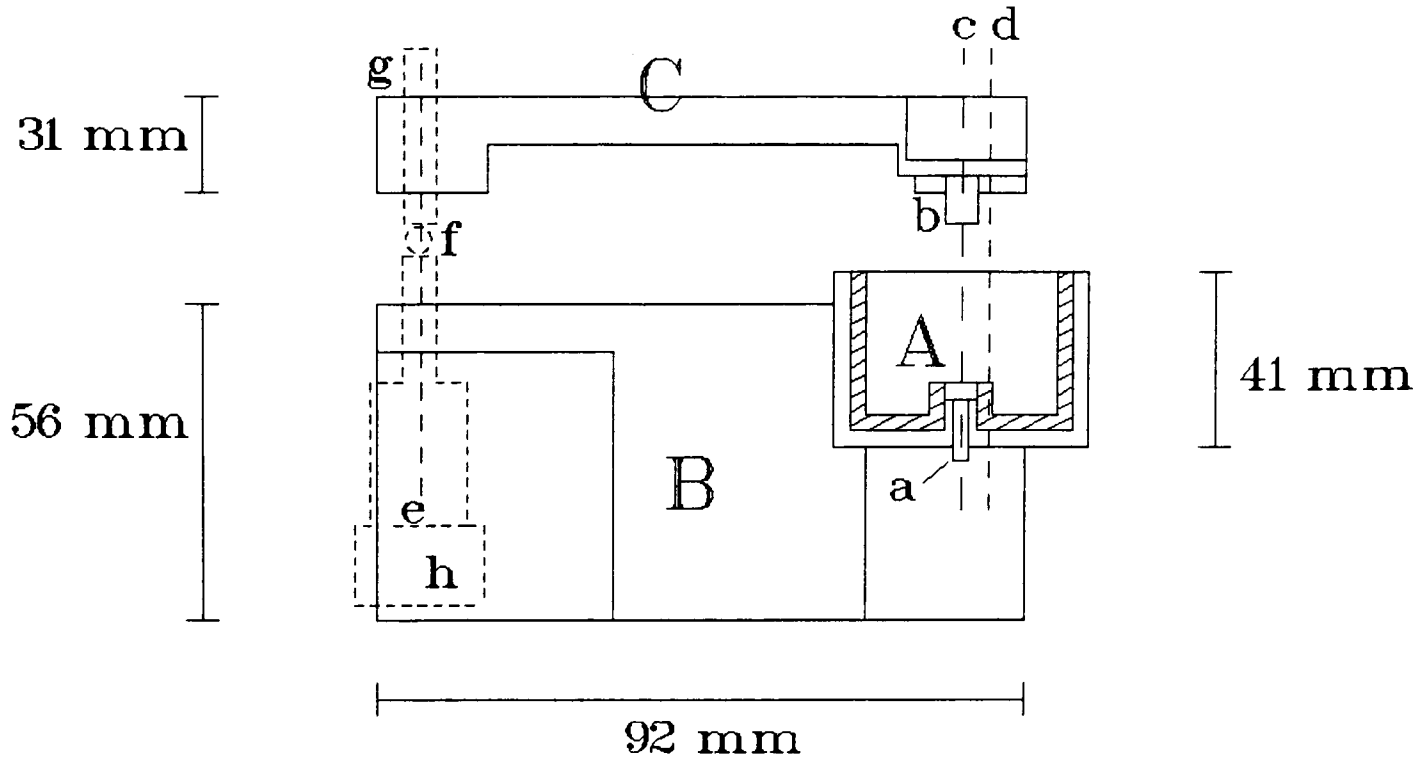

Fig. 3.1 (a). Schematic side elevation of the Mk.1 stage. (Not to scale). Front pivot bolts not shown for clarity.

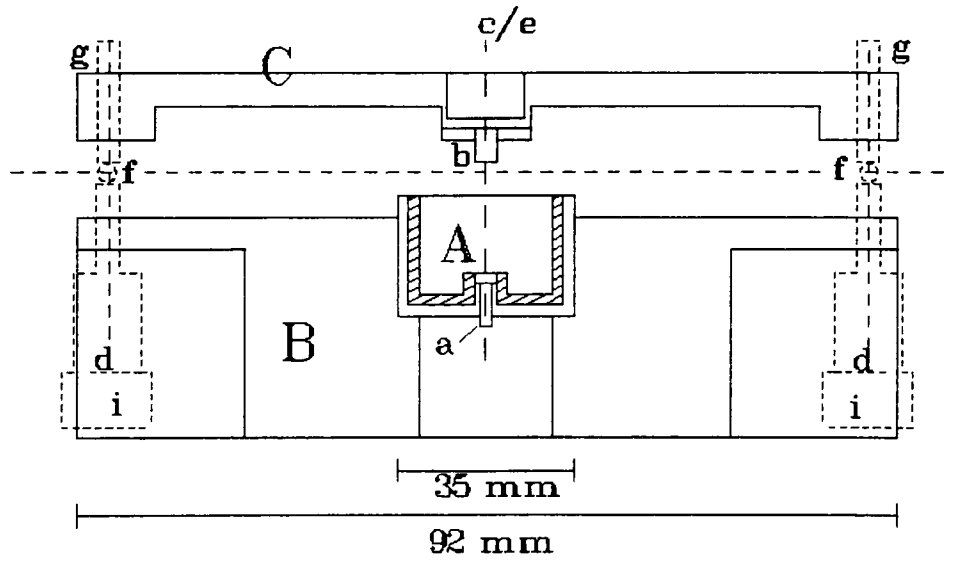

Fig. 3.1 (b). Schematic front elevation of the Mk.1 stage (Not to scale).

Key:

A Electrochemical cell
B Main stage body
C Top plate

a Sample support
b Piezo tube
c Tip/sample axis
d Front pivot axis
e Rear movement axis
f Ball bearing mount
g Position of brass coarse adjustment bolt
h position differential micrometer
i position standard micrometer

The electronic components of the instrument were provided by a feedback loop (built by the O.U. Materials department) and IBM supported software from a previous project[185]. The head amplifier was 'home-built' (design as in fig. 3.12, without the input protection resistor and trim potentiometer) and battery powered.

Initial use of the stage revealed a significant problem; the weight of the top plate made coarse approach by manual turning of the differential micrometer an extremely long, tedious and tiring process. The configuration of the stage meant that the approach could not be observed. Tip crashing was hard to avoid and tunneling currents were noisy.

It was decided to redesign the stage, around an automatic approach provided by a Burleigh Inchworm® motor. The commercial feedback loop, computing and software were subsequently acquired.

A visit to Prof. R.J.Behm's laboratory in Munich to see the operation of his groups electrochemical STM, provided much information which was used in the design of the second system. On the basis of the high quality results being obtained[95] it was decided to follow the Munich method of coarse vibration isolation, cell design and tip manufacture. The visit cleared up misconceptions; large cell volumes were seen not to be important,using a luggin capillery close to the sample was not required and in the vibration isolation stack Viton 'O' rings separating the plates are positioned *vertically* not horizontally as tried in the Mk. I. design. It was also noted that differential micrometers may be prone to excessive amounts of slip.

3.IV. Oxford Electrochemical STM: Mks. 2 and 3

3.IV.i. Introduction

Photographs of the current (third) stage are shown in figs. 3.3 (a) and (b), with a schematic diagram in fig. 3.2; more detailed technical drawings are supplied in Appendix C. The main feature of the unit is the automated coarse approach provided by a Burleigh Controlled Approach Inchworm® motor[186], a piezoelectric micropositioning device. It represents an advance over the second stage in that the head amplifier is

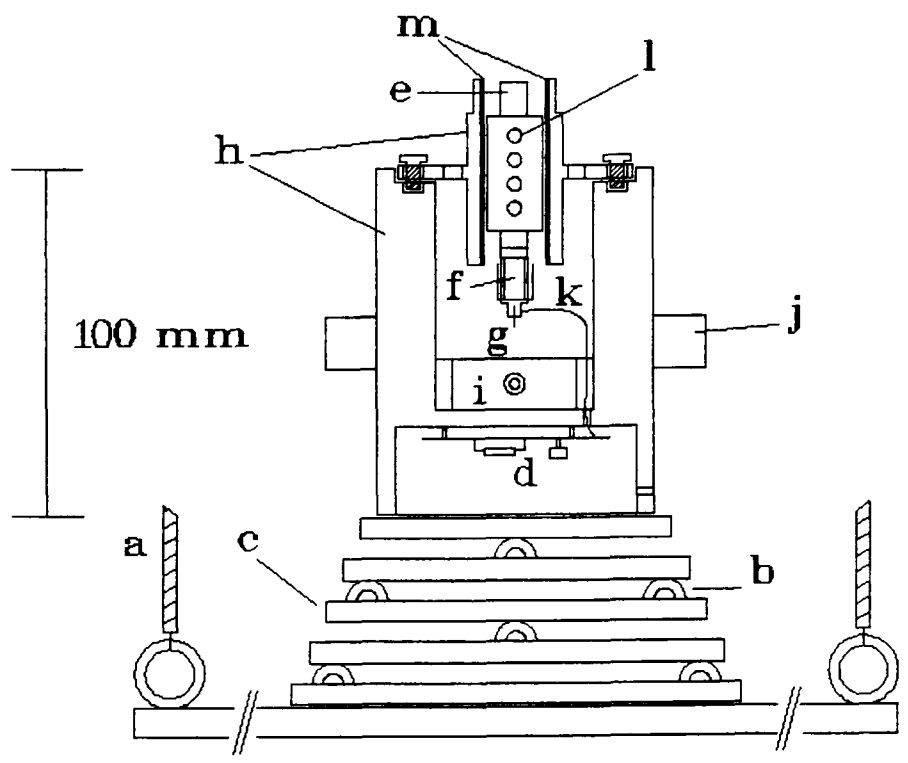

Fig. 3.2. Schematic section of the stage

Key:

a	*Elasticated cords for vibration isolation*
b	*Viton 'O' rings*
c	*Vibration isolation stack*
d	*Head amplifier*
e	*Inchworm motor*
f	*Piezo tube scanner and tip holder*
g	*Tip*
h	*Stainless steel body*
i	*Sample stage*
j	*Electrical connection box*
k	*Tip - head amplifier wire*
l	*Motor contact coils*
m	*Teflon spacers*

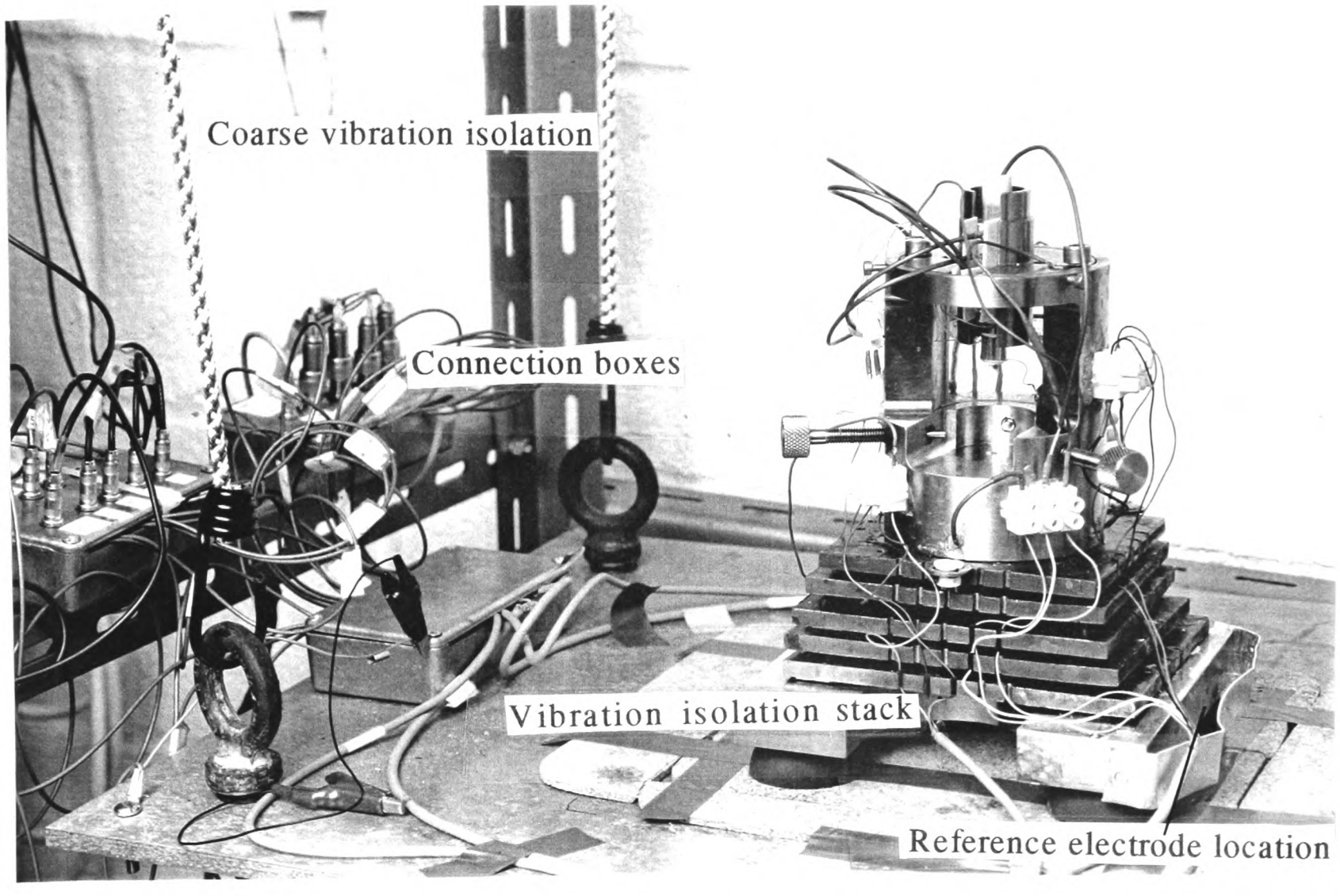

Fig. 3.3 (a). Photograph of the Oxford Electrochemical STM Mk.3.

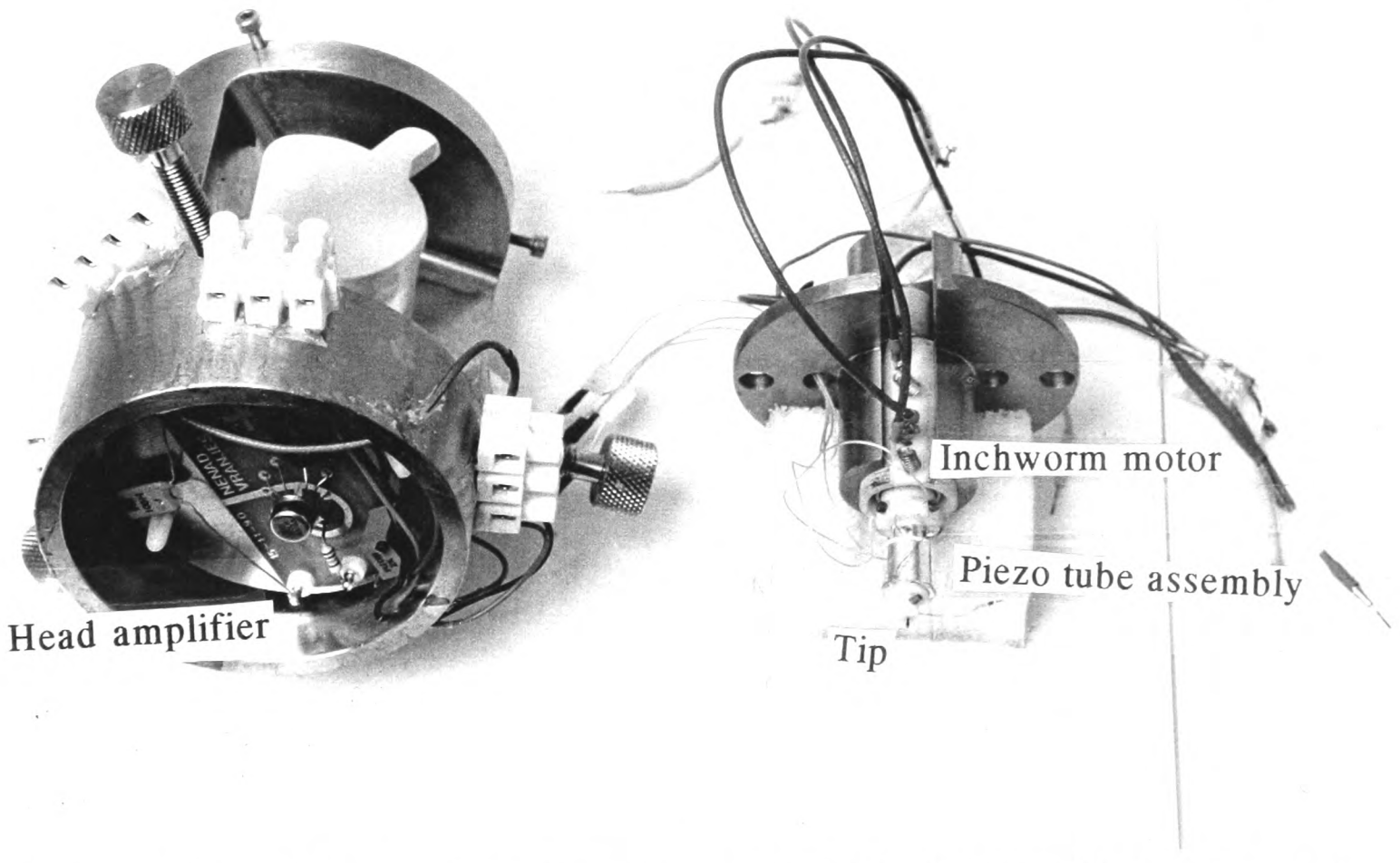

Fig. 3.3 (b). Photograph of the stage partially disassembled, showing the Inchworm holder and head amplifier.

directly incorporated into the stainless steel body of the STM instead of being in an external and separate box. Minor changes included increasing the visibility of the sample, simplifying the inchworm holder, tidying the electrical connections and improving the sample positioning.

In the system a piezo tube is used to scan the tip over a stationary sample. The piezo tube is attached to the spindle of the Inchworm motor which is perpendicular to the sample.

The system was never subject to rigorous mechanical characterisation partly due to a lack of experience in the area, but also because most of the components were tried and tested in other systems (although it was known that other groups were using inchworm motors, the Oxford designs were made independently); the vibration isolation was present in Behm's instrument in Munich; the tube scanner, Inchworm and Omicron electronics are all commercial. The STM was always operated with the feedback loop signal monitored on oscilloscope such that excessive noise/oscillations could be quickly detected.

3.IV.ii. Stage description

The stage is supported by a stack of five mild steel plates (6mm thick, approximately 100mm square increasing in size top to bottom) which are each separated by three Viton 'O' rings, to damp vibrations with frequencies of over 100 Hz[176]. Extra isolation was provided by sitting the stack on a stainless steel block and putting half a squash ball under each corner (fig. 3.3 (a).).

This arrangement sits on cork table matting on an aluminium plate which is suspended by elasticated cords from a Dexion® frame. So-called 'Bungee' cords, as used on luggage racks, were purchased from Halfords. Originally 48cm long, on use they stretched to 97cm, approximately 95%

full extension. Crude acoustic and electrical isolation is provided by a Perspex case covered internally by cork table matting, and externally by polystyrene blocks and an aluminium mesh. The cork matting was found to substantially reduce acoustic transfer through the case.

To reduce the possibility of vibration transmission to the stage via the wiring, a rather elaborate set of connections are made between the main electronics (feedback loop, potentiostat and Burleigh motor controller) and the stage. Wiring to the individual components of the stage is made from a set of connection boxes fixed to the stage body. From there each individual wire is pinned onto one of the plates in the vibration isolation stack, before entering (via shielded cable) another set of connection blocks, in an insulated box, on the side of the supporting plate. These are linked to a series of more substantial electrical connectors (LEMO or for the Inchworm, high voltage BNC) on the Dexion frame (to which the main electronic units are attached) by slack wires which ensure the effectiveness of the elasticated cords is not reduced.

As shown in fig. 2.3 (b) the feedback loop electronics and potentiostat were put on a separate Dexion frame, while the Burleigh motor controller was located below the stage. As this latter unit was switched off during scanning (see Section 3.IV.v.) vibration from cooling fans was not a problem.

The stage body is a symmetrical, effectively two piece, stainless steel unit; the lower housing the head amplifier and providing the sample support, the upper containing the inchworm motor. The latter component clamps the motor in position by the action of three screws around its circumference, which on tightening close the metal sleeve around the

motor body. This method allows adjustment of inchworm position for different sample heights. Bolts connect the upper and lower parts. Teflon spacers positioned between the motor contact coils and stage body prevent arcing due to the high voltages applied (or an accidental short circuit).

The tip current is of the order of nA and obviously such a small current can easily be overcome by electronic noise. To minimise noise pickup the signal is amplified as soon as possible by a large gain amplifier (head amplifier, see Section 3.IV.v.) and the tip-amplifier distance must be as short and shielded as possible. A compromise is needed however between the wire attached to the tip being light, to minimise the force on the tip holder (during both approach and scanning), and being well shielded.

Here approximately 40mm of 0.25mm diameter plastic coated wire connects the tip to a shielded wire, which passes through a hole in the sample mounting area to the head amplifier. The base and top vibration isolation plate electrically shield the amplifier. Silicon rubber compound was placed around the wire hole to prevent any liquid spill from reaching the head amplifier.

The piezo tube scanners (length 12.7mm, outside diameter 6.35mm, inside diameter 5.33mm) were based on the Binnig and Smith design[177] with four electrodes on the outside surface and one on the inside (fig. 3.4). They were made of a lead zirconate titanate ceramic, PC5, supplied by the Unilator division of Morgan Matroc[187]. Originally the tubes were configured with the inside electrode grounded and the outside electrodes being supplied with a combination of feedback and raster pattern voltages. After preliminary tunneling experiments the configuration was altered so feedback voltages were applied to the inside electrode, and only X,Y,

scanning voltages to the outer electrodes to reduce the possibilities of 'crosstalk'[188]. Fortunately only minor modification to the commercial electronics was required (section 3.IV.v.).

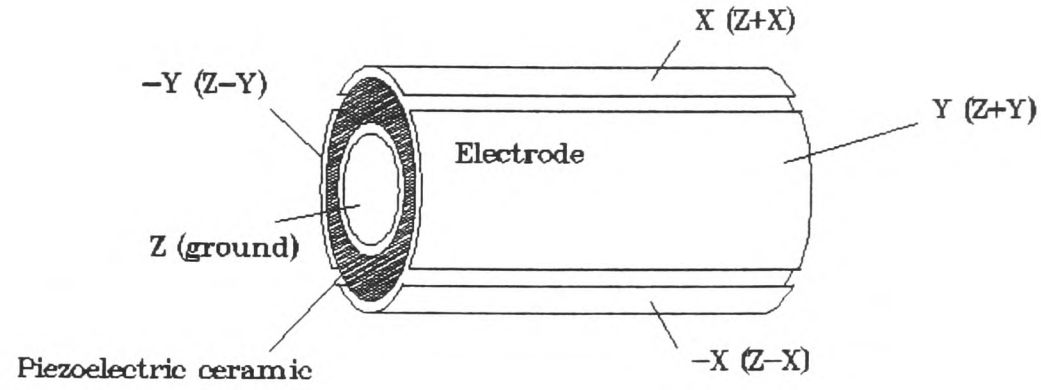

Electrode connections; current (original)

Length 12.7mm
Inner diameter 0.533mm
Outer diameter 0.635mm

Fig. 3.4. Piezo tube connections

The tip holder and piezo mounting (all made from non-conductive macor) are shown in figures 3.5 (a) and (b). During stage development, modification of the tip holder was a frequent occurrence. As this has always been glued (unless specified the glue used in the assembly was rapid setting cyanoacrylate or 'superglue') directly to the piezo tube any alteration required removal by sonication in acetone. In initial configurations piezos were glued indirectly to the inchworm shaft. Two problems with this system were that acetone has to be kept away from the inchworm motor, and simple modifications were rather time consuming.

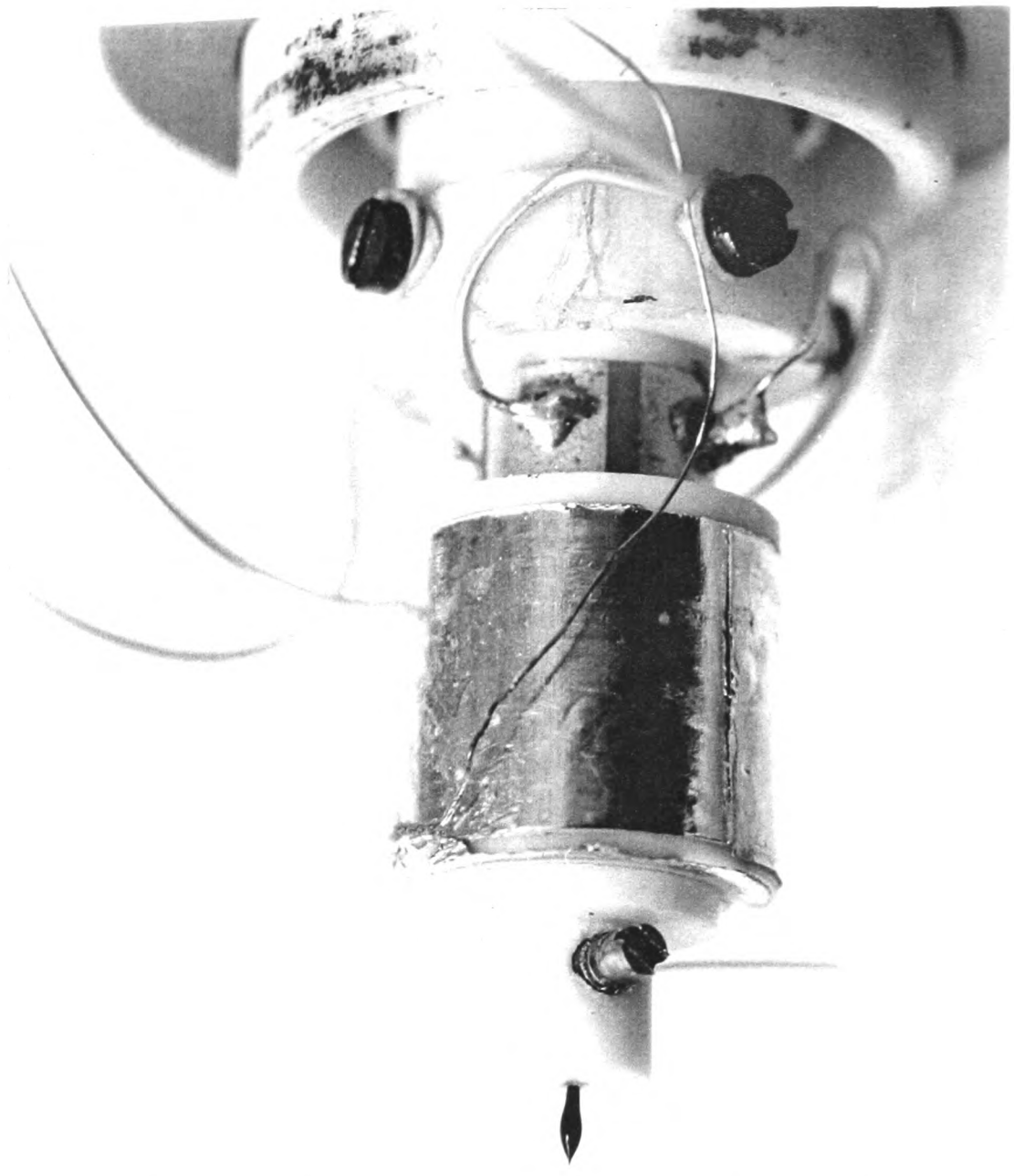

Fig. 3.5 (a). Photograph of the piezo tube, shield and tip holder

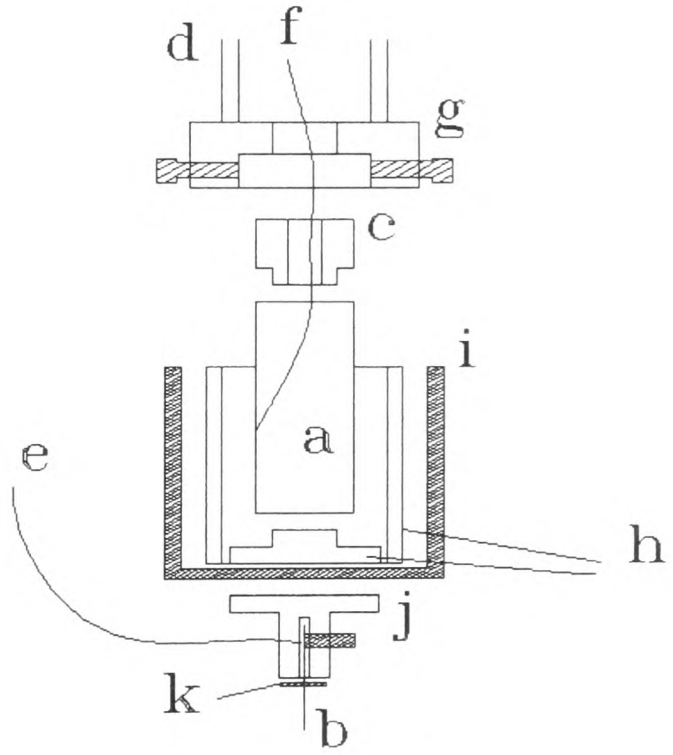

Fig. 3.5 (b). Exploded schematic of the piezo tube, shield and tip holder

Key:

a	*Piezo tube*	*i*	*Aluminium shield*
b	*Tip*	*j*	*Tip holder*
c	*Macor tube mount*	*k*	*Araldite plug*
d	*Inchworm shaft*		
e	*Tip-head amplifier connection*		
f	*Z-piezo connection*		
g	*Tube holder*		
h	*Macor plate and shield*		

The first attempt at a system to allow easy interchange of piezo tubes, and thus tip holders, involved a nut and bolt system between shaft and piezo. The arrangement was about 10mm long and was discarded as it appeared to contribute to system instability. In the current configuration piezo tubes are attached to macor mounts, which are fixed by screws, in a holder glued to the bottom of the inchworm shaft. An attempt was made to use the locating screws as electrical contacts, but the piezo tubes proved too brittle to withstand the pressure applied.

Contact to the piezo electrodes is achieved by soldering, a quicker, more durable and more easily reversible process than the originally used RS conductive paint. Care must be taken with the inner electrode not to strip the silvering off the ceramic because it is rather delicate.

Some trials were made with 'potted' piezo tubes i.e. the tube was filled with rubber compound[189], but imaging did not appear to be enhanced and the procedure was not adopted.

For stability and convenience the wire to the inner electrode is glued to the piezo mount, and soldered to a separate wire which runs through the inchworm shaft, while wires to the outer electrodes are fixed to the piezo holder.

Surrounding the piezo tube is a grounded aluminium shield, supported by Macor and connected to the stage body by wire attached by conducting paint. This intended to reduce pick-up of electrical noise by the tip-head amplifier wire. The Macor tip holder holds the tip by a small metal screw, and physical contact is made between tip, screw and tip-sample wire. The wire is fixed into the tip holder by epoxy glue. One drawback of this system is the brittle nature of the Macor which causes the screw thread to shear with use and require the tip holder to be replaced.

In an attempt to avoid liquid rising into the tip holder through accidental overfilling of the cell, (fig. 2.11.) at various points the bottom of the tip holder was coated with Teflon tape (hydrophobic, but tended to peal off with tip removal) and araldite (to reduce the tip holder opening). The latter solution seemed to work quite well but prolonged exposure to acidic solution did cause the glue to soften and fall off.

This piezo mount/tip holder configuration developed with the stage and in itself influenced tip insulation. Original experiments[190] under liquid involved insulating the tip with nail varnish while it was in position, an inconvenient method as experiments could not be started until the varnish hardened.

The sample mount has to support the sample rigidly while a bias voltage is applied between it and the tip. Among the first sample mounts used, for HOPG, gold SCS and thin film were brass stubs covered with glass, to which the sample was fixed with epoxy adhesive. Electrical connection was via conducting silver paint to an appropriate wire. This method is both time consuming and exposes the sample to potential contamination from gases evolved on curing (although none was ever detected). These were replaced for HOPG and gold on mica by the macor cells shown in fig. 2.10. Gold SCS samples were supported as shown in fig. 3.6, the Teflon sheath because of its hydrophobic nature functioned poorly as an electrochemical cell and was not used.

For electrochemical experiments the reference electrode and socket were supported at the side of the bottom block of the vibration isolation stack.

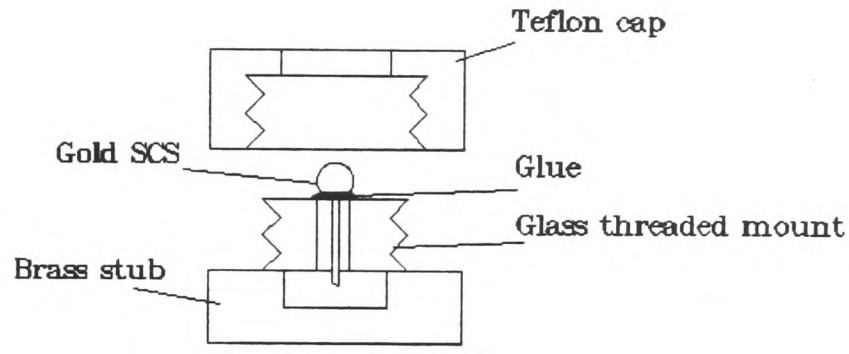

Fig. 3.6. Schematic section of a SCS mount

3.IV.iii. Piezo Calibration

A combination of three methods were used to calibrate the piezo tubes; calculation, observation of known features by using the STM and experimental determination.

The vertical motion of a tube scanner is relatively straightforward to measure, but the lateral movement, describing an arc (illustrated in fig. 3.7), gives a calibration related to tip length. A Michelson interferometer approach, reasonable for calibrating in the vertical direction, is thus not applicable for the horizontal deflection[157].

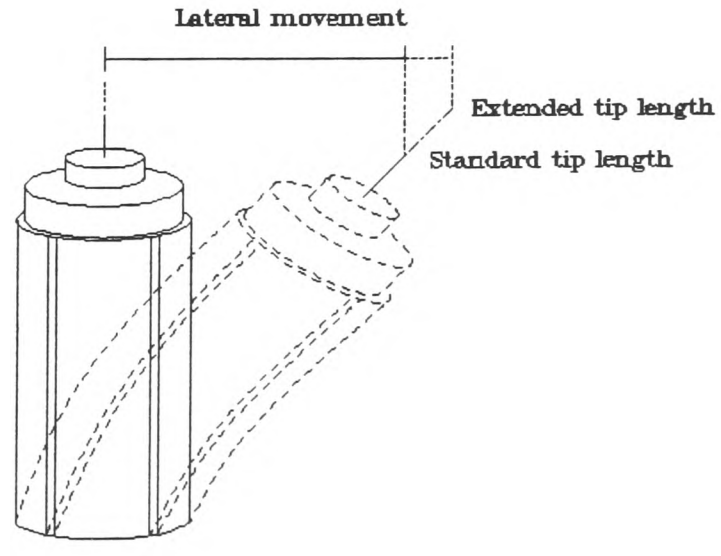

Fig. 3.7. Lateral movement of a piezo tube

For reasons of convenience, in addition to this complication, experimental monitoring of piezo movement was carried out by a Nanoindenter[191] operated by Dr. T.P.Weihs. The Nanoindenter is a micro-hardness tester which is able to monitor the displacement caused in a material on application of a known force (see fig. 3.8). It has a quoted resolution of ±2Å.

A diamond tip is used to indent materials, the movement of the shaft holding the tip is controlled by the relative motion of the electromagnetic coil and the magnet. The greater the repulsive force between the magnets, the greater the load applied to the surface and thus the deeper the indent. The displacement of the shaft is monitored by the capacitive sensor.

A piezo tube, with tip holder, was set up under the Nanoindenter tip. The tip was lowered onto the macor and the instrument set at constant load: movement of the piezo was therefore recorded by the Nanoindenter. The piezo tube was mounted on a brass cube and measurements were taken with the tube oriented so that vertical and lateral piezo movements could be monitored in turn.

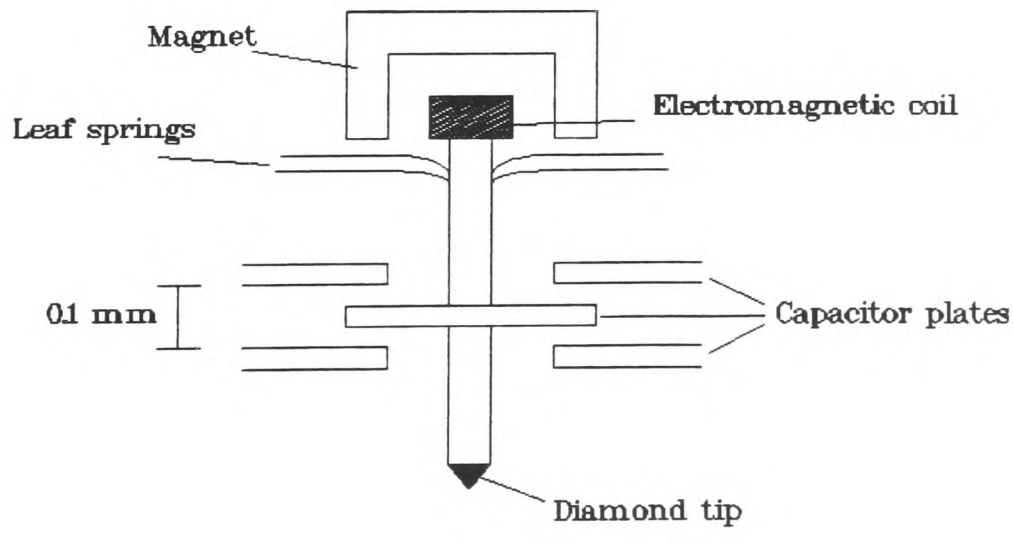

Fig. 3.8. Schematic representation of the main components of the Nanoindenter.

To calculate the Z calibration constant the following equation was used[187];

$$s = (l/t)d_{31}$$

where s is the movement of the tube along its axis, l the length of the tube, t the tube thickness and d_{31} the manufacturer supplied expansion (contraction) coefficient along the axis. For the tubes used here this yielded a calibration constant of about $42\text{Å}V^{-1}$. Experimental observation of monatomic steps on gold (approximately 2.4Å) supported this value as did Nanoindenter measurements.

Determination of a lateral calibration constant was more difficult; simple trigonometry on the configuration shown in fig. 3.7 implies on changing from a tip 8 mm from the end of the piezo tube to one 10 mm away (as the tip holder is approximately 6 mm long this corresponds to the difference between a bare and an insulated tip), there will be a difference in distance covered, for the same angle of bend of the piezo, of about 10%. This is a simplified 'ball-park' calculation. The movement of the tip relative to the surface, because of feedback control in the vertical direction, in addition to the actual lateral piezo action may not be that straightforward.

The ideal method of calibration would be to run a 'standard', like HOPG before (or immediately after) each experiment. As will be discussed in Chapter Four imaging HOPG was found to be difficult and this approach was not viable.

Nanoindenter measurements indicated a value of about $155\text{Å}V^{-1}$, but this measurement inevitably involved some degree of lateral tip-surface motion. The combination of movement over the circular tip mount and its surface roughness making the value calculated merely a rough guide.

An early result on HOPG had indicated a calibration of 115ÅV^{-1}, and this was adopted. This means horizontal distances quoted are unlikely to be 'true' values, though there should be a certain amount of self-consistency where images have been taken in the same medium. A reasonable estimate of the error in lateral values is ±25%, based on the rough piezo movement calculation and other imaging of the HOPG lattice. For many of the images presented, the precise size of the features is not crucial to the conclusions drawn, but a feeling for the uncertainty in horizontal resolution is required.

3.IV.iv. Coarse approach mechanism

Inchworm® motors move a shaft, along its own axis by the method shown in fig. 3.9, the piezoelectric components giving the possibility for high resolution movement with minimal backlash or overshoot. The nature and number of moving parts should also minimise vibrations within the tip-sample loop.

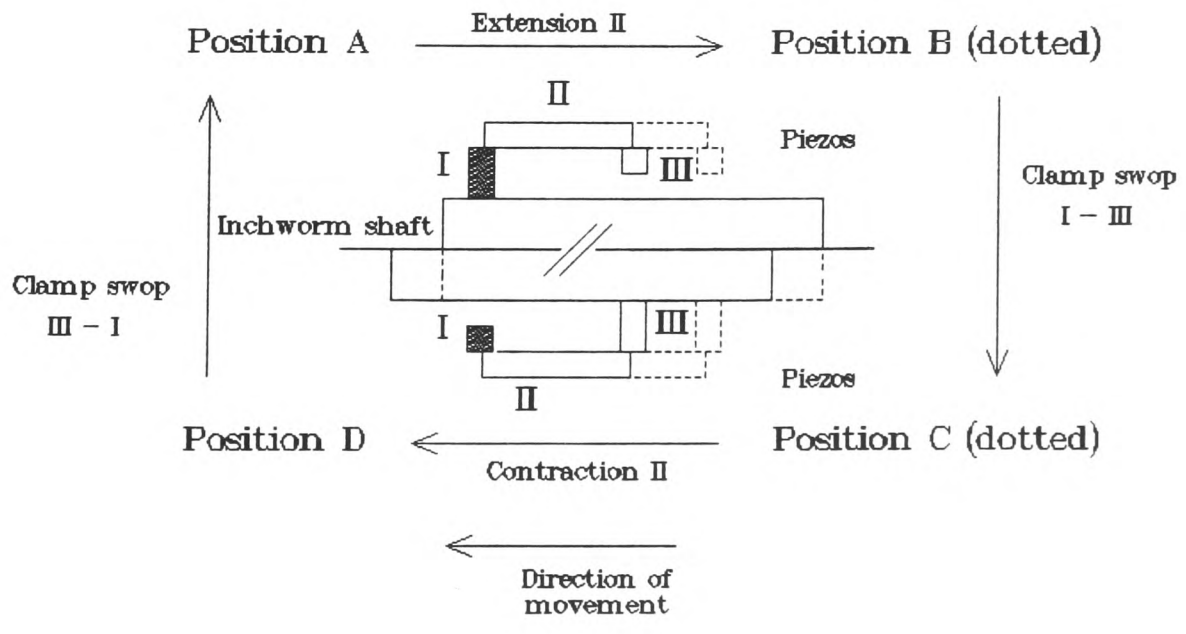

Fig. 3.9. Inchworm movement

The motor used was the UHVC-100 (hollow shaft option), chosen because of the 'controlled approach' capability. Inchworm motors have motion discontinuities at the point both clamps hold the shaft simultaneously. In a standard inchworm this discontinuity will be alternately towards or away from the direction of movement, as the clamps fix in order. In 'controlled approach' inchworms this motion discontinuity is set up such that the motion profile 'glitch' is always away from the direction of 'controlled approach'. Thus in STM work tip-surface contact due to faulty approach should be avoided. A second characteristic is that the motion is resolvable to 1 nm[192].

The coarse approach operation is based on that used in the Omicron UHV system. In this a ramped voltage causes the z piezo element to extend towards the surface and if an appropriate tunneling current is sensed the approach stops, the feedback loop is brought into operation and the STM experiment begins. If not the piezo is contracted and a 'louse' moves the sample towards the tip, by a distance *less* than the extension of the piezo, the piezo is then ramped forwards and the process repeated until tunneling is obtained. During the coarse approach step the feedback loop is disconnected, a particularly important point because the rapidly varying high voltage signals (0 - 700V) applied to the piezo components of the inchworm cause significant noise on the tunneling current. Despite attempts to shield the tip against this, the noise is sufficient to be detected by the head amplifier and hence feedback loop as a tunneling current. Consequently initial attempts at inchworm approach using the Materials department feedback loop and an interface, based on a comparator which halted inchworm movement on detection of a tunneling current, failed.

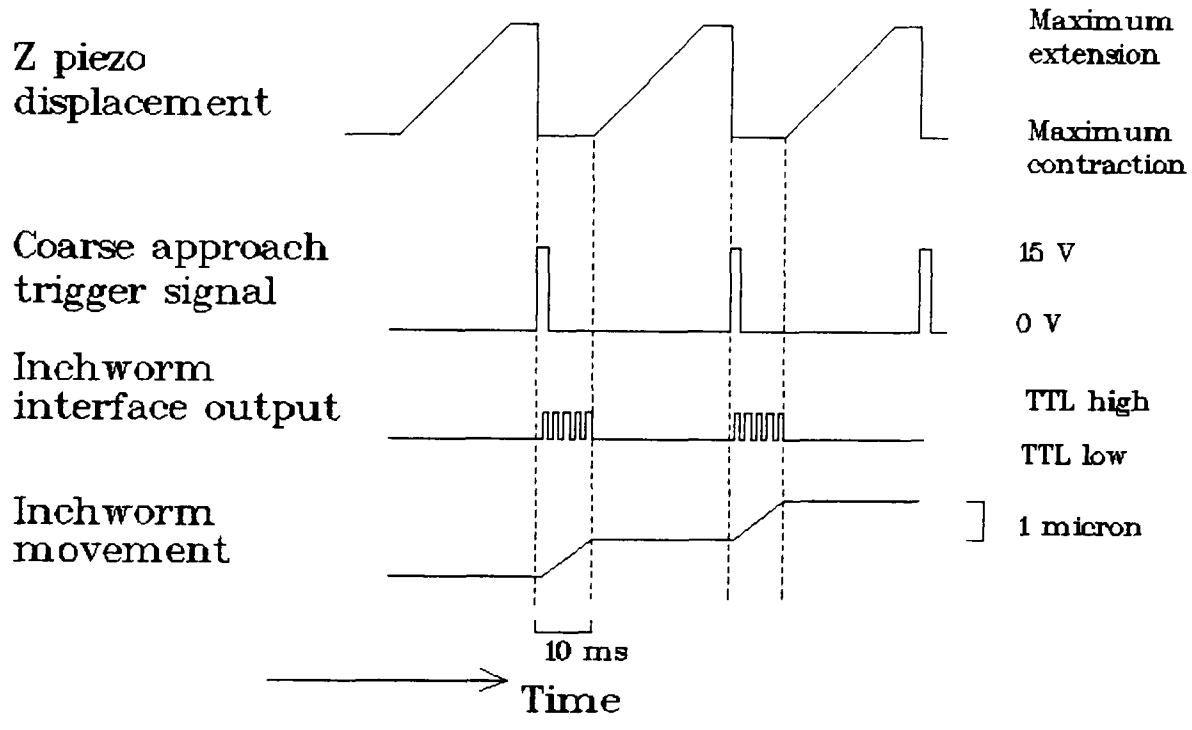

Fig. 3.10. Representation of the relative timing of electronic signals and mechanical movements during a coarse approach.

In the electrochemical STM the trigger signal used within the Omicron electronics to initiate the sample movement, is taken off from the Omicron feedback loop and used to drive a 'home-built' interface (designed by Dr. P.R. Trevellick) for controlling the motion of the inchworm motor. The interface also serves as basic control unit for the inchworm motor and replaces an original unit based around two HP function generators. A schematic diagram showing the relative motions of Z piezo and inchworm is given in fig. 3.10.

The Inchworm interface controls the motor controller by supplying TTL signals to a port on the motor drive card. A schematic circuit diagram is shown in fig. 3.11.

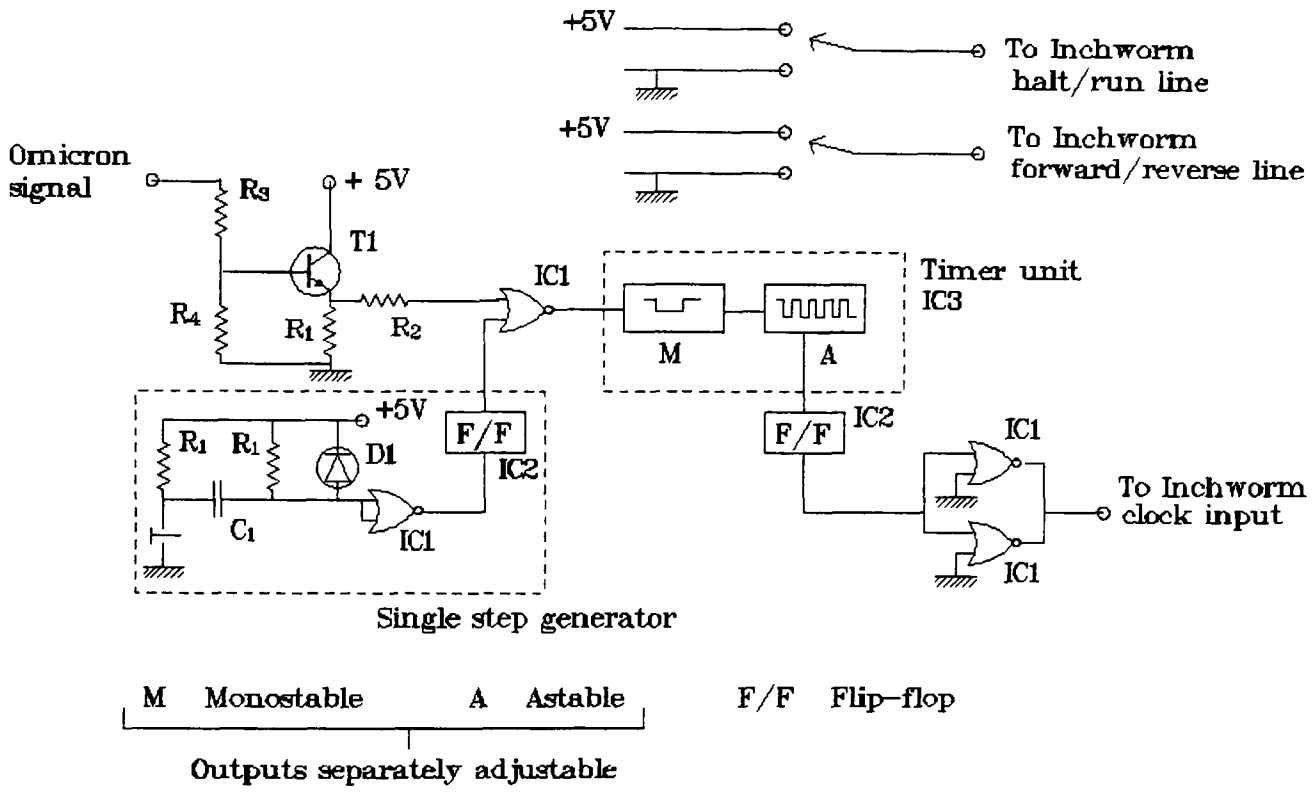

Fig. 3.11 (a). Schematic circuit diagram of the Inchworm interface

Key:				
R_1	*10KΩ*	T_1	*ZTX300*	
R_2	*4.7KΩ*	D_1	*IN41848*	
R_3	*22KΩ*	IC_1	*74HCT02*	
R_4	*12KΩ*	IC_2	*74HCT74*	
C_1	*1nF*	IC_3	*556*	

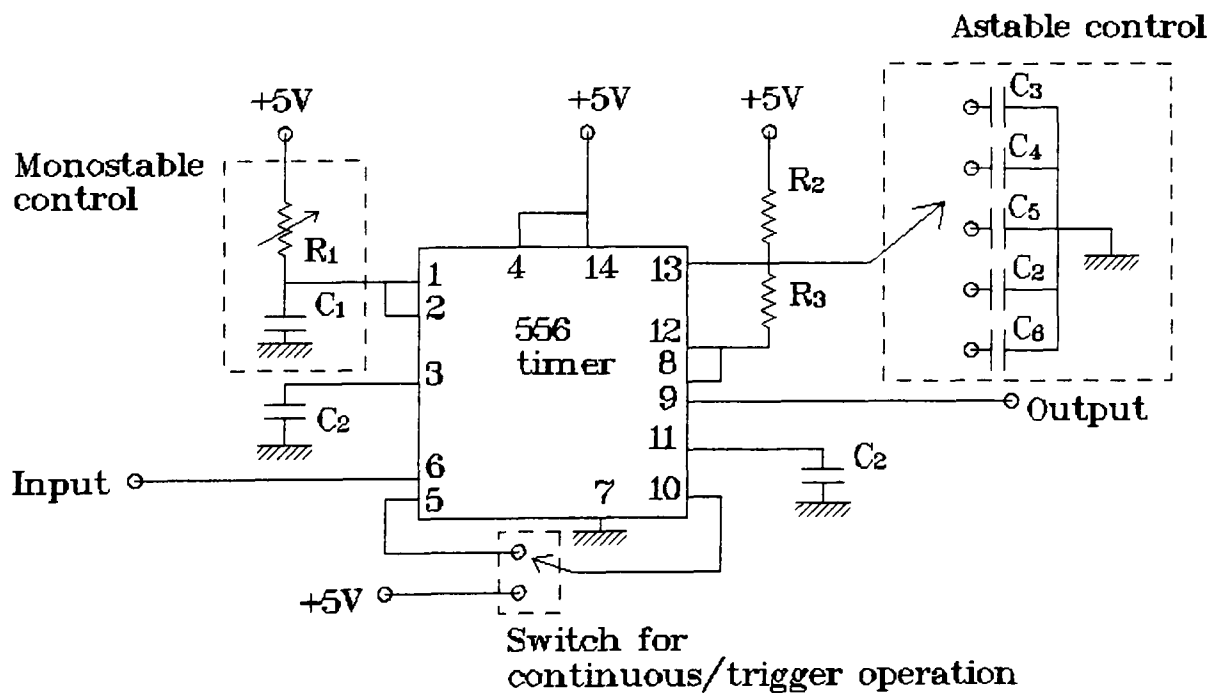

Fig. 3.11 (b). Timer circuit of Inchworm interface.

Key:					
C_1	*0.1μF*	C_6	*300pF*		*Monostable range*
C_2	*10nF*	R_1	*10-200KΩ*		*1-22ms*
C_3	*2nF*	R_2	*5KΩ*		*Astable range*
C_4	*4nF*	R_3	*3KΩ*		*13-400KHz*
C_5	*6nF*				

The Omicron trigger signal is transformed into a TTL signal by the transistor and this is connected to a 556 i.c. timer. This is configured as a tone burst generator (see fig. 3.11 (b).), the first timing circuit (configured for monostable operation) provides a variable length pulse to be applied to the second (astable operation) which then gives a variable frequency output. Here the monostable pulse had to be shorter than the time allowed for coarse approach by the Omicron circuitry, 10 ms, to ensure inchworm movement did not overlap with piezo ramping. This output is then passed through a 'flip-flop' which makes the waveform duty cycle acceptable to be 'read' by the Burleigh drive card (at the expense of halving the timer output frequency). At the drive card one high-low (or vice versa) TTL transition will give an incremental movement in Inchworm, here 1 nm, the speed of motion therefore depending on the frequency of the output waveform. For automatic approach, frequencies of about 50 KHz were used i.e. 50 μms^{-1}. Logic NOR gates were used to provide the correct signal for the first timer circuit and stable outputs for the inchworm controller.

Additionally the interface allows continuous and step movement, the latter actually being one pulse from the first timing circuit and thus the distance moved in a single step will depend on the frequency setting. Logic signals for activating the controller and specifying direction are also included. The continuous function allows rapid movement of the inchworm over large distances to allow sample changing. A 'flip-flop' was used in the single step circuitry to act as pulse shaper to prevent accidental multi-step operation.

When first using the Mk.2. stage there were problems with high resolution imaging (and periodic noise on images), and it was

subsequently concluded electrical noise from the motor controller was being picked up prior to the head amplifier. It was subsequently decided to operate the system with the motor controller switched off during tunneling[188,192]. The controlled approach inchworm electronics cause a clamp switchover to take place when a 'halt' signal is received by the motor controller with the lower clamp being activated (the rationale being that for vibration sensitive applications shortening the unfixed shaft length is advantageous) and this produces the previously mentioned 'glitch' away from the direction of controlled approach.

Unfortunately this 'glitch' throws the system out of tunneling. The first attempted solution was to step the inchworm further towards the surface once tunneling had been sensed, hence the step function on the 'homebuilt' interface. Note that the step function causes movement by switching the output waveform between a set value and 0 Hz while leaving the inchworm activated; switching the 'halt/run' signal with such small movements actually results in net movement away from the surface. The Omicron electronics supplies ±140V to the Z piezo divided on a front panel display into ±2000 units which represent about ±130V, even on going to maximum piezo contraction the 'glitch' still caused the system to lose tunneling, a distance of about 1 μm.

A maximum a.c. voltage of 250V is allowed by the piezo tube before it loses reversible piezoelectric behaviour, and thus the tube had spare translational motion not used by the Omicron electronics. To utilise this a 90V dry cell battery was put in line between the Omicron output and the Z piezo. On reaching tunneling a 90V offset (because of the direction of piezo poling the positive terminal was connected to the piezo) was put into the system allowing the piezo to contract by another 0.4 μm. After

stepping to a display value between -1200 and -1800 using the step function at a frequency of 12 KHz, the inchworm power was switched off, firstly by issuing a 'halt' signal and secondly by physically shutting down the motor controller. The 'glitch' takes the system out of tunneling which is usually regained on turning the battery offset off. In the worst case, reversing the polarity of the battery connections enables a 0.4 μm extension to be applied to the piezo, though this facility was rarely used to give stable tunneling, normally a reiteration of the step and power off procedure would be carried out. Although both clamps are deactivated when power is switched off, no shaft slippage is detected.

A subsequent fault in the original drive card led to a non-controlled approach drive card being fitted. This had a maximum resolution of 4 nm and did not give clamp changing on receiving a 'halt' command, but a 'glitch' was still observed on shutdown. The motion discontinuities still are away from the direction of controlled approach as that is a function of motor construction. The coarse approach 'glitch' was found to be on average slightly smaller with the latter card, and stage performance was not observed to be adversely affected. A frequency of 25 KHz was used for coarse approach.

3.IV.v. Electronics

This Section provides a description of the head amplifier and other miscellaneous electronic aspects of the system.

The head amplifier is a simple current follower (fig. 3.12) with a 10^8 gain i.e. a tunneling current of 1 nA yields an output of 100 mV, supported on a custom built circuit board. The grounded non-inverting input maintains the tip at virtual earth. Due to the low currents being measured the operational amplifier should have a low input bias current[156,157] and

an AD515 was chosen. It was configured as recommended[193], with a guard ring and input protection as shown. Some workers[157] compensate for the input capacitance of the tip and tip-sample wire by adding a capacitor to the feedback loop, but no advantage was found on adding one to this system. As added capacitance has the effect of lowering the bandwidth of the op-amp and, for optimum performance, requires adjustment if the input leads are changed, it was felt a capacitor would become an unnecessary inconvenience and this approach was not followed.

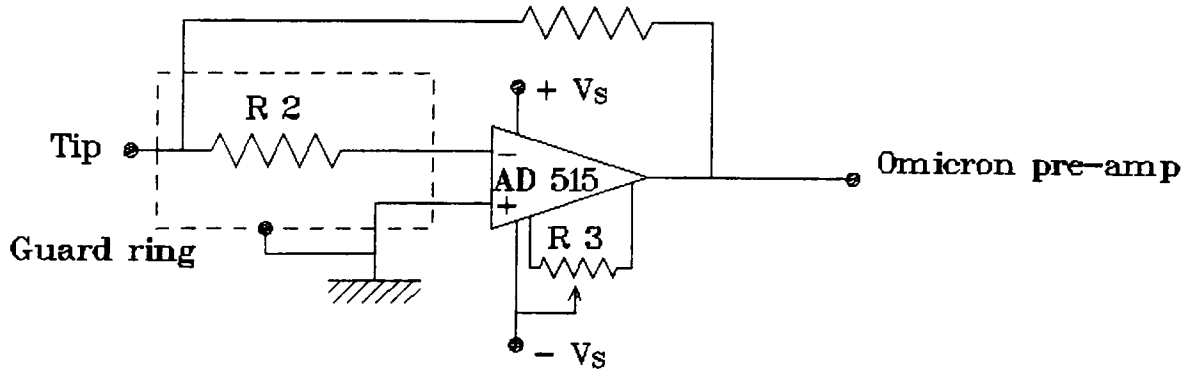

Fig. 3.12. Schematic circuit diagram of the head amplifier.

Key: *R1* *100 MΩ*
R2 *100 KΩ*
R3 *10 KΩ trim potentiometer*

To change the Omicron feedback electronics from supplying (Z ± X) and (Z ± Y) signals to a piezo tube with grounded inner electrode, to supplying Z, ± X and ± Y signals, a jumper connection was altered to give the correct polarity for the Z electrode, and the Z power supply was disconnected from the four scanning voltages.

To prevent ground loops the potentiostat and head amplifier were powered from the Omicron electronics and the Inchworm interface was powered from the motor controller. All box casings were grounded via the Omicron casing. On the stage, the piezo shield, stage body (and thus vibration isolation top plate) and aluminium supporting plate are all connected to ground.

3.V. Operational points: using the STM

This Section is intended to address some of the practical aspects of operating the STM.

3.V.i. Tunneling conditions

All experiments were carried out in constant current mode. Constant height mode was inappropriate for most surfaces studied and was never applied successfully. Spectroscopy was used sparingly and details are given where appropriate.

Although more exactly detailed in the results chapters; in air bias voltages were normally in the range 50 mV - 300 mV (sample positive) with tunneling currents in the range 1 nA - 5 nA; in electrolyte bias voltages were variable (see Section 2.III.iii.) with tunneling currents commonly 3 nA - 10 nA.

The response of the feedback loop is controlled by altering the time constant of an integrator. If the response is too slow features on the surface will not be detected and there is the possibility of a tip crash; if the response is too fast the feedback loop will respond to the inherent vibrations of the tip - sample loop and will send the system into oscillation. For constant current operation, the response was set to be as fast as possible (i.e. low time constant) to maximise sensitivity (also

allowing fast scan speeds to minimise the effects of drift) without causing oscillation on the tunneling current. For constant height operation the reciprocal time constant was set to the minimum and the software recorded signal was changed from Z piezo voltage to current.

3.V.ii. Tunneling

A complete approach to tunneling after tip and sample changing involved continuous motion of the inchworm towards the surface until, by optical microscopy observation, the tip and its reflection (all samples used were highly reflective) almost touched. At this point the Inchworm interface was switched to receive signals from the Omicron electronics and the approach was automatically controlled. The Faraday cage/acoustic box was normally put over the instrument at this point. Observation under liquids was more difficult and generally larger tip-surface distances were left after initial approach. Depending on operator judgement, an automatic approach in air typically took about five minutes and one under electrolyte one to two minutes longer. Unexpectedly long approach times often indicated failure of the feedback loop to operate.

The general stability of the tip-sample gap could often be gauged within the first 20 minutes of tunneling. If the system was stable repeatable linescans could be obtained in about five minutes of gaining a tunneling current. The software has an 'autoscan' facility where scanning in the X direction is carried out with no change in Y position, obviously for a completely stable system the 'image' would be composed of identical lines. Movement of features in an X or Y direction after initial tunneling at a speed of up to 100Å min^{-1} was usually caused by rapid Z drift towards, or more commonly away, from the surface resulting eventually in loss of tunneling. This was characteristic of poorly fixed samples. Some Z

drift after a coarse approach is inevitable while the piezo tube and piezoelectric components of the inchworm equilibrate, a half hour period was often left before imaging was seriously attempted.

For all samples initial responses to this problem could be to retract the tip and make another coarse approach, possibly after moving the sample horizontally, or to set the tunneling conditions momentarily to 10 V and 20 nA (tip 'zapping', field emission in the tunneling gap may modify the surface and the tip, and is often used to 'clean' the latter when imaging is poor). In both cases the aim is to dislodge any foreign material possibly causing instability in the tip-sample gap. Commonly, though re-fixing of the sample was necessary.

Occasionally with gold on mica, some areas of sample would give stable tunneling while others would not, possibly due to bowing of the sample on cutting it from a larger sheet. Under liquid the Z drift problem was reduced, and would allow imaging but of low quality. The thin layers of gold on mica were quite delicate; in electrochemical experiments prolonged gas evolution would cause the film to lift off the mica and break up.

3.V.iii. Imaging: general

The Omicron software allows scanning over an entire area of ±140 V in X and Y, but of this only a maximum scan area of 50 V in X and Y can be used in an image. To access other regions in the total scan area a manual offset in X and Y must be applied via the electronics front panel. To find appropriate areas for experimentation (often a long and tiresome process) the wider scan area could be probed by systematic imaging. A useful scan size for these purposes was 800 - 1500Å square. The lack of a

zoom facility coupled to drift often caused consternation when interesting areas were lost on moving to smaller scan sizes.

For large area scans (over 800Å square) X and Y increments, i.e. the distance between data points, were set at between 6 and 10Å for general area scanning. For normal imaging usually 160 - 300 points a side were recorded at point times (the length of time spent by the tip over a data point) of 800 - 2500 μs.

When imaging, a powerful method of checking the validity of the signal being detected is to rotate the image, vary the number of sampling points and vary the speed of sampling. If the image has features being caused by the effect of noise on the system the image will change appearance as the scan parameters change but possibly will not rotate. Features due to the surface alone will be rotated but will not change dimensions.

The software allowed recording of data in both directions (each X line was scanned forwards and backwards before the next Y increment was moved to). This facility showed up scan direction dependent surface features and enabled poor imaging to be detected.

A quick method of monitoring the progress of an experiment was to whistle near the experiment, if this was observed on the tunneling current, the tip-sample gap was responsive. If there was no response this implied lack of sensitivity in the gap, and tip movement or 'zapping' would be required to regain imaging ability. Area movement would be necessary after 'zapping' because of the probability of surface modification.

One problem commonly arising was the occurrence of linescans as shown below in fig. 3.13, the straight line presumably arising from a surface feature so sharp the tip could not follow it. If imaging was

continued until the straight line filled the scan area, the software would record noise of about 0.2Å height. Normal imaging could be resumed by stopping and restarting the scan. It was assumed the effect was an artifact of the data digitisation process.

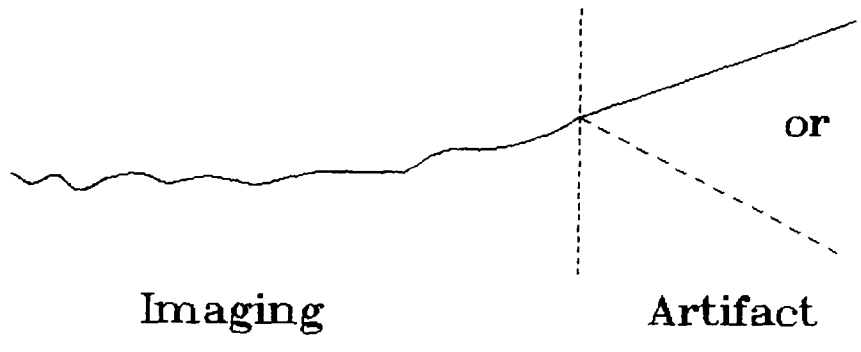

Fig. 3.13. Linescan artifact.

3.V.iv. Imaging under liquids

A problem with initial experiments under electrolyte, was the presence of a large d.c. offset on the tunneling current which prevented detection of a tunneling signal (normally the residual offset due to electrochemical effects at the tip is less than approximately 100 pA when the tip potential is optimised; residual electronic noise on the system is of the order of 50 pA). It was originally assumed this was due to poor tip insulation, until it was found to appear on approach to the liquid *before* tip-electrolyte contact and was reduced by blowing air through the stage. The problem was alleviated by gluing the tip-head amplifier wire into the tip holder with epoxy rather than cyanoacrylate glue after careful cleaning of the components of the tip holder. Presumably electrolyte left on the tip holder after accidental immersion evaporated leaving a crystalline

deposit which on exposure to water vapour caused electrochemistry at the metal components of the tip holder. The problem did resurface briefly with the epoxy glued system which, on cleaning, worked correctly.

Occasionally very bad lateral drift could be observed in an electrochemical experiment which was due to liquid leakage out of the cell; when using phosphate buffer solution, evaporation of the solution would leave small crystalline deposits along the reference electrode tubing which, if not carefully removed, would induce electrolyte to rise over the cell wall leading to rapid depletion of cell contents.

The loss of full potential control in electrochemical experiments due to evaporation could be monitored by two methods; withdrawal of the tip slightly, altering its potential and looking for variation in the offset of the tunneling current (which risks changing tip morphology and composition), or by slightly altering the potential of the sample, where the process of bias voltage alteration gives transient noise on the tunneling current if there is potential control. Ideas for using a fluid detector circuit were dropped because of the uncontrolled electrochemistry use of such a circuit would cause.

Loss of sensitivity in the tunnel gap here could not be easily rectified with tip 'zapping', because of the possible electrochemical processes that could take place. Instead it was often found that tip retraction and re-approach using the coarse approach battery would solve the problem.

3.VI. Summary

This Chapter has described the development of an STM system suitable for *in-situ* electrochemical studies. The ability of this equipment

to provide high resolution imaging is shown in subsequent Chapters.

There is however scope for improvement; the idiosyncratic approach of the current stage developed through a need to overcome some characteristics of the commercial piezoelectric motor used to provide the automatic approach. These problems may now have been overcome by Burleigh, who have developed a new motor controller. Burleigh are now marketing a smaller sized inchworm which future workers may find useful.

Hindsight and subsequent viewing of commercial equipment provokes the suggestion that an alternative configuration would be to use an inchworm to coarse approach the sample towards a vertically fixed scanning system. This would reduce the distance between tip and the nearest fixed point and may further increase the stability of the system.

Chapter Four

Instrument and Substrate Evaluation

4.1 Introduction

This Chapter is concerned with results obtained from tunneling in air; discussion of the instrument's use in *in-situ* work is contained in Chapter Five.

The first aim was to demonstrate that the system was operational and to provide some indication of the performance of the stage. In line with the project aims for the study of cytochrome *c* electrochemistry, substrates needed to be developed and characterised.

It was originally envisaged the STM would be used for carrying out high resolution studies of ordered adsorbate layers on electrode surfaces. A prerequisite for this type of work is that the substrates have sizable atomically flat regions: if the surface corrugation is larger than the effects being searched for, no results will be forthcoming! In addition the preparation should give reproducible surfaces with well characterised features. As pointed out earlier, the uncertainties in the features found on graphite surfaces has caused some concern in the area of biological imaging. The presence of well-defined features, for example atomic scale steps, is desirable to provide reference points during imaging.

For investigations related to cytochrome *c*, 'disposable' gold surfaces were needed because the work involved the irreversible modification of electrodes with organic molecules. Cleaning the surfaces by mechanical polishing and electrochemical cycling in acidic media, as customary in such studies[194], is not viable because of the microscopic roughening caused by such a procedure.

Note:

The results in this Thesis are mostly presented in the form of greyscale' images where the higher the tip is over a feature the lighter

in colour it is. The numbers attached to the vertical scaling represent the height of the tip over a datum. Images are balanced to take out effects due to sample slope, but have not been filtered unless otherwise stated.

It should be noted that the accuracy of lateral measurements are subject to the constraints outlined in Section 3.IV.

Image data acquisition is presented thus: pixel acquisition time (t), distance between pixels (inc) - increments in x and y directions are usually equivalent so only one number is presented, set-point tunneling current (I_T) and bias voltage (V_T). Additional information where required is given explicitly. Other instrumental details are contained in Section 3.V

4.II. Graphite

Despite the problems of anomalous corrugation heights[195] and unexpected structures[21], highly oriented pyrolytic graphite (HOPG) is still a popular substrate for exhibiting (and thus calibrating) the resolution of an STM in ambient or liquid environments. For experiments using graphite, fresh surfaces were exposed just prior to positioning in the microscope.

Examination of graphite was found to be a non-trivial exercise. On many of the approaches made, the system was relatively stable over large area scans and often surface features could be observed. However when small areas were scanned at high resolution, consecutive linescans were inconsistent. Fig. 4.1. shows a greyscale representation of one such large scale image with a chain-like features 20Å high, 80-120Å wide diagonally crossing an otherwise flat surface.

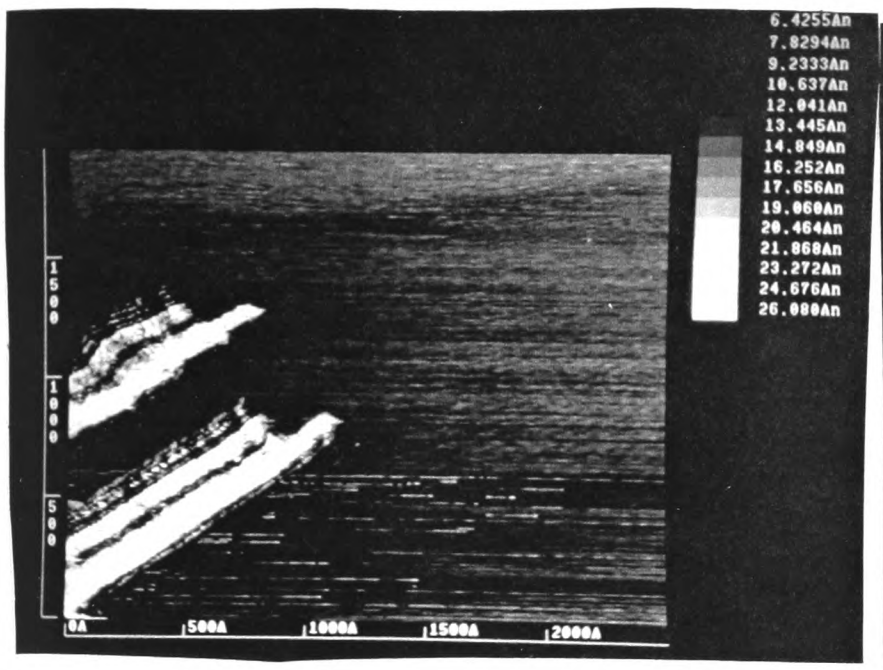

Fig. 4.1.

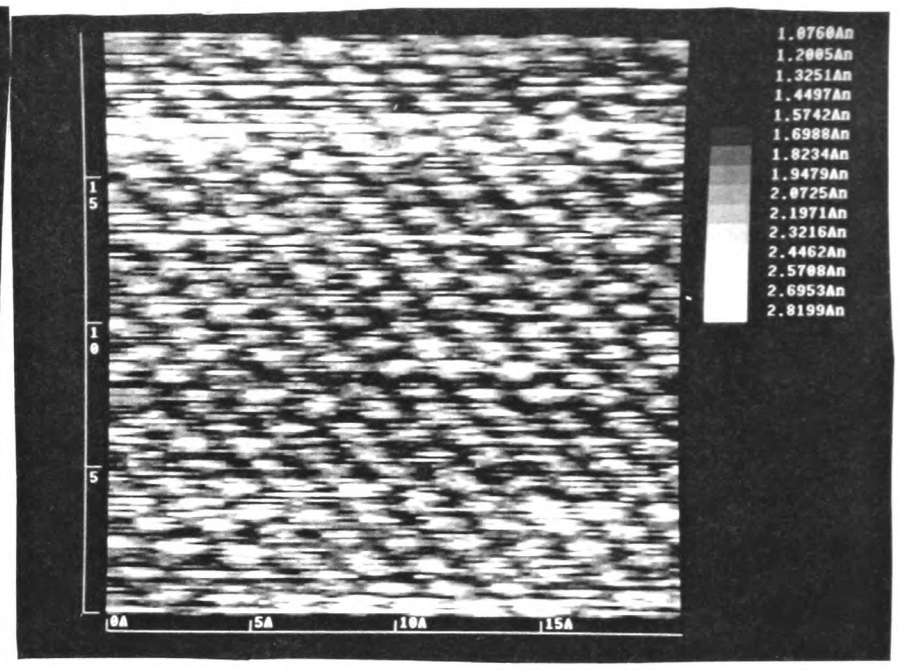

Fig. 4.2.

Fig 4.1. Image of an unidentified substrate feature on HOPG. t: 1.5 ms, inc: 5Å, I_T: 2 nA, V_T: 100 mV.

Fig. 4.2. Image of a graphite lattice. t: 0.15 ms, inc: 0.1Å, I_T: 2.5 nA, V_T: 100 mV.

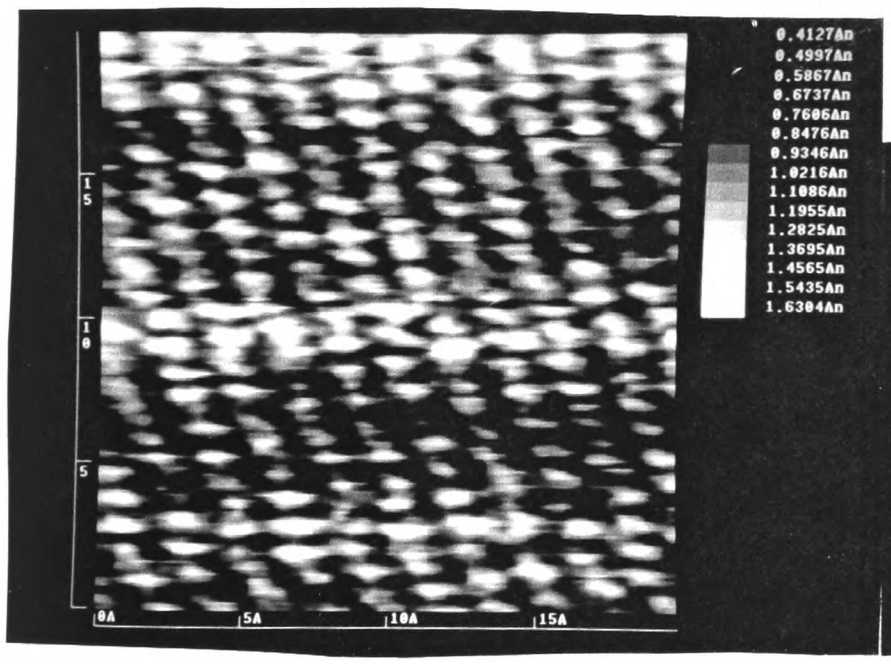

Fig. 4.3 (a).

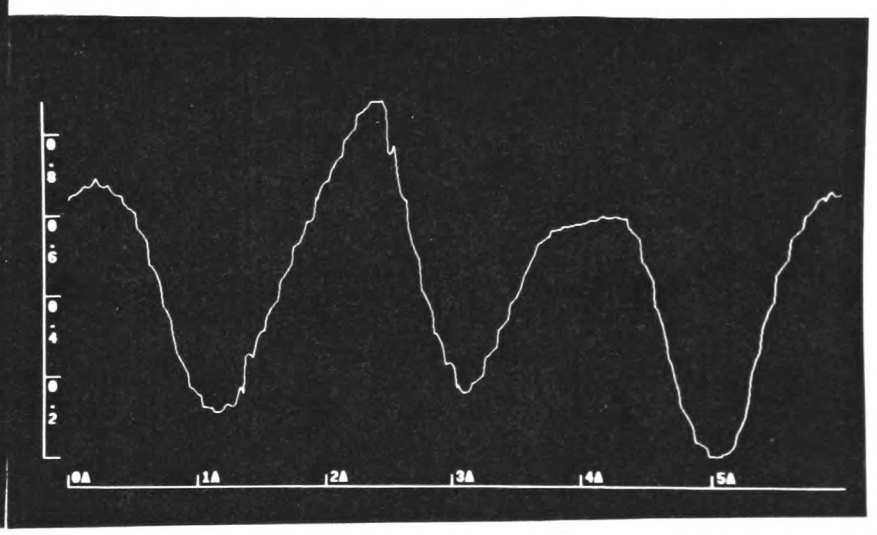

Fig 4.3 (b)

Fig. 4.3. (a). As fig. 4.2, except scan direction rotated by 30° and image smoothed by averaging of nearest neighbour pixels, (b) section through part of (a).

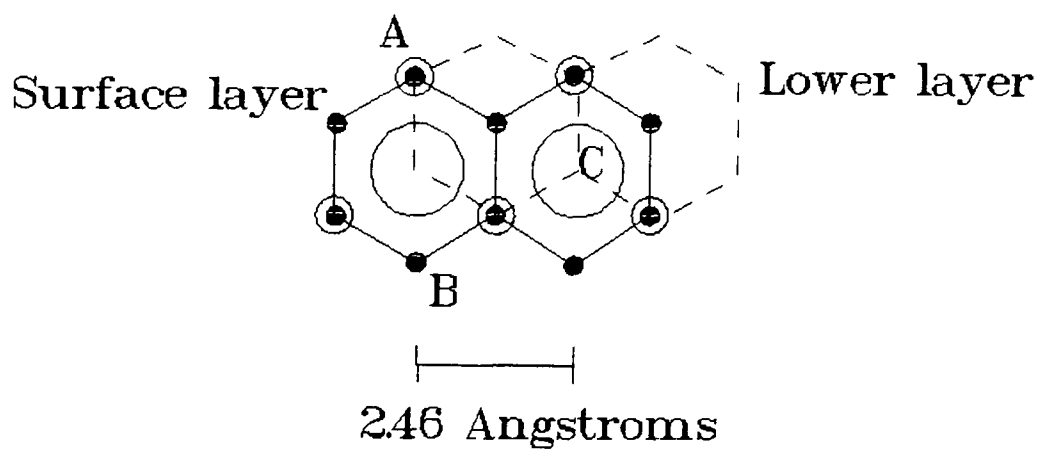

Fig. 4.4. Theoretically expected graphite lattice[196]; atoms at site A coincide with atoms in the layer beneath and appear slightly higher (ca. 0.15Å) than those at site B, maximum corrugation is between site C, where there are lower layer atoms alone, and site A (ca. 1Å).

It should be noted that the two features mimic each other topographically (although the upper set does not run parallel to the lower). This implies a multiple tip effect (see Section 4.III). Streaking of the image in the direction of scanning, e.g. around the lower feature, indicates degradation of the feature is due to interaction with the tip. As a 'one-off' observation in an ambient experiment this type of feature is impossible to interpret. It could be merely adsorbed contamination, or a carbon fibre resulting from substrate cleavage (see reference 23).

The STM linescans of small areas would often indicate a surface corrugation of below 5Å, implying the surface was flat; however the graphite lattice could not be imaged. Continued effort did give results: figs. 4.2. and 4.3 (a) show images of the HOPG lattice. The images were taken consecutively with a rotation of 30° in scan direction between them,

at a high pixel acquisition rate. The rotation of the image data with scan direction implies the features are not given by simple periodic noise and are associated with the surface. The distortion of the image away from the threefold symmetry of the HOPG lattice (especially noticeable in the smoothed image) may be ascribed to thermal drift[197], significant sample tilt[198] or slight differences in X and Y calibration. For comparison fig. 4.4 shows a schematic representation of the theoretically expected[196], and commonly found, basal plane graphite lattice. A cross section of part of the image (figs. 4.3 (a) and (b)) shows a 2Å spacing between parallel height points, with a corrugation of between 0.4 and 0.6Å. Within the margin of error discussed in Section 3.IV., the lateral measurement indicates the features shown are compatible with the graphite lattice.

4.III. Gold single crystal spheres

Single crystal sphere (SCS) facets (for preparation see Section 2.V.iv.) were found to yield a variety of markedly different surfaces. Fig. 4.5 shows part of a large atomically flat terrace with a monatomic step leading to another terrace in the bottom corner, and parts of three monatomic islands. This type of image is ideal for checking the vertical calibration of the instrument against the gold step height of approximately 2.4Å[199]. Such images also provide an indication of instrument stability, in this case the intrinsic random noise (no periodic noise components were identified) on the terrace, measured in a direction perpendicular to the scan direction, was about 1Å. In images with smaller scan sizes (e.g. 800Å x 800Å) this value could be reduced to 0.6Å. Attempts to gain atomic resolution on similar regions were unsuccessful, and this may have been due to a number of reasons; e.g. poor tip quality or lack of instrument stability.

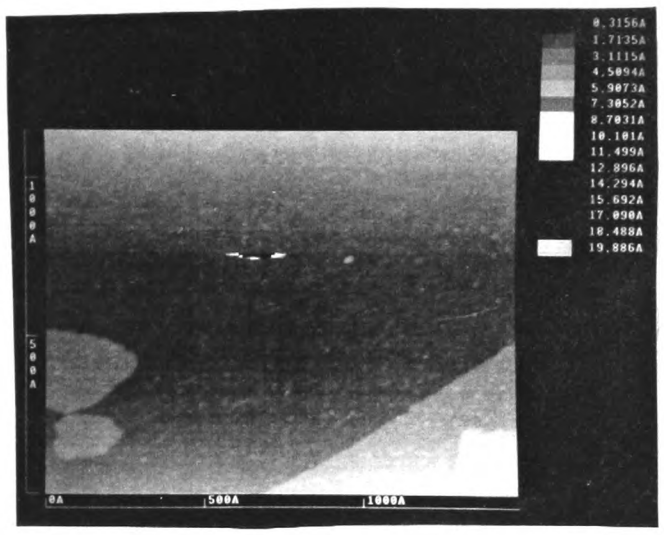

Fig. 4.5.

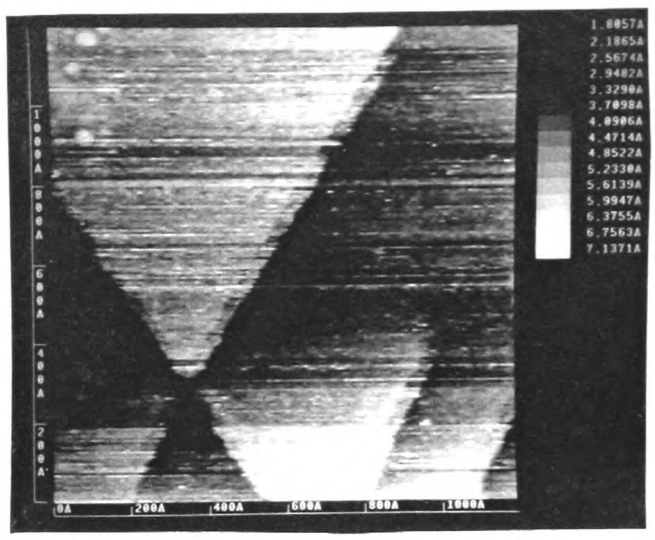

Fig 4.6 (a).

Fig. 4.5. An atomically flat region of a gold SCS sample. (t: 0.8 ms, inc: 6Å, I_T: 2 nA, V_T: 100 mV).

Fig. 4.6. (a) Atomically flat faceted region of a gold SCS showing multi-tip effect. Image parameters as fig. 4.5. (b) Schematic representation of possible image effects given by a multiple tip.

Fig. 4.6 (b)

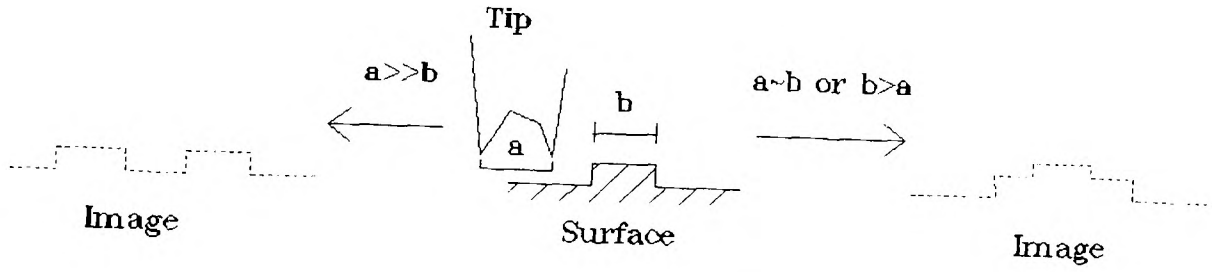

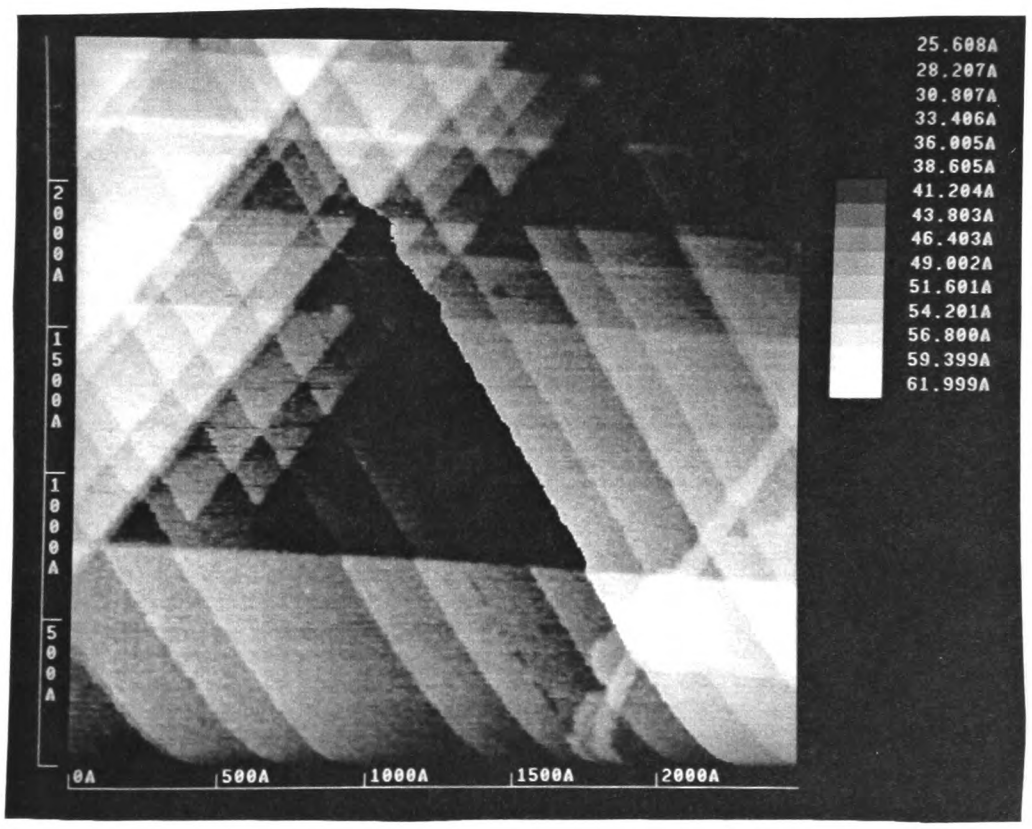

Fig. 4.7. Facets and terraces on a gold SCS. Scan parameters as fig. 4.5., except t: 2 ms, inc: 8Å.

Figs. 4.6 (a) and 4.7 show the 'classic' Au (111) surface of overlapping steps which meet at approximately 60° angles, characteristic of a surface exhibiting threefold symmetry. This type of surface has been reported by a number of workers using gold in the form of SCS[92,172], single crystals[70] and less commonly thin films on mica[200]. Wang and Moskovits[201] have observed such facets on an annealed gold foil sample attributing crystallographic orientation to the steps observed. In turn this has been used as evidence for the surface showing a 22 x $\sqrt{3}$ reconstruction. Fig 4.6 (a) illustrates artifacts caused by multiple tips; the large triangular facet appears to have a double step while below it another step comes out of apparently flat substrate. As indicated in fig. 4.6 (b), a multiple tip superimposes signals from different areas of surface giving a resultant image which is the sum of two tunneling currents. Here the triangular facets are 'real' features, but are summed yielding an image that does not show the true surface topography. The illustration shows a variety of potentially misleading structures can arise from multiple tips, however the repeating nature of such effects within the same image aids identification and interpretation.

Fig. 4.7 shows a large number of monatomic steps overlapping to form triangular terraces with a multi-atomic step, approximately 17Å in height, running diagonally through the centre of the image. The remarkable symmetry shown by the surface, where steps cross even relatively large changes in vertical height has prompted suspicions that tip-surface interaction is responsible for the faceting[200,202]. While acknowledging the possibility of some contribution to the image by multiple tips, rotation of scan direction showed consistency in the main features, and the non-symmetric features and holes in the bottom right

hand corner (also present on rotated images) appear to be irregular surface features. These observations imply the image is formed by monitoring a tunneling current from the surface rather than by a mechanism involving physical movement of the surface. This conclusion is consistent with the surface modification experiments carried out elsewhere[172].

Tip-surface interactions have been used by Wang and Moskovits to explain their observation of the development of features on a gold SCS[201]. Similarly Bard has recently reported the topography of gold on mica samples changed when repeatedly scanned[204]. Both of these experiments involved tunneling in air and it is clear that there are still many aspects of *ex-vacuo* tunneling which are not completely understood.

A different type of faceted surface is given in fig. 4.8, here again steps intersect at multiples of 60°, but the surface is not absolutely smooth, with a peak to trough corrugation of up to 2Å in places. This surface was imaged after a bead, left exposed to air for a couple of days, was annealed by gentle heating in a butane flame to a temperature below its melting point. This type of procedure when completed by quenching of the hot surface in distilled water is commonly used to clean gold single crystals and establish atomically flat regions. It is worth noting that recent atomic resolution studies on such gold surfaces prepared in a H_2/O_2 flame, showed the presence or absence of a reconstructed surface depended on the flame temperature[203] (similar results based upon investigations of quenching an annealed single crystal have also been published[83]).

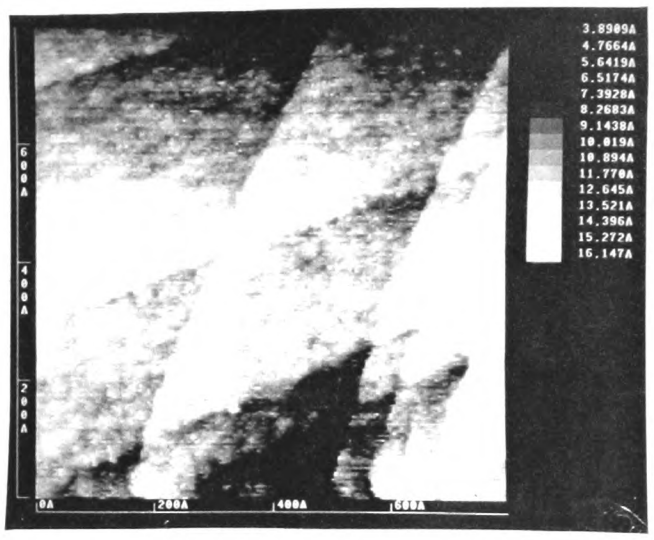

Fig 4.8.

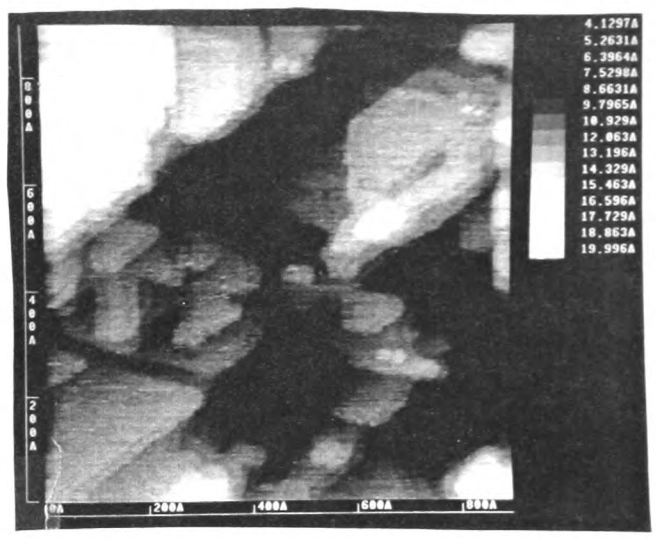

Fig. 4.9.

Fig. 4.8. Image of a 'corrugated' gold SCS facet. (t: 0.8 ms, inc: 4Å, I_T: 5 nA, V_T: 250 mV).

Fig 4.9. Uncommon, atomically flat, island topography on a gold SCS. Scan parameters as fig. 4.5.

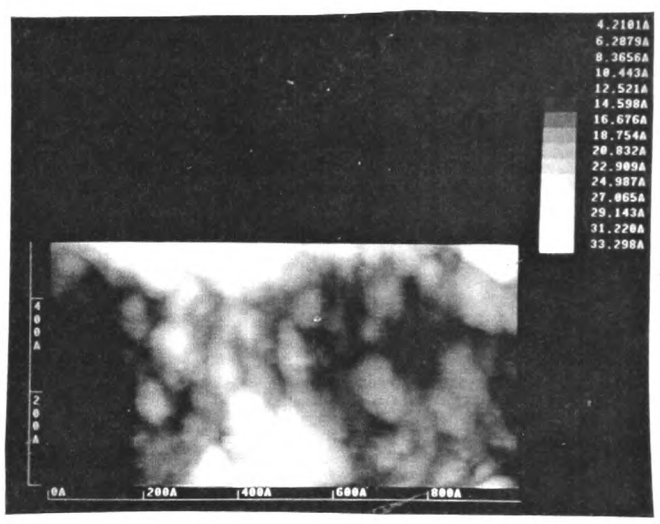

Fig. 4.10. Example of the irregular topography found on an Au SCS. Image parameters as fig. 4.5.

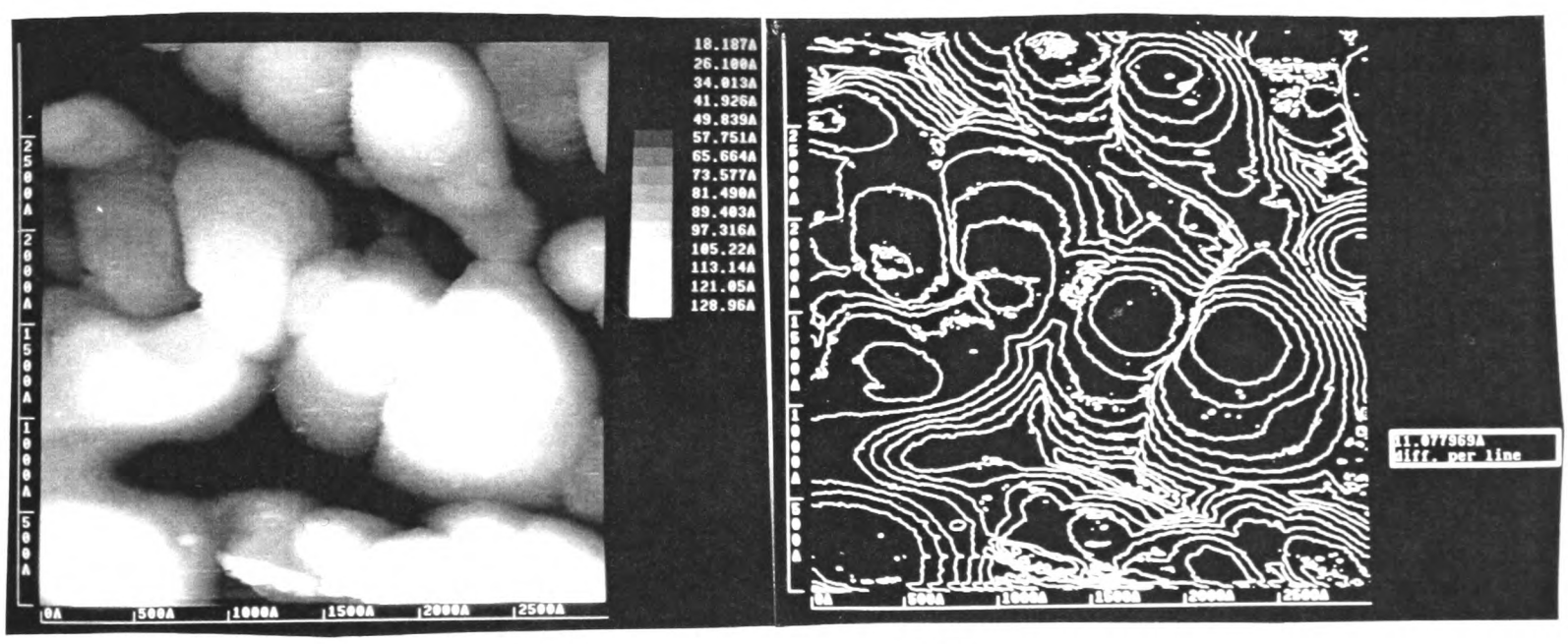

(a) *(b)*

Fig. 4.11. (a) A typical gold on mica topography. Sample Au 2. (t: 0.8 ms, inc 8Å, I_T: 1.5 nA, V_T: -250 mV, (b) contour line representation of (a).

As the √3 x 22 reconstruction so formed has a corrugation amplitude of 0.2Å, the same effect is not being observed here. A more likely explanation is that contaminants from the flame, normally removed on quenching, are responsible.

A collection of small atomically flat islands separated by monatomic steps is presented in fig. 4.9, this previously unobserved topography does not appear to show any specific crystallographic orientation.

A more common topography is shown in fig. 4.10, the surface is irregular and globular in appearance, while the lack of flat areas and well defined features means the surface is unsuitable for attempting to investigate deposition of materials. Ill-defined topographies such as this could be found on most surfaces.

In summary, the surface of gold single crystal spheres shows a variety of topographies, some of which (fig. 4.5) are extremely good for the type of work outlined, others are poorer (fig. 4.6) while surfaces such as shown in fig. 4.10 are useless and potentially misleading in the case of large molecule deposition. The distribution of the various topographies while not closely monitored, is in broad agreement with other work[172].

4.IV. Gold on mica

Substrate preparation and nomenclature was outlined in Section 2.V.iii. A typical gold on mica surface is shown in fig. 4.11 (a), accompanied by a contour map of the image to indicate more clearly the surface topography. In this area there are a number of islands which have atomic or multi-atomic steps forming atomically flat terraces that eventually lead up to an atomically flat plateau. Many examples of this are given throughout Chapters 5 and 6, but an interesting illustration of this in fig. 4.12, exhibits two such plateaus grown beside one another with

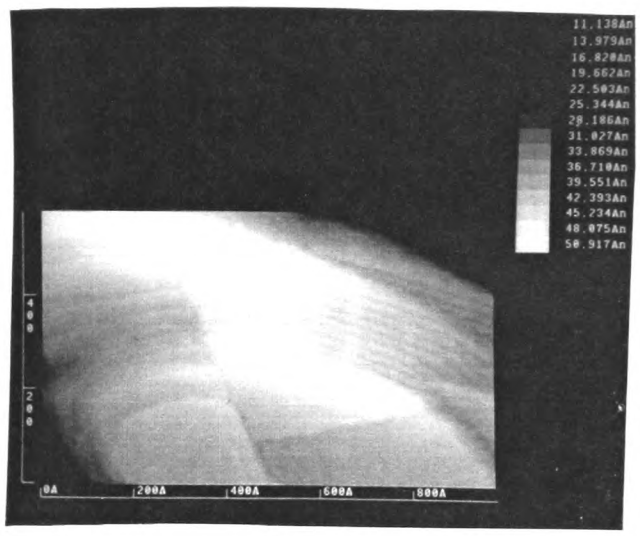

Fig. 4.12. Gold on mica plateau, sample Au 4. t: 2 ms, inc: 5Å, I_T: 2.5 nA, V_T: 250 mV.

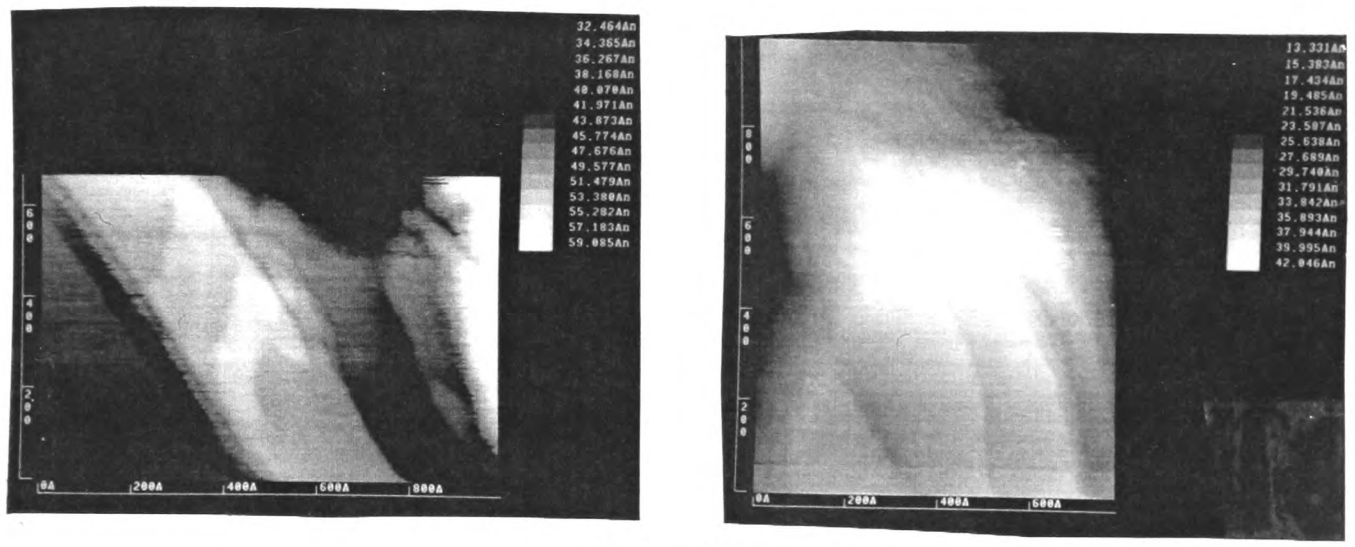

(a) *(b)*

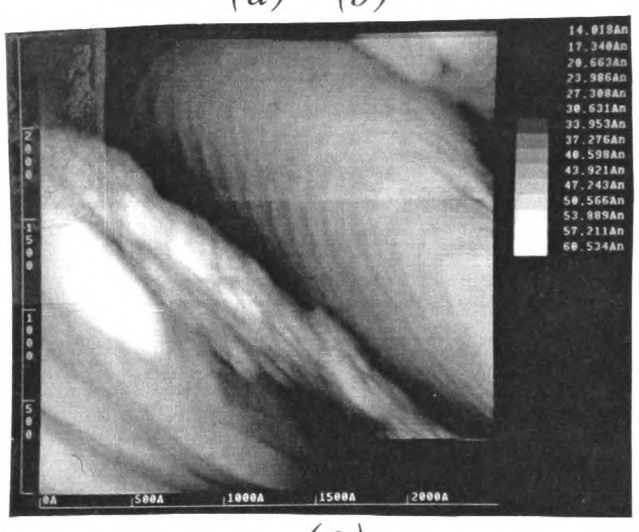

(c)

Fig. 4.13. Examples of topographies noted during imaging gold on mica substrates, (a) Au 4, t: 1.5 ms, inc: 4Å, I_T: 2.5 nA, V_T: 250 mV, (b) Au 4, t: 1.5 ms, inc: 5Å, I_T: 2 nA, V_T: -500 mV, (c) Au 4, t: 2 ms, inc: 10Å, I_T: 2 nA, V_T: 100 mV

different terrace spacing.

The epitaxial growth of gold on mica to yield Au (111) surfaces is well known[171]. Film formation occurs by growth around isolated nuclei and as these crystallites expand and meet, island-like grains are formed. Subsequent deposition on this surface will reflect the topography of the original grains, thus forming the isolated 'hillocks' as shown in 4.11, while diffusion of atoms gives terraces and plateaus.[171]. At the intermediate temperatures of *ca.* 200°C used here (others have used deposition temperatures of 500°C[200]), the original grains will fuse together yielding larger grains than at room temperature, but since the mobility of the condensing gold atoms is not great enough to fill in the depressions between the grains the plateaus and terraces remain isolated. The substantial misregistry of terraces shown in fig. 4.12 is probably due to a feature in the underlying mica.

An obvious difference between these surfaces and SCS surfaces is the lack of features explicitly showing the crystallographic orientation of the substrate, i.e. here the step edges are rough. The terraced structure given for the gold on mica surfaces is however extremely useful; the flat plateaus are ideal for adsorbate support, while the steps provide convenient reference points - in addition to providing features that may be important in various processes, e.g. adsorption of bio-molecules may be stronger at step sites.

For reference a number of other images obtained on this type of sample are shown in figs. 4.13 and 4.14; fig. 4.13 (a) shows an elongated plateau with some terrace structure adjacent to poorly defined areas while figs. 4.13 (b) and (c) exhibit a more typical terrace/plateau type region again surrounded by less regular areas.

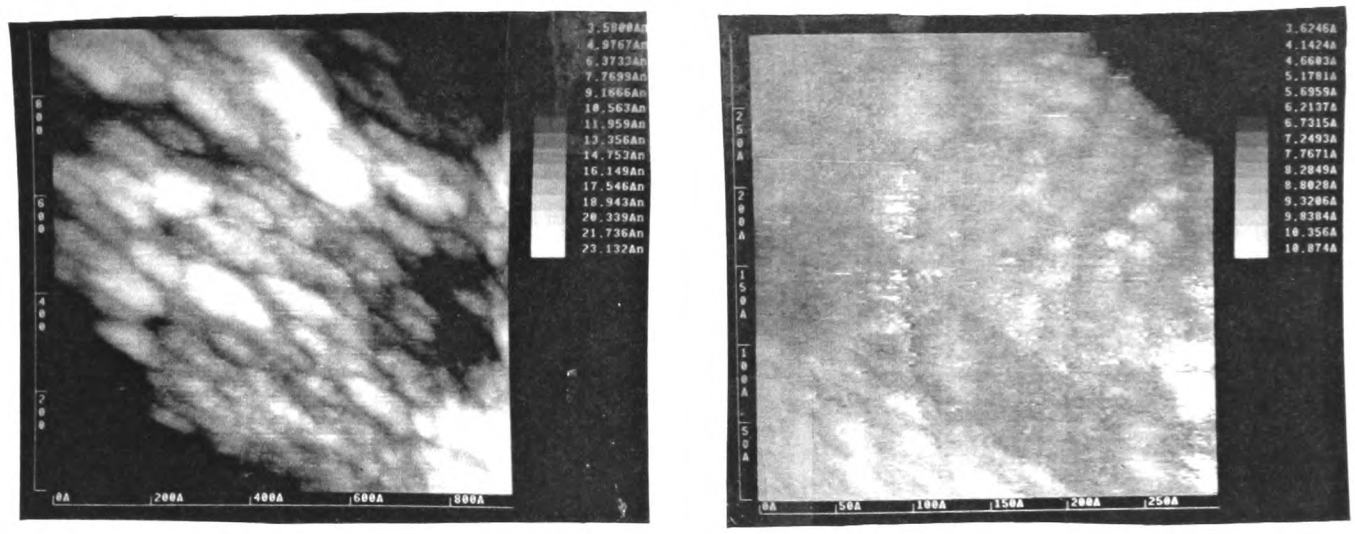

(a) *(b)*

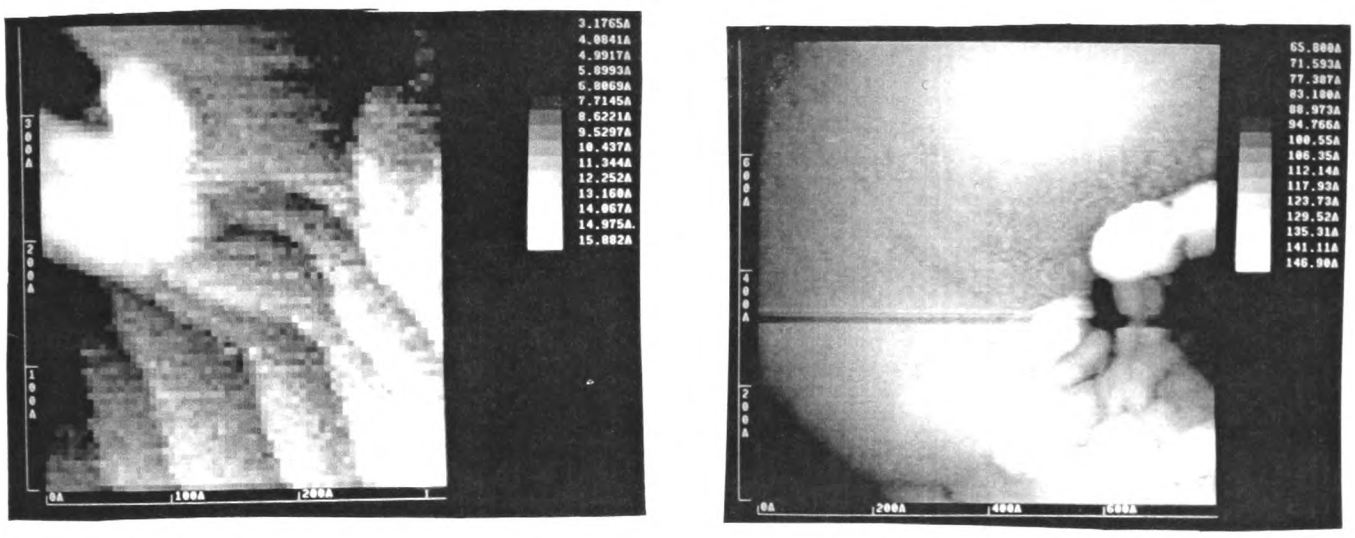

(c) *(d)*

Fig. 4.14. (a) Au 4, t: 2 ms, inc: 5Å, I_T: 2 nA, V_T: 100 mV, (b) Au 2, t: 1 ms, inc: 1Å, I_T: 2 nA, V_T: 250 mV, (c) Au 4, t: 1.9 ms, inc: 5Å, I_T: 2 nA V_T: 50 mV, (d) Au 4, t: 1.8 ms, inc: 4Å, I_T: 2nA, V_T: 200 mV.

Fig. 4.14 (a), shows one such 'globular' area. The vertical corrugation of the region is low yet no atomically flat regions are visible. Similar behaviour is given in fig. 4.14 (b), where again the area has low corrugation without giving any flat areas. It must be constantly remembered that the images are taken while tunneling in air, thus the surface, and consequently the tip, may easily pick up contaminants. This could easily explain the lack of structure in images such as fig. 4.14 (b). Emch *et al.*[205] have commented that they found 'rolling hills' type geometry to be mostly attributable to tip contamination, fig. 4.14 (b) could be thought of in this category, although the appearance of such types of feature adjacent to well defined regions as in fig. 4.13 (c) imply the image is related to the surface topography. One problem in surface characterisation is the difficulty in comparing ill-defined topographies, in addition to the vagaries of surface/ tip contamination. Of importance to Chapter 6 are the images in figs. 4.14 (c) and (d) where almost discrete 'globular' features are observed (in the latter the feature is adjacent to a hole on a well defined terraced region).

In comparison to other results[171,200], these substrates exhibit comparatively small plateaus and terraces, which is almost certainly due to the low mica outgassing and gold deposition temperatures used (a limitation of the deposition apparatus used), temperatures of 400°C or more would certainly seem to be advantageous.

For the marginally different sample preparations used here, no large difference between samples was noted. The exception to this was the Au 4 sample, which seemed to have far more disordered regions (i.e. regions lacking terraced grains) than previous samples, and following this a different supply of mica was used for a comparative test (Au 5/6 samples).

No noticeable variation in sample quality was observed.

Atomic resolution imaging was attempted and only once was an appropriate image observed. Quality was poor however and subsequent image rotation was unable to substantiate the first image. Stage resolution on these substrates was consistent with that found on SCS surfaces.

4.V. Conclusions

The stage was found to be capable of a sufficiently high vertical resolution that monatomic steps on gold surfaces (approximately 2.4Å) could be observed easily and repeatably. Lateral resolution was harder to estimate due to the problems encountered during graphite imaging, but from inspection of the width of terraces resolved, it could be estimated at better than 10Å. Intrinsic noise perpendicular to the scan direction was often approximately 0.6Å.

This chapter has presented results from topographic imaging of two gold substrates successfully evaluated for use in later experiments. Attempts to form gold SCS by electron beam bombardment (courtesy Dr. P. Dobson) were unsuccessful - the melted portion of wire exhibited no facets and much contamination. Chemical treatment (cyanide electropolishing courtesy Dr. T. Cataldi) of the mechanically polished Au (111) single crystal left a tarnished surface[73] and subsequent UHV Ar sputtering and annealing failed to reveal a LEED pattern. Further mechanical polishing followed by flame annealing gave a surface which on STM investigation gave no useful areas.

Although both gold SCS and gold on mica samples gave excellent surfaces, in line with the requirements outlined in Section 4.I., most of the results presented in this Thesis use gold on mica samples. This is for a number of reasons; firstly it was originally found hard to locate

suitable areas on gold SCS samples, whereas the distinctive gold thin film plateau regions were quickly observed; secondly, for reasons enlarged upon in Chapter 6, it was felt necessary to reproduce features originally seen on an SCS sample and thirdly thin film samples proved easier to set up in the microscope.

The variety of topographies illustrated show just how important it is to image a surface carefully before begining modification of it, surface characterisation is now an accepted component of STM studies. To gain some perspective of the possibilities for imaging different topographies, use of an STM at the scan sizes used in this study may be considered, at least metaphorically, to taking football pitch sized samples of the surface of the British Isles! In ambient conditions the problem of contaminants causing unusual features is another factor to be aware of.

Additionally the results serve to reinforce the point that on an atomic scale, unless prepared extremely carefully, an electrode surface will be rough. Thus when envisaging the role of surface structure in interfacial processes one should remember, especially with polycrystalline electrodes, well-defined steps and terraces will be the exception. Thus as previously implied the arrival of *in-situ* STM will further establish the trend for using carefully prepared electrode surfaces. One area for further study is the effect, on the final surface, of varying aspects of the SCS preparation, e.g. changing flame composition or cooling method.

Another experimental aspect, is that all the surfaces will have been covered by adsorbates on exposure to the atmosphere[206], yet although some images do show instability due to spurious debris, monatomic steps may usually be resolved. It appears much of this contamination is not detected by the STM experiment, and it may be speculated such adsorbates

are either being pushed aside by the tip or not interfering with the tunneling process within the limits of the resolution of the instrument, i.e. presenting a homogeneous or negligible modification to the tunneling barrier.

In conclusion, gold on mica substrates were chosen as the main surface to be used for the project as they optimally fulfilled the criteria discussed in Section 4.I., i.e. that of easily characterised, 'disposable' surfaces with atomically flat regions. Gold SCS substrates were found to give more unpredictable results and were inconvenient to use practically. As Nichols *et al.* have found some indications of alloying when studying the bulk deposition of copper on gold[97], the use of disposable surfaces may become important in even apparently macroscopically reversible processes.

The size of atomically flat terraces on the gold thin films could probably be enlarged by higher temperature mica outgassing and gold deposition. Attention to sample storage and transfer from deposition chamber to storage to stage may yield improved results.

Chapter Five

In-situ STM of gold surfaces

5.I. Introduction

This Chapter describes the evolution in the experimental use of the STM during the course of the project; Section 5.II. considers tunneling under electrolyte without potential control while Section 5.III. discusses the electrochemical oxidation of gold under phosphate buffer. Subsequent improvement in the potentiostat electronics yielded the more attractive results of Section 5.IV. Here again the process was the electrochemical oxidation of gold, but the electrolyte was sulphuric acid. Discussion and rationalisation of the images is presented in Section 5.V.

The work using phosphate buffer was intended to test the capabilities of the STM under an electrolyte and was also of importance to cytochrome *c* investigations, being a commonly used electrolyte in those studies. The experiments using sulphuric acid were carried out partly as a comparison with the phosphate experiments, but mainly to provide the background characterisation to facilitate future work on underpotential- and bulk-deposited metal species.

There are some aspects of a few of the results presented here (e.g. image 5.1), that, for reasons of completeness, are discussed in the next chapter.

All potentials (even when originally measured against other reference electrodes) are quoted relative to the standard calomel electrode (S.C.E.). For the figures involving STM images, sample potentials are presented alongside each individual image while general scan parameters are described in captions at the end of a series of images. The slight irregularity in the values of the recorded potentials is due to the manual control of the potentiostat.

5.II. *In-situ* Electrochemical STM without potential control

5.II.i. Phosphate buffer

Fig. 5.1 shows a gold on mica surface imaged under a phosphate buffer (0.02M phosphate, 0.1M perchlorate) solution; characteristic 'plateau' regions are covered by small irregular approximately monatomic high islands. The image was obtained at high set point current to overcome an effect due to Faradaic current flowing through the tip (the bias voltage was adjusted to minimise this problem). This residual current is observed as a slowly varying d.c. offset present on the tunneling current signal while the tip was submerged but far from tunneling.

This method of imaging, apart from giving no control over the tip and substrate condition, is inherently unstable as there is no way of minimising the residual Faradaic current over a prolonged period of time.

As in all the experiments with aqueous electrolytes the gold surfaces were hydrophobic, an observation consistent with their exposure to air and uptake of atmospheric contaminants[205].

5.II.ii. Distilled water

Fig. 5.2 shows consecutive forward and reverse scans of a gold surface under distilled water. Again the bias voltage was manually adjusted to minimise residual currents. The ill-defined feature at the top left is likely to be liquid supported contaminant. The substrate surface, although poorly defined, is reversibly imaged while the feature shows streaking in the direction of scanning indicative of tip contact. As the substrate is still clearly observable around the object it is likely that the streaking is caused by movement rather than tip induced breakup (which would be expected to affect the tip and degrade the image).

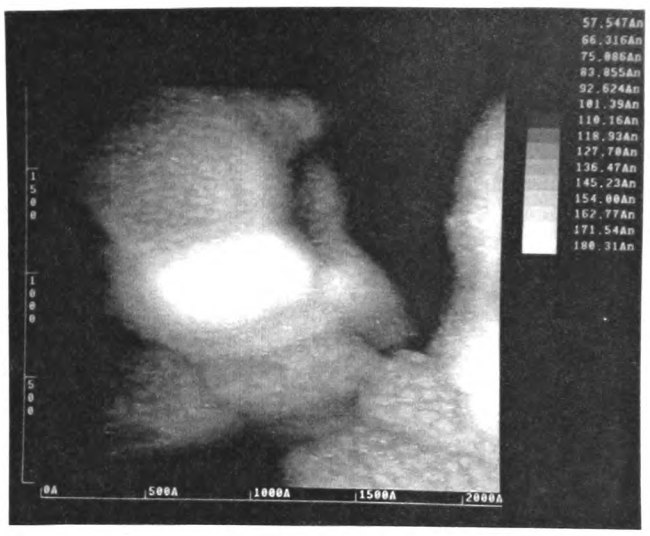

Fig. 5.1. Gold surface imaged in phosphate buffer; sample Au 2. t: 2 ms, inc: 6Å, I_T: 28 nA, V_T: 700 mV.

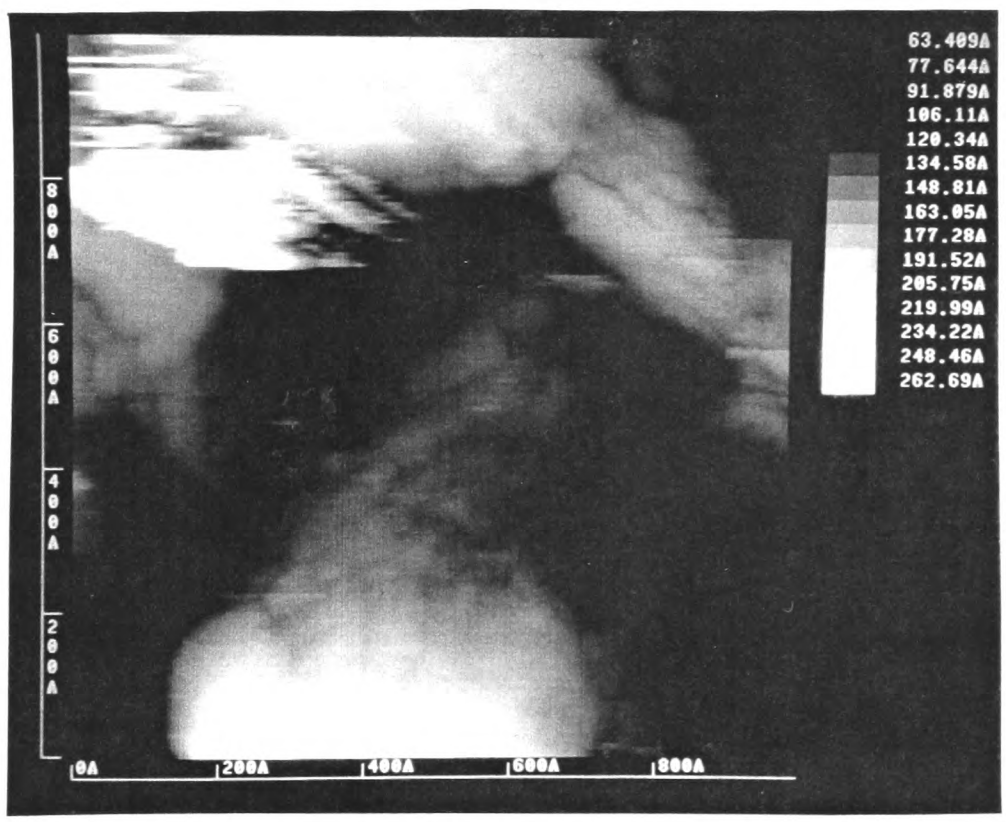

(a)

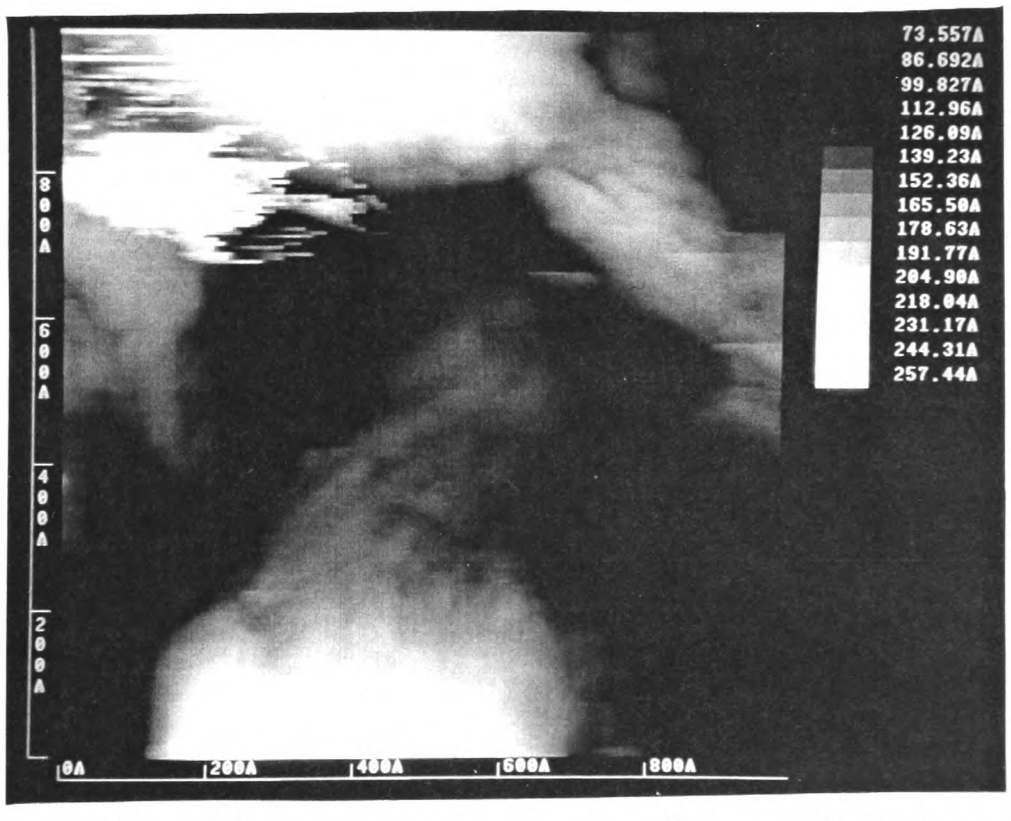

(b)

Fig. 5.2. Forward (a) and reverse (b) scans of a gold surface in distilled water; sample Au 4. t: 1.5 ms, inc: 5Å, I_T: 3 nA, V_T: 100 mV

Imaging under distilled water was used for comparison with effects seen under electrolyte. It has been suggested that very weak electrolytes give poor images[207] but no conclusive evidence for this was found during these studies.

5.III. STM observation of the electro-oxidation of gold under phosphate buffer

The first practical comment to make about electrochemistry using thin film electrodes is that they are very delicate; accidental biasing into a region of gas evolution for more than a couple of seconds will cause the film to lift off the mica support.

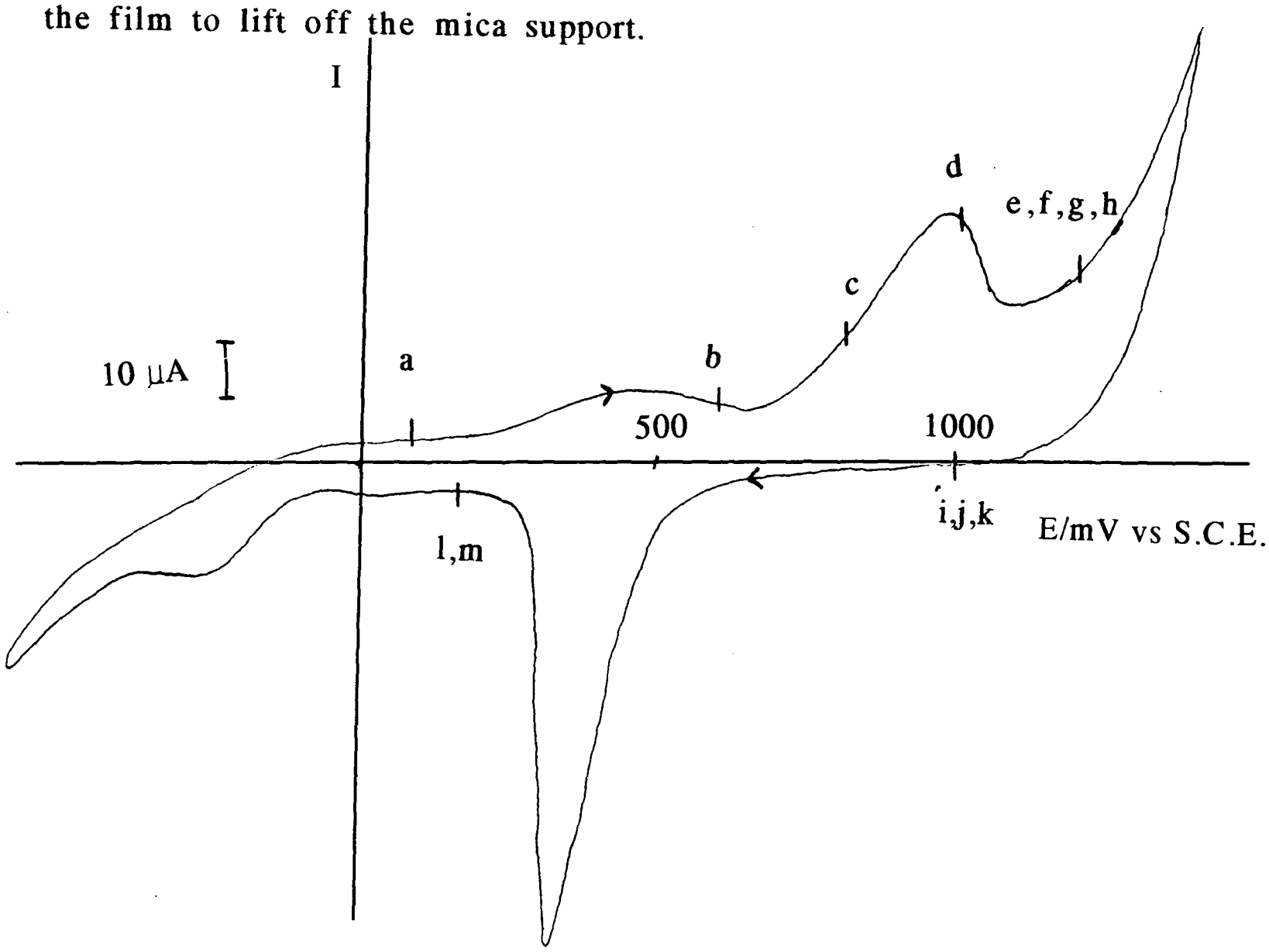

Fig. 5.3, Cyclic voltammogram for a gold on mica surface in phosphate buffer (air saturated). Scan rate 50 mVs^{-1}. Points a - m are described in the text.

Fig. 5.3. shows a cyclic voltammogram for a gold on mica substrate in a phosphate buffer solution. The solution was not deaerated prior to cycling and thus is directly comparable to the situation in the STM system where it is not possible to exclude oxygen. The phosphate buffer solution consisted of 0.02M NaH_2PO_4, 0.026M Na_2HPO_4 and 0.1M $NaClO_4$ at pH 7. Apart from peaks due to the reduction of dissolved oxygen at cathodic potentials, and consequental slope on the voltammogram, the CV is substantially similar to those quoted elsewhere[208].

The tip potential that minimised residual Faradaic currents through the tip was found by trial and error to be approximately -220 mV vs S.C.E. The cell was set up as described in Section 2.III.iii. with phosphate buffer in the tubing leading to the S.C.E. supporting salt bridge, which was filled with 3M KCl.

The results of observing the change in surface topography with applied potential are shown in fig. 5.4 (a-m) and the approximate potentials of the images are marked by the appropriate letter on fig. 5.3. Figs. 5.4 (e-h) and (i-k) were taken consecutively at the same potential to study the time dependence of features observed. Each of the scans took approximately 100 seconds. The experiment was conducted by imaging at a given substrate potential, stopping the scan while the potential was manually altered and scanning again. The tip was not withdrawn from the surface during this process and the majority of the images, (c-k), were taken in the same area. Instrumental drift exacerbated by surface processes caused by structural change resulted in some movement of scan area between images. It was decided that as the processes occurring were dynamic it was better to complete a full oxidative cycle than spend too much time precisely locating areas.

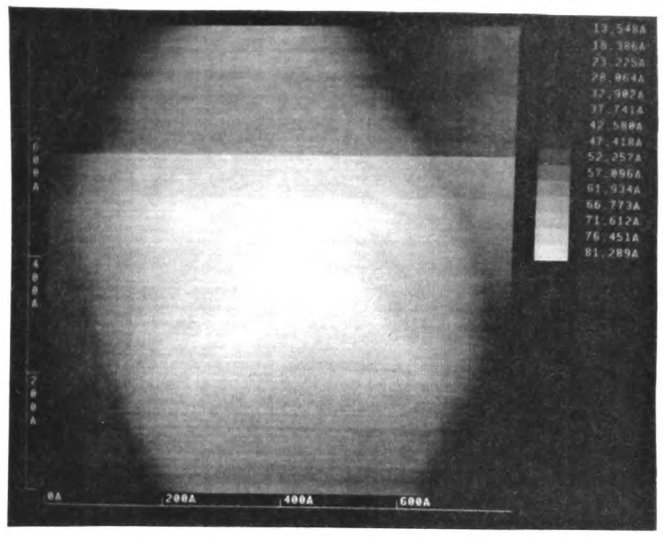

(a) 75 mV

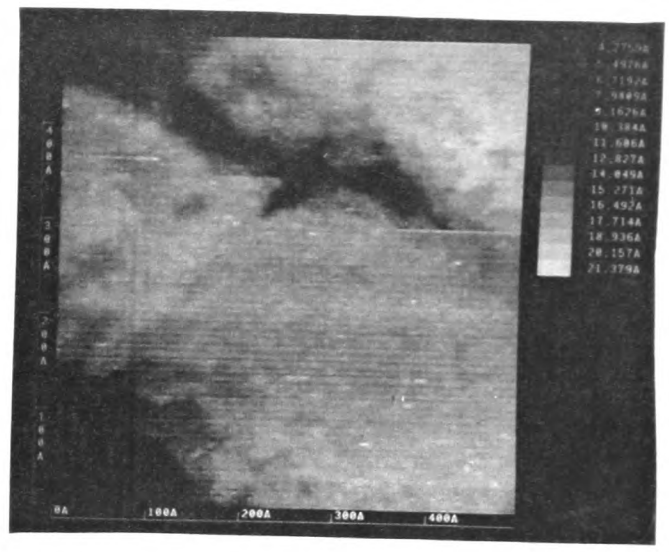

(b) 600 mV

(c) 800 mV

(d) 1000 mV

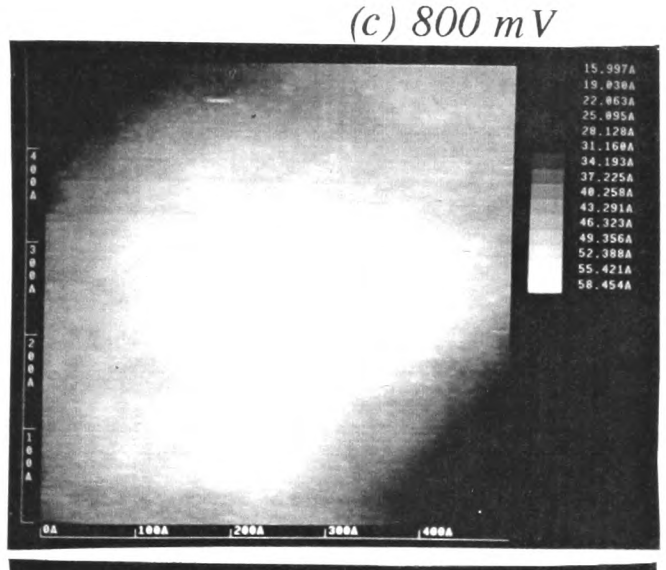

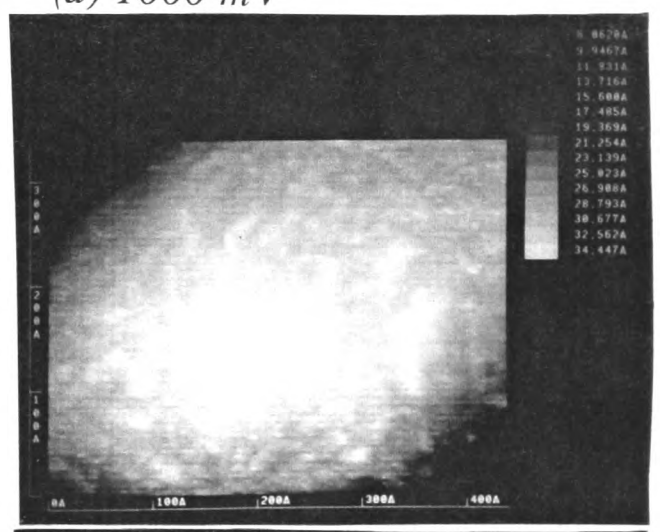

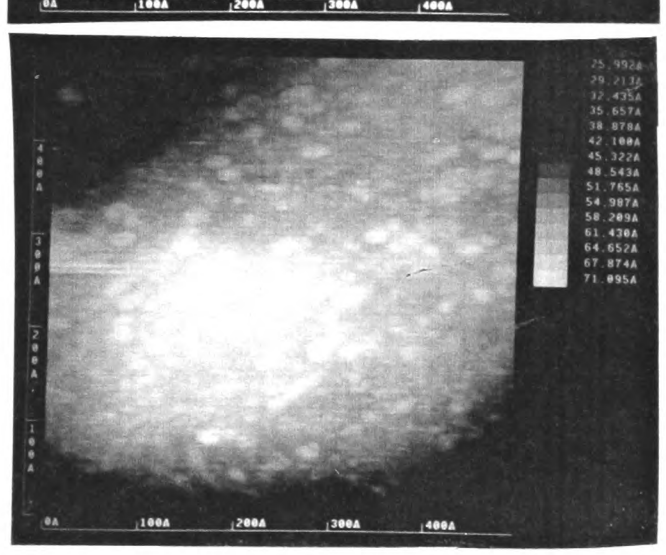

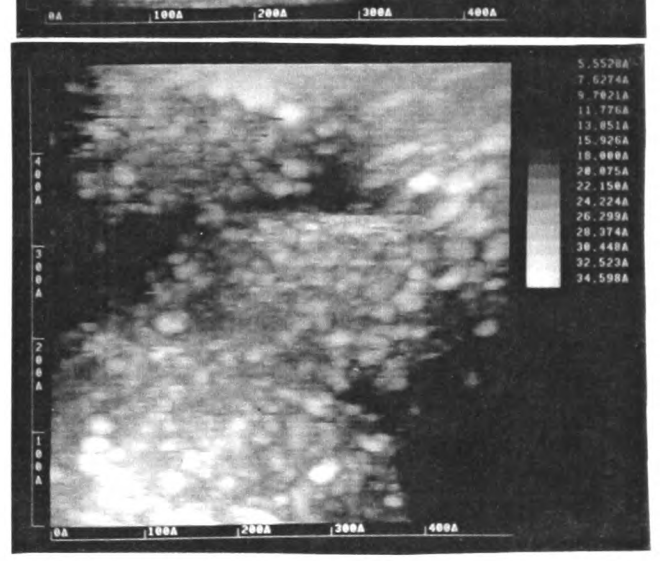

(e) 1200 mV

(f) 1200 mV

(g) 1200 mV

(h) 1200 mV

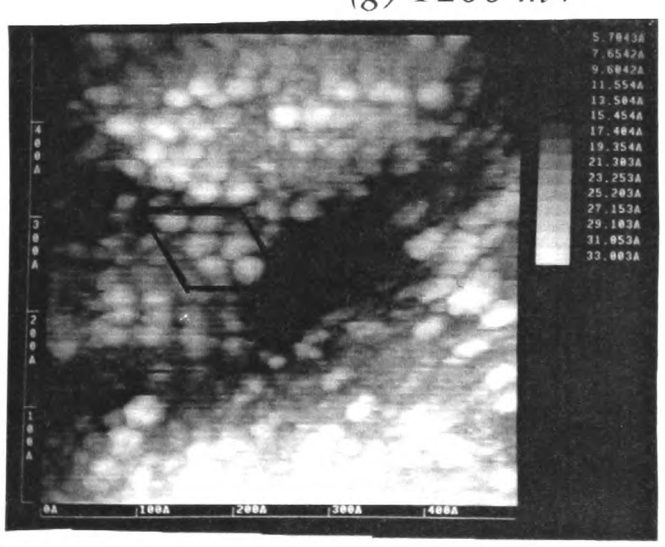

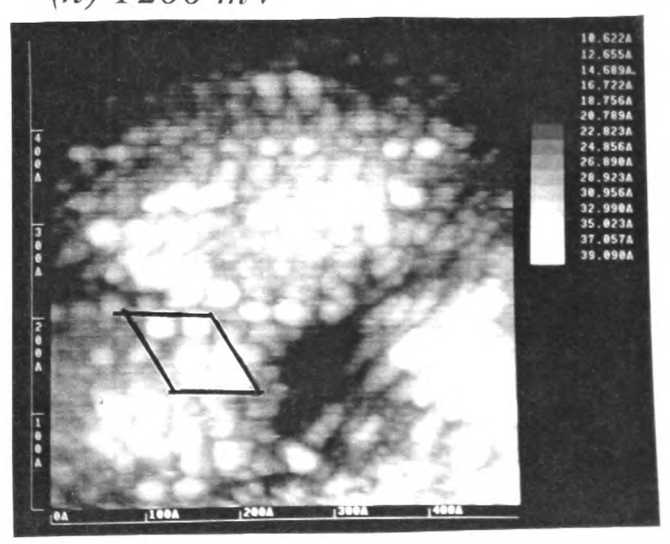

Fig. 5.4. Sample potentials only shown, full caption at end of series.

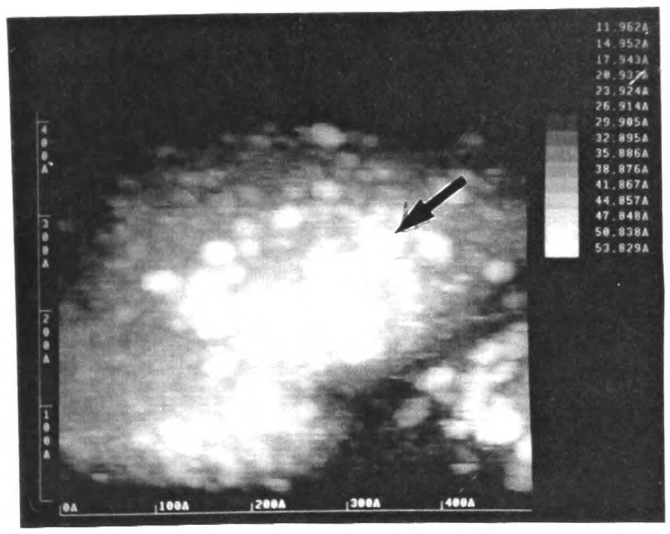

(i) 1000 mV

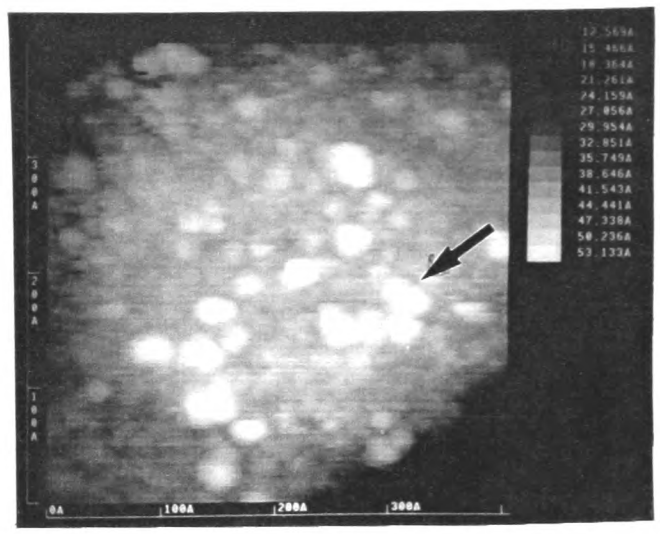

(j) 1000 mV

(k) 1000 mV

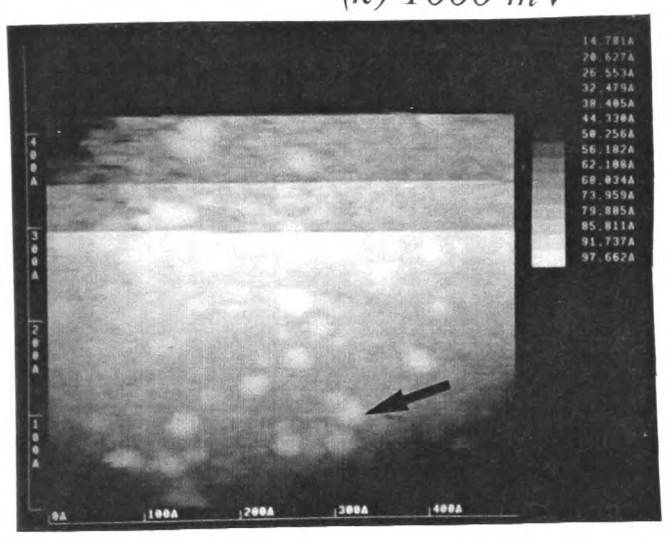

(l) 200 mV

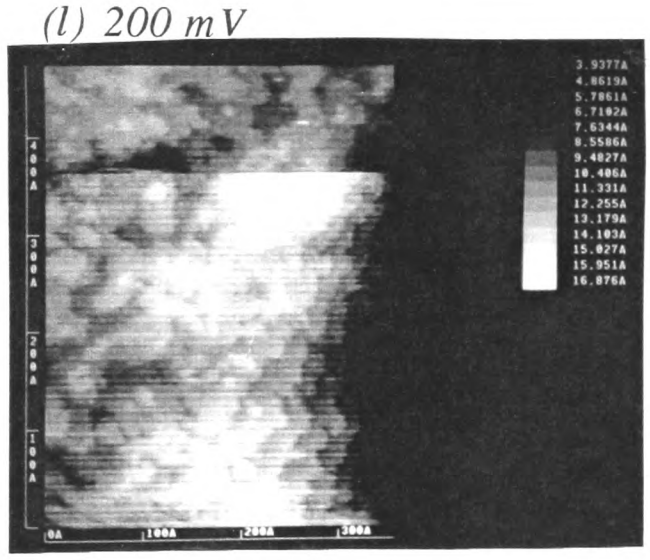

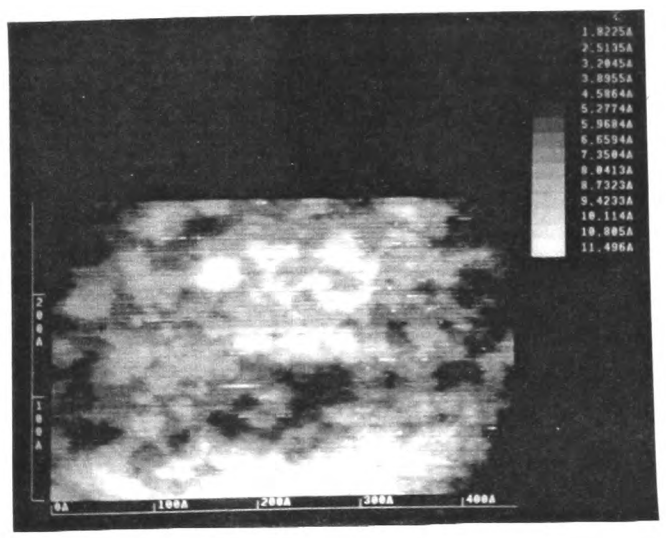

(m) 200 mV

Fig. 5.4. Images of gold electro-oxidation in phosphate buffer. Tip bias in all images -220 mV vs S.C.E., sample Au 4, image parameters fig. 5.4 (a) t: 2.5 ms, inc: 4Å, I_T: 12 nA, all other images t: 1.8 ms, inc: 3Å, I_T: 3 nA.

The tunneling bias voltage, for each image is the sum of the potential of the tip and the potential of the substrate, i.e. in fig. 5.4 (a), V_T is 295 mV.

The images may be described according to potential:

Potential/mV (vs S.C.E.)	Image	Comments
75	(a)	Poorly resolved grain, blurred plateau visible at bottom of image.
600	(b)	Flat plateau with terraces just resolved, irregular surface structure at top right apparently indicates holes in topmost gold layer.
800	(c)	Resolution of surface lost, although underlying topography that of a terraced grain.
1000	(d)	Topography appearing to be dominated by island growth.
1200	(e,f,g,h)	Surface becoming dominated by islands which increase in size with time (up to 15Å high in (h)). Some comparison between surfaces and an indication of instrumental drift is shown by the marked box.
1000	(i,j,k)	Island growth reversed as surface starts to smooth, an arrow indicates features common to each image.
200	(l,m)	Highly stepped irregular surface, (l) appears to show terracing. The surface is full of monatomic steps with the residual noise on each contour of the same height 1Å.

The irregular surface observed in (l) and (m) had not previously been imaged on a bare substrate, however there are similarities to features visible in (b).

Repetition of the experiment by potential stepping from the double layer region reproduced the behaviour described i.e. significant island formation did not begin until about 1200 mV vs S.C.E. and this growth was removed by returning to below 300 mV.

5.IV. *In-situ* STM study of gold under sulphuric acid.

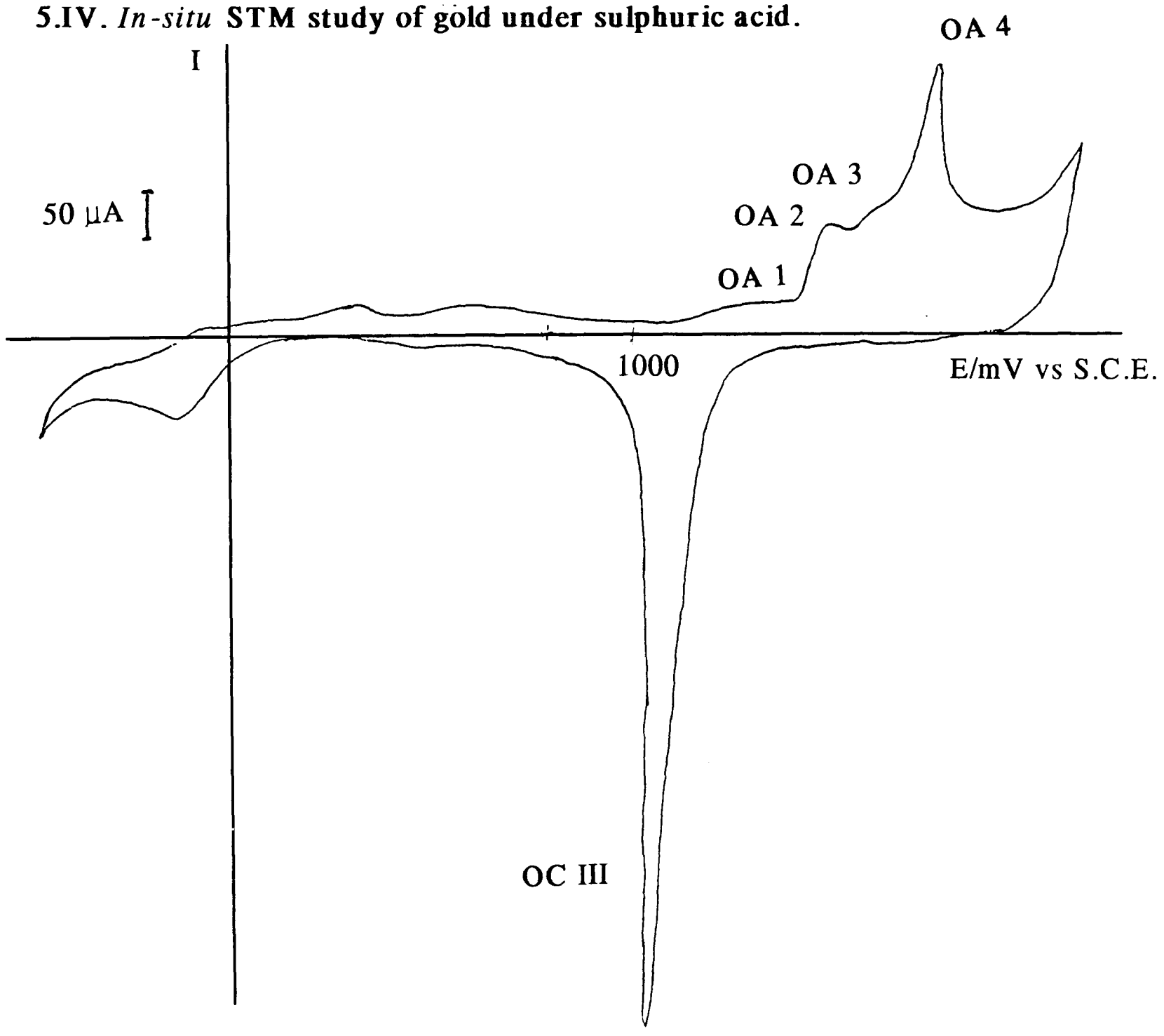

Fig. 5.5. Cyclic voltammogram of gold on mica in 0.5M H_2SO_4, scan rate 50 mVs^{-1}.

In these experiments the electrolyte was 0.5M H_2SO_4, and this was also used in the salt bridge supporting the mercury/mercurous sulphate (M.M.S.) reference electrode (400 mV vs S.C.E.). Following experimental observation and referring to Behm's work[88] the tip was biased at -400 mV vs the reference electrode (i.e. 0V vs S.C.E.). A representative CV for the *in-situ* system is shown in fig. 5.5. Bias voltages here are equal to the potential of the substrate, measured against a S.C.E. reference. All the samples shown here were Au 5.

5.IV.i. Imaging at potentials positive of the double layer region

Fig. 5.6 (a-n) shows a collection of images taken in an investigation of the oxidation of the gold surface. The experiment involved collecting images in a stepwise fashion; one at a potential in the double layer region, the other at a potential around the anodic oxidation peaks. Thus figs. (c), (e), (g), (i), (j), (k), and (m) are all taken at about 400 mV vs S.C.E. Approximately two minutes elapsed between each image as the potential was manually adjusted and the scan area slightly altered to compensate for drift and maintain imaging of the same area.

The images taken around the double layer region show a terraced region with an atomically flat plateau and monatomic steps clearly resolved. At more positive potentials the surface becomes covered with small islands and the bulk topography is only just discernible. The exception to this is at 745 mV, where although the surface is noticeably less well-defined than around 400 mV, steps are still visible.

The images show the oxidative processes causing significant surface rearrangement. Fig. 5.6 (a) shows a plateau and terraces adjacent to a bulk feature at the top right. On the flat area are two islands 15-20Å high

remaining from a sweep into the more cathodic potentials (presented in Section 5.IV.ii.) and holes adjacent to the bulk feature. After stepping to 1154 mV, fig. 5.6 (b), the islands (and some surface pits previously apparent) have been removed, fig. 5.6 (c), and the surface has rearranged to give a complete plateau. Moving to and from 1209 mV (figs. 5.6 (d) and (e)), causes more changes with a third step appearing around the now smaller plateau, possibly by collapse of the large terrace in the bottom left of fig. 5.6 (c), and the presence of a monatomic high island on the remaining terrace. This island is removed on the subsequent sweep to 1301 mV and again the plateau shrinks with movement of adjacent terrace step edges.

Figs. 5.6 (i), (j) and (k), consecutively taken at 402 mV after imaging at 1400 mV, show a monatomic pit has formed in the terrace surface and this, along with the now extremely small plateau visible at the top right of figs. (i) and (j), shrinks in size slightly over the three images. Step motion within these images is not noticeable. This hole disappears after the electrode potential was stepped to 1500 mV and again some rearrangement of steps between images is observable. Fig. 5.6 (k) taken after some scan area adjustment, appears to show the same area but here the plateau that seemed to have decreased in size considerably by fig. 5.6 (i), is now almost back to the size it was at the start of the series. Images above this potential were not attempted because of the possibility of the gold film lifting off the mica.

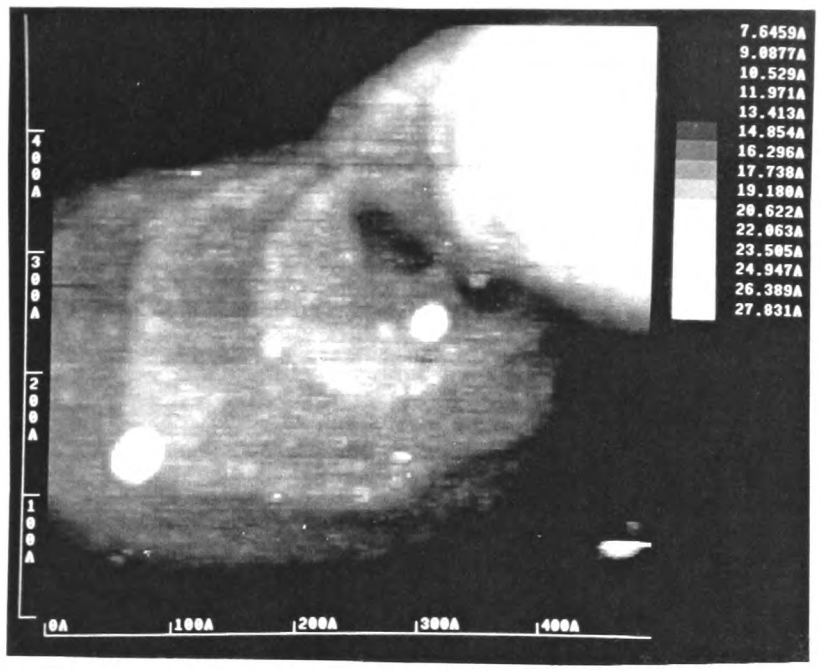

(a) 745 mV

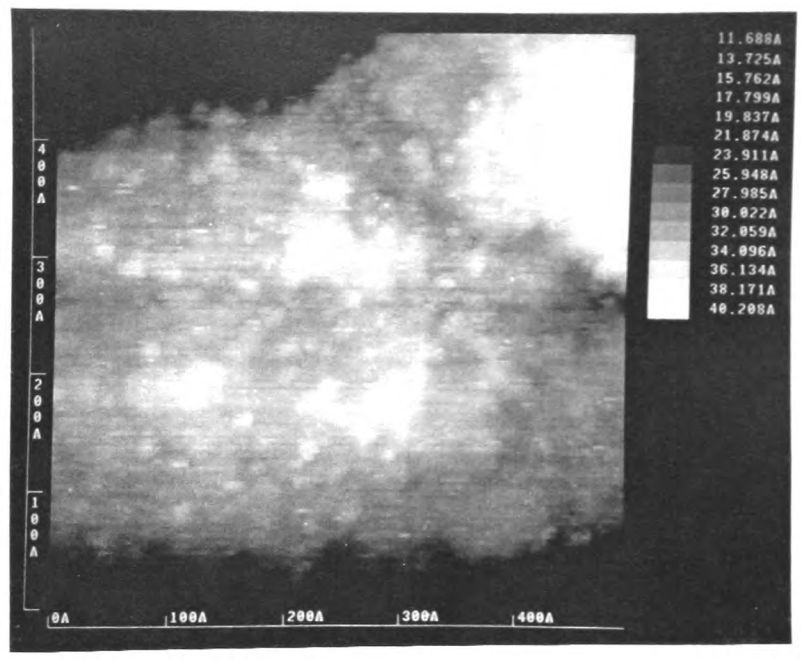

(b) 1154 mV

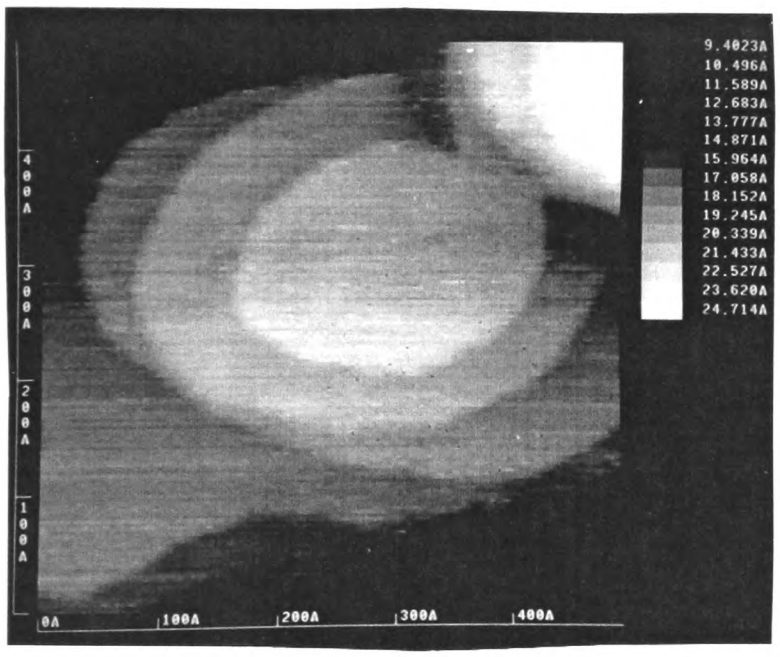

(c) 397 mV

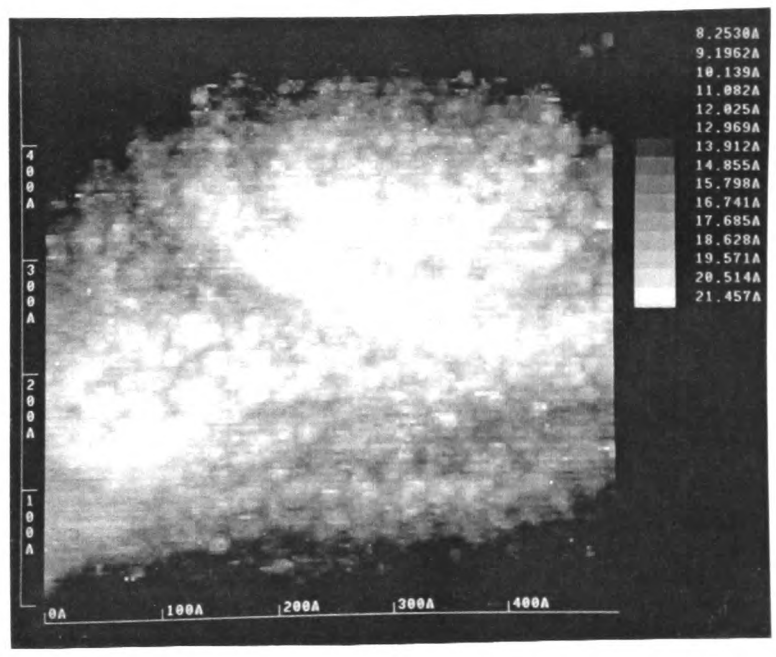

(d) 1209 mV

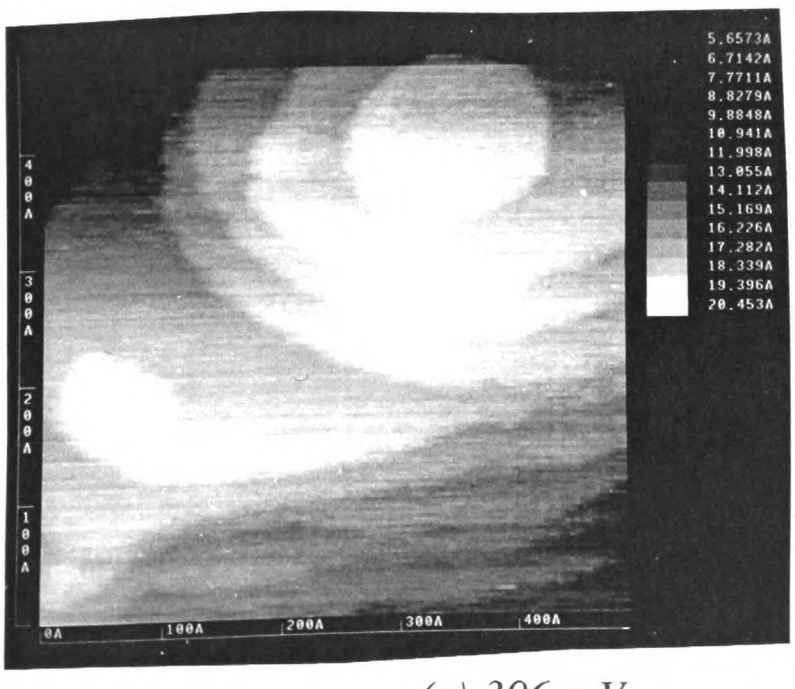

(e) 396 mV

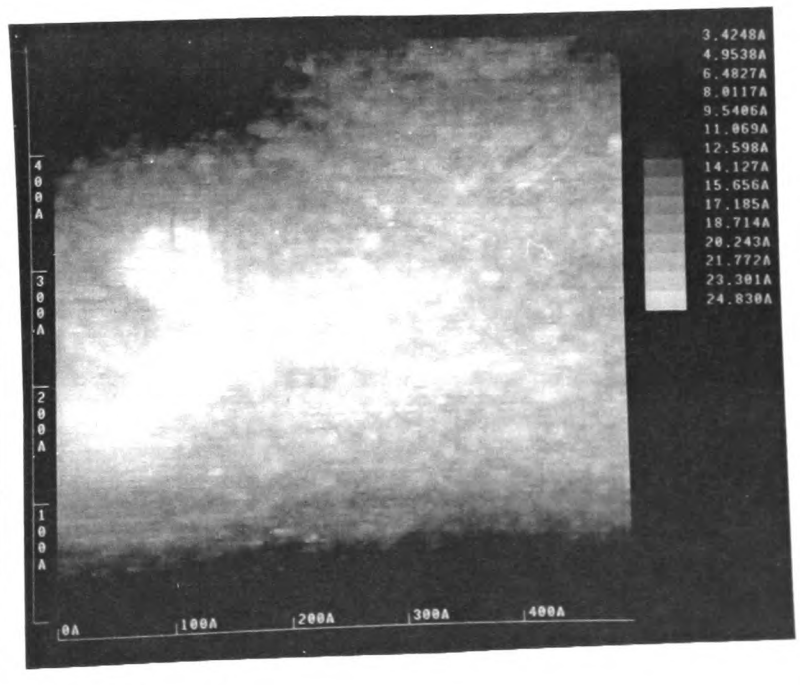

(f) 1301 mV

Fig. 5.6. Sample potential only shown, full captions at end of series.

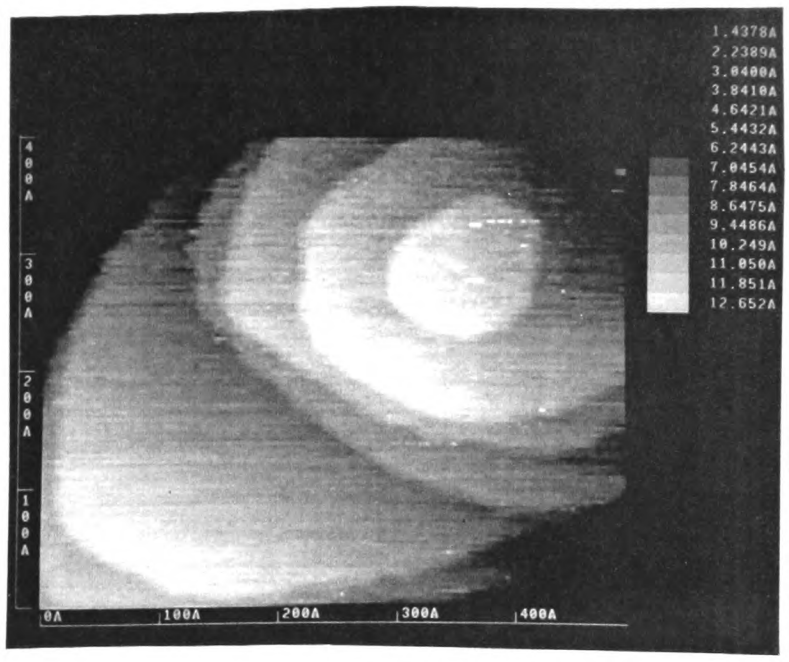

(g) 397 mV

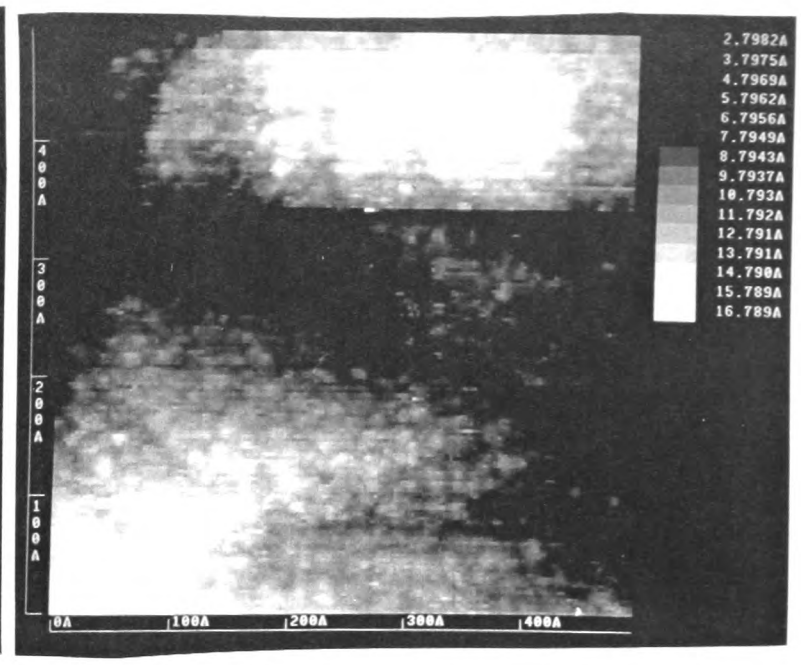

(h) 1400 mV

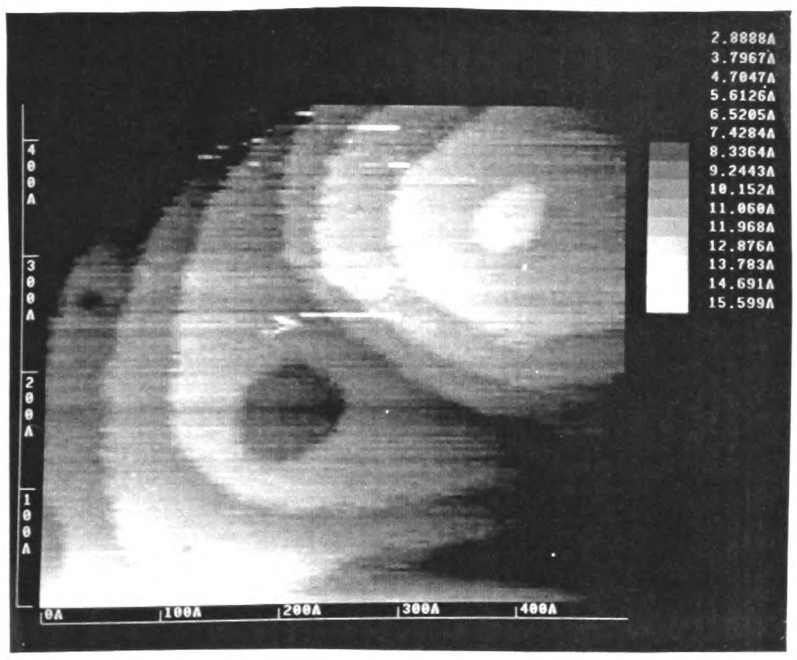

(i) 402 mV

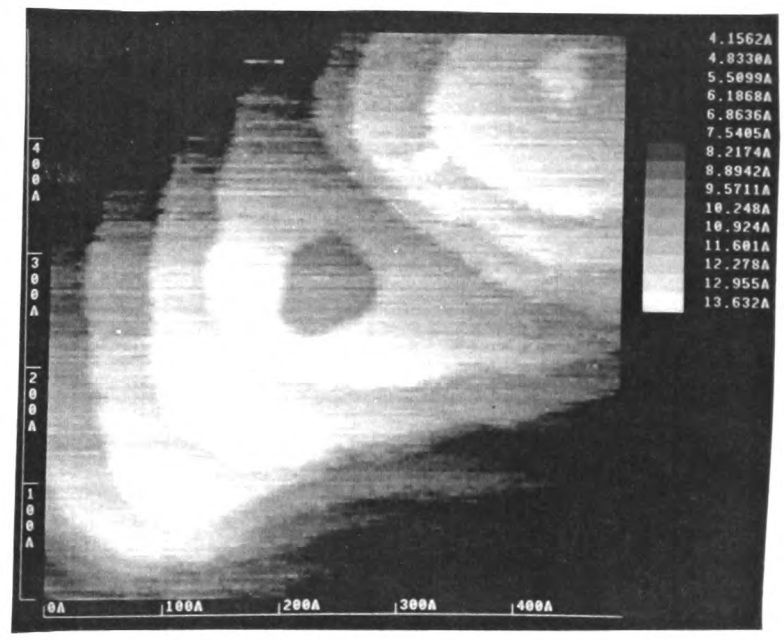

(j) 402 mV

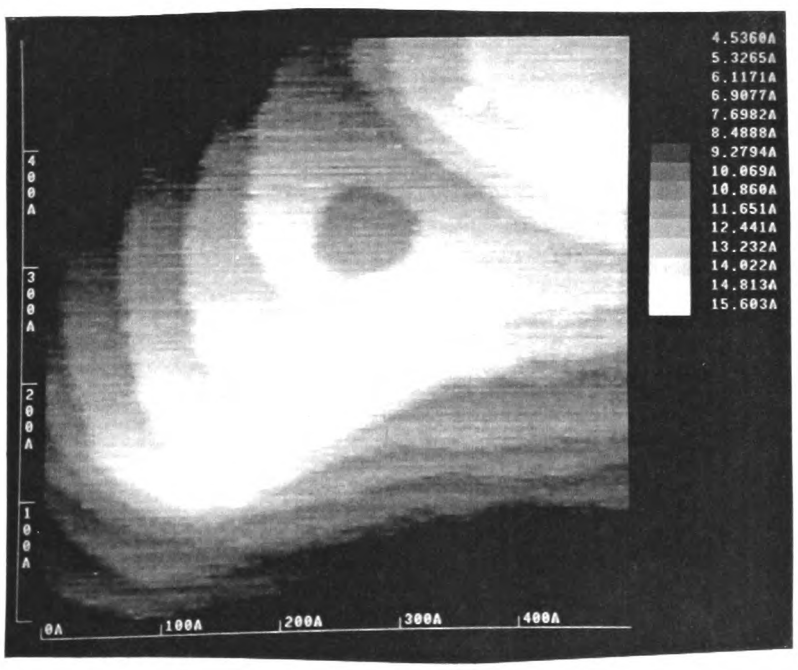

(k) 402 mV

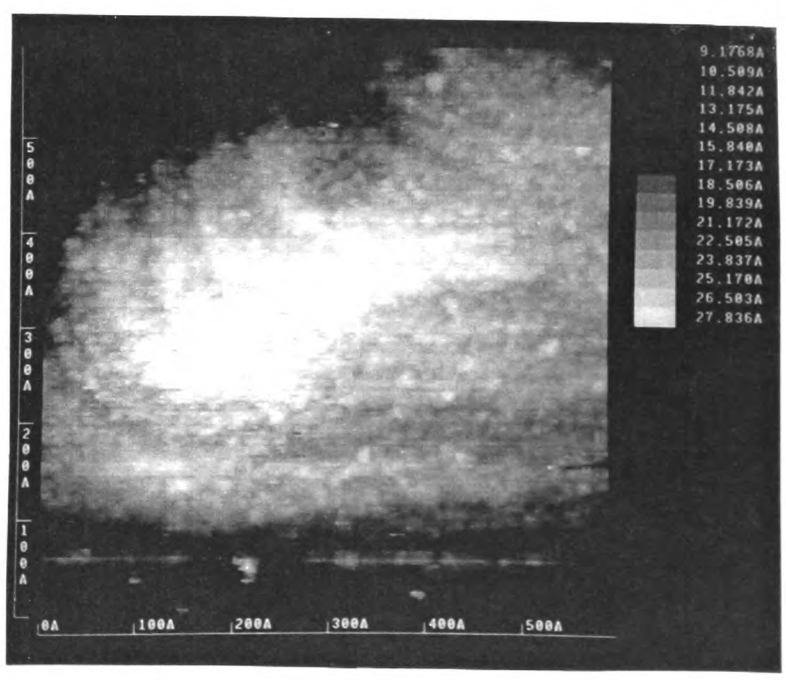

(l) 1500 mV

Fig. 5.6. Sample potential only shown, full captions at end of series.

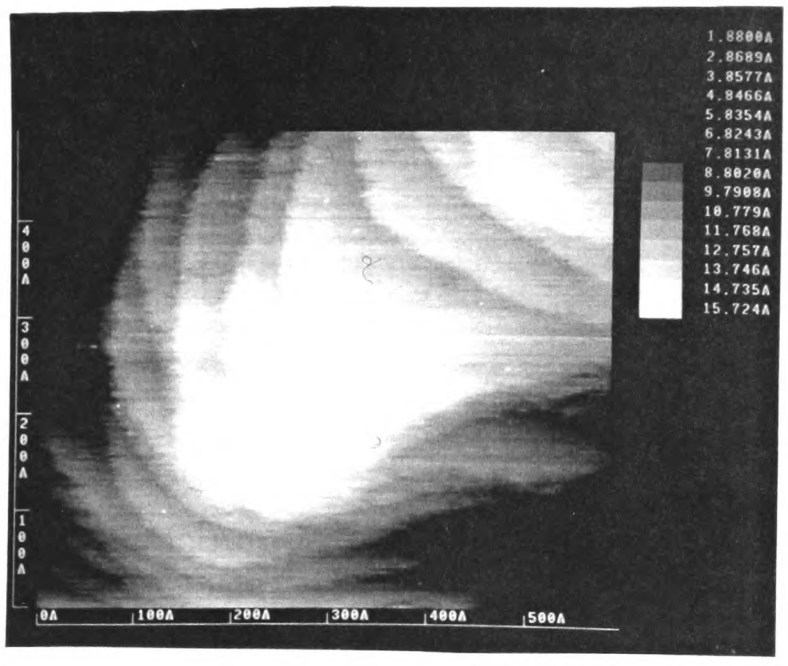

(m) 392 mV

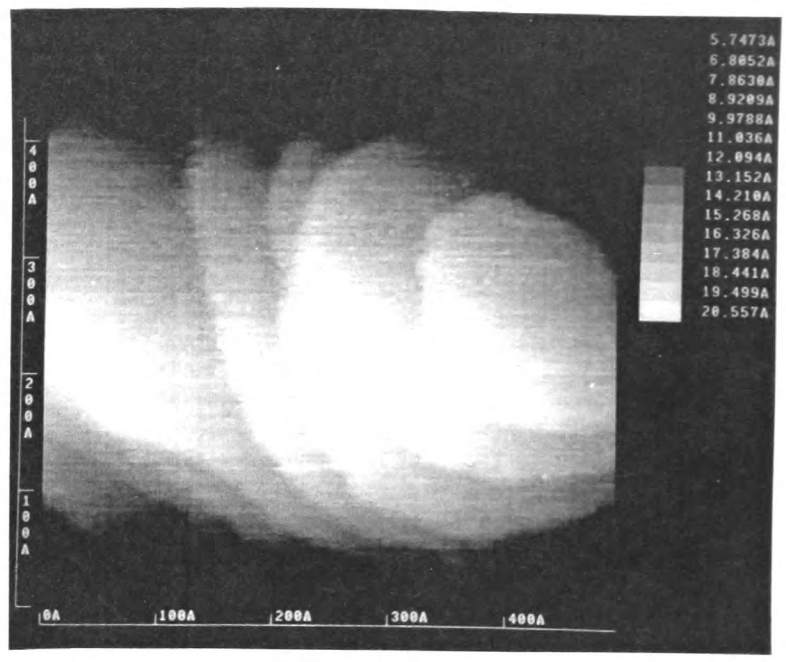

(n) 202 mV

Fig 5.6. Images showing the electro-oxidation of gold on mica by 0.5M H_2SO_4. All images t: 1.5 ms, inc: 3Å, tip potential 0V vs S.C.E. I_T: 3 nA.

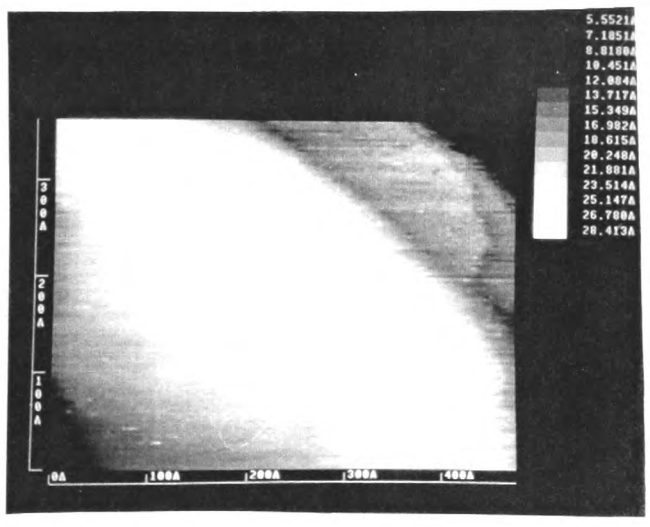

(a) 650 mV

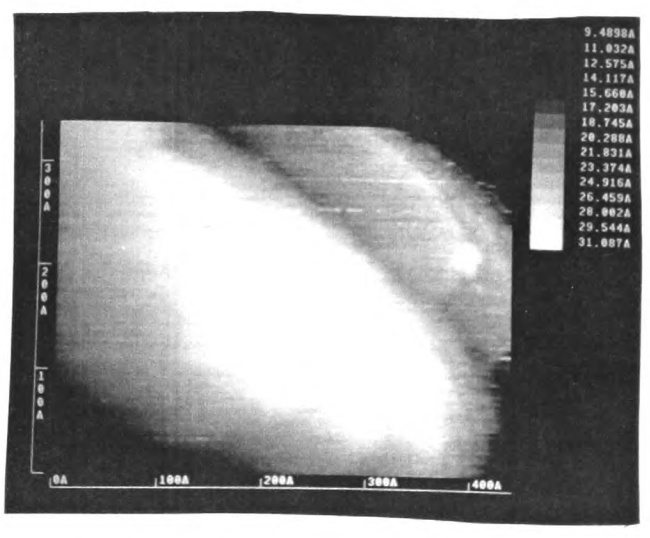

(b) 450 mV

Fig 5.7. Image of a gold substrate in 0.5M H_2SO_4. Tip potential 0V vs S.C.E., t: 1.8 ms, inc: 3Å, I_T: 4 nA.

A previous study using this stepwise method of imaging yielded the results shown in figs. 5.7, 5.8 and 5.9. These three sets of images were all collected in the same experiment but, because of drift and general instability, it was not possible to image the same area for a prolonged period. Thus each figure, although part of the same investigation was collected at a physically different location. Fig. 5.7 (a), taken at 650 mV, shows slight surface roughening which is similar to that shown in fig. 5.8 (a) taken at 860 mV. At 965 mV, fig. 5.8 (c), the surface is showing mobility and there the plateau step edges have rearranged considerably compared to the topography given in the double layer. Obscuring of the surface by roughening is shown in fig. 5.9 (b) taken at 1002 mV and some hole formation is shown on the top left plateau.

Holes like those seen in fig. 5.6 (a) have not been imaged on bare gold on mica samples, and it is proposed that they are present due to cycling the substrate to over 1000 mV vs S.C.E. earlier in the experiment. It appeared over a number of experiments that pitting of the surface could take place at potentials higher than 900 mV vs S.C.E.

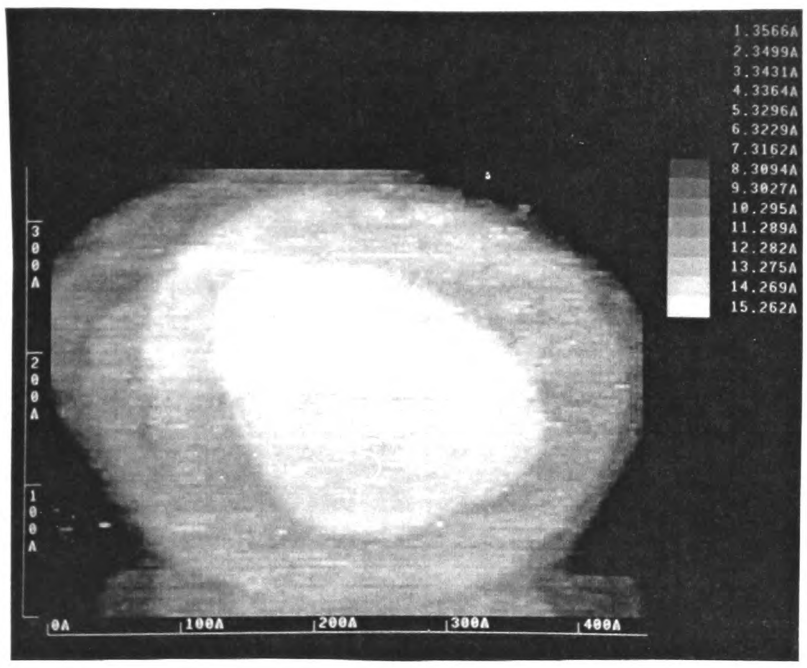

(a) 860 mV

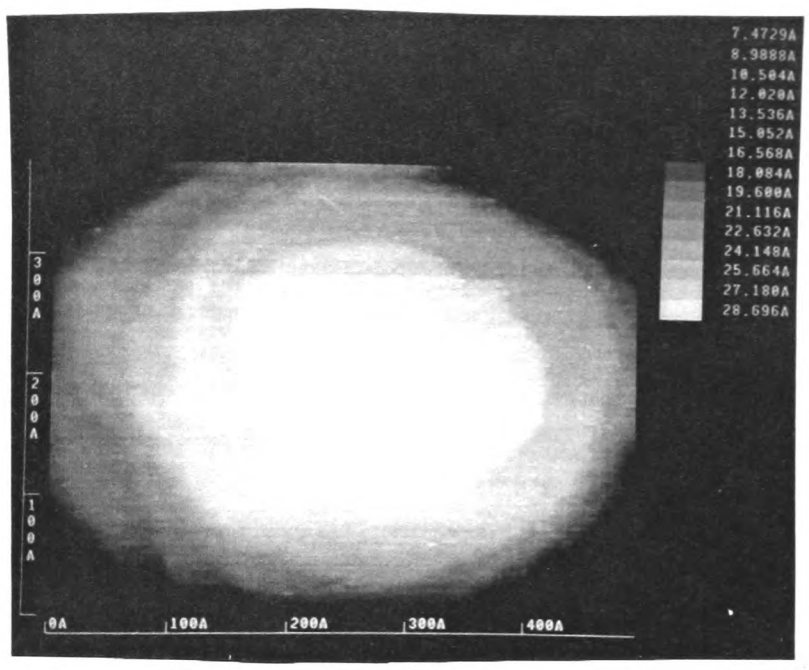

(b) 446 mV

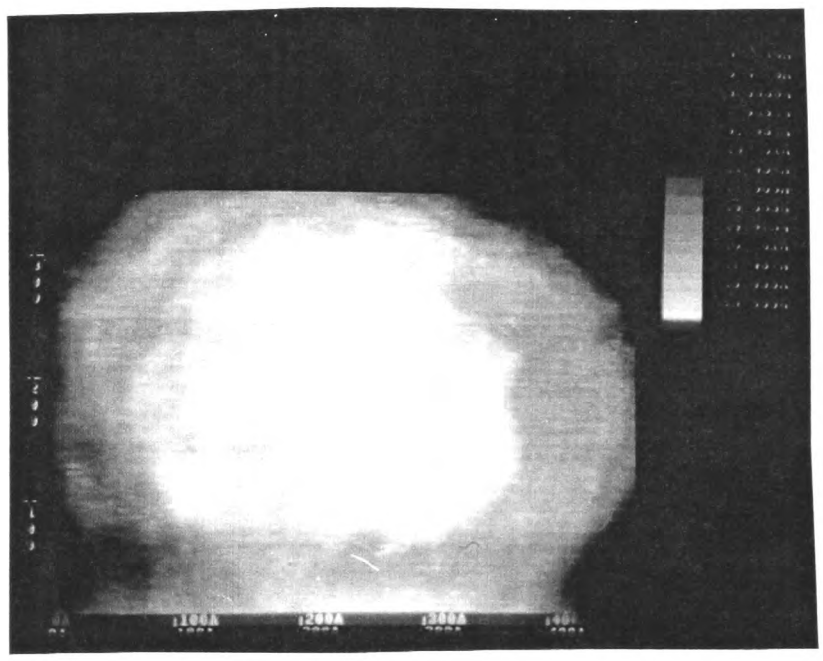

(c) 965 mV

Fig 5.8. Scan parameters as 5.7.

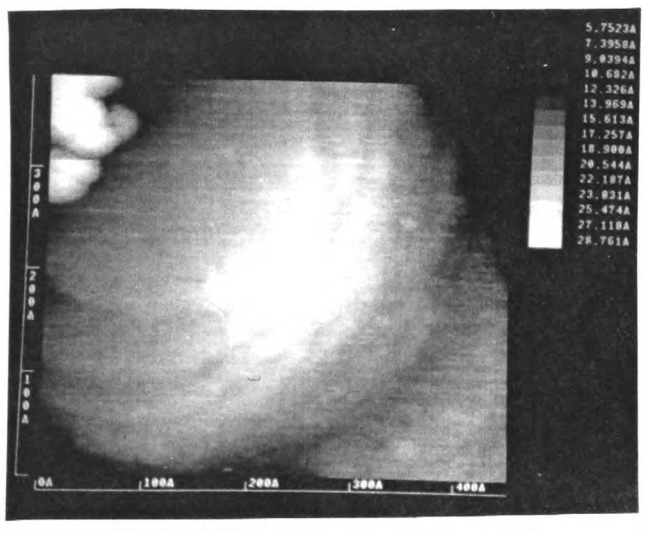

(a) 425 mV

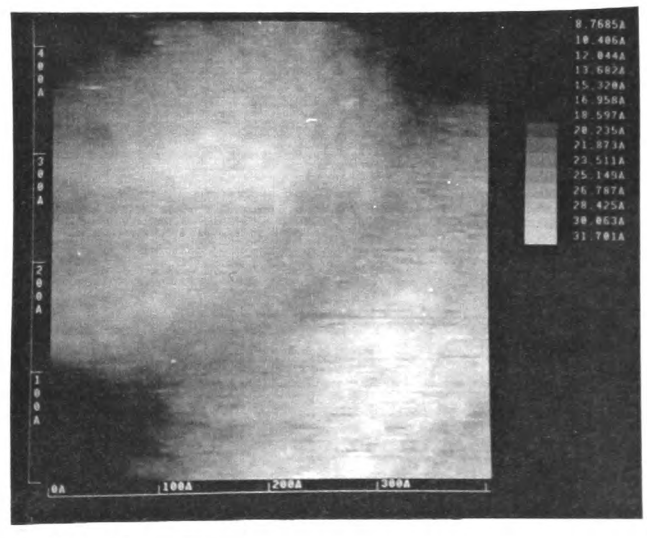

(b) 1002 mV

Fig. 5.9. Scan parameters as fig. 5.7.

5.IV.ii. Imaging at potentials negative of the double layer region.

Figs. 5.10 (a)-(e) show the region of image 5.6 (n) during a sweep to potentials negative of the double layer region. Here, as the surface modifications were less obvious, consecutive images were taken at increasingly negative potentials without returning to the double layer region. As shown in fig. 5.6 (n) the surface is smooth and clear at 202 mV but on the series of images in fig. 5.10 small (approximately 30Å wide, monatomic height) islands are visible, which are removed on returning to 395 mV (fig. 5.10 (e)). No step edge motion is visible in the images. Repetition of the experiment at lower resolution failed to image the same features, but at -501 mV the surface started to break up due to gas evolution.

Figs. 5.11 (a)-(c) show a surface after biasing for approximately 80 minutes at -207 mV, an arrow locates a step edge common to each image. The experiment was unintentional and resulted due to a complication in setting tunneling parameters. At -207 mV the surface is covered with monatomically high islands while at 205 mV, the number of islands has decreased until at 409 mV the surface is clear.

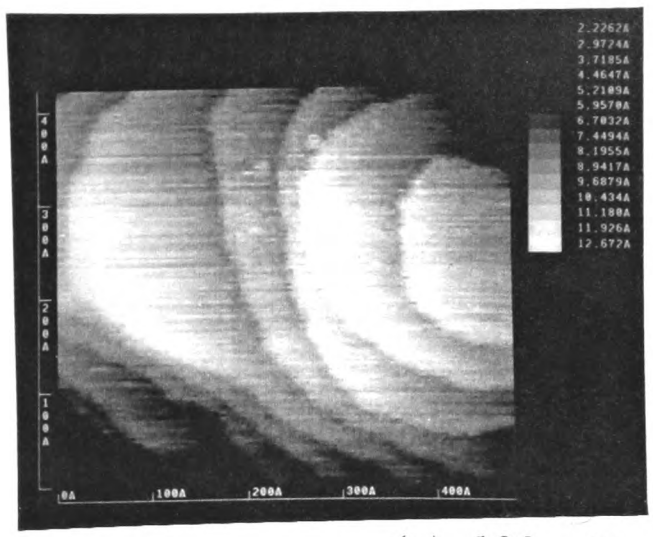

(a) -100 mV

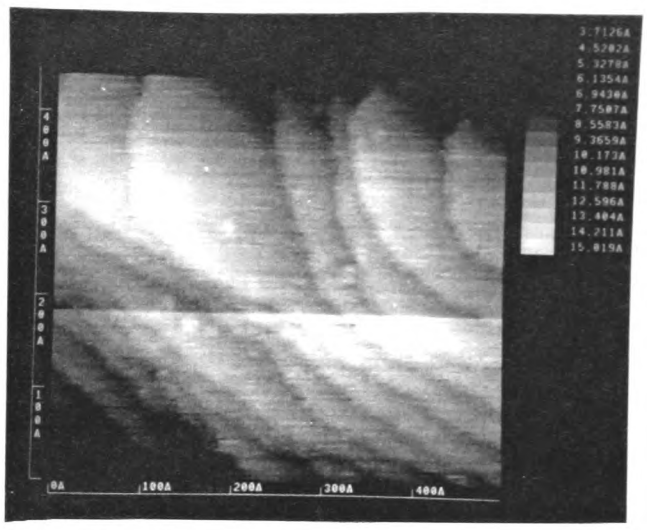

(b) -200 mV

(c) -320 mV

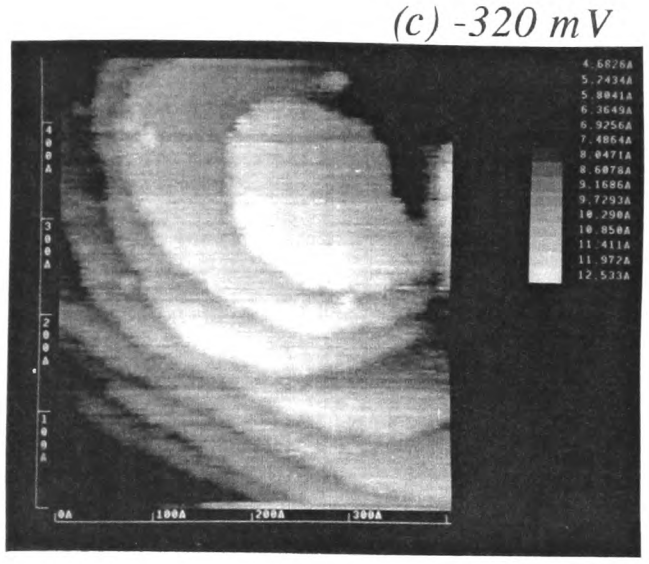

(d) -400 mV

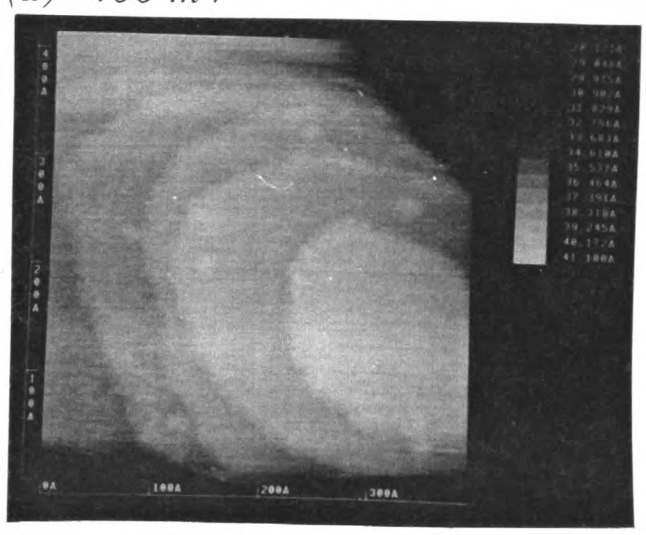

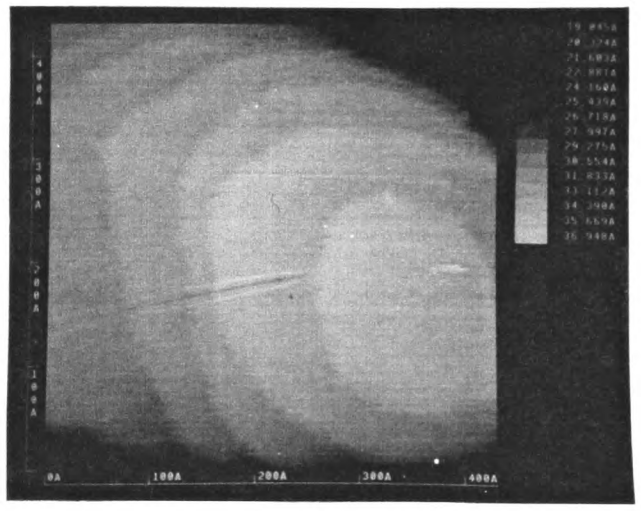

(e) 395 mV

Fig. 5.10. Images of a gold substrate in 0.5M H_2SO_4 during a potential sweep towards the hydrogen evolution region. Imaging parameters as fig. 5.6. Potentials vs S.C.E. as shown.

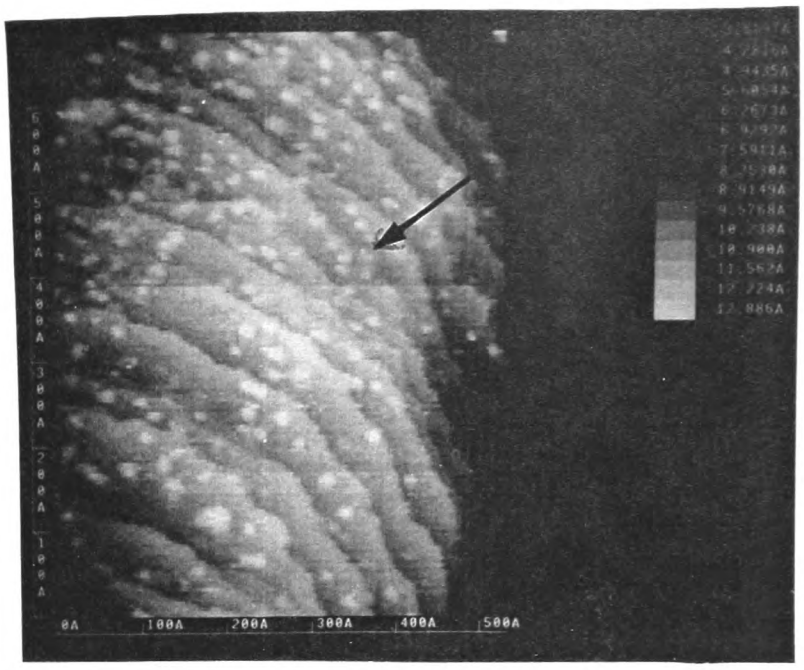

(a) -207 mV

(b) 205 mV

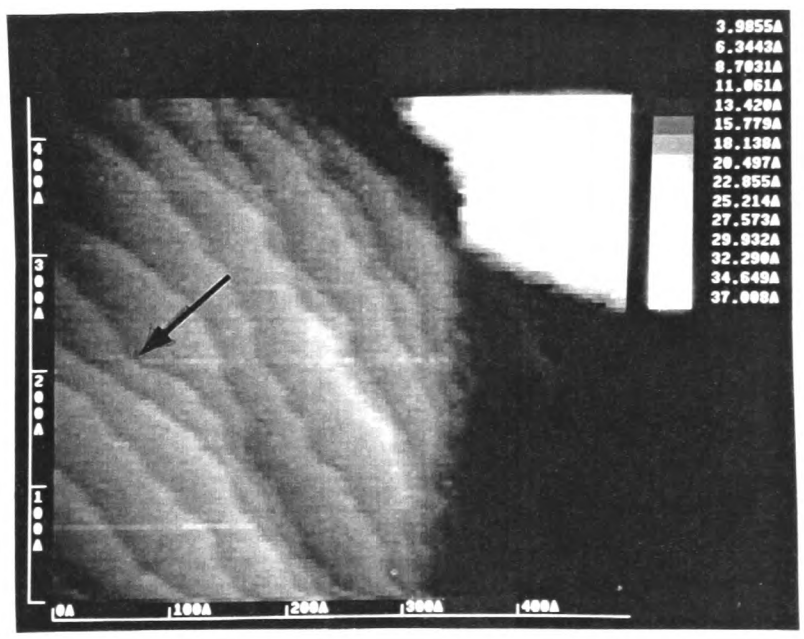

(c) 409 mV

Fig. 5.11. Images of potential dependent features found on gold after biasing at -207 mV. (t: 1.6 ms, inc: 4Å), I_T 5 nA. Potentials vs S.C.E. as shown.

Figs. 5.12 (a) and (b) show the results from another experiment where the surface potential was manually adjusted to -900 mV and immediately taken back to the double layer region (402 mV), while between images (b) and (c) the potential was stepped down to -950 mV.

All the images in fig. 5.12 show the presence of monatomic high islands, not seen on bare substrates or in the double layer region. These islands slowly decrease in width with time spent at the double layer region as shown by figs. 5.12 (c) and (d) (reference point on image arrowed) and their disappearance is speeded by the increase in potential shown by fig. 5.12 (e), taken at 502 mV.

To further investigate the implication of this observation, excursions to positive potentials were carried out. Figure 5.13 (a) shows a terraced area of surface at 1023 mV. As expected from the results in Section 5.IV.i. the surface is rougher, there is evidence of pitting in the lower terrace and a feature appears to be forming on the steps. This feature is not present in the following scan, fig. 5.13 (b), taken at 401 mV. Image 5.13 (c) (401 mV) of an adjacent area of surface shows the presence of monatomic islands on the terraces. The surface was then swept to 1105 mV, fig. 5.13 (d), and returned to 396 mV, fig.5.13 (e), where larger islands, 10Å high, have been formed. The series of images (e)-(h) taken at 396 mV appear to show some mobility of these objects as an extra island appears between (e) and (f) and some islands around the main feature at the top left have disappeared by the last image. It should be noted some multiple tip imaging is taking place as indicated by the repetition of features in the image about the axis indicated, and the arrowed features in fig. 5.13 (f) are artifacts.

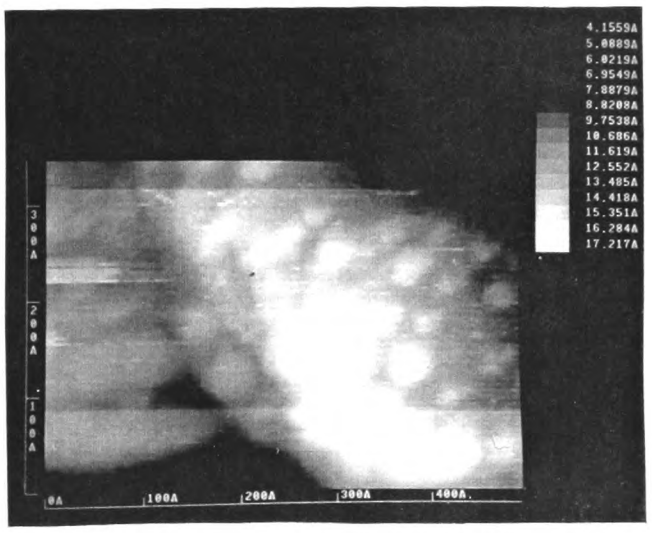

(a) 402 mV

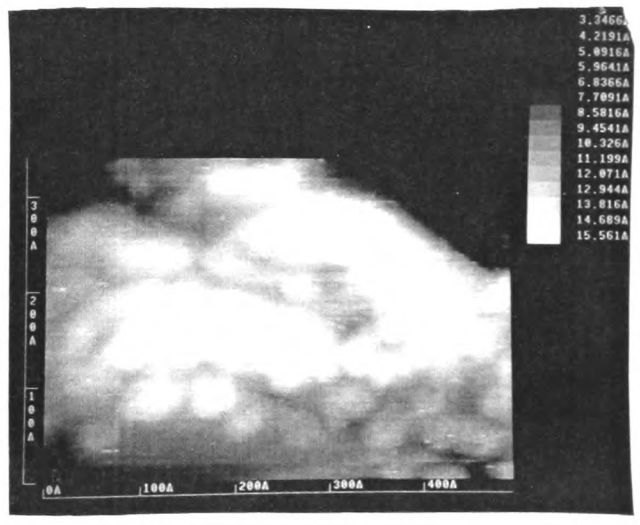

(b) 402 mv

(c) 385 mV

(d) 385 mV

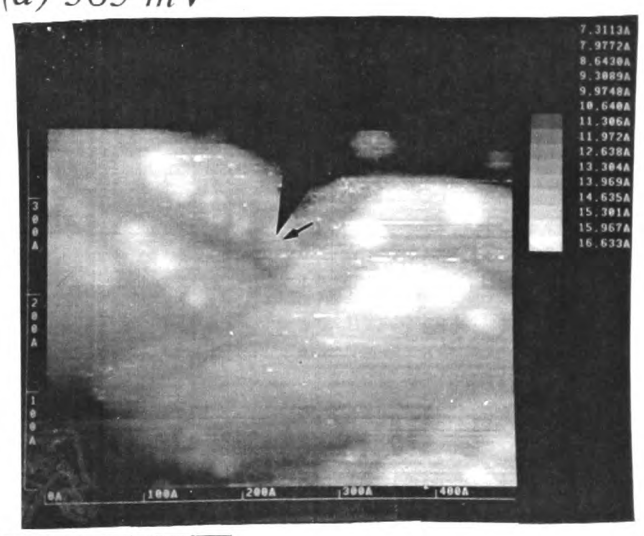

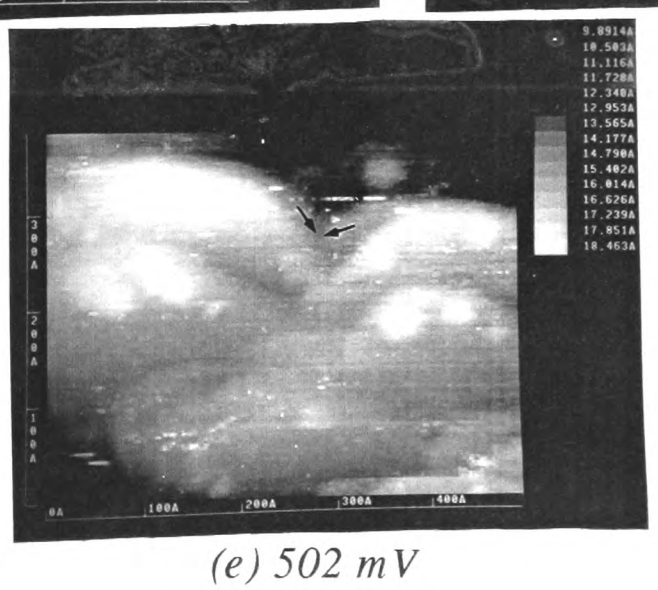

(e) 502 mV

Fig. 5.12. Images of a gold surface after transient excursion into hydrogen evolution. Scan conditions as fig. 5.6. Potentials vs S.C.E. as shown.

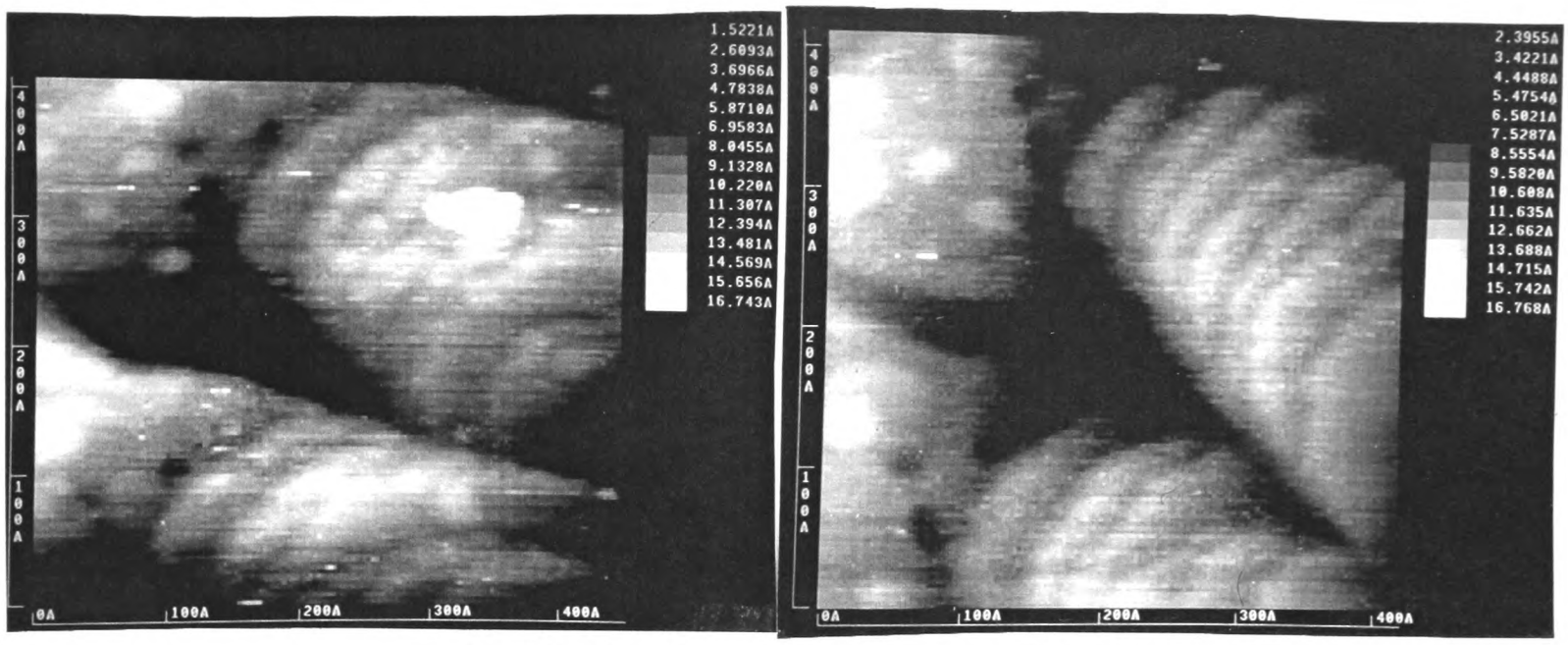

(a) 1023 mV *(b) 401 mV*

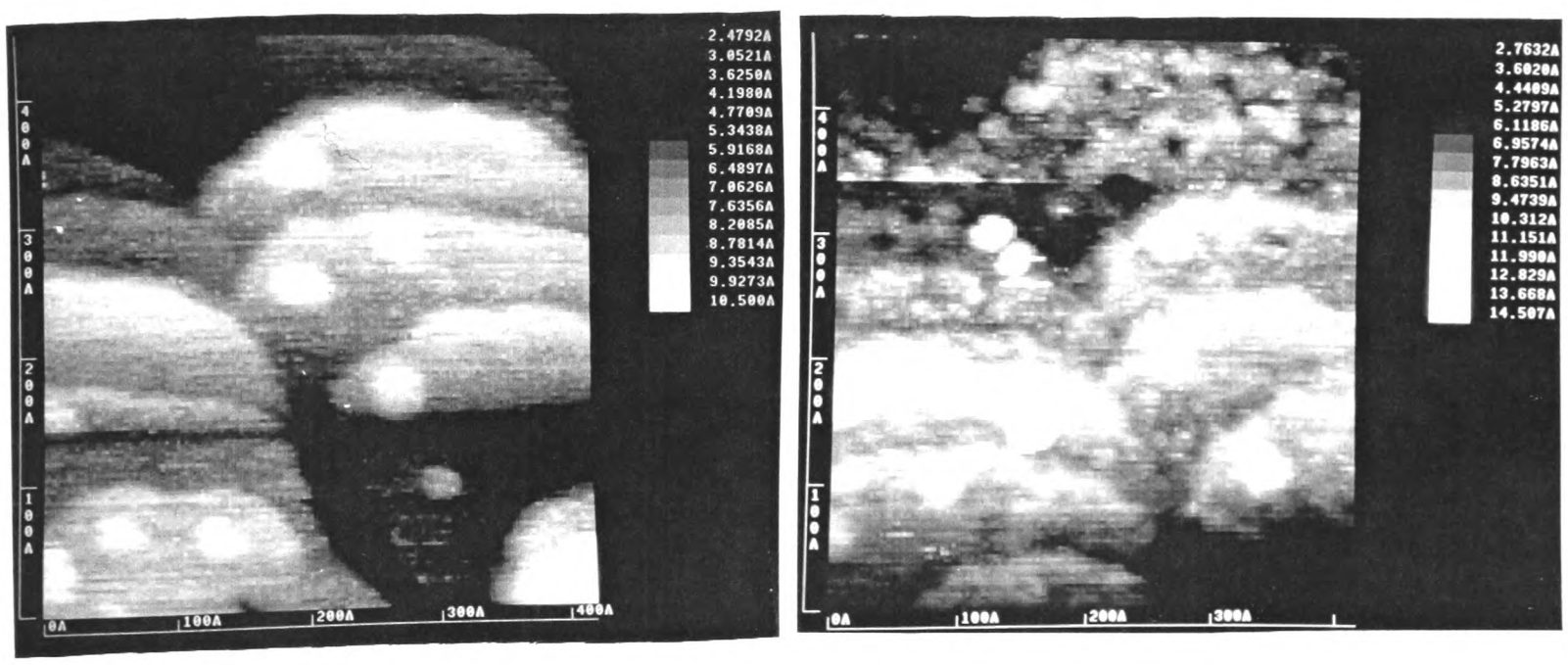

(c) 401 mV *(d) 396 mV*

Fig. 5.13. Caption on following page.

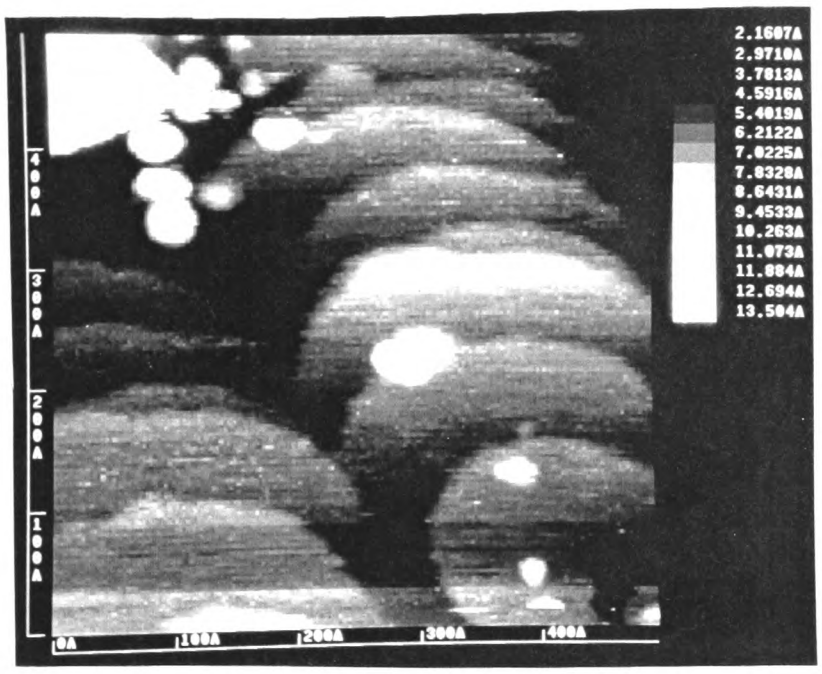

(e) 396 mV

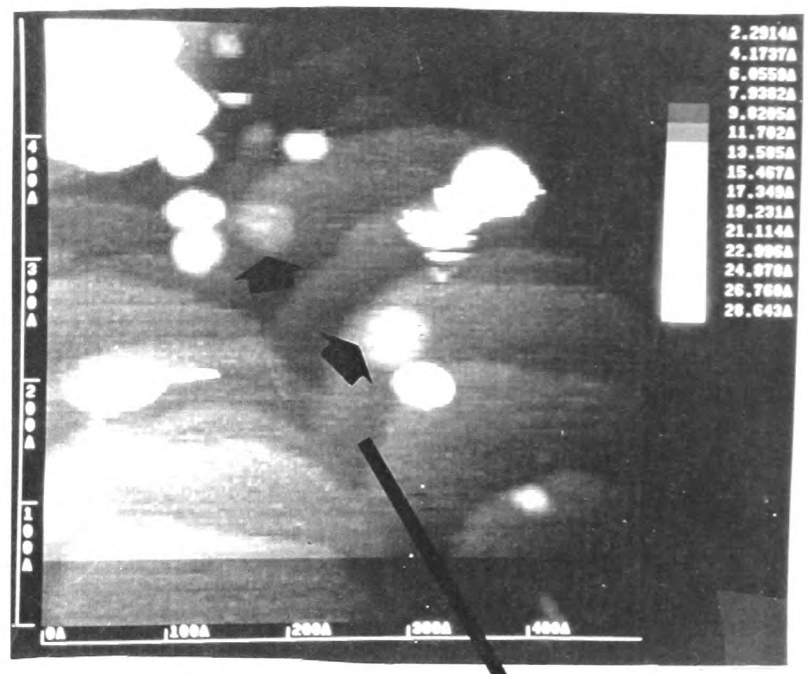

(f) 396 mV

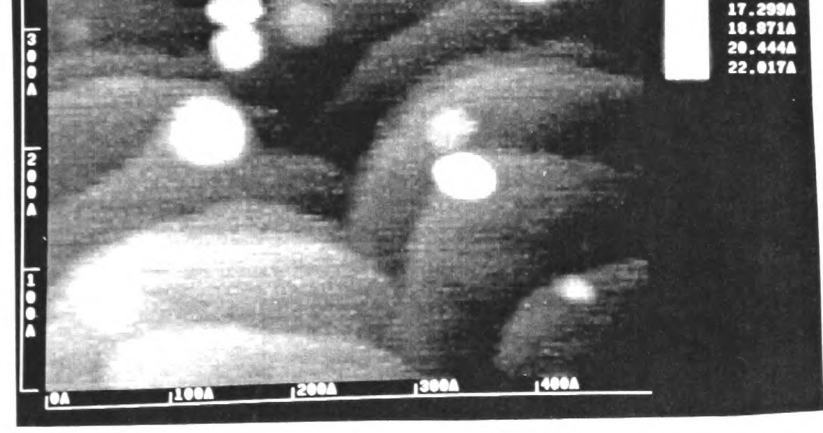

(g) 396 mV

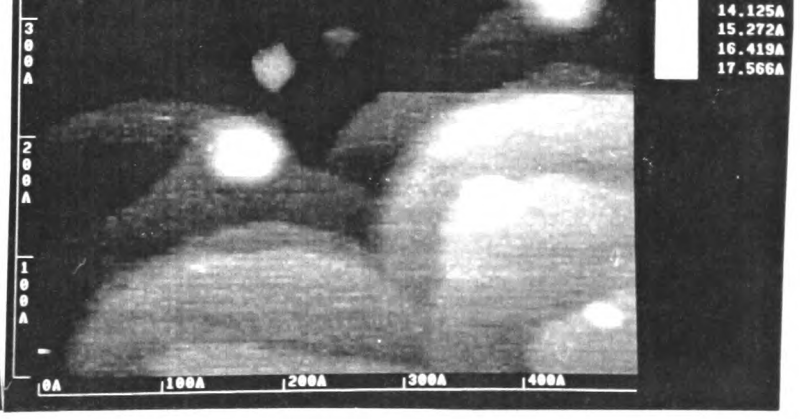

(h) 396 mV

Fig. 5.13. Images of the gold surface of fig. 5.12 during and after excursions to oxidative potentials. Scan parameters as fig. 5.12.

5.V. Discussion

In this Section the results from imaging gold surfaces at potentials positive of the double layer region are dealt with before those results arising from excursions negative of the double layer region. Within this framework as the studies under sulphuric acid electrolyte gave the most comprehensive results, those images are analysed before discussing the electro-oxidation of a gold surface under phosphate buffer.

5.V.i. Tip condition

Figures 5.14 and 5.15 show the cyclic voltammetry of tungsten wire in phosphate buffer and sulphuric acid respectively. Around 50 mm of 0.2 mm diameter wire was cleaned in tip etching solution (approximately 2M sodium hydroxide) at 2.5V a.c. with a platinum counter electrode, to mimic the surface state of the tip after preparation. About 30 mm of wire was in contact with the solution when the cyclic voltammetry was carried out using the STM cell. Fresh samples were used for each CV, the sample for the sulphuric acid experiment was stored in distilled water prior to use.

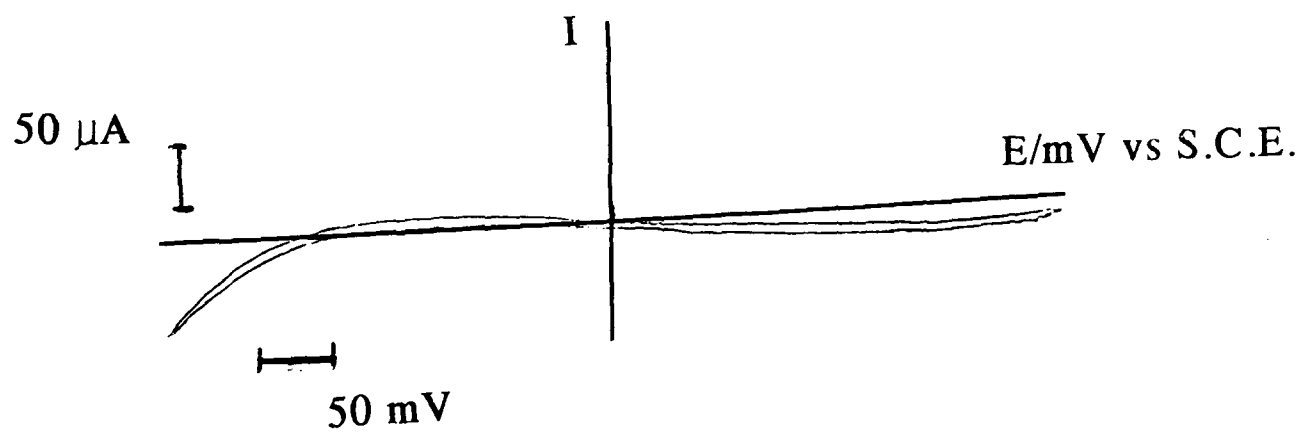

Fig 5.14. Cyclic voltammogram of 'cleaned' tungsten wire in phosphate buffer. Scan rate 50 mVs^{-1}.

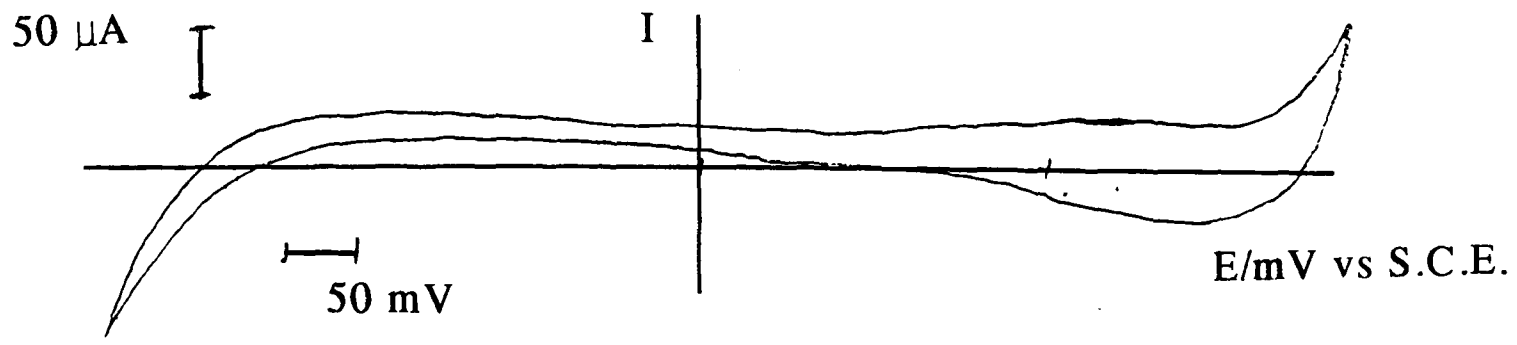

Fig 5.15. Cyclic voltammogram of 'cleaned' tungsten wire in 0.5M H_2SO_4. Scan rate 50 mVs^{-1}.

Both voltammograms show the tip was biased in the double layer region during *in-situ* STM experiments. It thus appears that at these potentials the tip is neither being corroded nor causing electrolysis of the solution. It is probable that the tip has some type of oxide coating.

5.V.ii. General comments

STM can be at times a rather temperamental technique with drift, jumps to different areas and tip instability all giving problems. Such problems are exacerbated while working *in-situ* under electrochemical control, particularly when a series of images at varying potentials is required. Thus sequences of images were often collected without fully investigating the time-dependent behaviour of modified surfaces at a given potential.

It should again be noted that the tunneling bias voltages vary continuously throughout these experiments, although as the surfaces are predominantly metallic in character this is not thought to make any significant difference to imaging (see Section 1.IV).

It is possible that the tip 'shields' the surface and hinders the approach of species to the electrode surface in *in-situ* STM work (a double layer thickness of 10-20Å may be of the same order of magnitude as the

tip-sample separation), but as yet no evaluation of this has been carried out. As the processes discussed here involve interaction of the surface and electrolyte immediately close to the surface, 'shielding' is unlikely to be important here.

5.V.iii. Electro-oxidation of the gold surface in sulphuric acid

Angerstein-Kozlowska *et al.* have carried out a thorough study of the oxidation of low index planes of gold[209,210] in perchlorate and sulphate electrolytes and the CV shown in fig. 5.5 is in good agreement with that expected for an Au (111) oriented surface in sulphuric acid (some convolution of the CV with that for a polycrystalline sample is to be expected because of the gold wire connection used). This result is consistent with the sample preparation method used (see Section 4.IV.). In this system the sulphate and/or hydrogen sulphate anions are strongly specifically adsorbed.

The oxidation of gold to form a monolayer oxide is a two electron process and can be represented by[210] :

$$M + H_2O \Longleftrightarrow MOH + H^+ + e^-$$

$$MOH \Longleftrightarrow MO + H^+ + e^-$$

where MOH and MO do not represent stoichiometric phases but indicate the state of adsorbed species. The oxide formation region of fig. 5.5 is labelled according to the nomenclature of references 209 and 210 where the order of numbering of the anodic (A) peaks is based upon the order in which they appear in the CV and the associated degree of surface oxidation. The labelling of the cathodic (C) peaks correlates to the reduction of the appropriate surface state formed on the anodic sweep. The proposed mechanism for gold electro-oxidation is outlined briefly. OA I,

II and III are oxidation peaks due to the formation of consecutive MOH sublattices, each requiring a slightly different energy, which overall represent the transfer of one electron to the gold surface, per gold atom, giving an MOH monolayer.

In the gold/sulphuric acid system the strong adsorption of the electrolyte anions means the rearrangement of the surface (place exchange, see Chapter 1, fig.1.6), induced by the repulsive interactions of the MOH dipoles, is only possible by the gradual desorption of the HSO_4^-/SO_4^{2-} species. The process leading to what is thought to be a two atom thick layer is termed 'replacement turnover' and this phase is the basis for bulk oxide formation at more positive potentials. As there are now no longer separate lattices the second electron is transferred in a single peak OA 4, in the same way the reduction process only yields a single peak. The blocking effect of the anions in this electrolyte is proposed to hinder the formation of the MOH species to such an extent that the replacement turnover process is indistinguishable from the formation of MO.

The results presented in Section 5.IV. (figs. 5.6 - 5.9) are comparable to the work of Itaya *et al.*[92] and Trevor *et al.*[90] who studied the oxidation of gold under a perchlorate electrolyte (used in the mechanistic studies outlined above as a weakly adsorbing anion). Also relevant is the work by Behm *et al.* on the Au (100) surface[88].

Inspection of these images provides three distinct regions (the discontinuities between regions arise from the STM data);

A from the double layer region (200 mV) up to approximately 650 mV the surface structure is apparently unaffected by changes in potential,

B between 750 mV and 1050 mV imaging shows a 'cloudy' surface and considerable step movement is visible, returning to the double layer region from these potentials shows movement of steps,

C above 1150 mV the surface is visibly roughened with a corrugation below that of the height of a gold monatomic step, returning to the double layer from these potentials may show pitting or island formation on the surface in addition to step movement.

The roughening and mass transfer associated with region C, can be attributed to the 'replacement turnover' process where place exchange causes lifting of gold atoms out of the first substrate layer. Mass transport leading to pitting may be rationalised by gold dissolution and/or surface diffusion by displaced material on reduction of the oxide layers[92]. Deposition (and/or nucleation) of this gold provides an explanation for island formation. In contrast to work in perchloric acid[90,92], pitting here was found after excursions to potentials around OA 3/4 whereas in those studies potentials between OA 4 and bulk oxide formation were required. Suggestions that species such as Au_2O_3 are responsible for gold dissolution[92] may be appropriate here although more work needs to be done before arriving at this conclusion.

The low corrugation height of the images at higher potentials supports the proposal that the phase formed at this point is only due to reaction of a monolayer of gold. The observation of both the island in fig. 5.6 (f) and the pit in fig. 5.6 (l), before their removal, is in agreement with Itaya *et al.*[92] who thought that large scale topographic changes were produced on reduction cycles.

Although study of the time dependent stability of topographically

modified surfaces such as fig. 5.6 (i) was not made, the stability of the image for the five minutes of imaging is consistent with the other work in the area.

Unlike Itaya *et al.*[92], who resolved differences between MOH and MO phases, no clear difference between the roughened images is visible. Difference between the perchlorate and sulphate electrolytes may be responsible for this, as in perchloric acid the MOH replacement turnover peak OA 3 and the MO formation wave OA 4 are distinct, which is not the case in sulphuric acid. The disappearance of the pit observed in images 5.6 (i) - (k), is rather remarkable when it is noticed the surrounding step topography seems relatively unchanged; it is not clear from these images where the required gold came from.

Region B is below the potential where the OA 1 and 2 peaks are present although at the positive end of the double layer region (300 - 800 mV vs S.C.E.) Angerstein-Kozlowska *et al.* have resolved small peaks which they attribute to charge transfer from chemisorption of electrolyte anions[210]. It was proposed that the peaks also show reordering of the anions on the gold surface. The STM results presented above imply that at least the processes towards higher potentials may in fact be indicative of significant restructuring of step edges. Due to the problems with electrolyte deaeration from the cyclic voltammetry and subsequent STM use, 400 mV vs S.C.E. was used as the rest point for imaging. Behm *et al.*[88] found similar restructuring on Au (100) in the double layer with no observable difference between perchloric and sulphuric acids. However Itaya *et al.*[92] commented on the lack of step movement in their studies in perchloric acid. It would appear from the electrochemical studies[210] that these peaks are significantly less pronounced in the presence of

perchlorate than sulphate anions.

It can be hypothesised that this process is a major contributor to step motion, but would not be expected to contribute to mass transfer of gold atoms out of a terrace to give pitting. In this proposal, charge transfer from sulphate anions weakens the coordination of exposed gold atoms and increases their mobility over the surface until a more energetically favourable site is found. This is consistent with the dissolution of small islands on Au (100) previously observed[88] (and also the enhanced mobility of surfaces under chloride containing electrolytes). In the same way formation of MOH and MO species is also expected to make the surface more mobile. As the process leading to pitting is as yet unclear the contribution of dissolution reactions to step edge movement cannot be estimated.

Additional support for this analysis is provided by the imaging of hydrogensulphate adlayers on Au (111) by Behm and co-workers[87] at potentials more positive than 750 mV vs. S.C.E.. These workers ascribed the appearance of the structured layer to the transition from a disordered to an ordered phase with accompanying charge transfer. No information on step edge movement was given in the report. Since this group of workers reported a similar adlayer could *not* be imaged on an Au (100) surface, repetition of the work described in Section 5.IV. on such a surface may yield interesting results.

The apparent discrepancy between the groups of Behm and Itaya with respect to step edge movement in perchloric acid may be due to two reasons; firstly Behm's group used a S.C.E. reference which could conceivably have caused some contamination of the electrolyte with chloride ions[88], while Itaya's group carefully excluded all traces of

chloride from the system and used a bright platinum wire quasi-reference[92]. Secondly the topographies investigated were substantially different; in the first case the step edges were highly irregular and small islands were present, while in the latter a gold SCS substrate with thermodynamically more stable straight steps was used. This may be one of the more unexpected aspects of sample preparation, use of equilibrated surfaces may cause some surface processes to be overlooked. In this case, at the potentials used it is not necessarily suspected that a process giving surface equilibration is in operation.

Similar allegations of contamination could be levelled against the results presented here; care was taken to ensure the cells were thoroughly washed with Milli-Q water before use, but more persuasively the images 5.6 (i) - (k) do show the relative stability of a topography formed after an excursion to 1400 mV. If chloride was present it is expected the surface would show considerably more instability.

If the step movement is associated with peaks found in the double layer region prior to OA 1 etc., this may indicate differences in activity in perchlorate and sulphate electrolytes but this will require continued detailed and careful work.

Summary

It would appear that these results imply, for Au (111) surfaces at oxidative potentials, two processes may contribute to surface rearrangement;

(i) Coordination of anions to surface atoms facilitates surface mobility towards a thermodynamically more stable topography (presumably following the Terrace-Ledge-Kink model of surfaces).

(ii) Place exchange causes more substantial mass transfer including pitting of previously flat terraces: the location of pit formation is not yet understood.

Differences in the image quality between the three potential regions are discernible, at lower potentials the surface is atomically flat, while in the potential range B, the topography appears 'cloudy'. It may be postulated that the lack of resolution at this point, may be due to the charge transfer processes occurring between chemisorbed anions and the surface, giving local inconsistencies in the barrier height to tunneling. Such analysis is *not* supported by Behm *et al.* who see no difference in height between regions of ordered and disordered hydrogensulphate anions, implying no change in barrier height at the surface has occurred.

In the replacement turnover region the conductivity of the surface layer may not be homogeneous (or even well defined), but the underlying structure could still be resolved implying the resultant roughness was below the height of a gold step. The accusation that significant tip-surface interaction was allowing this resolution (i.e. the tip was pushing through a poorly conducting surface layer) and thus giving a false

representation of the height, is countered by comparison to the images of bulk oxide deposition under phosphate electrolyte, that show larger features and no underlying structure.

5.V.iv. Electro-oxidation of the gold surface in phosphate buffer

This Section considers the results presented in Section 5.III. and draws on the preceding discussion of the oxidation of gold under sulphuric acid.

The cyclic voltammogram of gold under phosphate buffer (fig. 5.3) shows a broad peak corresponding to oxidation of the surface without resolution of components of the process possible.

Although the starting point for the cycle under phosphate buffer (shown in fig. 5.4) is poorly resolved, the image at 600 mV shows a clear surface. The topography of images 5.4 (c) and (d) is directly comparable to the appropriate images in the sulphuric acid oxidation, with the lower potential giving a 'cloudy' surface. At 1000 mV, fig. 5.4 (d), the surface exhibits roughening consistent with that expected for monolayer reaction. The images at 1200 mV, figs. 5.4 (e) - (h), show features developing as bulk oxide formation occurs. This process is halted by reversing the potential sweep and the apparent smoothing of the surface is presumably due to the surface mobility of oxide species.

The images given after reduction of the oxide layer show that bulk oxide formation has involved atoms from several atomic layers beneath the original surface. Thus the topography formed by expulsion of oxygen from the structure involves pitting to a depth of greater than one monolayer. The irregularity of this surface reflects the amorphous nature of the bulk oxide.

As the experiments here used a S.C.E. reference in a chloride

containing salt bridge there is some possibility that, over the timescale of the experiment described (a couple of hours), some chloride contamination of the solution may have taken place. This is somewhat countered by the observation of the highly irregular topography exhibited in figs. 5.4 (l) and (m) which would be expected to self-anneal significantly in the presence of chloride. In any case although chloride contamination would act to exaggerate the results observed, the main result would be unchanged.

5.V.v. Behaviour of the surface at potentials negative of the double layer region in sulphuric acid

In rigorously clean electrochemical systems, the cyclic voltammogram of gold at potentials negative of the double layer region in sulphuric acid merely shows the onset of hydrogen evolution. In the CV presented in figure 5.5, the onset of hydrogen evolution is at about -300 mV while at -100 mV there is a peak due to the reduction of dissolved oxygen to give peroxide species.

The STM results of fig. 5.10 are much as expected from this; no step movement or any other surface process is observed until hydrogen evolution physically affects image stability and the sample disintegrates. Less predictable are the small islands apparent after imaging at -100 mV.

The results of fig. 5.11 appear to be due the same effect, magnified through biasing the sample for a long period of time. The image is very similar to that shown by Lindsay *et al.* in their *in-situ* observation of the 22 x $\sqrt{3}$ reconstruction of an Au (111) surface[86], where it was speculated that the 'blobs' could have been due to excess atoms in the reconstructed layer being forced upwards upon the loss of the reconstruction. The

process appeared irreversible although no information was given about the surface at higher potentials. Reversibility was not tested for the results given here. Unfortunately there are two problems; firstly there are only approximately 4.5% more atoms in the reconstructed structure than the unreconstructed[85], thus the images of both Lindsay and fig. 5.11 (a) appear to show an excessive amount of displaced material, secondly Weaver *et al.*[85] have imaged the phase transition, showing it to be reversible, without observing a similar effect.

Assuming figs. 5.10 and 5.11 show the same effect, the images presented here are hard to reconcile with those of Tao and Lindsay; here the 'blobs' arise as the potential is dropped and are removed on going to positive potentials whereas in the literature a reconstructed surface was imaged until the potential was shifted to positive values.

Although being unable to advance a strong explanation for these effects, several suggestions may be made: the 'blobs' may be a deposit as the apparent lack of step edge movement on their removal would appear to imply they were not part of the surface (here a platinum counter electrode was positioned within the sample cell - dissolution of this would provide a source of contaminant). Alternatively Brooker *et al's.* observation of large scale surface rearrangements of a gold surface activated by biasing in the hydrogen evolution region[93], may indicate that the important process leading to these effects is the interaction of hydrogen with the gold surface.

It is clear from this type of result that *in-situ* electrochemical STM has the potential for opening up new avenues of research, but it may not necessarily be easy distinguishing artifacts from interesting effects. Irrespective of the source of the 'blobs', further characterisation of this

particular effect is desirable because these potential regions are visited during deposition studies, e.g. bulk deposition of copper on gold and underpotential deposition of lead on gold.

Regarding figs. 5.12 and 5.13, it is not clear if they show the same effect. The behaviour of the features as the potential of the surface is varied is hard to reconcile with the conclusions already drawn, and it would appear that they are not part of the gold surface. Also the physical movement apparent in some images would tend to suggest the features are discrete units - perhaps some type of deposit caused by electrochemistry of contaminants in the electrolyte. For the present time the cause of these images is unclear.

5.VI. Suggestions for further work

Investigations of the electro-oxidation of the gold surface in sulphuric acid appear to indicate surface rearrangement processes active at potentials below that originally expected from cyclic voltammetry. It would be informative to extend this work to other electrolytes and to different crystallographic faces and look for differences in behaviour. Observation of the time dependence of the processes observed here (i.e. stability of pits formed in sulphuric acid, highly stepped surface after bulk oxide formation) would provide useful data; however to obtain consistent results by remaining over one area for a prolonged time may be hard work! The effect on surfaces of different basic topology may also be relevant.

This work could be extended to investigate the effects of the adsorption of cations such as Bi^{III} and Pb^{II} on the electro-oxidation of gold[211]. The CV for the oxidation of gold in the presence of these species shows considerable modification (with the oxidation peaks reduced in

height, broadened and shifted to more positive potentials and the reduction peak moved to more negative potentials) and topological imaging of the process may aid in rationalising the electrochemical measurements.

Imaging the surface after biasing towards potentials below 0V vs S.C.E. caused features of uncertain origin. Pinpointing the cause of these features is necessary for the characterisation of the behaviour of gold surfaces at these potentials. This is important because of the interest in the study of deposition processes.

As previously indicated the work under sulphuric acid was a precursor to the study of the underpotential deposition of Sn^{II} on gold. This system provided a UPD system not previously studied by *in-situ* STM and has been shown to promote the direct electrochemistry of cytochrome *c*[212] (see Section 6.I). Recent work[213] has also shown tin to adsorb irreversibly on gold; a topographical study of this could make interesting secondary research. Unfortunately the basic electrochemistry for the process seemed rather hard to reproduce, with the air sensitivity of $Sn^{II}_{(aq)}$ being somewhat incompatible with the current STM system. Similarly, preliminary investigation of the behaviour of a tungsten tip in the Sn/H_2SO_4 solution implied that it was difficult to find a region of stability. Despite this gloomy prognosis an experiment was attempted, in the hope that even if the UPD process could not be observed, bulk tin deposition might be seen, but imaging was very poor and no results were otained.

Longer term aims in this area could be focused towards studies of processes on platinum substrates (although the ease with which platinum surfaces become contaminated may cause some practical difficulties). These electrodes are of great catalytic importance for electro-oxidation of

small molecules, a process required in many potential fuel cell systems. Modification of the platinum electrodes by ad-atoms often enhances their activity by decreasing the poisoning of the surface. The sensitivity of the electrochemical process to structure has long been considered and *in-situ* STM provides a method of studying this directly. Investigation of the ordering of the ad-atom species is an obvious starting point (*cf.* the AFM investigation of Bi adlayers on gold (111) which provided support for a model of H_2O_2 oxidation[139]), more ambitiously, spatially resolved observation of poisoning would be useful. It should be remembered that, except in exceptional circumstances, the surfaces currently investigated by *in-situ* STM are far flatter and well defined than those often used for electrochemical measurements.

5.VII. Conclusions

The STM system constructed was shown to be effective at *in-situ* real time, reproducible, high resolution imaging of electrochemical processes. The ability of STM to provide real space information easily correlated with established techniques like cyclic voltammetry was once again exhibited.

In summary:

1. Imaging of the electro-oxidation of a gold surface in a sulphuric acid electrolyte at potentials above MOH formation gave results consistent with those already published and could be correlated with cyclic voltammetry.
2. Step motion at potentials below MOH formation has been observed and related to peaks due to charge transfer from chemisorbed anions.
3. In a phosphate electrolyte, bulk oxide formation and the surface

resulting from subsequent reduction have been imaged.

4. Characterisation of surface structure at potentials below 0V vs S.C.E. has revealed features arising from an as yet unclarified source. Identification of such features is important for the future use of STM in imaging processes occurring in these potential regions.

5. Areas for future research have been identified.

Chapter Six

Investigation of Aspects of the Direct Electrochemistry of Cytochrome *c* at Gold Electrodes

6.I. Introduction

As pointed out by Armstrong *et al.*[214], study of the direct electrochemistry of redox proteins may yield information applicable to a diverse range of topics, including mechanistic studies of protein electron transfer and biosensors. Observation of the unmediated electrochemistry of these species is often not trivial; they have a tendency to irreversibly adsorb to the electrode surface whilst undergoing a conformational change and subsequent loss of activity. Some of the early work in this area centered on the electron transfer protein cytochrome *c*, a relatively simple species with a known structure[215]. It has a molecular weight of 12400 and the electroactive functionality, a single heme centre, is mostly contained within the molecule, only one edge of the porphyrin group being exposed to solvent. The oxidised molecule has a +9 charge at pH 7 (due to an excess of basic residues) with a dipole moment of 324 D.

The quasi-reversible cyclic voltammetry of horse heart cytochrome *c* was shown in 1977 by Yeh and Kuwana[216] and Eddowes and Hill[217] separately on, respectively, a tin doped indium oxide electrode and a gold electrode with an adsorbed monolayer of 4, 4'-bipyridyl. The conclusion drawn from the research was that the structure and character of the interface was critically important in facilitating the non-degradative electrochemistry to take place. Subsequent work has shown a large range of molecules and species can promote the direct electrochemistry of cytochrome *c* at a gold electrode[218,219]. Alongside this, investigations have been made of the structure of the electrode-electrolyte interface to elucidate the interaction between the protein and the modified gold surface.

Ellipsometric probing of an adsorbed layer of 4, 4'-dithiodipyridine

(SSBPY) on gold electrodes[208] gave results consistent with an 'end - on' adsorption of the molecule, in agreement with previous surface enhanced Raman spectroscopy (SERS) studies[220]. Ellipsometry showed that the molecular orientation was time-dependent and taking into account the SERS data the following adsorption scheme seems likely:

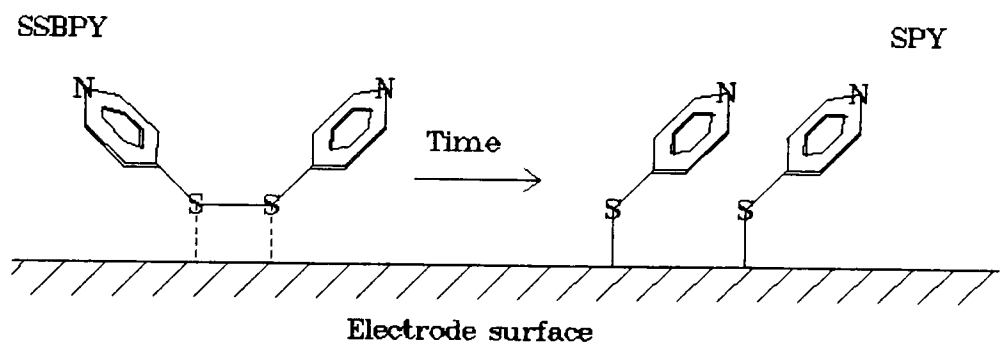

The strong adsorption of SSBPY onto gold makes it a particularly useful promoter, as electrodes can be modified without the necessity for the species to be present in the electrolyte during cytochrome *c* electrochemistry.

The mechanism, proposed by Hill *et al.*[218], for the direct electrochemistry of cytochrome *c* at such modified electrodes involves the protein weakly binding to the modified surface. This is achieved via hydrogen bonding between the weakly basic pyridyl nitrogen and the lysine $-NH_3^+$ groups close to the heme unit of the cytochrome *c* (fig. 6.1). Electron transfer is facilitated by the protein being optimally oriented at the electrode with the short term electrode - protein interaction allowing turnover of molecules at the electrode surface. It is known that the electrochemistry requires areas of adsorbed promoter rather than isolated molecules[221] and there is a likelihood that the protein - surface interaction is dynamic with the cytochrome species traversing the surface.

The mechanism is applicable to other organic surface modifiers found to be effective promoters[218]; they are all capable of interacting with the protonated cytochrome lysine groups by forming either a hydrogen bond (species containing pyridyl nitrogens or aniline type amines) and/or a salt bridge (anionic species e.g carboxylate). Most of these species include a functionality which gives strong adsorption onto the electrode surface.

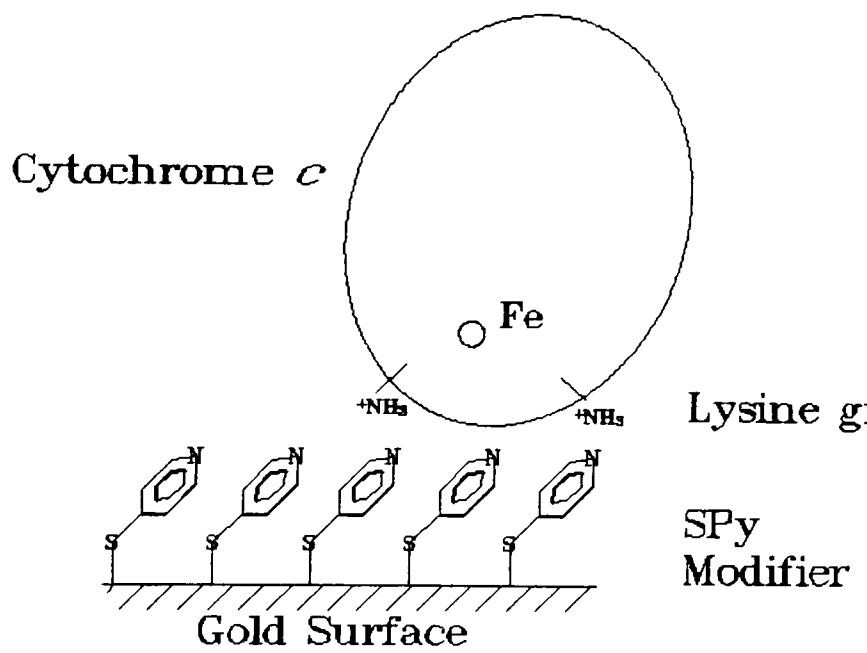

Fig. 6.1. Schematic representation of the interaction of cytochrome c with a modified electrode surface.

In addition to small organic molecules it was found that sulphur ad-atoms acted as promoters. Shibata *et al.* have extended this work by modifying gold electrodes with a number of ad-atom species and studying the electrochemistry of cytochrome *c* as a function of both ad-atom electronegativity and electrode coverage[212]. It was concluded that the ad-atoms suppressed the irreversible binding of cytochrome *c* to the electrode whilst providing an electrostatic attraction to the protein residues around

the heme group that allowed reversible electrochemistry.

Niki and co-workers have investigated the adsorption of cytochrome *c* at bare and SSBPY modified gold electrodes by infra-red reflection adsorption spectroscopy (IRRAS)[222] and electroreflectance[223] while Bockris and co-workers have carried out similar work using ellipsometry[224]. The results indicated cytochrome *c* strongly adsorbs to both bare gold *and* on modified surfaces.

It was shown the redox potential of cytochrome *c* irreversibly adsorbed on a bare gold electrode is 0.5 V more negative than cytochrome *c* in bulk solution, whereas adsorption at a modified electrode had no effect on the species redox potential[223]. The shift in electrochemical properties at the bare electrode are believed to be caused by the conformational changes undergone by the molecule as it adsorbs. This work has led to an alternative explanation for the action of SSBPY; the SSBPY monolayer prevents unfolding of the cytochrome *c* and immobilises a layer of the protein which mediates electron transfer between the electrode and protein molecules in the bulk solution. In this case the redox potential of the adsorbed cytochrome *c* allows reversible electrochemistry while in the case of the bare electrode only the reduction process can be mediated[224].

Work is currently being carried out to elucidate the precise nature of shortlived reversible cytochrome *c* electrochemistry observed at a *bare* gold electrode[225].

The possibility of real space imaging of the interaction between cytochrome *c* and an electrode surface by scanning tunneling microscopy is therefore of great relevance to this field. Imaging could provide more information on the mechanism of interaction and in addition may indicate

the influence surface topology has on the process (a question none of the previous studies are in a position to address properly). The imaging of an adsorbate layer or cytochrome *c* molecule in itself, has implications for the application of STM to biological studies.

The ability of *n*-alkanethiols and organic disulphides to give self-assembled films has long attracted interest because they offer a controllably versatile approach to surface modification (see for e.g. references 65 and 226), and it was hoped study of the SSBPY/gold system would have application to this area.

As a precursor to STM studies it was decided to follow up previous investigations on the adsorption of SSBPY on gold using *in-situ* FTIR[227]. It was hoped the newer instrumentation available would have increased sensitivity and this was subsequently borne out by experiment which resolved signals 100x less intense than those previously detected. The ambitious long term goal of the STM studies was to observe the adsorption/interaction of cytochrome *c* at both bare and modified electrodes in a potential controlled environment, in addition to gaining information on the SSBPY monolayer.

6.II. *In-situ* external reflectance IR investigation of the adsorption of SSBPY on gold

6.II.i. Results

In these experiments the solutions were approximately 1mM SSBPY (Aldrithiol-4 from Aldrich, as received) in a supporting phosphate buffer electrolyte (0.02M NaH_2PO_4, 0.026M Na_2HPO_4, 0.1M $HClO_4$, pH 7.1). In the CV shown below the solution was deaerated by saturating with nitrogen before being admitted to the spectroelectrochemical cell. For the

reflectance spectra it was necessary to further purge the solution of oxygen *in-situ*, by using a second platinum wire electrode (see fig. 2.7) set at potentials giving O_2 reduction (-0.5V vs S.C.E.). In all cases the solution in the cell *during* IR experiments was 1mM SSBPY in phosphate buffer. To check the state of the system and electrode, CV's of the polycrystalline gold electrode were observed in the buffer alone, and potential cycling carried out to clean the electrode if required, prior to replacing the solution *in-situ* by admitting SSBPY solution. Before starting the series of experiments CV's analogous to those already published[220] were observed, and subsequently the presence of SSBPY in the cell was indicated by the suppression of small impurity peaks in the CV (this point is discussed further in 6.IV.).

The reversible electrochemistry of cytochrome *c* takes place in the potential range -0.3 V to 0.3 V vs S.C.E. and SSBPY is electro-inactive in this region as shown below in fig. 6.2.

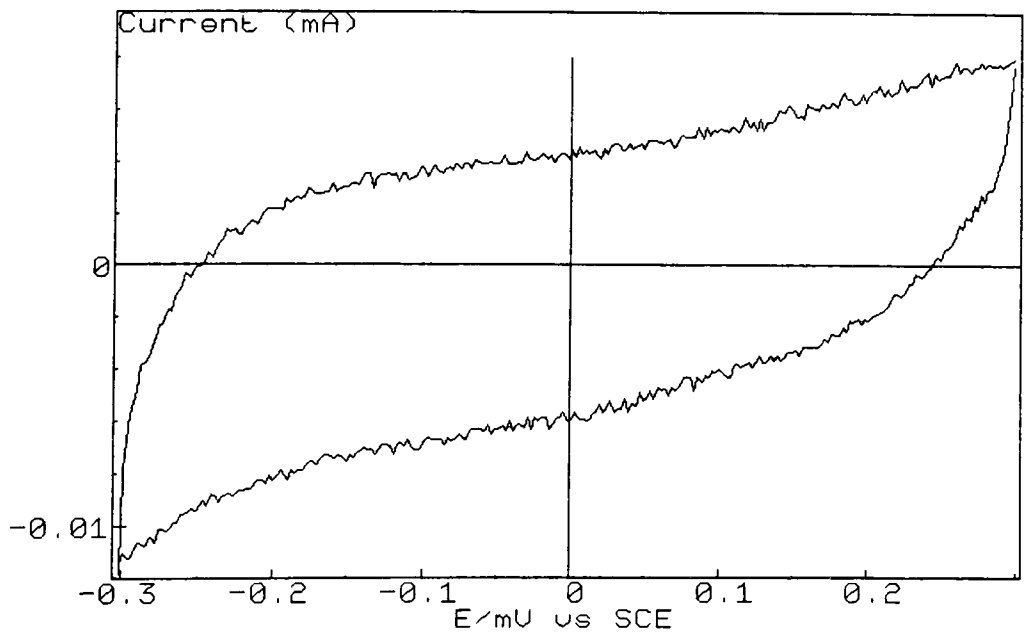

Fig. 6.2. Cyclic voltammogram of a SSBPY covered gold electrode in 1mM SSBPY/phosphate buffer solution. Scan rate 50 mVs^{-1}.

Initial FT-IR experiments were carried out using p-polarised light, by recording and averaging 1000 scans at -0.3V, 0.3V and -0.3V. Conventional data treatment (see Section 2.II.ii.) for both the -0.3V to 0.3V, and the 0.3V to -0.3V steps showed the presence of reversible peaks at around 1460, 1570 and 1610 cm^{-1}. These were, however, obscured by fine structure attributed to variations in water vapour concentration in the sample compartment over the time taken to record the spectra (about five minutes). It was found however that the subtraction method shown below gave a clearer result;

$$0.3/-0.3a - -0.3b/0.3$$

where -0.3a and -0.3b are the first and second spectra collected at -0.3V respectively and 0.3 is the spectrum taken at 0.3V. The method is algebraically equivalent to subtracting the two normalised spectra from each other and is valid in this case because of the reversibility of the process, hence the peaks are constructively reinforced while the noise is reduced.

To further clarify the situation, a square wave data collection was employed using 250 scans at each potential to maximise the total data collected, while reducing the time for water vapour changes between potentials;

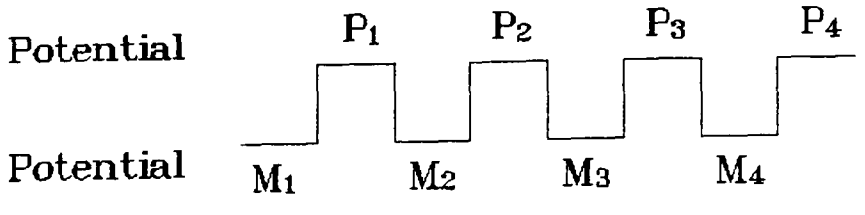

nd the subtraction formula was;

$$[(P_1/M_1 - M_2/P_1) + (P_2/M_2 - M_3/P_2) + (P_3/M_3 - M_4/P_3)]/6$$

he division by the number of steps used means the spectra are effectively ormalised as for a conventional spectra. In fact the procedure was epeated several times with different scan numbers, giving almost identical pectra with varying peak clarity.

Using -0.2V and 0.3V as the stepped potentials studied yielded for p-olarised light the spectrum shown in fig. 6.3 and for s-polarised light nat shown in fig. 6.4:

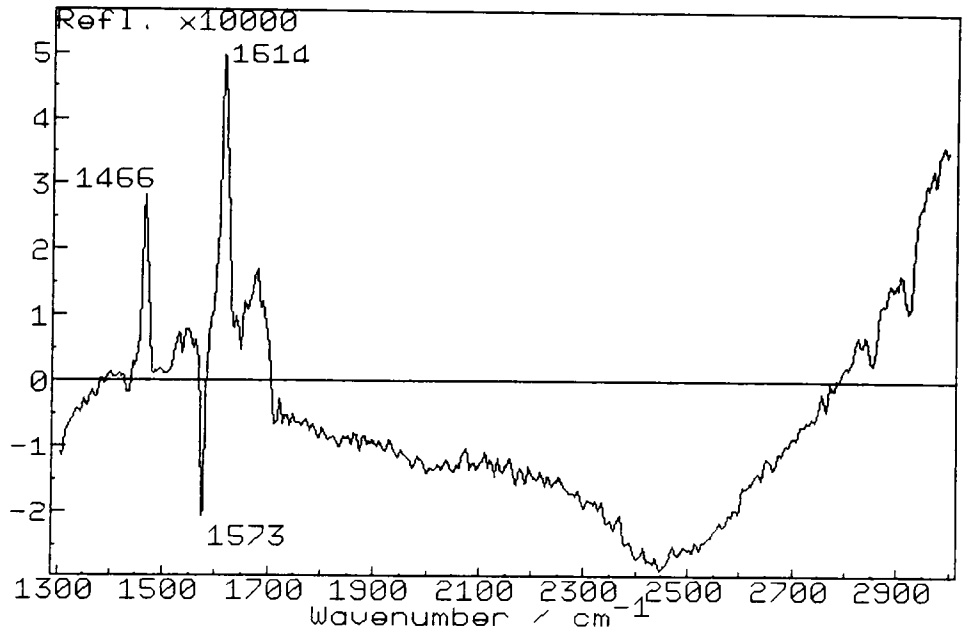

Fig. 6.3. Reflectance spectrum of SSBPY adsorbed at gold using p-polarised light (6 potential steps averaged).

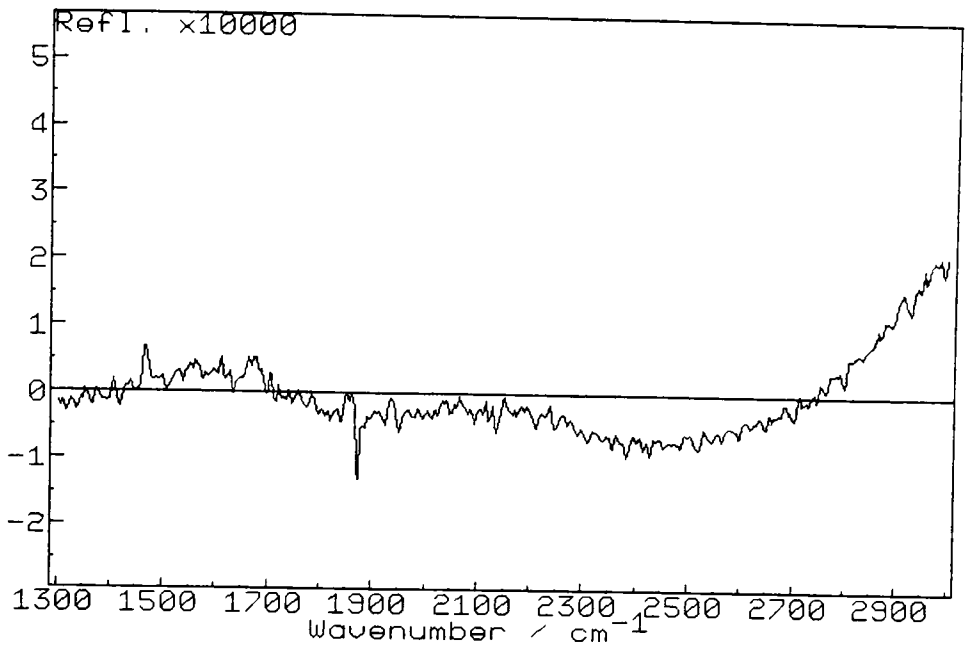

Fig. 6.4. Reflectance spectrum of SSBPY adsorbed at gold using s-polarised light (only 4 potential steps averaged).

Repetition of the experiment with p-polarised light with different potential steps showed variation in intensity of the bands as shown in figs. 6.5 and 6.6;

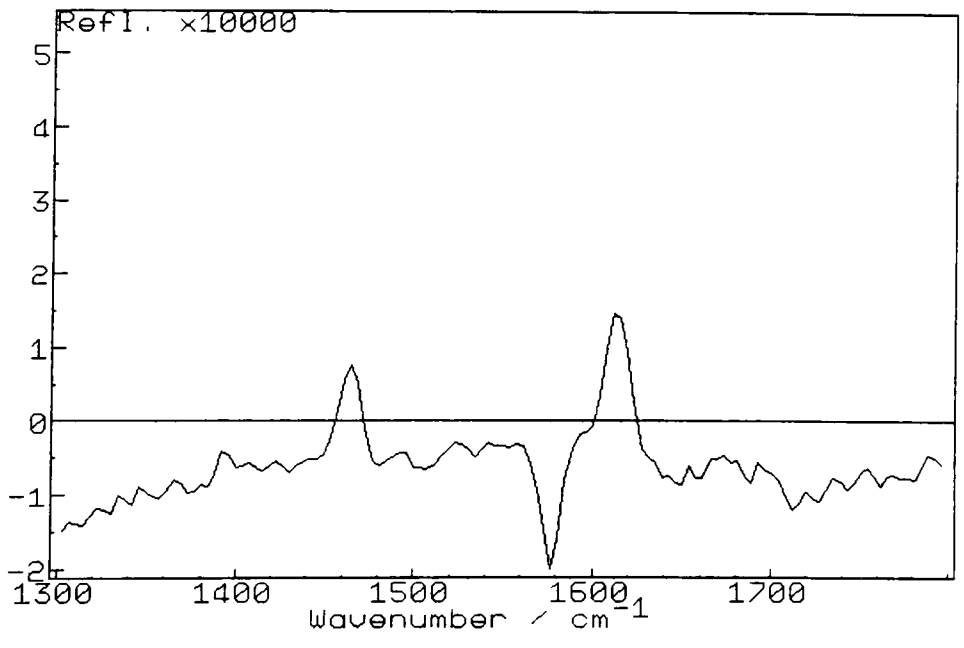

Fig. 6.5. Reflectance spectrum of SSBPY adsorbed at gold using p-polarised light, stepped potentials -0.2V and 0V

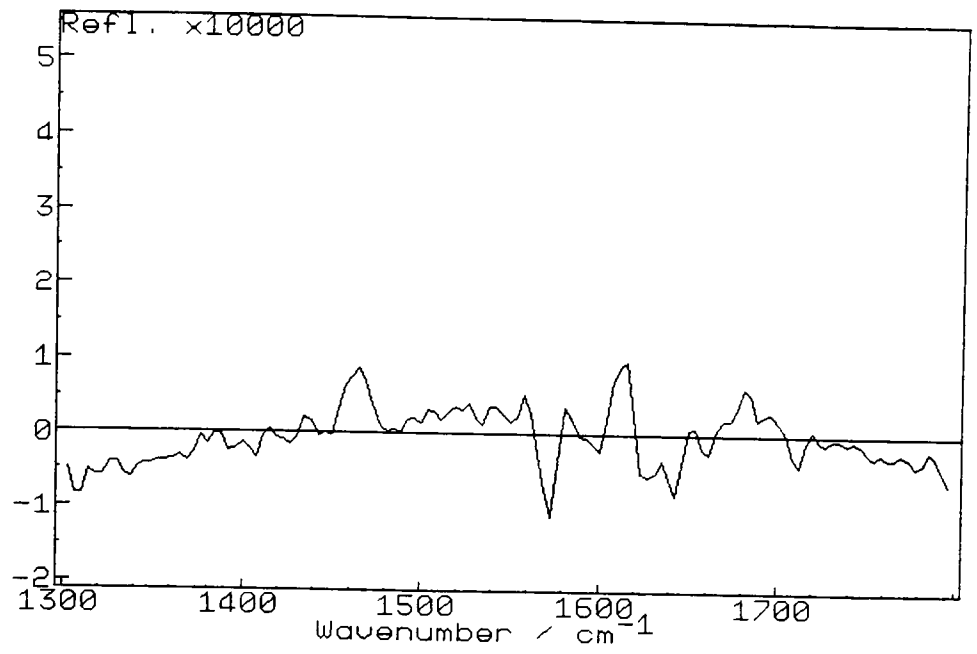

Fig.6.6. Reflectance spectrum of SSBPY adsorbed at gold using p-polarised light, stepped potentials 0V and 0.3V.

To obtain a transmission spectra (fig. 6.7), SSBPY was dissolved in methanol, then the solution was dropped onto the germanium window and allowed to evaporate. The spectra recorded were normalised against the blank window.

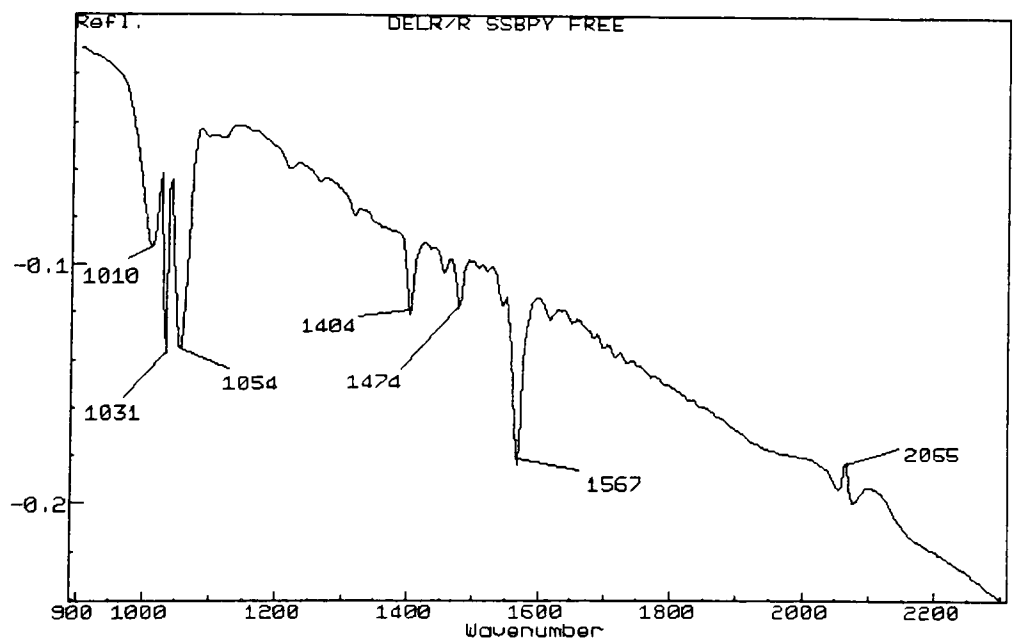

Fig. 6.7. Normalised transmission spectrum of free SSBPY

6.II.ii. Discussion

The spectra were only analysed in the region 1400 to 3000 wavenumbers because below about 1400 cm^{-1} the spectra are dominated by bands due to the movement of ClO_4^- in and out of the thin layer[228]. This is also the region in which phosphate absorbs.

The absence of bands observable with p-polarised light in the spectra obtained under irradiation with s-polarised light (figs. 6.3 and 6.4) shows the operation of the surface selection rule (see Section 2.II.), pointing to a surface specific process. Since there is no chemical change in the system it is a reasonable premise that the process monitored is a reversible, potential-dependent orientation change.

The transmission spectrum contains peaks at between 1000 and 1100 cm^{-1} due to pyridine ring breathing vibrations. The other peaks between 1400 and 1570 cm^{-1} can be attributed to C=C and C=N stretches[222,228]. There is no simple direct correlation between the transmission and the reflectance spectra, as noted by Niwa *et al.*[222], but this may be due to shifts in absorbance frequency caused by close packing of species on the electrode surface.

Ring modes may be assigned by reference to the work of Kline and Turkevich who made a detailed IR study of pyridine[229]. Consider the SPy fragment oriented vertically (fig. 6.8 with angle $= 0°$). The surface selection rule dictates that only dipole changes perpendicular to the surface will significantly contribute to the IR spectrum. The so called 8a and 19a modes (consisting of C=C and C=N stretches) have the most appropriate dipole changes (fig. 6.9).

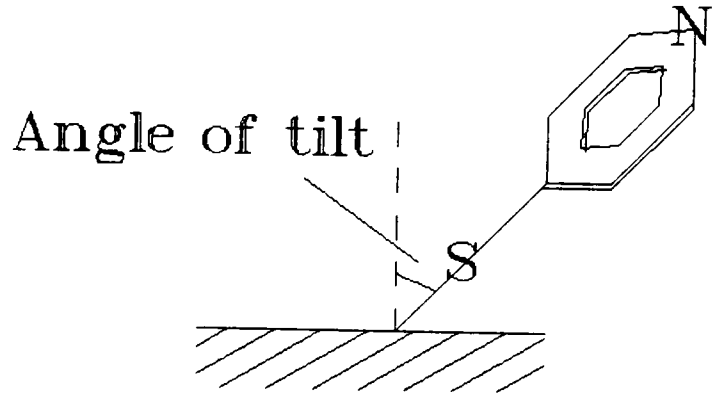

Fig. 6.8. Schematic representation of the orientation of a SPy fragment on a gold surface.

In pyridine these are at 1580 cm^{-1} and 1484^{-1} respectively and thus may be considered to give the loss features at about 1614 cm^{-1} and 1465 cm^{-1} in the reflectance spectra. Inspection of the modes of vibration shows only mode 8b will satisfy the surface selection rule to give a gain feature as the species tilts towards the surface. This is only true, however, as long as the plane of the pyridine ring remains perpendicular to the surface and thus the fragment does not show a tendency to lie flat, but instead to tilt edge on to the surface (fig. 6.8, angle $>0°$).

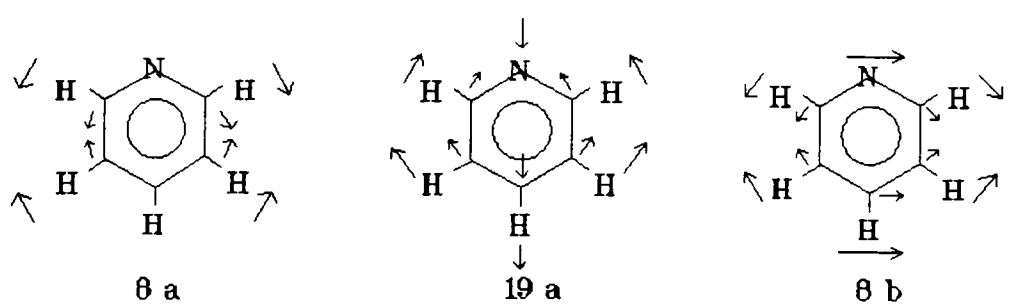

Fig. 6.9. Molecular vibrations giving rise to observed IR absorptions

Information on the dissociative adsorption of SSBPY is not given by this work for two reasons; firstly the S-S and S-C bond stretches are outside the range of the detector and secondly the large scale reorientation noted by Elliott *et al.*[208] took place within about 3 minutes of SSBPY being put in contact with the electrode. *In-situ* purging of the solutions here took about ten minutes.

The variation of band intensity with potential shown in figs. 6.3, 6.5 and 6.6 has since been exploited more systematically to support the model outlined above[230]. In this set of experiments it was found tilting occurred up to about 0.2V vs S.C.E. above which steric effects are assumed to be responsible for a lack of movement.

6.III. STM investigation of aspects of the direct electrochemistry of cytochrome *c*

The studies described in this section were carried out concurrently with instrumental development and as in Chapter five, as the instrument evolved so the complexity of the experiments attempted was increased. Unless explicitly stated otherwise the surfaces used were gold on mica thin films.

6.III.i. Studies of adsorbed promoters

Early work in this area by Dr. T.R.I. Cataldi, imaging a gold single crystal sphere (SCS) after exposure to a solution containing SSBPY, produced the image shown in figure 6.10. This image was taken under water with a tip insulated with nail varnish. The oval structure near the centre of the image implied that the image was not merely due to noise, though subsequent attempts to reproduce this behaviour were unsuccessful. Later, similar results were observed in air on another bead

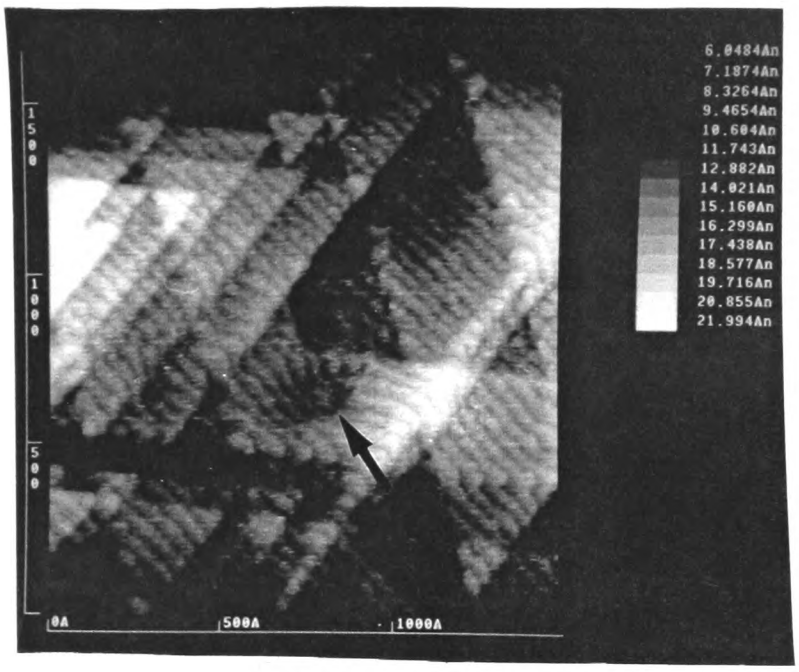

Fig. 6.10.

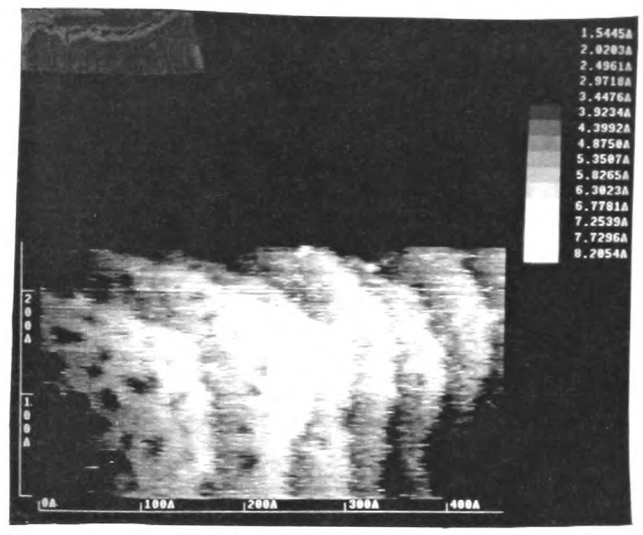

Fig. 6.11

Fig. 6.10. Image of a gold SCS under distilled water after exposure to SSBPY solution. (t: 0.9 ms, inc: 3Å, I_T: 6 nA, V_T: 200 mV) The periodicity of the corrugations is 35-45Å and the height is from 1-3Å. Image courtesy Dr.T.R.I.Cataldi.

Fig. 6.11. Pitting on an Au I sample after exposure to 1 mM sodium sulphide solution (t: 0.8 ms, inc: X 3Å, Y 1Å, I_T: 1.5 nA, V_T: -250 mV)

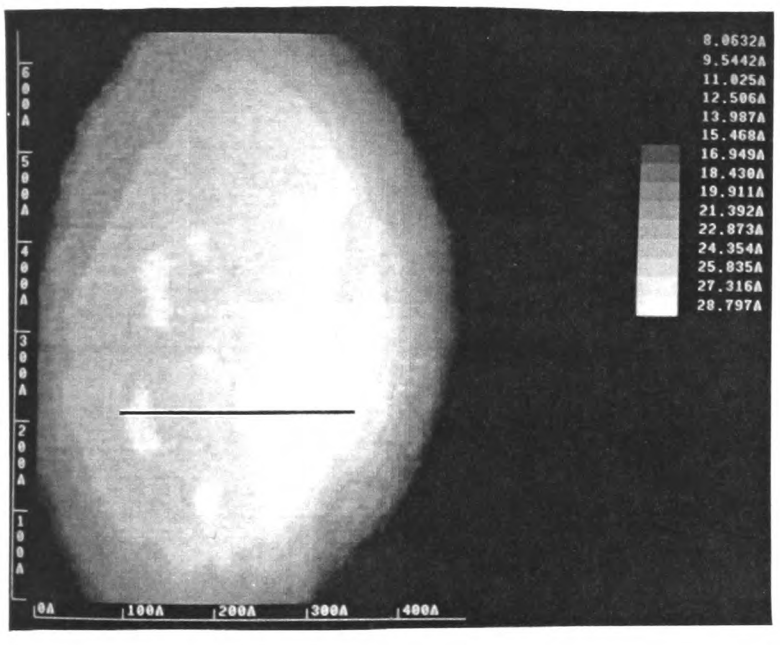

Fig. 6.12. An Au 4 sample imaged in ambient conditions after exposure to 1.2 mM SSBPY solution (t: 1.8 ms, I_T: 2 nA, V_T:100 mV) (a)inc: 5Å, (b) section along line shown in (a), (c) high resolution scan inc: 3Å.

(a)

(b)

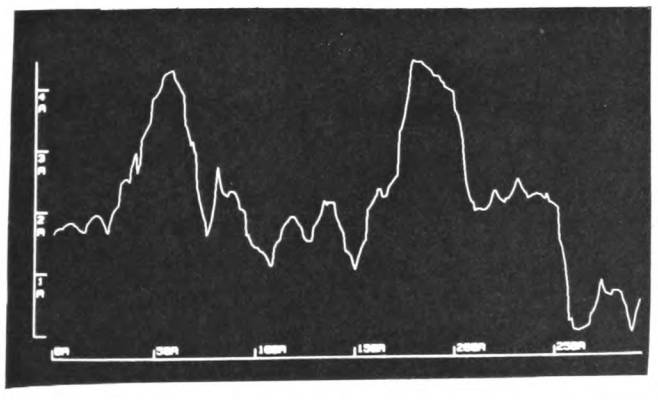

(c)

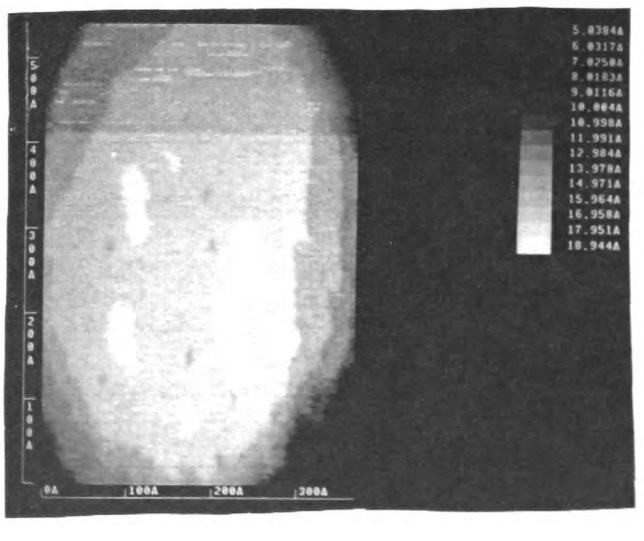

surface which had not been exposed to SSBPY but had been washed with phosphate buffer. Attempts to rationalise these observations provided a basis for the experiments outlined in this Section. Additional motivation for the use of gold thin films was provided by the confusion over these observations. It was hoped a change of substrate would either confirm them, or provide a more conclusive indication of noise.

Studies in ambient conditions

In collaboration with Mr. D. Reay, attempts were made firstly to image adsorbates of a physically larger size than SPy fragments and secondly to image adsorbed sulphur, an inorganic promoter[231]. The aim of the former experiments was to reproduce the effect observed in fig. 6.10 with a similar compound. If the effect arose from tunneling from molecular species, images displaying features with a different periodicity to that seen in fig. 6.10 would be expected with different adsorbates.

PMHC [2-(phenylmethylene) hydrazinecarbothioamide, see reference 219] and a peptide-substituted ferrocene, both supplied by Dr. K. Di Gleria, were dissolved in ether and ethanol and dropped onto a gold on mica surface, but unfortunately stable tunneling could not be obtained. This lack of success prompted experiments using a sodium sulphide solution. A 10 mM solution dropped onto a gold on mica substrate showed no particular effect but during scanning on a sample exposed to a 1 mM solution the image shown in fig. 6.11, was obtained. Here depressions several angstroms deep are visible on a plateau and adjacent terrace, though the effect was not conclusively observed in other parts of the same sample within the same experiment. The features in the area described appeared more clearly after repeated scanning. Time constraints meant

that this specific avenue of investigation was not followed up. It should be noted that this topography has not been observed on bare gold on mica samples.

Following this sideline, work using SSBPY solutions was restarted. Modified surfaces were obtained by dipping gold on mica samples into an approximately 1.2 mM aqueous solution of SSBPY for 2 minutes. The sample was then carefully washed with distilled water and left to dry in a covered container.

Initial attempts at imaging such samples failed due to poor tips and sample surfaces. After leaving one sample overnight the images shown in fig. 6.12 were obtained. As indicated by the fig. 6.12 (b), the islands on top of the plateau have a height equivalent to a monatomic gold step and are of the order 20-40Å by 60-100Å.

Higher resolution imaging reveals 1.5Å deep pits with a diameter of 10Å; the pit features became clearer with repeated scanning. Repeated imaging of the area led to image breakup of the type exhibited at the top of image 6.12 (c). There is some evidence of surface mobility as the 'islands' change dimensions between images. The features shown here were also observable on other plateaus.

On repetition of the experiment monatomic high islands on plateaus were again obtained. The surface shown in fig. 6.13 (a) was subject to CITS (see Section 2.I.ii.) between 1 and -1V but no variation in the I/V curve obtained for different regions of surface was discernible. A considerable effect on the surface was observed, as a large number of pits were formed on both the plateau and surrounding terraces with the result that the clarity of the steps was lost.

As a control experiment a gold on mica sample was dipped into distilled water alone and dried as above. This experiment showed only the standard gold on mica topography. In a separate experiment a gold on mica sample was clamped into the STM cell, and covered with N_2 purged distilled water which was then removed via the tubing normally used for the reference electrode. Subsequently monatomic high 'islands' were imaged on a plateau. The cell, tubing and connections had been cleaned in distilled water, ethanol and acetone prior to the experiment and a new tip had been fitted with the only other possible source of contaminants being the tip holder. Gold on mica samples were also imaged in air after coverage by ethanol and a phosphate buffer solution but due poor imaging no conclusive results were obtained.

As a continuation of this work, gold SCS samples were exposed to distilled water, ethanol, an 11 mM ethanolic solution of SSBPY and phosphate buffer. Only in the latter experiment were features not previously identified on a 'bare' SCS imaged (in fact fig. 4.7 was obtained after exposing the bead to ethanol) and this is shown in fig. 6.14.

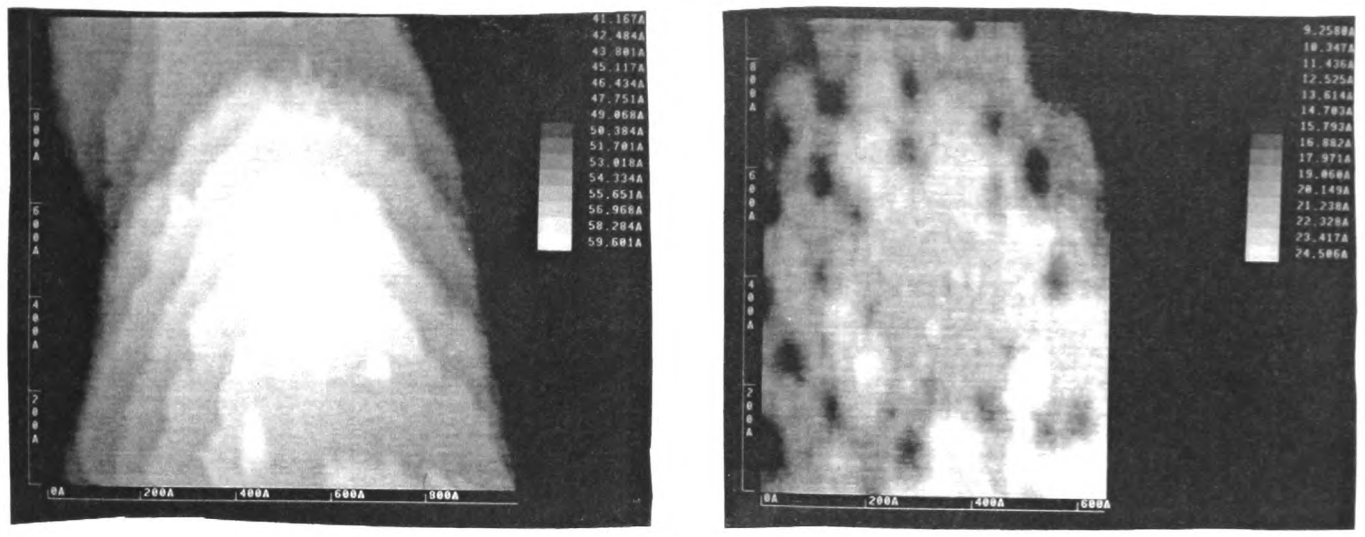

(a) *(b)*

Fig. 6.13. Au 4 sample after exposure to 1.2 mM SSBPY solution, (t: 1.8 ms, inc: 5Å, I_T: 2 nA, V_T: 50 mV, (a) plateau and terrace surface showing 'island' features, (b) plateau region after spectroscopy.

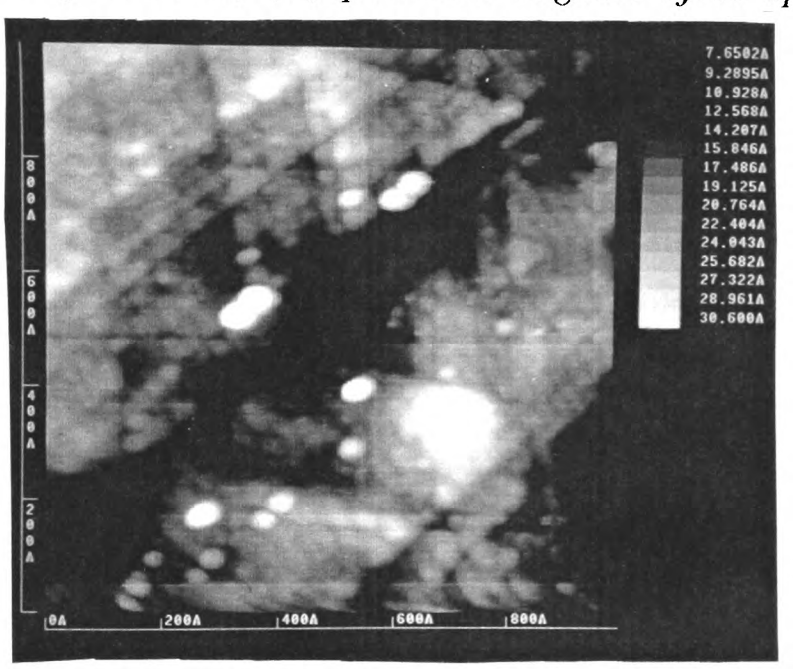

(a)

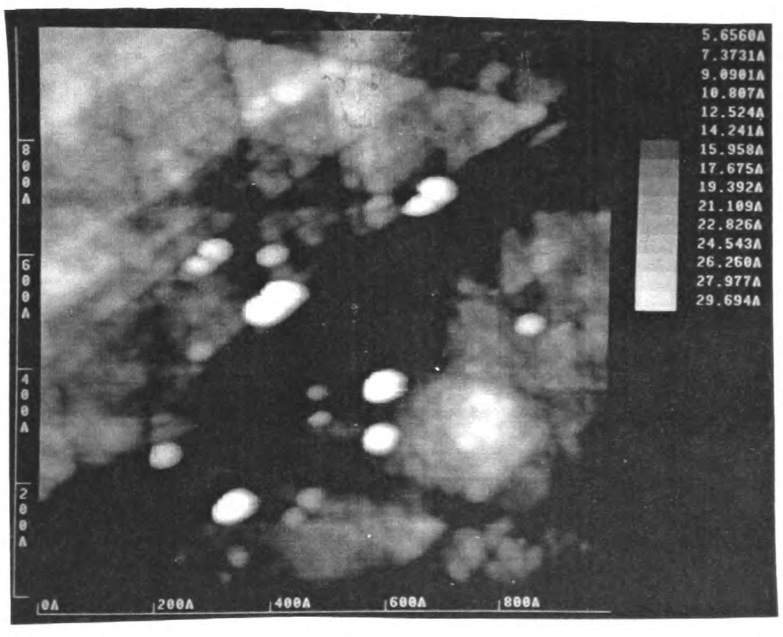

(b)

Fig. 6.14. 'Island' features on a corrugated SCS surface after exposure to phosphate buffer (t: 0.8 ms, inc: 4Å, I_T: 2 nA, V_T: 200 mV) The features are of the order of 30Å high and 60Å in diameter, some mobility of features is apparent between the two consecutive images (6.14 (b) taken approximately 1 minute after 6.14 (a)).

Studies under liquid without potential control

Imaging SSBPY modified surfaces submerged beneath distilled water was unproductive; plateau regions were imaged but no uncharacteristic features were observed.

Figure 5.1 showing irregular monatomic high islands on a gold on mica surface under phosphate buffer, provides an additional 'control' result relevant to this work.

6.III.ii. STM investigation of adsorbed cytochrome species

Studies on bare gold in air

The first attempt to image cytochrome *c* molecules on a gold surface involved exposing the sample to an approximately 0.2 μM solution of horseheart cytochrome *c* (Sigma type VI) supported in 300 μM phosphate buffer for one hour. As before the sample was dried under cover. Fig. 6.15 shows the results given.

The 'islands' given in fig. 6.15 (a) are pseudospherical in appearance and are 4 - 6Å in height and 40 - 70 Å in diameter. They are unlike features previously presented. Images 6.15 (b) and (c) exhibit monatomic high 'islands' on a plateau in a topography analogous to those shown in the previous Section albeit at higher coverage, while in image 6.15 (d) islands 6Å high are clustered on a flat area.

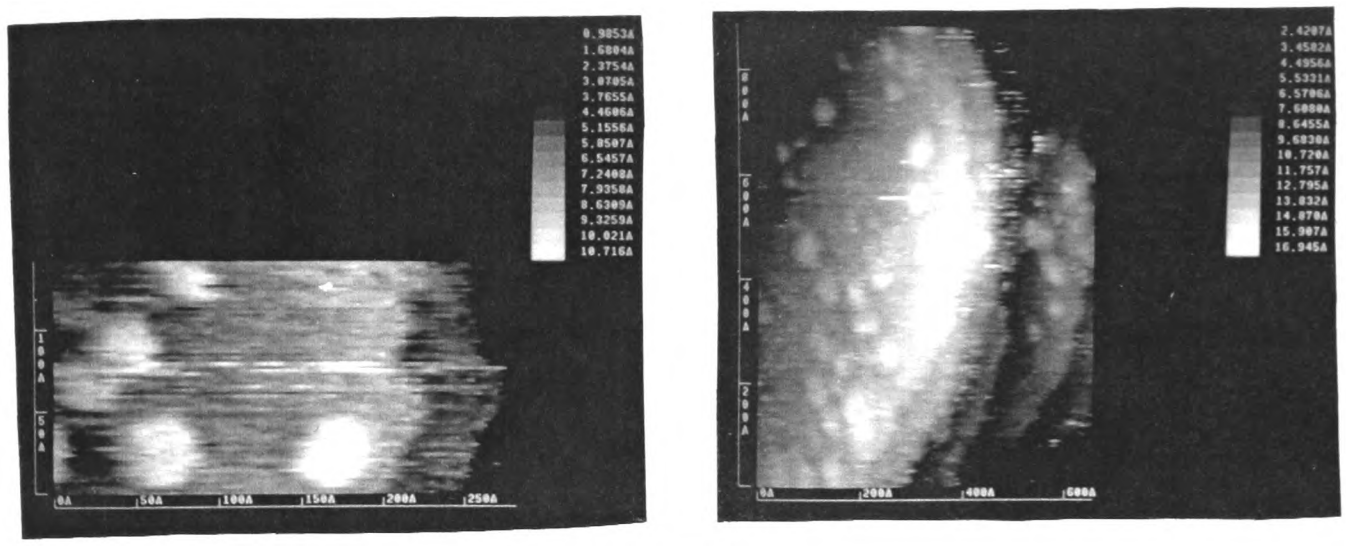

(a) *(b)*

(c) *(d)*

Fig. 6.15. Features observed on an Au 3 sample after exposure to a cytochrome c containing phosphate buffer solution, (a) t; 0.5 ms, inc: 2Å, I_T; 1 nA, V_T; 50 mV, (b) t: 1.0 ms, inc: 5Å, I_T: 1 nA, V_T: 50 mV, (c) conditions as (b) except inc: 4Å, (d) as (b) but inc: 2Å, I_t: 1 nA.

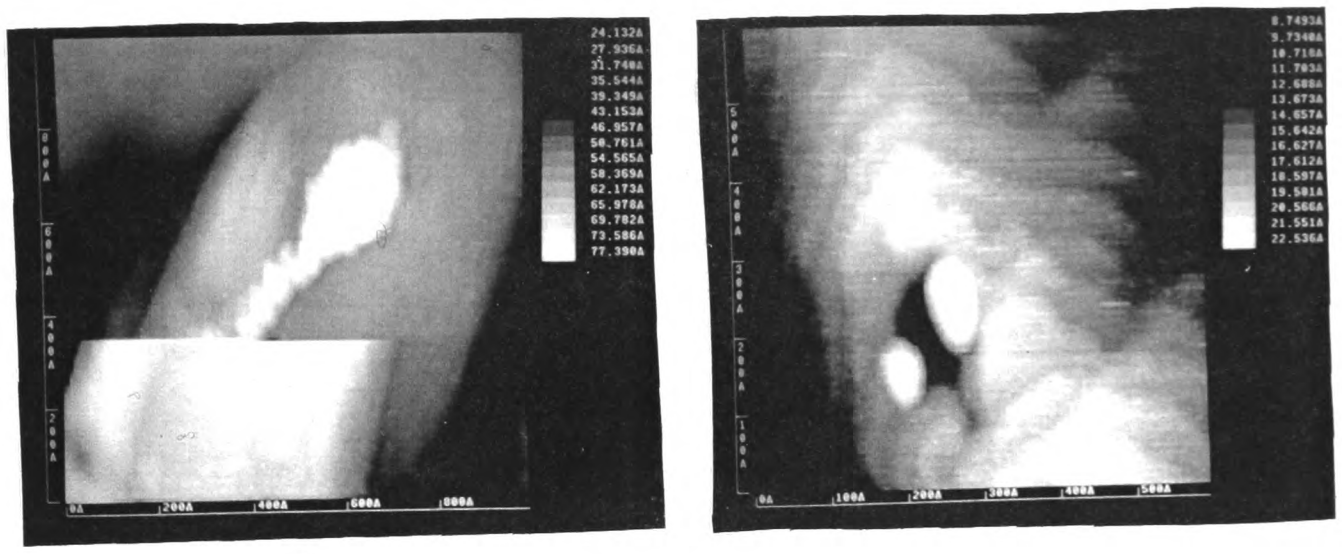

(a) *(b)*

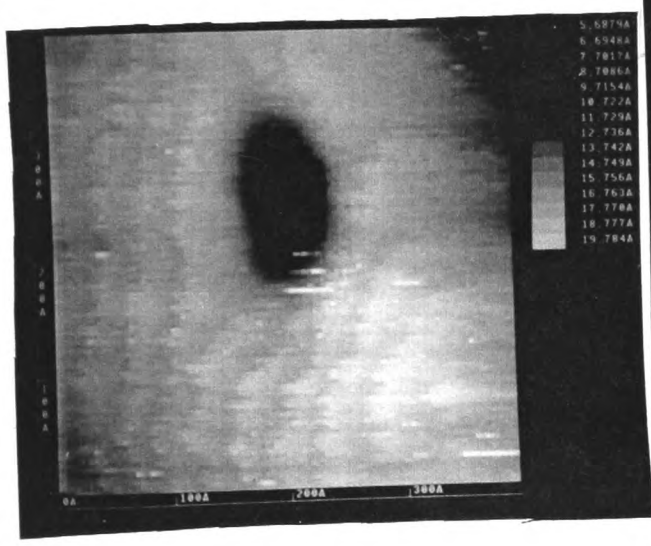

(c)

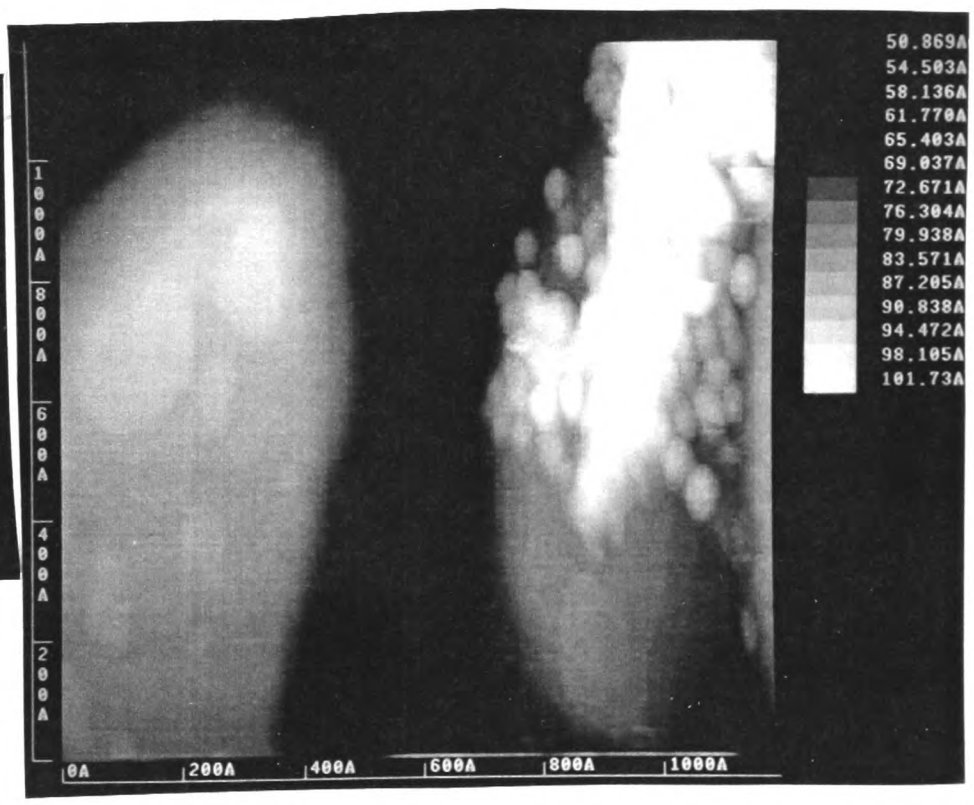

(d)

Fig. 6.16. Features observed on an Au 4 sample after exposure to an aqueous solution of cytochrome c, all images t: 2.0 ms (a) the lower left corner of this image shows an image of a different area of substrate possibly a multiple tip effect, unfortunately area was lost after spectroscopy, inc: 8Å, I_T: 2 nA, V_T: 100 mV, (b) inc: 5 Å, IT; 2 nA, VT: 100 mV, (c) 1V layer of a CITS image inc: 4Å, I_T: 2 nA, (d) inc: 6Å, I_T: 1 nA, V_T: 50 mV.

The similarity of the features in fig. 5.1 and fig. 6.15 (d) suggested the possibility of phosphate buffer being responsible for the effect. Thus for further experiments cytochrome *c* was supported in distilled water alone. A number of experiments were made using this solution, with most showing no deviation from features characteristic of the substrate, however, using the preparation method already outlined with an approximately 20 μM solution the results shown in fig. 6.16 were observed.

As in previous experiments monatomically high 'islands' can be seen on the plateau surface in fig. 6.16 (d) and on the 'unstable' part of fig. 6.16 (a). These 'islands' were imaged on some other plateaus but again many plateaus showed no exceptional features. More interesting are the features not previously observed on plateau surfaces with the appearance of adsorbates. In fig. 6.16 (a) the mound region has a height of 20Å with the strand-like region one of 15Å, whereas in fig. 6.16 (d) the individual 'units', where distinguishable, have the approximate dimensions of 12Å high by 40Å wide and 80Å long. In both images the material imaged appears to have formed a coagulate.

The use of higher voltages during spectroscopy on the, *ca.* 10Å high, features shown in fig. 6.16 (b) caused the removal of the features and it appears some surface mobility with the step structure at the lower end of the hole changing between images.

As the 'visibility' of the molecule to STM was not known, experiments were also made using an aqueous solution of cytochrome c_3. This protein has four exposed haem groups and is a molecule which gives direct electrochemistry at bare gold surfaces. The experiments yielded no conclusive results, although monatomically high 'islands' were observed

on a plateau in one experiment.

Studies on modified surfaces in air

Investigations of the combined SSBPY/cytochrome *c* system were attempted. Here sample preparation involved exposing the gold surface to 1.2 mM SSBPY for 2 minutes, washing with distilled water, exposing to aqueous cytochrome *c* solution for between 45 and 90 minutes and then allowing to dry under cover for another hour. Again monatomically high 'islands' were commonly observed, an interesting example being shown in fig. 6.17 (a), where an 'island' is present on a terraced area close to an emerging step. It is possible that this image shows a screw dislocation; fig. 6.17 (b) shows more clearly the step rising out of the surface.

The problems of attempting to find and identify isolated molecules in this work is indicated by fig. 6.18. In this image the arrowed 'humps' are steep sided features about 30Å high. The comparatively small size and topography of the features implies they are not necessarily part of the surface, and on repeated scanning of the area when the tunneling current was increased and the bias voltage reversed the features lost definition. Unfortunately this behaviour provides little information on characterising the possible molecules.

Fig. 6.19 shows a feature observed in a repeat experiment. The 'blobs' are approximately 25Å high and are situated over an apparent hole in the surface in an analogous manner to that of fig. 6.16 (b). Again spectroscopy failed to yield any extra information on the features.

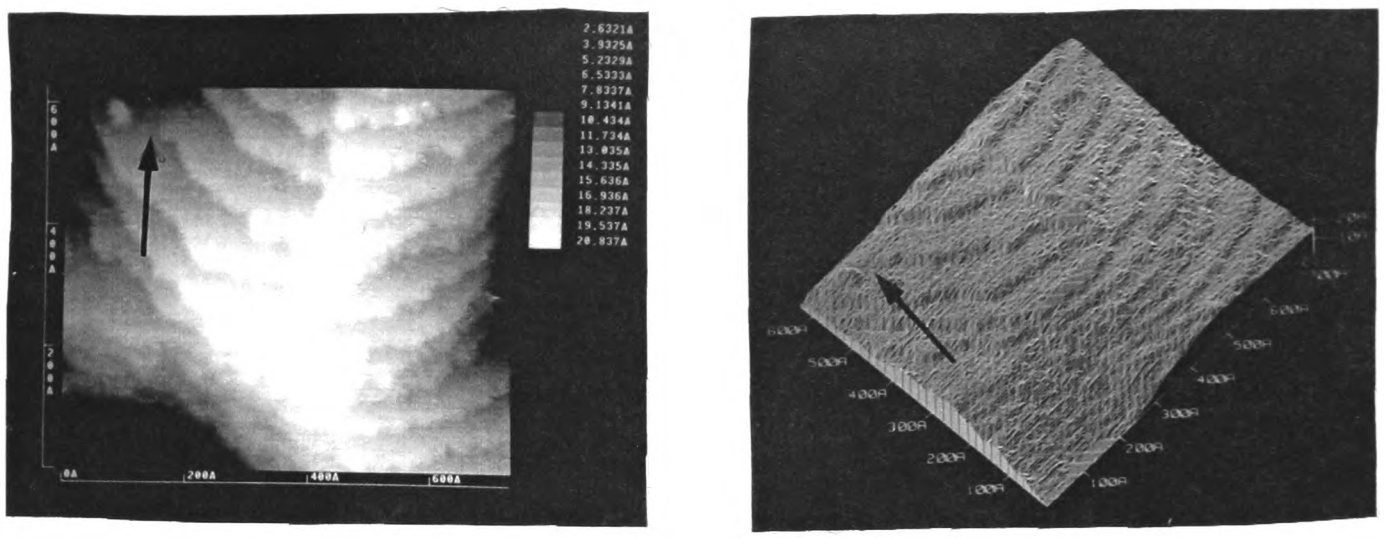

(a) (b)

Fig 6.17. (a) An Au 3 sample after exposure to aqueous solutions of SSBPY and cytochrome c, the emerging step is arrowed for clarity, t: 1.0 ms, inc: 4Å, I_T: 2 nA, V_T: 150 mV, (b) a 3D linescan representation of (a).

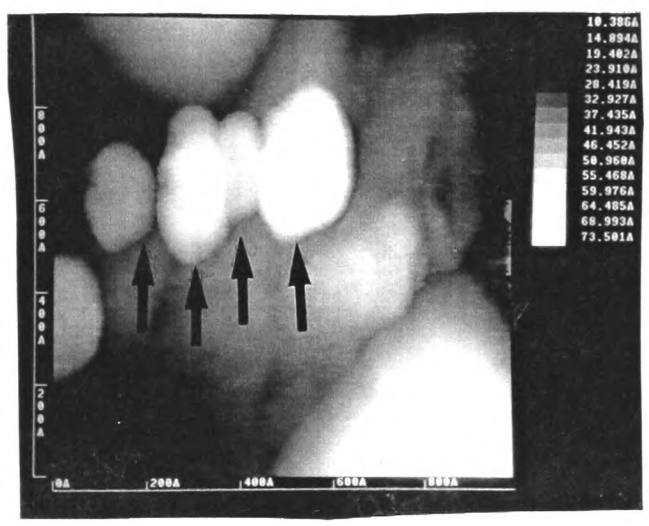

Fig. 6.18

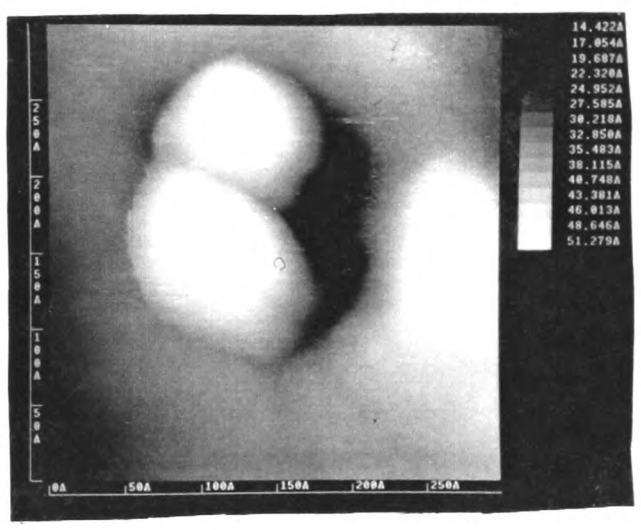

Fig.6.19

Fig. 6.18. Au 4 sample after exposure to aqueous solutions of SSBPY and cytochrome c, t: 2.0 ms, inc: 5Å, I_T: 2 nA, V_T: 50 mV.

Fig. 6.19. 25Å high features seen after exposing an Au 4 sample to SSBPY and cytochrome c solutions, t: 2.5 ms, inc: 1Å, I_T: 1 nA, V_T: 50 mV.

An interesting phenomena observed on this sample and seen previously on other such samples was the presence of regions where stable tunneling was not possible. An example of this is shown on the left side of fig. 6.20, the region is sharply defined but linescans of the area itself showed no consistency from line to line, unlike the right hand area which despite appearing rather amorphous still gave stable linescans. In the attached I/V and derivative curves (from a CITS scan) the flatter curve represents the 'stable' area. Although interpretation of such data is especially difficult with the contaminated surfaces present in ambient experiments, it is obvious the conductivity of the two regions is vastly different. The flatter curve is typical of that found when carrying out CITS in ambient conditions on these gold surfaces. On the current available information it is not possible to attribute this I/V behaviour to either deposited organic material or general contamination.

Fig. 6.21 shows another disordered region adjacent to a flat, but poorly resolved 'metal-like' region. Here the lower part of the image shows more discrete features which may be compared with the 'adsorbate' effects observed in fig. 6.16 (d).

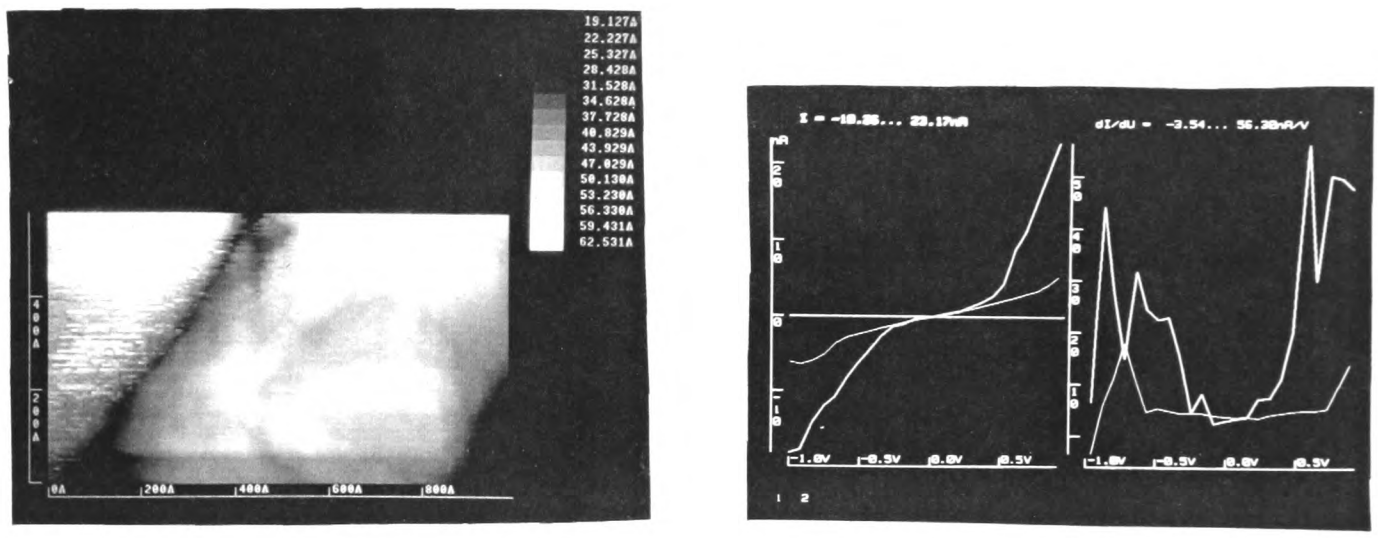

(a) (b)

Fig 6.20. (a) STM image of a defined disordered region adjacent to a normally conducting region, t: 1.5 ms, inc: 5Å, I_T: 10 nA, V_T: 50 mV, (b) CITS data of regions in (a); flatter I/V curve from stable region, steeper from disordered region, CITS: step time 0.35 ms, I_T 2 nA, 80 mV steps.

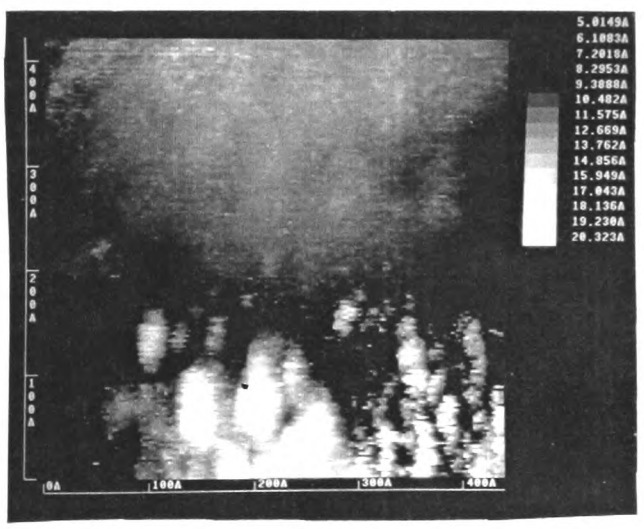

Fig. 6.21. Possible adsorbate effects, sample as for fig. 6.19. t: 1.5 ms, inc: 2.5Å, I_T: 2 nA, V_T: 50 mV.

Studies in aqueous solution

Preliminary experiments were made with the cytochrome *c*/SSBPY system under distilled water and cytochrome *c*/bare gold under phosphate buffer in a potential controlled environment. In both cases streaked features as illustrated in fig. 5.2, were imaged but it is not possible to assign the streaking to cytochrome *c* species or foreign material.

6.III.iii. Discussion

The results presented are most easily rationalised by discussion as three topics; (a) the observation of 'islands' on gold on mica plateaus after exposure to certain aqueous solutions, (b) the inability to resolve SPy species, (c) aspects relating to cytochrome *c*.

Behaviour of gold substrates after exposure to aqueous solutions

The most commonly observed feature after exposing a gold surface to the aqueous solutions used were monatomically high 'islands'. These were imaged in ambient conditions after contact with aqueous solutions of SSBPY and cytochrome *c* and c_3 and *in-situ* with phosphate buffer. These islands were only noted with distilled water when the exposure to water was carried out in the STM cell.

The slightly different features observed after exposure of gold on mica to a cytochrome *c* solution in phosphate buffer and on a gold SCS after exposure to phosphate buffer are considered later.

The correspondence between the vertical height of the islands and the monatomic step height on gold, coupled to the observation of the effect with several solutions, strongly implies the islands are derived from the gold surface itself not adsorption of any solution species. CITS

experiments and use of different bias voltages (including reverse polarities) failed to show noticeable differences between the islands and the rest of the plateau surface, supporting this hypothesis.

Despite extensive use of gold (111) surfaces in STM experiments only Behm's group have reported analogous features[88]. In this publication an Au (100) surface was studied (it was stated that similar features had also been observed, albeit at lower frequency, on Au (111) surfaces): by analogy with previous work on a Pt (100) surface, the islands were attributed to specific adsorption of anions lifting the reconstruction of the gold surface giving a (1x1) structure. As this structure has 20% fewer surface atoms the excess atoms are forced upwards with surface diffusion leading to island formation. As already pointed out in Section 5.V.v., the unreconstructed gold (111) surface has only *ca.* 4.5% fewer atoms, so again the images here seem to show more movement of material than expected.

Aside from this apparent inconsistency, it is still a reasonable proposition that the 'islands' observed are formed due to the lifting of a 22 x $\sqrt{3}$ reconstruction of the gold surface with excess atoms being pushed upwards, and diffusing together. The vertical corrugation of this reconstruction has been quoted as 0.2Å[199], resolution of which is beyond the capabilities of the STM used here. For the majority of the results the *ex-situ* sample preparation implies this transition is driven by the adsorption of species. The *ex-situ* control experiments using distilled water and phosphate only, would appear to imply the surface was unaffected in these cases. Effects were, however, seen when distilled water and phosphate buffer (fig. 5.1) were used *in-situ*, but because the system was not electrochemically controlled, movement of potential could have

raised the reconstruction. Due to the small sampling area of STM far more control experiments are required to fully support this hypothesis. Similarly the lack of observation of these features under sulphuric acid, in contrast to Behm *et al.* may be ascribed to not scanning the 'correct' area or using inappropriate potentials.

For the samples exposed to SSBPY, formation of a self assembled monolayer of SPy (see Sections 6.I. and 6.II.) would provide adequate driving force for a phase transition. For samples exposed to cytochrome *c* and c_3 solutions alone the obvious adsorbates are the proteins themselves, yet it may be expected that features due to the proteins would frequently be found adjacent to the 'islands' and this was not observed. A second possibility is that the protein samples contained some foreign material (e.g. buffer) retained from the extraction procedure which induces lifting of the reconstruction.

The features noted here have been observed on samples several hours after immersion, however as evidenced by images such as fig. 6.12, there is still some surface mobility. Surface diffusion of nanolithographic features formed by STM on gold surfaces has been studied by many workers but in some cases contradictory results have been obtained[172] and this inconsistency has led to speculation about the role of surface cleanliness in the process. Certainly the surfaces discussed above will be covered by some adsorbates from exposure to the atmosphere in addition to those added during immersion.

Obviously much work remains to be done to clarify the suggestions made; the most constructive would be to attempt to observe the processes, *in-situ* with careful electrochemical control, as a species is introduced to the solution. It is worth noting, with regard to this general area of

surface reconstructions under electrolyte, that observation of the 22 x √3-(1x1) transition by *in-situ* STM has provided a solution to the controversy between Kolb and co-workers[232,233] and D'Agostino and Ross about the stability, or otherwise, of the unreconstructed structure in electrolyte[234].

A further unexplained observation is the higher density of 'islands' in cases where the substrate has been exposed to a phosphate containing solution (figs. 5.1 and 6.15 (b), (c) and (d)) than a phosphate free solution. Image 6.15 (d) resembles the 1 x 1 microdomains observed on a platinum (100) surface after replacing an iodine adlayer by CO (fig. 3 in reference 110), though the vertical heights in the two cases are different; 1.5Å in reference 163, 6Å in fig. 6.15. Since the authors of that paper had previously imaged a 1 x 1 surface structure under the iodine adlattice they were not able to rationalise the apparent formation of smaller domains of the same structure.

Ex-situ experiments on gold SCS failed to reproduce the features found in image 6.10. In addition although it shows the wrong symmetry for the 22 x √3 reconstruction (both in the line structure and the lack of 60° changes of direction[199]), the features do have a similarity to the anomalous structure reported by Tao and Lindsay[86]. The irreproducibility of the result together with a lack of supporting literature leaves the observation without adequate explanation.

Effect of sulphide and SSBPY on gold on mica substrates

Unfortunately during this study no individual adsorbed SPy fragments were imaged. Chidsey *et al.*, who added *n*-octadecyl thiol to a gold surface[171], similarly found the organic layer had no apparent effect on the STM experiment, and could not be resolved. More recently Porter and co-workers have observed $\sqrt{3}$ x $\sqrt{3}$ R30° overlayers after exposing gold surfaces to ethanolic solutions of ethanethiol and *n*-octadecyl thiol[65] (nearest neighbour and next-nearest neighbour distances were approximately 5 and 9 Å respectively). They attribute the contrast mechanism to tunneling between the STM tip and sulphur atoms bound to the gold surface. Subsequent work with AFM indicated the same structure, although it was claimed some imaging was attributable to interaction between AFM tip and the hydrocarbon chains[66].

In the light of these sets of work it would appear that the resolution of the Oxford stage was not high enough to allow imaging, though again it should be emphasized the contrast mechanisms giving rise to such STM images are not fully understood. This has been highlighted by Bard and co-workers who again imaged the same $\sqrt{3}$ x $\sqrt{3}$ R30° structure for adsorbed long chain thiols[204]. On moving to thiol molecules with bulky substituents which prevent the same packing of the molecules the same structure was observed! Provisional interpretation has been that the adsorbed thiol species are causing a charge density wave effect to be set up at the gold surface.

Images 6.11 and 6.12 (c) show the unexpected result that surfaces after exposure to sulphide and SSBPY solutions exhibit pitting. Such effects have been reported by Bard[204] and it appears that a similar effect was also observed (but not emphasised) by Sun and Crooks[67].

Two possible interpretations of these features are; (a) the pits are physical depressions in the gold surface, (b) the features are non-conducting regions of surface of undefined topography appearing as pits because no tunneling current is detected from the area. In both cases the cause of these features can be ascribed to the action of sulphur-containing species on either the gold surface or surface impurities (Bucholz and co-workers observed a topography similar to that shown in fig. 6.11 on bare gold surfaces and described the features as characteristic of the surface[235] caused by impurities segregating to the surface). CITS scans of SSBPY covered surfaces showed no variation in electronic properties at different points of the surface but did cause substantial changes in the surface as shown in fig. 6.13 (b).

The dynamic nature of the formation of the pits (i.e. after application of high bias voltages during CITS, and their increased visibility with repeated scanning) and the lack of indication of different electronic properties between the pits and other parts of the surface would tend to favour the suggestion that the pits are physical not electronic effects. Such interpretation is consistent with the suggestion of Bard that the pitting develops due to the effect of the localised electric field given by STM, on a surface covered with adsorbates bonded through sulphur[204]. Further work on this subject is contained in Section 6.IV.

It is far from obvious that imaging the hydrocarbon parts of individual molecules within this adlayer is possible with STM; the aromatic ring is approximately 'edge-on' to the surface, being separated from the surface by an intermediate atom and as shown by the *in-situ* FTIR can alter orientation (see fig. 6.8). Possibly the most appropriate published work is by Wöll and co-workers who have imaged benzene[236]

and copper phthalocyanine[237] molecules lying flat on a surface and have tentatively interpreted features found in an investigation of napthalene on platinum (111) to molecules tilted on edge[238].

The adsorbed SPy species are not envisaged to take part in electron transfer, however they facilitate the direct electrochemistry of cytochrome *c*; a continuation of this area of research could be to study molecular assemblies that are specifically designed to act as electron transfer agents. Kunitake and co-workers have recently reported a mercaptan monolayer membrane which they envisage using to study highly oriented organic reaction sites[239].

A variation on this theme has already been reported by Aviram *et al.*, who investigated the ability of an organic molecule, chemisorbed to a gold surface, to display a switching effect when accessed in a STM experiment[240]. Thus investigation of these systems is an area where information obtained has relevance to electrochemists and those interested in molecular electronics.

Comments on the exposure of gold substrates to cytochrome *c* solutions

The importance of carefully characterising bare samples is underlined when attempting to image randomly adsorbed species, where the appearance of the species (when adsorbed on a surface), to an STM cannot be predicted. Consider images 6.16 (b) and 6.19, exhibiting raised features adjacent to apparent holes in the surface, where using large bias voltages during spectroscopy caused removal of the raised features. Certainly the images contain uncommon features, but these are also similar to images 4.13 (g) and (f). Thus with the available information, the most reasonable

interpretation is that the holes and adjacent hillocks are artifacts of sample preparation dislodged during the spectroscopy scan.

The major point arising here is the *lack* of commonly occurring features that could be interpreted as attributable to cytochrome *c*. The experiments as carried out aimed to image isolated molecules on flat areas of sample; there are many potential problems with this, e.g. molecules may preferentially adsorb in highly disordered areas *not* flat ones, distribution of molecules over the exposed area may be highly uneven - decreasing the probability of scanning an appropriate area, the molecules may be so weakly co-ordinated to the surface that the tip pushes them aside during scanning. Even the ability of the STM experiment to image such molecules was unknown. The most likely candidates for images of cytochrome *c* are images 6.16 (a) and (d); intuitively the images have the appearance of a collection of isolated molecules and the features were not seen on bare substrates.

Cytochrome *c* has the dimensions (from X-ray crystallography) of approximately 25 x 25 x 37Å. Images 6.16 (a) and (d) show collections of particles with lower vertical heights, but larger lateral dimensions, even allowing for the ± 25% uncertainty in lateral measurement, than would be expected from the X-ray data (the individual units in fig. 6.16 (d) have dimensions of 12 x 40 x 80Å). Such disagreement between STM and X-ray measurements is not unusual and suggestions can be made to rationalise this e.g. that the protein unfolds on adsorption at the surface or tip-molecule interactions causes distortion of the molecule. Understanding of why such macromolecules can be observed at all by STM is still causing debate, and many feel the observed structural differences are due to electronic factors: Lindsay and co-workers, in their

attempts to theoretically model the mechanism of imaging of biological molecules by STM, decided height measurements were not necessarily directly related to the physical topography of the molecule[45]. Nawaz *et al.* reported imaging cytochrome c_3 and c_{551} in UHV and found similar contradictions[241].

It is thus probable that the features observed in images 6.16 (a) and (d) (and similarly 6.21) are due to an agglomeration of cytochrome *c* molecules. Unfortunately, in the absence of distinguishing electronic characteristics, e.g. contrast change with reversed polarity, it is not possible to provide more information on the species or make the same assignments for images 6.15 (a) or 6.18. As already stated the speculative potential controlled experiments failed to provide additional information.

Assuming the features are due to cytochrome *c*, the most obvious conclusion from the work is that it is possible to image the protein using STM, although it appears a more careful deposition method is required. A suggestion here is to electrochemically deposit the protein and then image in ambient conditions. The work regrettably does not give much insight into the mechanism of operation of the cytochrome *c*/SSBPY bilayer system apart from appearing to contradict the ideas of Niki *et al.*[223] and Bockris *et al.*[224] who conclude that cytochrome *c* forms a strongly adsorbed layer at the gold surface and also at modified surfaces. Since bare and modified gold surfaces were imaged easily after exposure to cytochrome *c* containing solutions, if a protein layer was formed it was not visible to STM, a conclusion inconsistent with the interpretation of images 6.16 (a) and (d).

6.IV. Study of the electro-oxidation of a modified gold surface in sulphuric acid

Since the previous studies of SSBPY modified surfaces had failed to give any information on the adsorbed organic species themselves, a more indirect approach was tried. In this study of the electro-oxidation of a gold surface after exposure to SSBPY solution, the aims were to find (i) if the effect of adsorption of such a species on the behaviour of the gold surface under potential cycling could be observed and (ii) if any information could be gleaned on the structure of the organic layer. Thus because the gold/sulphuric acid system had already been well studied, sulphuric acid was chosen as the supporting electrolyte for this experiment.

6.IV.i. Results

Fig. 6.22 shows a cyclic voltammogram of a gold on mica electrode in 0.5M sulphuric acid after the addition of 4 drops (approximately 0.2 ml) of 1mM SSBPY solution. The conditions were as given in Section 5.IV.

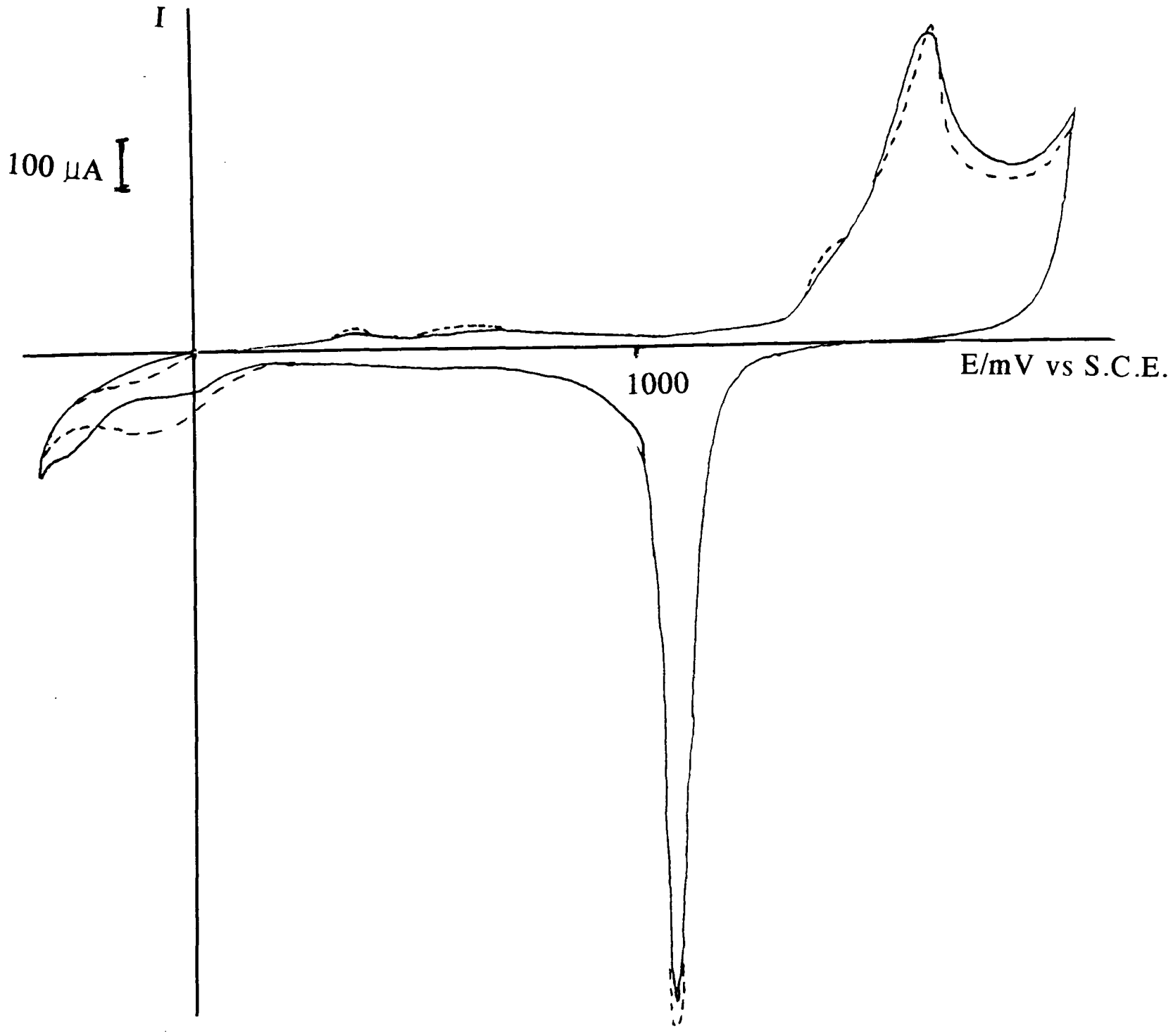

Fig. 6.22. Cyclic voltammogram of an SPY covered gold on mica electrode in 0.5M H_2SO_4. Scan rate 50 mVs^{-1}. Full line - first scan, dotted line - second scan.

The images shown in figure 6.23 were obtained after adding a similar amount of 1mM SSBPY to the experiment that produced the images in figure 5.6. The substrate was set to 400 mV during addition of the SSBPY after an excursion to 1500 mV. Initial images showed a noisy or slightly roughened surface with some evidence of pitting. On applying a potential of 1010 mV the image became less distinct (an effect consistent with the observations of Chapter 5), although the outlines of the three step edges present on the previous image are faintly visible. Significant changes in the topography of the terraces can be observed. The surface structure on returning to the double layer region exhibits an irregularly pitted topography not dissimilar to that observed after oxidation under phosphate buffer. The flecking present at 452 mV, fig. 6.23 (c), has disappeared at 200 mV, fig. 6.23 (d). Reducing the potential to -109 mV fig. 6.23 (e), reveals considerable step edge movement, expansion of pits already present and additional pitting.

Instability at -403 mV, caused an area change and break in the series of images. Subsequently altering the potential to 1293 mV fig. 6.23 (f) and returning to the double layer region gave a terraced surface without pits. This behaviour was reproduced on stepping up to 1491 mV, fig. 6.23 (i).

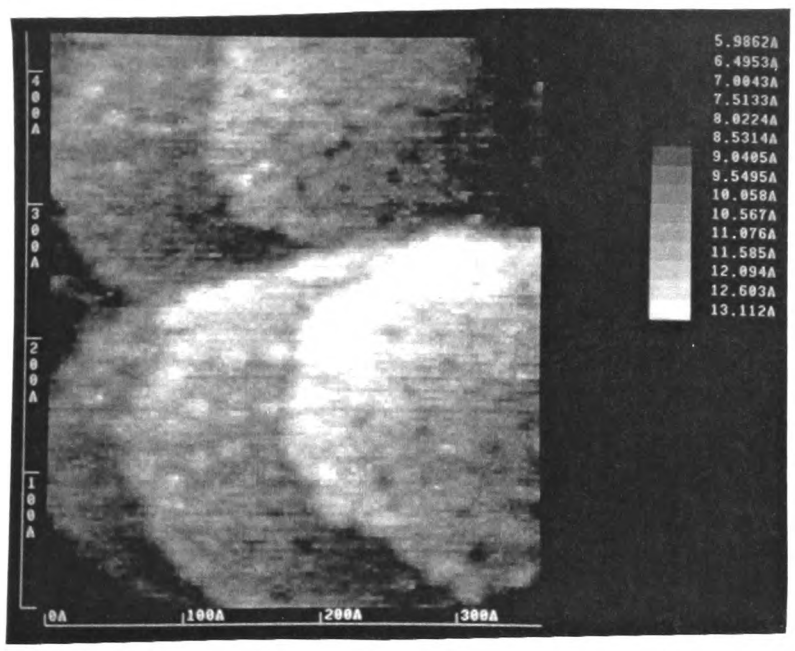

(a) 400 mV

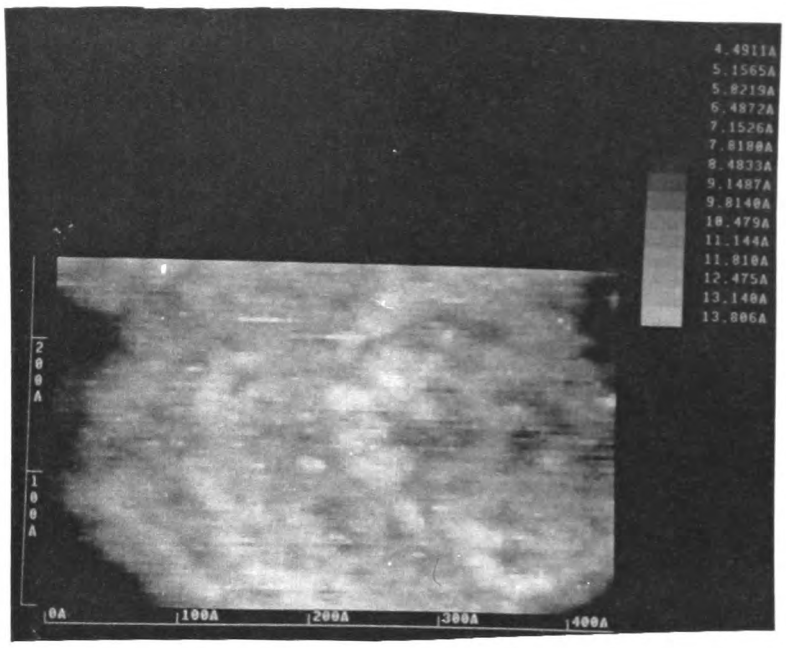

(b) 1010 mV

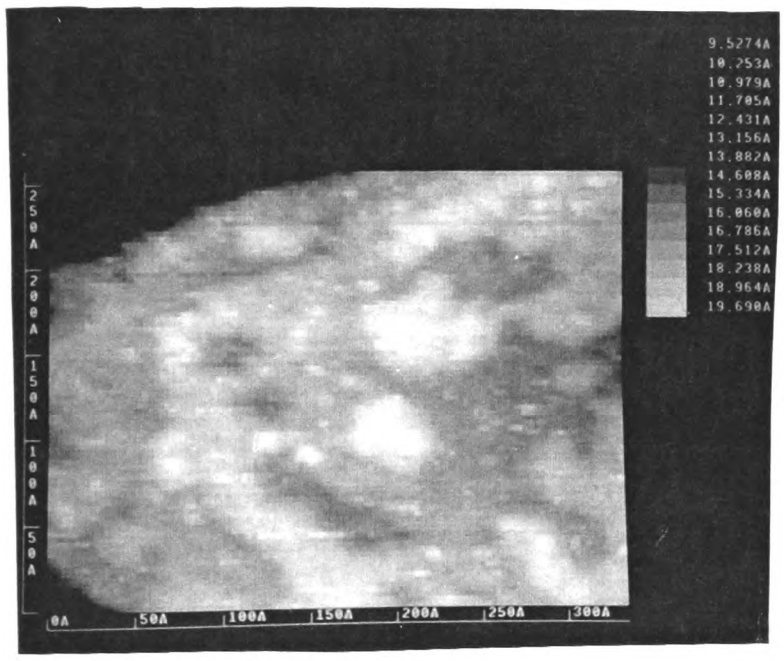

(c) 452 mV

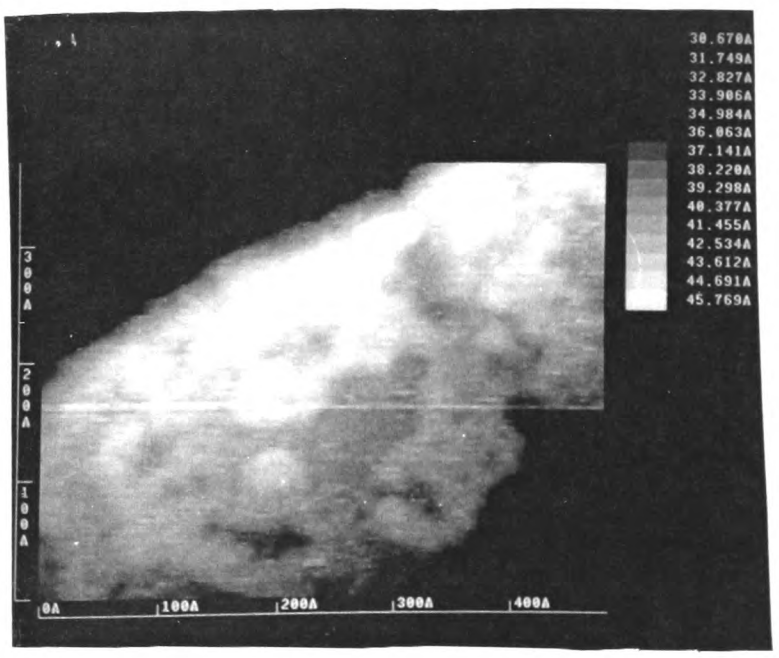

(d) 200 mV

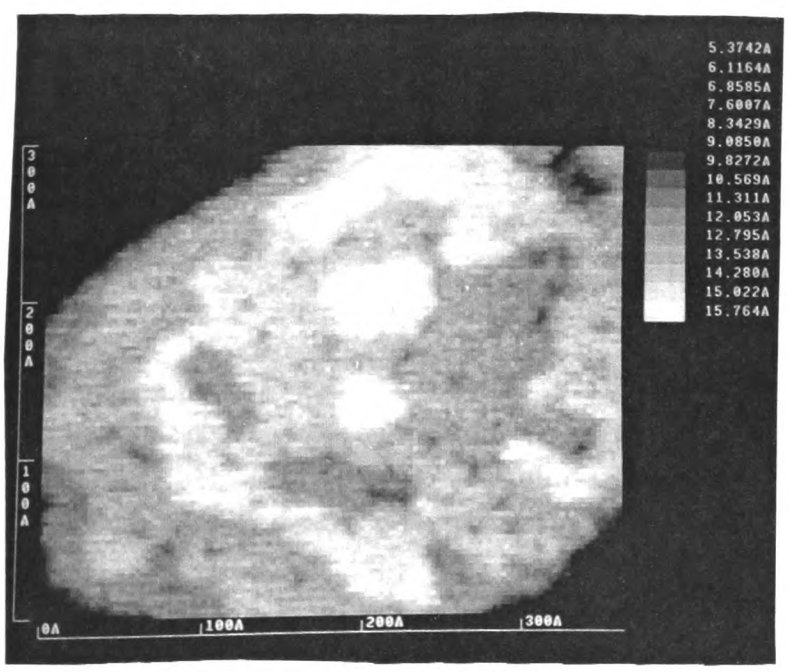

(e) -109 mV

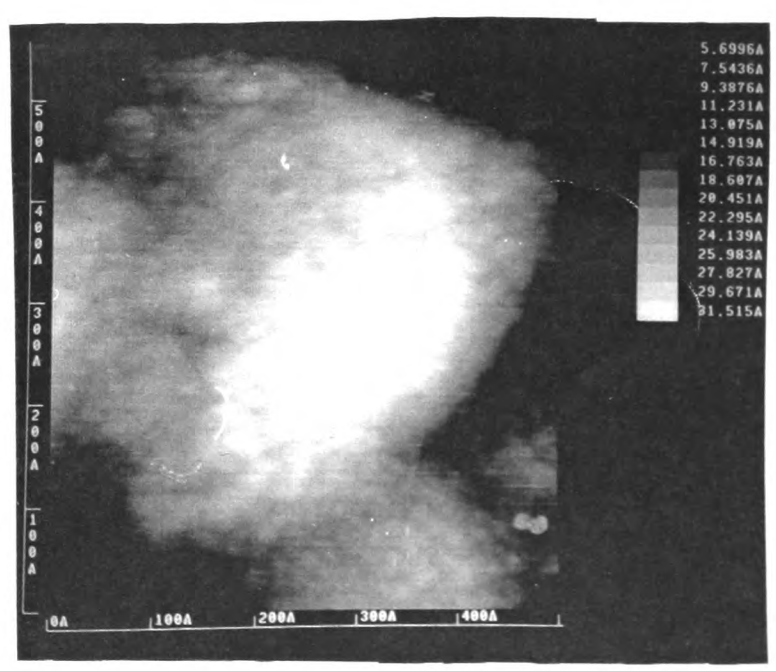

(f) 701 mV

Fig. 6.23 Sample potential only shown, full caption overleaf.

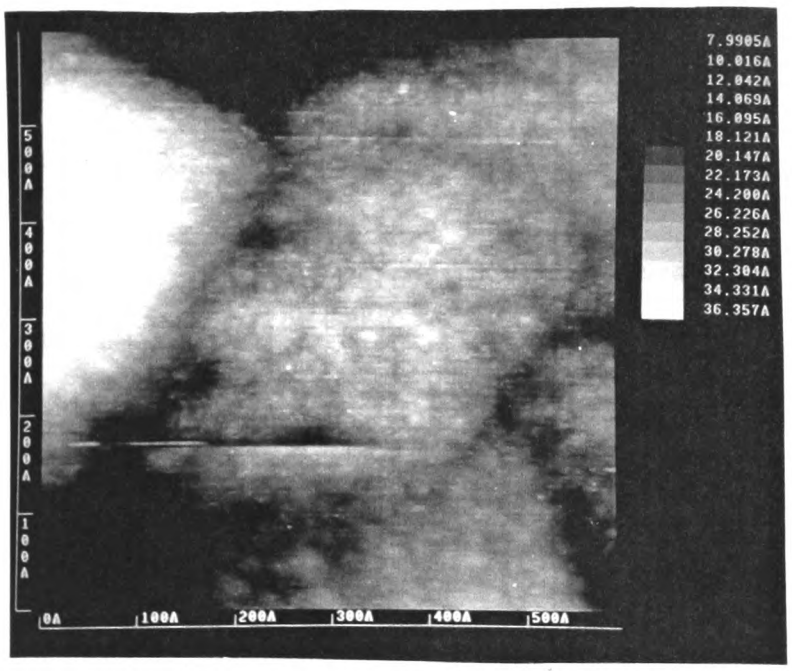

(g) 1293 mV

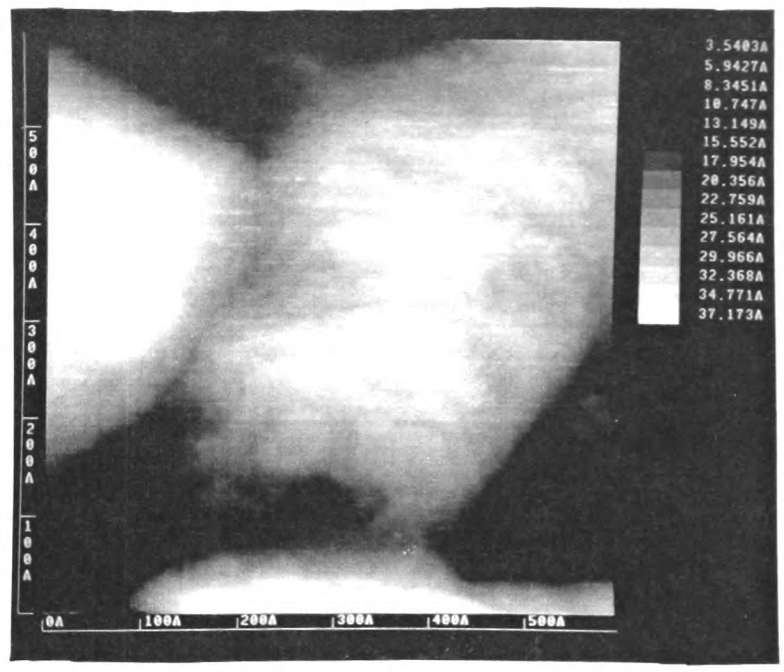

(h) 462 mV

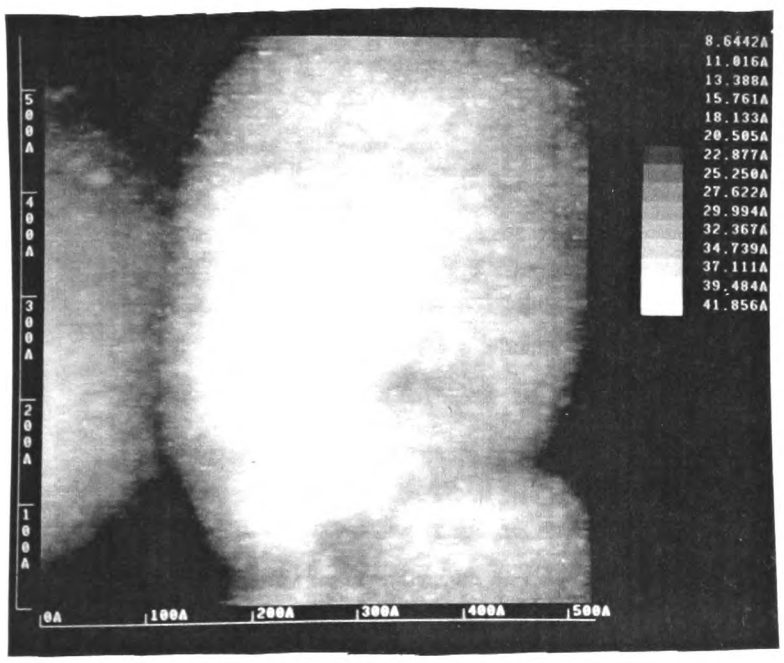

(i) 1491 mV

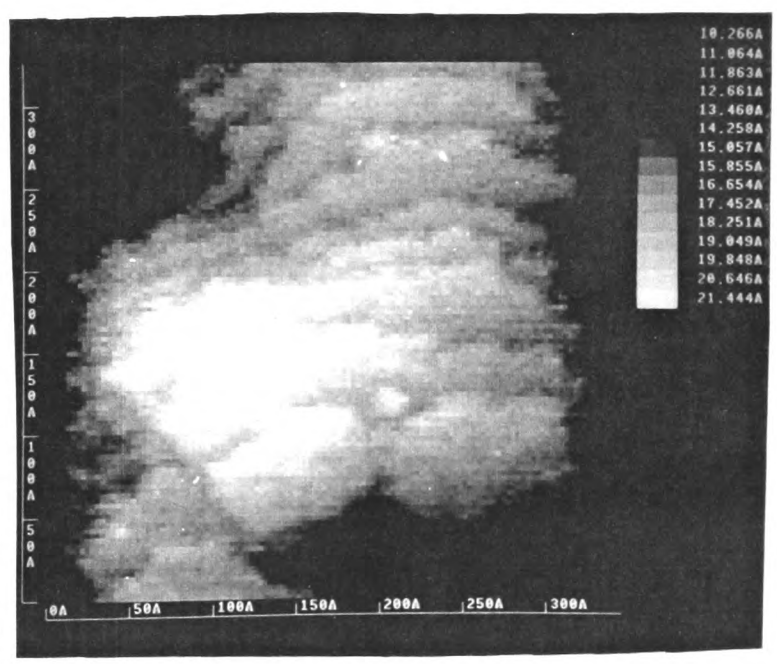

(j) 404 mV

Fig. 6.23. Images of electro-oxidation of a SPY covered gold on mica electrode in 0.5M H_2SO_4 (t: 1.5 ms, inc: 3Å, I_T 3 nA) Potentials vs S.C.E.

6.IV.ii. Discussion

Comparison of the cyclic voltammogram in fig. 6.22 against that shown in figure 5.5 indicates the adsorption of SSBPY causes the OA 1 and OA 2 peaks to be almost completely suppressed and the OA 3 and OA 4 processes to become compressed into one peak. Although the onset of oxidation is slightly shifted to higher potential the overall charge passed is approximately the same (see OC III). At negative potentials peaks due to peroxide formation are suppressed. As can be seen on the second scan the OA 1 and 2 peaks begin to become reappear as does the peroxide peak. Since the OA 1 and 2 peaks are due to MOH formation, already partially blocked on the Au (111) surface, it is not surprising that the presence of an organic monolayer inhibits the process further. The OA 3 shoulder is similarly lost. The surface is still able to oxidise and the replacement turnover mechanism remains operational as indicated by the OA 4 peak.

Reappearance of these peaks (together with those related to the presence of dissolved oxygen), implies that during this process, or at the onset of bulk oxide formation, the effect of the organic monolayer is reduced. This could be through, for example, irreversible loss of SPy from the surface or rearrangement to expose fresh gold.

It is conceivable, though unlikely in the light of experience, that the pitting present on image 6.23 (a) was due to the prior sweep up to 1500 mV. The extent of pitting and movement apparent at 1010 mV, is unexpected as this is at least 100 mV before the replacement turnover process crucial for pit formation by surface oxidation is considered to be important. In addition the lack of island growth implies that this 'turnover' process is not taking place. The results of Chapter 5 showed that step movement at this potential was possible, but not pit formation.

The next set of images show continuing 'dissolution' of the surface with pit formation in evidence by -109 mV. This is again surprising - the surface previously has shown stability at these potentials. The lack of correlation with the voltammogram implies that the process observed is chemical not electrochemical. The large scale nature of the process observed shows the process involves the whole surface, negating suggestions that the effect is due to small amounts of surface segregated impurities. These observations support the hypothesis (made previously in the discussion concerning images 6.11, 6.12 (c) and 6.13 (b)) that the surface pitting is induced by the interaction of the STM experiment and the gold-sulphur bond.

The surface under electrolyte was far more dynamic than similarly modified surfaces investigated in air, but since the electrolyte contained other coordinating species, this is not particularly surprising (*cf.* Section 5.V.). The observation of a 'standard' non-pitted surface in images 6.23 (h) and (j), taken after excursions to higher positive potentials, is consistent with the cyclic voltammetry. Porter *et al.* have proposed adsorbed thiol layers are irreversibly oxidised to sulphonic acids on electro-oxidative desorption in acidic media[243]. Such a proposal would fit into the observations made here; exposure of the gold surface would allow the standard CV to be regained and no pitting would be expected. The highly roughened topography formed by the pitting is obviously smoothed by the sweep to high potentials as expected from the results presented in Chapter 5.

Although the *in-situ* electrochemical work was not successful in providing information on the structure of the organic layer these results, together with those from *ex-situ* studies, provide evidence of a novel

process that should be investigated more thoroughly. An obvious starting point is a thorough investigation of the effect of tunneling conditions (i.e. bias voltage, tunneling current and pixel acquisition time) on the pitting process. It is not obvious were the displaced gold is moved to and this depends on the actual reaction occurring: in air presumably appropriate gold atoms gain enough energy to become mobile, in a mechanism analogous to that allowing lithography by voltage pulse, to diffuse to step edges. Under electrolyte the gold may be displaced to a different part of the surface or even into solution.

Another obvious experiment is to attempt to reproduce this effect not only with other sulphur containing compounds but other inorganic species, e.g. the other chalcogenides.

It may be that initial pitting occurs preferentially at specific sites and this could be examined by high resolution STM work. There are some indications in image 6.23 (e) that there is pitting in regions that had previously been covered by gold, i.e. reaction with the second gold layer. Further work is needed to confirm this, but observation of pitting on gold not previously bonded to sulphur may imply the thiol monolayer to be mobile.

6.V. Conclusions

In-situ FTIR was used to provide further evidence for the adsorption of SSBPY at gold electrodes to give a monolayer of SPy bonded to gold through sulphur. This work is consistent with that already published. Furthermore the orientation of the SPy species was shown to be potential dependent. The relation between this observation and the direct electrochemistry of cytochrome *c* at modified electrodes remains to be elucidated. This work was originally intended to support STM

investigations of the SSBPY/cytochrome *c* system, but subsequent STM studies did not provide information that could be easily correlated with the FTIR data. It is not clear if STM is able to image the aromatic part of the SPy adsorbate.

STM investigations of the SSBPY/cytochrome *c* system unexpectedly led to indications of surface rearrangement of the gold surface after exposure to aqueous solutions whereby discrete monatomic high islands are formed. It is clear much additional work is required to identify the cause and mechanism of this transition. Other features formed after exposure of gold to these solutions (e.g. the dense 'blob' effect apparent on images 5.11 and 6.14) have been reported. It is not possible to completely rationalise these features with the information currently available.

Attempts to image cytochrome *c* molecules on the gold substrate were of limited success, although a small number of images contained features which were attributable to the protein. It would appear from this set of experiments that while cytochrome *c* is detectable by STM it does not form a strongly adsorbed monolayer on the gold surface as concluded by some workers. This work highlighted a number of problems with imaging discrete biomolecules: firstly it was extremely hard to locate and identify the molecules and secondly the molecules themselves, when observed, appeared as part of a large coagulation. It must therefore be concluded that more attention needs to be paid to developing deposition procedures - the most promising method is to use electro-deposition within a potential controlled experiment. Utilisation of this type of approach may also facilitate easier characterisation of material by either reversibly adsorbing and desorbing molecules themselves and correlating the

potentials of the process to known characteristics or using potentials at which the supporting surface is modified to differentiate surface and molecule.

STM imaging of gold surfaces after exposure to SSBPY and sulphide containing solutions showed pitting of the modified surfaces. In a subsequent investigation of the electro-oxidation of a SPy modified gold surface in sulphuric acid substantial surface mobility and pitting were observed. This is the first time this process has been imaged by STM. Movement of the substrate to higher potentials where the organic monolayer is apparently lost from the surface (as indicated by cyclic voltammetry) returned the surface topography to its original state. The results have been shown to be consistent with a hypothesis that the pitting is caused by interaction of the STM experiment with the gold-sulphur bond.

This set of results provides evidence of the unintentional manipulation of a surface by STM. Here the technique is potentially invasive and thus may cause confusion by modifying the surface as it is investigated. This effect may subsequently be highly relevant to one of the long term aims of this work - that of high density data storage. Depending on the process actually causing the pitting it is not hard to envisage a data storage system based around selective removal of gold atoms from a surface. 'Writing' could be achieved by carefully controlled STM, while non-invasive 'reading' could be via AFM. Certainly the investigations started here on the STM of SSBPY modified surfaces merit further attention.

References

1 G.Binnig, H.Rohrer, Ch.Gerber, E.Weibel, *Phys. Rev. Lett.*, **49**, (1982) 57.

2 G.Binnig and H.Rohrer, Nobel prize winners in physics 1986, *Rev. Mod. Phys.*, **59**, (1987) 615.

3 STM '91, Interlaken, Switzerland, August 1991.

4 R.G.Compton, A.Hamnett (Eds.), Comprehensive chemical kinetics, Vol 29, Elsevier, Amsterdam, 1989.

5 R.J.Gale (Ed), Spectroelectrochemistry: Theory and practice, Plenum, New York, 1988.

6 R.Parsons in ref. 4, p. 105.

7 P.A.Christensen and A.Hamnett in ref.4, p. 1.

8 R.E.Hester in ref. 4, p. 79.

9 R.Greef in ref. 4, p. 427.

10 L.M.Peter in ref. 4, p. 353.

11 D.M.Kolb in ref. 5, p. 124.

12 A.Wieckowski in R.E.White, J.O'M.Bockris and B.E.Conway (Eds.), *Modern Aspects of Electrochemistry* Vol. 21, Plenum, New York, 1990, p. 65.

13 H.D.Abruña in R.E.White, J.O'M.Bockris and B.E.Conway (Eds.), *Modern Aspects of Electrochemistry* Vol. 20, Plenum, New York, 1989.

14 For e.g. M.L.Lynch, B.J.Barner, R.M.Corn, *J. Electroanal. Chem.*, **300**, (1991) 447.

15 D.A.Scherson in ref. 5, p.399.

16 X. Gao, A.Hamelin, M.J.Weaver, *Phys. Rev. Lett.*, **67**, (1991) 618.

17 O.M.Magnussen, J.Hotlos, G.Beitel, D.M.Kolb, R.J.Behm, *J. Vac. Sci. Technol.*, **B9**, (1991) 969.

18 T.Hachiya, H.Honbo, K.Itaya, *J. Electroanal. Chem.*, **315**, (1991) 275.

19 Proc. 1st Int. STM Conf. (1986) in *Surf. Sci.*, **181**, (1987), Proc. 2nd Int. STM Conf. (1987) in *J. Vac. Sci. Technol.*, **A6**, (1988), Proc. 3rd Int. STM Conf. (1988) in *J. Microsc.*, **152**, (1988), Proc. 4th Int. STM Conf. (1989) in *J. Vac. Sci. Technol.*, **A8**, (1990), Proc. 5th Int. STM Conf. (1990) in *J. Vac. Sci. Technol.*, **B9**, (1991).

20 R.J.Behm, N.Garcia and H.Rohrer (Eds.), Scanning tunneling microscopy and related methods. NATO ASI Series E, Vol. 184, Kluwer, Dordrecht, 1990.

21 C.R.Clemmer, T.P.Beebe, *Science*, **251**, (1991) 640.

22 M.L.Myrick, N.V.Hud, S.M.Angel, D.G.Garvis, *Chem. Phys. Lett.*, **180**, (1991) 156.

23 H.Chang, A.J.Bard, *Langmuir*, **7**, (1991) 1143.

24 M.P.Everson, J.H.Helms, *Synth. Metals*, **40**, (1991) 97.

25 C.F.Quate, Paper presented at NATO Science Forum 1990; Highlights of the Eighties and Future Prospects in Condensed Matter Physics. To be published in a NATO Series by Plenum Press.

26 H.J.Mamin, P.H.Guenthner, D.Rugar, *Phys. Rev. Lett.*, **65**, (1990) 2418.

27 D.M.Eigler, E.K.Schweizer, *Nature*, **344**, (1990) 525.

28 M.O.Watanabe, T.Kuroda, K.Tanaka, A.Sakai, *J. Vac. Sci. Technol.*, **B9**, (1991) 924.

29 B.Drake, R.Sonnenfeld, J.Schneir, P.K.Hansma, G.Slough, R.V.Coleman, *Rev. Sci. Instrum.*, **57**, (1986) 441.

30 R.Sonnenfeld, J.Schneir, B.Drake, P.K.Hansma, D.E.Aspnes, *Appl. Phys. Lett.*, **50**, (1987) 1742.

31 J.Schneir, O.Marti, G.Remmers, D.Gläser, R.Sonnenfeld, B.Drake, P.K.Hansma, V.Elings, *J. Vac. Sci. Technol.*, **A6**, (1988) 283.

32 J.Schneir, R.Sonnenfeld, O.Marti, P.K.Hansma, J.E.Demuth, R.J.Hamers, *J. Appl. Phys.*, **63**, (1988) 717.

33 J.Schneir, P.K.Hansma, *Langmuir*, **3**, (1987) 1025.

34 J.S.Foster, J.E.Frommer, P.C.Arnett, *Nature* **331**, (1988) 324.

35 G.C.McGonigal, R.H.Bernhardt, D.J.Thomson, *Appl. Phys. Lett.*, **57**, (1990) 28.

36 R.H.Bernhardt, G.C.McGonigal, R.Schneider, D.J.Thomson, *J. Vac. Sci. Technol.* **A8**, (1990) 667.

37 J.D.Todd, J.B.Pethica, *J. Phys.: Condens. Matter.*, 1, (1989) 9823.

38 M.Sawamura, J.F.Womelsdorf, W.C.Ermler, *J. Phys. Chem.*, **95**, (1991) 8823.

39 R.Sonnenfeld, P.K.Hansma, *Science*, **232**, (1986) 211.

40 F.R.F.Fan, A.J.Bard, *J. Electrochem. Soc.*, **136**, (1989) 166.

41 R.J.Driscoll, M.G.Youngquist, J.D.Baldeschwieler, *Nature*, **346**, (1990) 294.

42 G.Travaglini, H.Rohrer, M.Amrein, H.Gross, *Surf. Sci.* **181**, (1987) 380.

43 S.M.Lindsay, B.Barris, *J. Vac. Sci. Technol.*, **A6**, (1988) 544.

44 G.Lee, D.F.Evans, V.Elings, R.D.Edstrom, *J. Vac. Sci. Technol.*, **B9**, (1991) 1236.

45 S.M.Lindsay, O.F.Sankey, Y.Li, C.Herbst, A.Rupprecht, *J. Phys. Chem.*, 94, (1990) 4655.

46 J.-Y. Yuan, Z.Shao, C.Gao, *Phys. Rev. Lett.*, **67**, (1991) 863.

47 A.J.Arvia, *Surf. Sci.*, **181**, (1987) 78.

48 M.M.Dovek, M.J.Heben, N.S.Lewis, R.M.Penner, C.F.Quate, Electrochemical Surface Science: Molecular Phenomena at Electrode Surfaces. ACS Symp. Ser. **378**, (1988) 174.

49 R.Sonnenfeld, J.Schneir and P.K.Hansma in R.E.White, J.O'M.Bockris and B.E.Conway (Eds.), *Modern Aspects of Electrochemistry* Vol. 21, Plenum, New York, 1990, p. 1.

50 T.R.I.Cataldi, I.G.Blackham, G.A.D.Briggs, J.B.Pethica, H.A.O.Hill, *J. Electroanal. Chem.*, **290**, (1990) 1.

51 P.A.Christensen, *Chem. Rev.*, 21, (1992) 197.

52 J.Gomez, L.Vasquez, A.M.Baro, C.L.Perdriel, A.J.Arvia, *Electrochimica Acta*, **34**, (1989) 619.

53 L.Vazquez, J.Gomez, A.M.Baro, N.Garcia, M.L.Marcos, J.Gonzalez Velasco, J.M.Vara, A.J.Arvia, J.Presa, A.García, M.Aguilar, *J. Am. Chem. Soc.*, **109**, (1987) 1730.

54 J.M.Gomez-Rodriguez, A.M.Baro, R.C.Salvarezza, *J. Vac. Sci. Technol.*, B9, (191) 495.

55 A.J.Arvia, C.Alonso, R.C.Salvarezza, J.M.Vara, L.Vazquez, A.Bartolome, A.M.Baro, *J. Electrochem. Soc.*, **137**, (1990) 2161.

56 G.Kreysa, J.Gomez, A.Baro, A.J.Arvia, *J. Electroanal. Chem.*, **265**, (1989) 67.

57 L.M.Siperko, *J. Electrochem. Soc.*, **137**, (1990) 2791.

58 I.Otsuka, T.Iwasaki, *J. Vac. Sci. Technol.*, **A8**, (1990) 530.

59 R.Yang, K.M.Dalsin, D.F.Evans, L.Christensen, W.A.Hendrickson, *J. Phys. Chem.* **93**, (1990) 6117.

60 R.Yang, K.Naoi, D.F.Evans, W.H.Smyrl, W.A.Hendrickson, *Langmuir* 7, (1991) 556.

61 T.L.Porter, S.Jeffers, G.Caple, B.L.Wheeler, R.Swift, *Surf. Sci. Lett.*, **238**, (1990) L433.

62 D.A.Bonnell, M.Angelopoulos, *Synth. Metals*, 33, (1989) 301.

63 B.C.Schardt, S.L.Yau, F.Rinaldi, *Science*, **243**, (1989) 1050.

64 S.-C.Chang, S.-L.Yau, B.C.Schardt, M.J.Weaver, *J. Phys. Chem.*, **95**, (1991) 4787.

65 C.A.Widrig, C.A.Alves, M.D.Porter, *J. Am. Chem. Soc.*, **113**, (1991) 2805.

66 C.A.Alves, E.L.Smith, M.D.Porter, *J. Am. Chem. Soc.*, **114**, (1992) 1222.

67 L.Sun, R.M.Crooks, *J. Electrochem. Soc.*, **138**, (1991) L23.

68 A.J.Bard, L.R.Faulkner, Electrochemical Methods: Fundamentals and Applications. J.Wiley and Sons, N.Y. 1980.

69 P.Lustenberger, H.Rohrer, R.Christoph, H.Siegenthaler, *J. Electroanal. Chem.*, **243**, (1988) 225.

70 J.Wiechers, T.Twomey, D.M.Kolb, R.J.Behm, *J. Electroanal. Chem.*, **248**, (1988) 451.

71 S.-L.Yau, X.Gao, S.-C.Chang, B.C.Schardt, M.J.Weaver, *J. Am. Chem. Soc.*, **113**, (1991) 6049.

72 J.K.Sass, J.K.Gimzewski, *J. Electroanal. Chem.*, **251**, (1988) 241.

73 M.Binggeli, D.Carnal, R.Nyffenegger, H.Siegenthaler, R.Christoph, H.Rohrer, *J. Vac. Sci. Technol.*, **B9**, (1991) 1985.

74 J.K.Sass, J.K.Gimzewski, *J. Electroanal. Chem.*, **308**, (1991) 333.

75 W.Schmickler, *J. Electroanal. Chem.*, **296**, (1990) 283.

76 V.A.Merichev, *Surf. Sci.*, **250**, (1991) 220.

77 R.Sonnenfeld, B.C.Schardt, *Appl. Phys. Lett.*, **49**, (1986) 1172.

78 K.Itaya, S.Sugawara, *Chem. Lett.*, (1987) 1927.

79 B.Drake, R.Sonnenfeld, J.Schneir, P.K.Hansma, *Surf. Sci.*, **181**, (1987) 92.

80 J.Schneir, V.Elings, P.K.Hansma, *J. Electrochem. Soc.*, **135** (1988) 2774.

81 K.Itaya, K.Higaki, S.Sugawara, *Chem. Lett.*, (1988) 421.

82 O.Lev, F.-R.Fan, A.J.Bard, *J. Electrochem. Soc.*, **135**, (1988) 783.

83 A.Hamelin, X.Gao, M.J.Weaver, *J. Electroanal. Chem.*, **323**, (1992) 361.

84 X. Gao, A.Hamelin, M.J.Weaver, *Phys. Rev. B.*, **44**, (1991) 10983.

85 X. Gao, A.Hamelin, M.J.Weaver, *J. Chem. Phys.*, **95**, (1991) 6993.

86 N.J.Tao, S.M.Lindsay, *J. Appl. Phys.*, **70**, (1991) 5141.

87 O.M.Magnussen, J.Hageböck, J.Hotlos, R.J.Behm, *Faraday Discuss.*, **94**, (1992) to be published.

88 R.J.Nichols, O.M.Magnussen, J.Hotlos, T.Twomey, R.J.Behm, D.M.Kolb, *J. Electroanal. Chem.*, **290**, (1990) 21.

89 P.N.Ross, *J. Vac. Sci. Technol.*, **A5**, (1987) 948.

90 D.J.Trevor, C.E.D.Chidsey, D.N.Loiacono, *Phys. Rev. Lett.*, **62**, (1989)

91 D.J.Trevor, C.E.D.Chidsey, *J. Vac. Sci. Technol.*, **B9**, (1991) 964.

92 H.Honbo, S.Sugawara, K.Itaya, *Anal. Chem.*, **62**, (1990) 2424.

93 J.Brooker, P.A.Christensen, A.Hamnett, R.He, C.A.Paliteiro, *Faraday Discuss.*, **94**, (1992) to be published.

94 E. Holland-Moritz, J.Gordon II, K.Kanazawa, R.Sonnenfeld, *Langmuir*, **7**, (1991) 1981.

95 O.M.Magnussen, J.Hotlos, R.J.Nichols, D.M.Kolb, R.J.Behm, *Phys. Rev. Lett.*, **64**, (1990) 29291.

96 N.Batina, T.Will, D.M.Kolb, *Faraday Discuss.*, **94**, (1992) to be published.

97 R.J.Nichols, D.M.Kolb, R.J.Behm, *J. Electroanal. Chem.*, **313**, (1991) 109.

98 M.P.Green, K.J.Hanson, D.A.Scherson, X.Xing, M.Richter, P.N.Ross, R.Carr, I.Lindau, *J. Phys. Chem.*, **93**, (1989) 2181.

99 M.P.Green, K.J.Hanson, R.Carr, I.Lindau, *J. Electrochem. Soc.*, **137**, (1990) 3493.

100 N.J.Tao, S.M.Lindsay, *J. Phys. Chem.*, **96**, (1992) 5213.

101 X.Gao, Y.Zhang, M.J.Weaver, *J. Phys. Chem.*, **96**, (1992) 4156.

102 K.Itaya, S.Sugawara, K.Sashikata, N.Furuya, *J. Vac. Sci. Technol.*, **A8**, (1990) 515.

103 K.Sashikata, N.Furuya, K.Itaya, *J. Vac. Sci. Technol.*, **B9**, (1991) 457.

104 K.Uosaki, H.Kita, *J. Electroanal. Chem.*, **259**, (1989) 301.

105 M.J.Armstrong, R.H.Muller, *J. Electrochem. Soc.*, **138**, (1991) 2303.

106 K.Sashikata, N.Furuya, K.Itaya, *J. Electroanal. Chem.*, **316**, (1991) 361.

107 N.Kimizuka, K.Itaya, *Faraday Discuss.*, **94**, (1992) to be published.

108 S.-L.Yau, C.M.Vitus, B.C.Schardt, *J. Am. Chem. Soc.*, **112**, (1990) 3677.

109 H.Baltruschat, U.Bringemeier, R.Vogel, *Faraday Discuss.*, **94**, (1992) to be published.

110 C.M.Vitus, S.-C.Chang, B.C.Schardt, M.J.Weaver, *J. Phys. Chem.*, **95**, (1991) 7559.

111 J.S.Chen, T.S.Devine, D.F.Ogletree, M.Salmeron, *Surf. Sci.*, **258**, (1991) 346.

112 M.H.J.Hottenhuis, M.A.H.Mickers, J.W.Gerritsen, J.P. Van der Eerden, *Electrochimica Acta*, **34**, (1989) 1141.

113 M.Höpfner, W.Obretenov, K.Jüttner, W.J.Lorenz, G.Staikov, V.Bostanov, E.Budevski, *Surf. Sci.*, **248**, (1991) 225.

114 R.Christoph, H.Siegenthaler, H.Rohrer, H.Wiese, *Electrochimica Acta*, 34, (1989) 1011.

115 W.Obretenov, U.Schmidt, W.J.Lorenz, G.Staikov, E.Budevski, D.Carnal, U.Müller, H.Siegenthaler, E.Schmidt, *Faraday Discuss.*, **94**, (1992) to be published.

116 R.Houbertz, U.Memmert, R.J.Behm, *Appl. Phys. Lett.*, **58**, (1991) 1027.

117 E.Tomita, N.Matsuda, K.Itaya, *J. Vac. Sci. Technol.*, **A8**, (1990) 534.

118 K.Itaya, E.Tomita, *Chem. Lett.*, (1989) 285.

119 P.Carlsson, B.Holmström, H.Kita, K.Uosaki, *J. Electroanal. Chem.*, **283**, (1990) 425.

120 S.Eriksson, P.Carlsson, B.Holmström, K.Uosaki, *J. Electroanal. Chem.*, 313, (1991) 121.

121 K.Uosaki, M.Koinuma, *Faraday Discuss.*, **94**, (1992) to be published.

122 T.Thundat, L.A.Naghara, S.M.Lindsay, *J. Vac. Sci. Technol.*, **A8**, (1990) 539.

123 A.A.Gewirth, A.J.Bard, *J. Phys. Chem.*, **92** (1988) 5563.

124 J.Wang, T.Martinez, D.R.Yaniv, L.D.McCormick, *J. Electroanal. Chem.*, 313, (1991) 129.

125 J.Wang, T.Martinez, D.R.Yaniv, L.D.McCormick, *J. Electroanal. Chem.*, 286, (1990) 265.

126 D.R.Yaniv, L.D.McCormick, J.Wang, N.Naser, *J. Electroanal. Chem.*, **314**, (1991) 353.

127 X.G.Zhang, U.Stimming, *J. Electroanal. Chem.*, **291**, (1990) 273.

128 H.W.Pickering, Y.C.Wu, D.S.Gregory, S.Geh, T.Sakurai, *J. Vac. Sci. Technol.*, **B9**, (1991) 976.

129 R.C.Bhardwaj, A.Gonzalez-Martin, J.O'M.Bockris, *J. Electroanal. Chem.*, 307, (1991) 195.

130 R.C.Bhardwaj, A.Gonzalez-Martin, J.O'M.Bockris, *J. Electrochem. Soc.*, **138**, (1991) 1901.

131 T.Thundat, L.A.Nagahara, P.I.Oden, S.M.Lindsay, M.A.George, W.S.Glaunsinger, *J. Vac. Sci. Technol.*, **A8**, (1990) 3537.

132 L.A.Nagahara, T.Thundat, P.I.Oden, S.M.Lindsay, R.L.Rill, *Ultramicroscopy*, **33**, (1990) 107.

133 G.Binnig, C.F.Quate, Ch.Gerber, *Phys. Rev. Lett.*, **56**, (1986) 930.

134 A.J.Gratz, S.Manne, P.K.Hansma, *Science*, **251**, (1991) 1343.

135 B.Drake, C.B.Prater, A.L.Weisenhorn, S.A.C.Gould, T.R.Albrecht, C.F.Quate, D.S.Cannell, H.G.Hansma, P.K.Hansma, *Science*, **243**, (1989) 1586.

136 R.D.Edstrom, M.A.Miller, V.B.Elings, X.Yang, R.Yang, G.Lee, D.F.Evans, *J. Vac. Sci. Technol.*, **B9**, (1991) 1248.

137 S.Manne, J.Massie, V.B.Elings, P.K.Hansma, A.A.Gewirth, *J. Vac. Sci. Technol.*, **B9**, (1991) 950.

138 S.Manne, P.K.Hansma, J.Massie, V.B.Elings, A.A.Gewirth, *Science*, 251, (1991) 183.

139 C.-H. Chen, A.A.Gewirth, *J. Am. Chem. Soc.*, **114**, (1992) 5439.

140 C.-H. Chen, S.M. Vesecky, A.A.Gewirth, *J. Am. Chem. Soc.*, **114**, (1992) 451.

141 C.-H. Chen, A.A.Gewirth, *Phys. Rev. Lett.*, **68**, (1992) 1571.

142 H.Heinzelmann, E.Meyer, H.Rudin, H.-J.Güntherodt in ref. 20, p. 443.

143 T.P.Weihs, private communication.

144 T.P.Weihs, Z.Nawaz, S.P.Jarvis, J.B.Pethica, *Appl. Phys. Lett.*, in press.

145 A.J.Bard, F-R.F.Fan, J.Kwak, O.Lev, *Anal. Chem.*, **61**, (1989) 132.

146 A.J.Bard, F.-R.Fan, D.T.Pierce, P.R.Unwin, D.O.Wipf, F.Zhou, *Science*, 254, (1991) 68.

147 P.K.Hansma, B.Drake, O.Marti, S.A.C.Gould, C.B.Prater, *Science,* **243**, (1989) 641.

148 H.Rohrer in ref. 20, p. 8.

149 Y.Kuk, P.J.Silverman, *Rev. Sci. Instrum.*, **60**, (1989) 165.

150 P.K.Hansma, J.Tersoff, *J. Appl. Phys.*, **61**, (1987) R1.

151 J.Tersoff, D.R.Hamann, *Phys. Rev. Lett.*, **50**, (1983) 1998 and *Phys. Rev. B,* **31**, (1985) 805.

152 R.M.Feenstra, J.A.Stroscio, J.Tersoff, A.P.Fein, *Phys. Rev. Lett.*, **58**, (1987) 1192.

153 J.Tersoff in ref. 20, p. 86.

154 C.J.Chen, *Phys. Rev. Lett.*, **65**, (1990) 448.

155 R.M.Feenstra in ref. 20, p. 230.

156 S.-I.Park, C.F.Quate, *Rev. Sci. Instrum.*, **58**, (1987) 2010.

157 S.Grafström, J.Kowalski, R.Neuman, *Meas. Sci. Technol.*, 1, (1990) 139.

158 Omicron Vakuumphysik GMBH, Idsteiner Str. 78, D-6204, Taunusstein 4. Germany.

159 A.Bewick and S.Pons in R.J.H.Clark and R.E.Hester (Eds.), Advances in Infrared and Raman Spectroscopy, Vol.12, Wiley Heyden, London, 1985, p. 1.

160 P.A.Christensen, A.Hamnett, P.R.Trevellick, *J. Electroanal. Chem.*, 242, (1988) 23.

161 Oxsys Micros Ltd., 15 Alma Place, Oxford.

162 Southampton Electrochemistry Group, Instrumental Methods in Electrochemistry, Wiley and Sons, Chichester 1985.

163 S.A.Weeks, *D. Phil. Thesis,* Oxford (1987).

164 McGeoch Ltd., 124, Electric Avenue, Witton, Birmingham, B6 7DZ.

165 Description/code no. 6.0724.XXX, Metrohm Ltd. CH-9101 Herisau, Switzerland.

166 A.J.Melmed, *J. Vac. Sci. Technol.*, **B9**, (1991) 601.

167 M.J.Heben, R.M.Penner, N.S.Lewis, M.M.Dovek, C.F.Quate, *Appl. Phys. Lett.*, **54**, (1989) 1421.

168 A.A.Gewirth, D.H.Craston, A.J.Bard, *J. Electroanal. Chem.*, **261**, (1989) 477.

169 Longreach Scientific Resources, RFD 1, Box 549, Orr's Island, ME 04066 U.S.A.

170 L.A.Nagahara, T.Thundat, S.M.Lindsay, *Rev. Sci. Instrum.*, **60**, (1989) 3128.

171 C.E.D.Chidsey, D.N.Loiacono, T.Sleator, S.Nakahara, *Surf. Sci.*, **200**, (1988) 45.

172 D.A.Sommerfeld, R.T.Cambron, T.P.Beebe, *J. Phys. Chem.*, **94**, (1990) 8926.

173 D.W.Pohl, *IBM J. Res. Develop.*, **30**, (1986) 417.

174 Companies offering STM and AFM instruments include Digital Instruments, U.S.A., Park Scientific Instruments, U.S.A., Omicron Vakuumphysik, Germany, W.A. Technology, U.K., VG Instruments, U.K., Hitachi, Japan, Jeol, Japan.

175 G.Binnig, H.Rohrer, *IBM J. Res. Develop.*, **30**, (1986) 355.

176 Ch. Gerber, G.Binnig, H.Fuchs, O.Marti, H.Rohrer, *Rev. Sci. Instrum.*, 57, (1986) 221.

177 G.Binnig, D.P.E.Smith, *Rev. Sci. Instrum.*, **57**, (1986) 1688.

178 J.E.Demuth, R.J.Hamers, R.M.Tromp, M.E.Welland, *J. Vac. Sci. Technol.*, A4, (1986) 1320.

179 G.W.Stupian, M.S.Leung, *Rev. Sci. Instrum.*, **60**, (1989) 181.

180 B.G.Orr, C.W.Snyder, M.Johnson, *Rev. Sci. Instrum.*, **62**, (1991) 1400.

181 M.Welland, Cambridge University, private communication.

182 N.Shimizu, T.Kimura, T.Nakamura, I.Umeba, *J. Vac. Sci. Technol.*, **A8**, (1990) 333.

183 D.W.Pohl, *Rev. Sci. Instrum.*, **58**, (1987) 54.

184 M.M.Dovek, M.J.Heben, C.A.Lang, N.S.Lewis, C.F.Quate, *Rev. Sci. Instrum.*, **59**, (1988) 2333.

185 J.D.Todd, *D. Phil. Thesis*, Oxford (1991).

186 Burleigh Instruments (UK) Ltd., 11 Hatfield Rd, St.Albans, Herts, AL1 3RR.

187 Unilator Ltd., Vauxhall Industrial Estate, Ruabon, Wrexham, Clwyd. LL14 6HY

188 Ch.Gerber, private communication.

189 D.P.DiLella, J.H.Wandass, R.J.Colton, C.R.K.Marrian, *Rev. Sci. Instrum.*, **60**, (1989) 997.

190 T.R.I.Cataldi, unpublished results.

191 Nano Instruments Inc., P.O.Box 14211, Knoxville, TN 37914, U.S.A.

192 Burleigh Instruments technical guide; The inchworm approach in STM, C.W.Snyder, B.G.Orr, L.Rapp.

193 Analog Devices, Linear Products Databook, 1988, Analog Devices MA. U.S.A.

194 H.A.O.Hill, private communication.

195 J.B.Pethica, *Phys. Rev. Lett.*, **37**, (1986) 3235.

196 A.Selloni, P.Carnevali, E.Tosatti, C.D.Chen, *Phys. Rev. B*, **31**, (1985) 2602.

197 S.-I.Park, C.F.Quate, *Appl. Phys. Lett.*, **48**, (1986) 112.

198 J.Schneir, R.Sonnenfeld, P.K.Hansma, J.Tersoff, *Phys. Rev. B*, **34**, (1986) 4979.

199 J.V.Barth, H.Brune, G.Ertl, R.J.Behm, *Phys. Rev. B*, **42**, (1990) 9307.

200 J.A.Derose, T.Thundat, L.A.Nagahara, S.M.Lindsay, *Surf. Sci.*, **256**, (1991) 102.

201 Z.Wang, M.Moskovits, *J. Appl. Phys.*, **71**, (1992) 5401.

202 J.B.Pethica, private communication.

203 J.Hossick Schott, C.R.Arana, H.D.Abrûna, H.Hurrell Petach, C.M.Elliott, H.S.White, *J. Phys. Chem.*, **96**, (1992) 5222.

204 A.J.Bard, Introductory Lecture, Faraday discussion meeting No. 94: The liquid/solid interface at high resolution, *Faraday Discuss.*, **94**, (1992) to be published.

205 R.Emch, J.Nogami, M.M.Dovek, C.A.Lang, C.F.Quate, *J. Appl. Phys.*, **65**, (1989) 79.

206 C.J.Roberts, B.Hoffman-Millack, W.S.Steer, *Surf. Sci.*, **224**, (1989) 1.

207 J.Hotlos, private communication.

208 D.Elliott, A.Hamnett, O.C.Lettington, H.A.O.Hill, N.J.Walton, *J. Electroanal. Chem.*, **202**, (1986) 303.

209 H.Angerstein-Kozlowska, B.E.Conway, A.Hamelin, L.Stoicoviciu, *Electrochimica Acta*, **31**, (1986) 1051.

210 H.Angerstein-Kozlowska, B.E.Conway, A.Hamelin, L.Stoicoviciu, *J. Electroanal. Chem.*, **228**, (1987) 429.

211 R.R.Adžic, N.M.Markovic, *Electrochimica Acta*, **30**, (1985) 1473.

212 M.Shibata, K.Nakamura, N.Furuya, M.Watanabe, *J. Electroanal. Chem.*, **314**, (1991) 179.

213 A.Rodes, J.M.Feliu, A.Aldaz, J.Clavilier, *J. Electroanal. Chem.*, **256**, (1988) 455.

214 F.A.Armstrong, H.A.O.Hill, N.J.Walton, *Acc. Chem. Rev.*, **21**, (1988) 407.

215 F.R.Salemme, *Ann. Rev. Biochem*, **46**, (1977) 299.

216 P.Yeh, T.Kuwana, *Chem. Lett.*, (1977) 1145.

217 M.J.Eddowes, H.A.O.Hill, *J. Chem. Soc. Chem. Comm.*, (1977) 3154.

218 P.M.Allen, H.A.O.Hill, N.J.Walton, *J. Electroanal. Chem.*, **178**, (1984) 69.

219 H.A.O.Hill, D.J.Page, N.J.Walton, D.Whitford, *J. Electroanal. Chem.*, **187**, (1985) 315.

220 I.Taniguchi, M.Iseki, H.Yamaguchi, K.Yasukouchi, *J. Electroanal. Chem.*, **186**, (1985) 299.

221 H.A.O.Hill, D.J.Page, N.J.Walton, *J. Electroanal. Chem.*, **217**, (1987) 141.

222 K.Niwa, M.Furukawa, K.Niki, *J. Electroanal. Chem.*, **245**, (1988) 275.

223 C.Hinnen, K.Niki, *J. Electroanal. Chem.*, **264**, (1989) 157.

224 A.Szucs, G.D.Hitchens, J.O'M.Bockris, *Electrochimica Acta*, **37**, (1992) 413.

225 H.A.O.Hill, L.Pinaheiro, N.Hunt, private communication.

226 For example R.G.Nuzzo, F.A.Fusco, D.L.Allara, *J. Am. Chem. Soc.*, 109, (1987) 2358.

227 A.Hamnett, P.A.Christensen, O.C.Lettington, unpublished results.

228 G.Socrates, Infrared Characteristic Group Frequencies, Wiley - Interscience, Chichester, 1980.

229 C.H.Kline, Jr., J.Turkevich, *J. Chem. Phys.*, **12**, (1944) 300.

230 P.A.Christensen, A.Hamnett, I.G.Blackham, *J. Electroanal. Chem.*, 318, (1991) 407.

231 D.Reay Pt.II. thesis, Oxford 1991.

232 D.M.Kolb, G.Lehmpfuhl, M.S.Zei, *J. Electroanal. Chem.*, **179**, (1984) 289.

233 A.Friedrich, B.Pettinger, D.M.Kolb, G.Lüpke, R.Steinhoff, G.Marowsky, *Chem. Phys. Lett.*, **163**, (1989) 123.

234 A.T.D'Agostino, P.N.Ross Jr., *Surf. Sci.*, **185**, (1987) 88.

235 S.Bucholz, H.Fuchs, J.P.Rabe, *J. Vac. Sci. Technol.*, **B9**, (1991) 857.

236 H.Ohtani, R.J.Wilson, S.Chiang, C.M.Mate, *Phys. Rev. Lett.*, **60**, (1988) 2398.

237 P.H.Lippel, R.J.Wilson, M.D.Miller, Ch.Wöll, S.Chiang, *Phys. Rev. Lett.*, **62**, (1989) 171.

238 V.M.Hallmark, S.Chaing, J.K.Brown, Ch.Wöll, *Phys. Rev. Lett.*, **66**, (1991) 48.

239 M.Kunitake, K.Akiyoshi, K.Kawatana, N.Nakashima, O.Manabe, *J. Electroanal. Chem.*, **292**, (1990) 277.

240 A.Aviram, C.Joachim, M.Pomerantz, *Chem. Phys. Lett.*, **146**, (1988) 490.

241 Z.Nawaz, T.R.I.Cataldi, J.Knall, R.Somekh, J.B.Pethica, *Surf. Sci.*, 265, (1992) 139.

242 C.A.Widrig, C.Chung, M.D.Porter, *J. Electroanal. Chem.*, **310**, (1991) 335.

243 A.Zangwill, Physics at surfaces, Cambridge University Press, Cambridge, 1988.

Appendix A

Reference list of *in-situ* electrochemical STM (and AFM) literature

FEATURE/PROCESS	SYSTEM	REFERENCE
Surface inspection	Ag	113
	Si	116, 117
	n-TiO_2	118
	$GaAs^2$	121
	Carbon paste electrode	125
	Glucose oxidase electrode	126
Potential dependent reconstruction	H^+/Au (100)	16, 83
	H^+/Au (110)	84
	H^+/Au (111)	85, 86
Electrolyte adlayer	HSO_4^-/Au	87
Potential controlled topographic changes	H^+/Au	70
	OH^-/Au	93
	Aq. salt/Au	94
	Cl^+/Ag	111
	H^+/GaP	119
	OH^-/GaAs	120
	OH^-/Ta	131
Oxidation/Reduction	H^+/Au (111)	88, 90, 91, 92, 137 (AFM)
	H^+/Pt	102, 103
	H^+/Rh,Pd	103
	H^+/HOPG	123
	Phenol/HOPG	124
Underpotential deposition (UPD)	Cu/Au	17, 95, 97, 18, 96, 138 (AFM)
	Pb/Au	73, 98, 99
	Bi/Au	139 (AFM)
	Ag/Au	140 (AFM)
	Hg/Au	141 (AFM)
	Cu/Pt	106
	Ag/Pt	107
	Pb/Ag	114, 115

Deposition	Cu/Pt	104, 105
	Ag/Ag	112
	Ni/Ge	122
Adsorbate	halide/Au	100
	S/Au	101
	halide/Pt	108, 109
	I^-/CO/Pt	110
	CO/Rh	71
	DNA/Au	132
Dissolution	Cu	127, 128
Passivation	OH^-/Al	129
	borate/Fe	130

Appendix B

Reconstruction and adlayer nomenclature[243]

A two dimensional periodic structure can be described by defining a surface net by the vectors $\mathbf{a}_S$ and $\mathbf{b}_S$, where every lattice point can be reached from the origin by a translation of the form $\mathbf{T} = m\mathbf{a}_S + n\mathbf{b}_S$. This leads to five nets (although the centered rectangular net is a version of the oblique net), as shown in figure B.1.

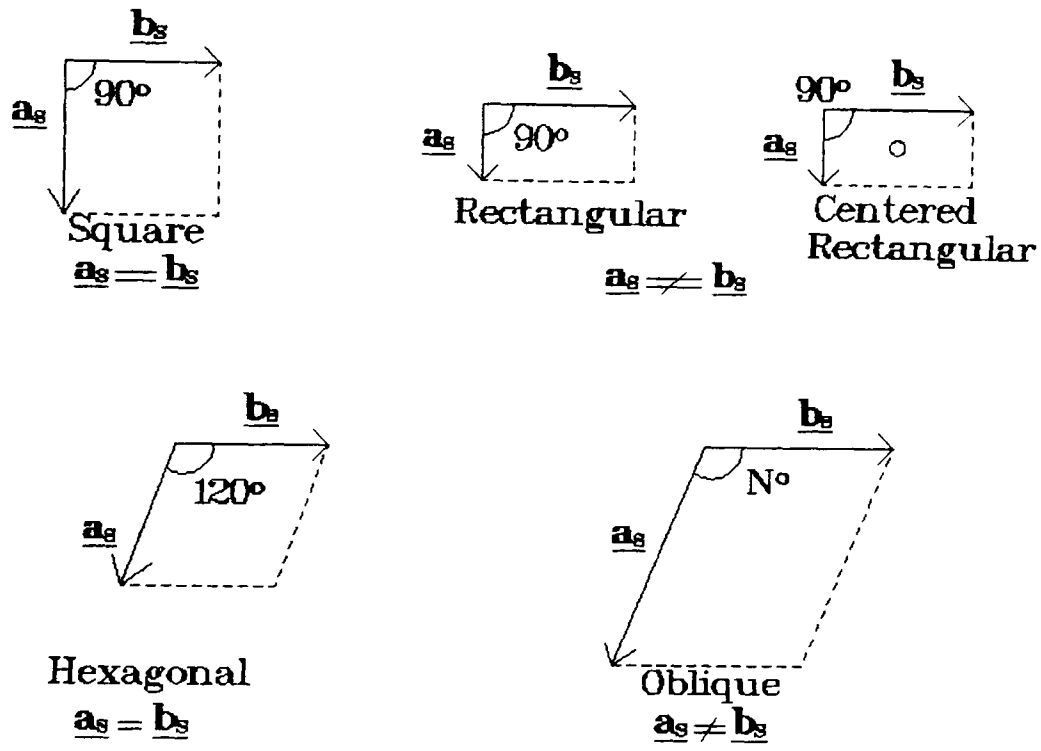

Fig. B.1. The five surface nets

Ideal or simply relaxed surfaces have structures identical to the underlying bulk lattice (**a** and **b**) and, as the translation vectors of the surface are identical to the bulk, they are termed (1 x 1) structures of the appropriate exposed plane, e.g. Au (110) 1 x 1.

For a reconstructed surface the periodicity and orientation of the surface net differs from that of the ideal surface; $\mathbf{a}_S = N\mathrm{a}$ and $\mathbf{b}_S = N\mathrm{b}$. Here the nomenclature is R(*hkl*) *N* x *M*. e.g. Au (110) 2 x 1. The angle of rotation relative to the bulk lattice is noted after the vectors.

Similarly for ordered overlayers the ratios of the lengths of the adsorbate (*A*) and substrate (*S*) unit mesh translation vectors and relative rotational orientation (Φ) and written *S* (*hkl*) (*N* x *M*) - *A* RΦ. An example of this is illustrated in figure 1.7.

Appendix C

Technical diagrams of the Oxford Electrochemical STM (Mk. 3)

These diagrams are best used in conjunction with the photographs, diagrams and descriptions contained in Chapter 3.

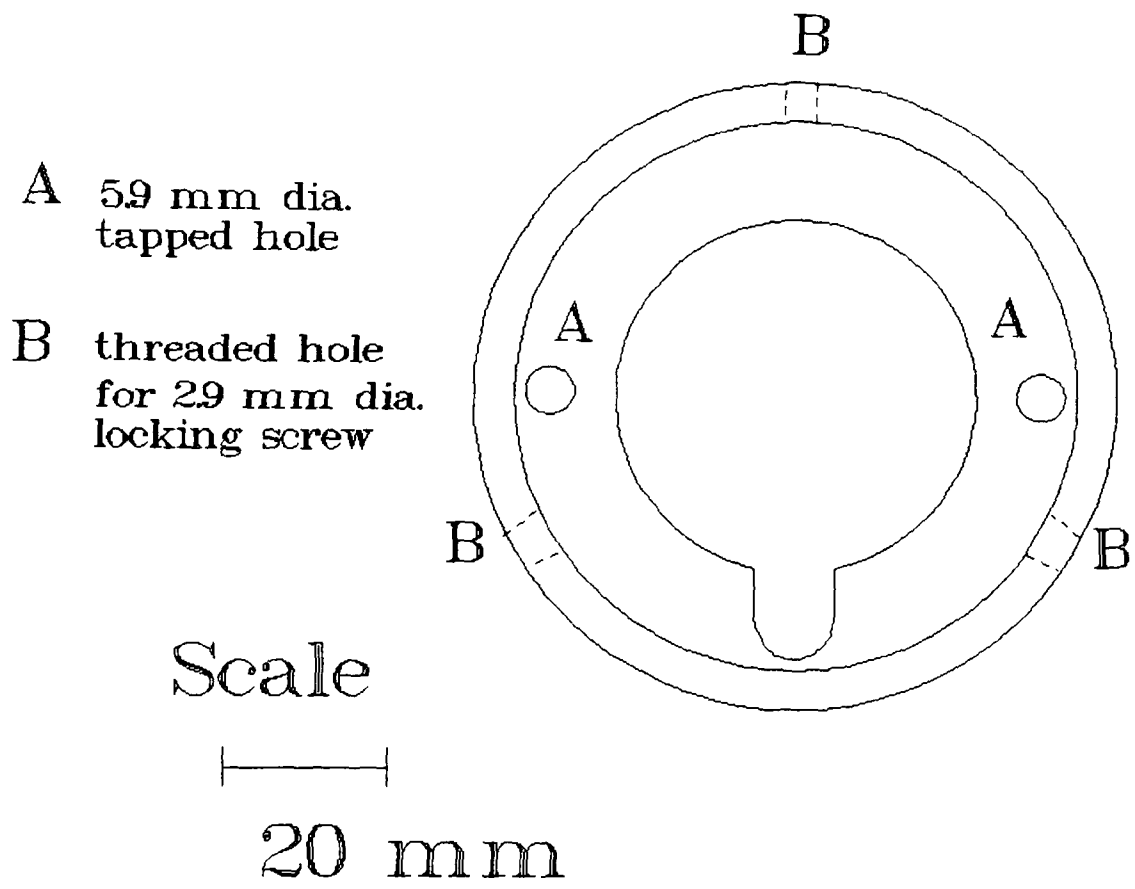

Fig. C.1. View of STM body from above showing Inchworm holder location (Simplified view - sample stage not shown)

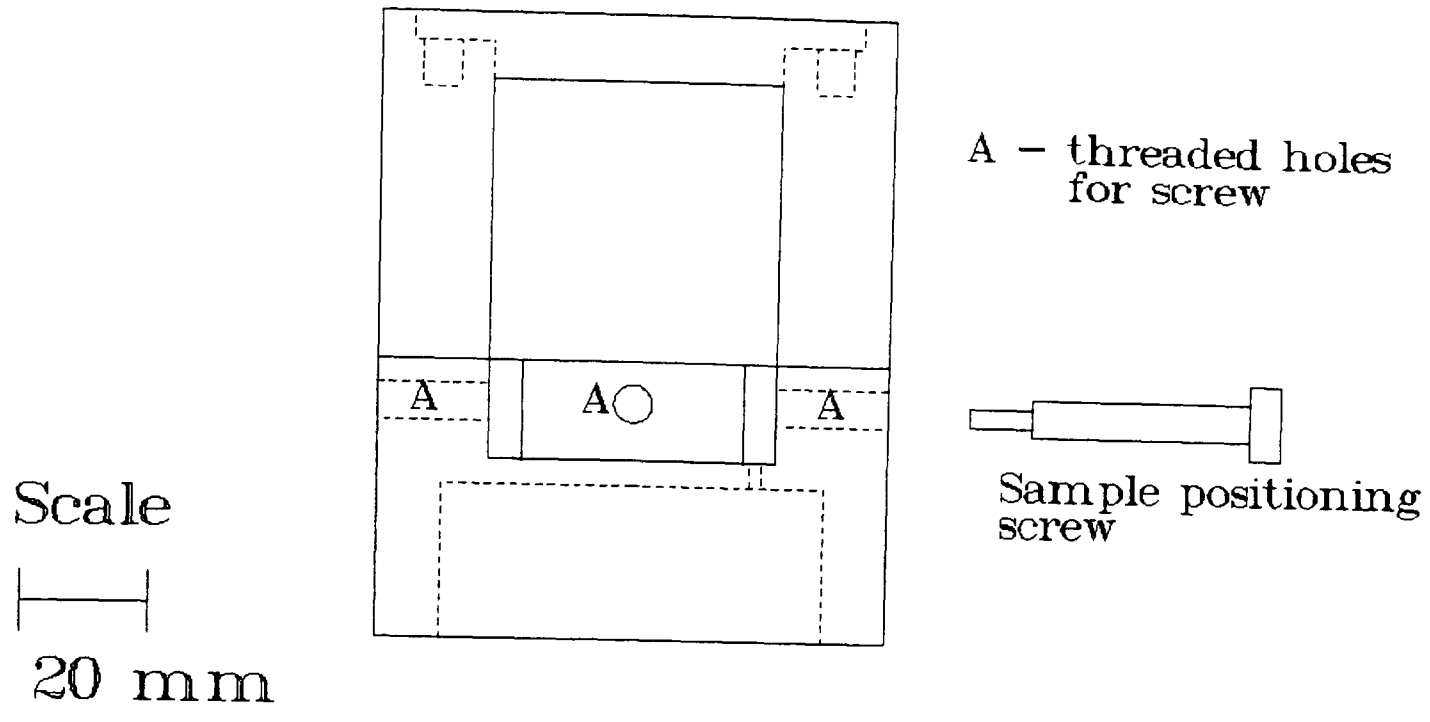

Fig. C.2. Front view of STM body

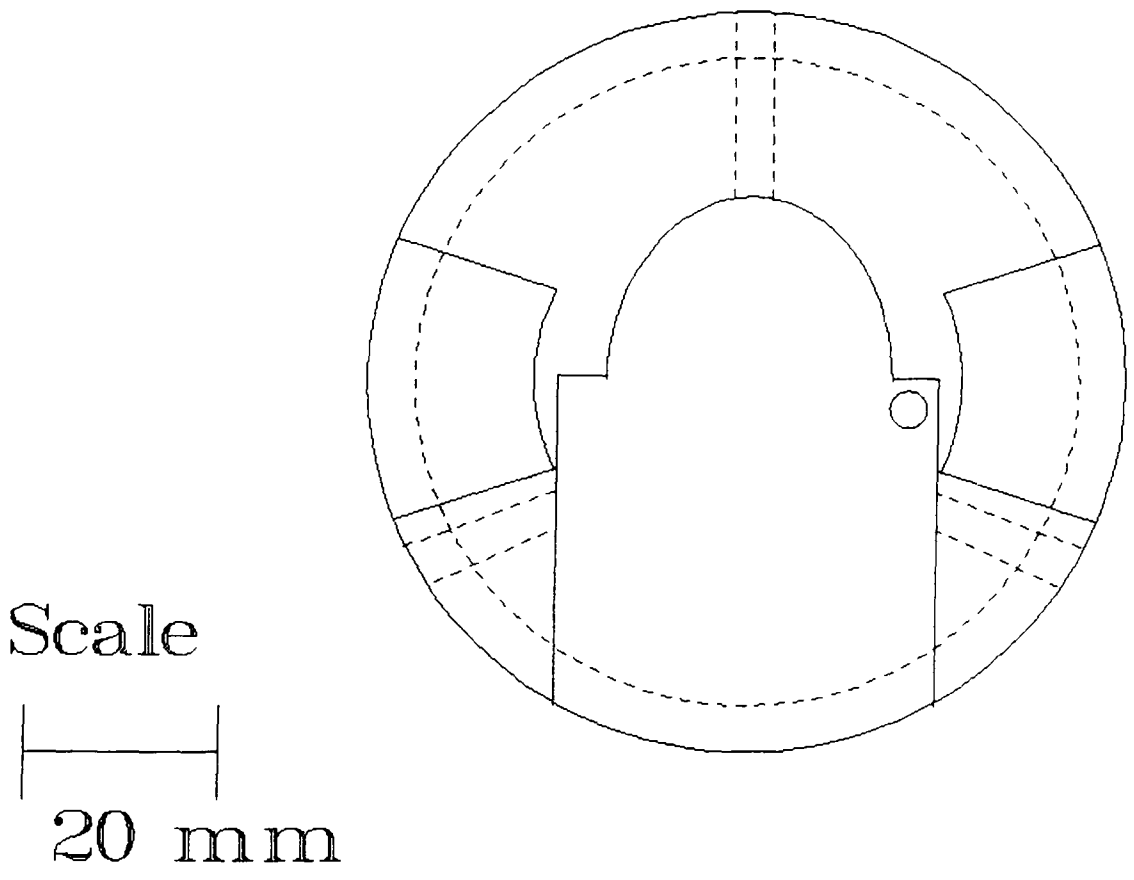

Fig. C.3. Horizontal section through STM body showing sample stage

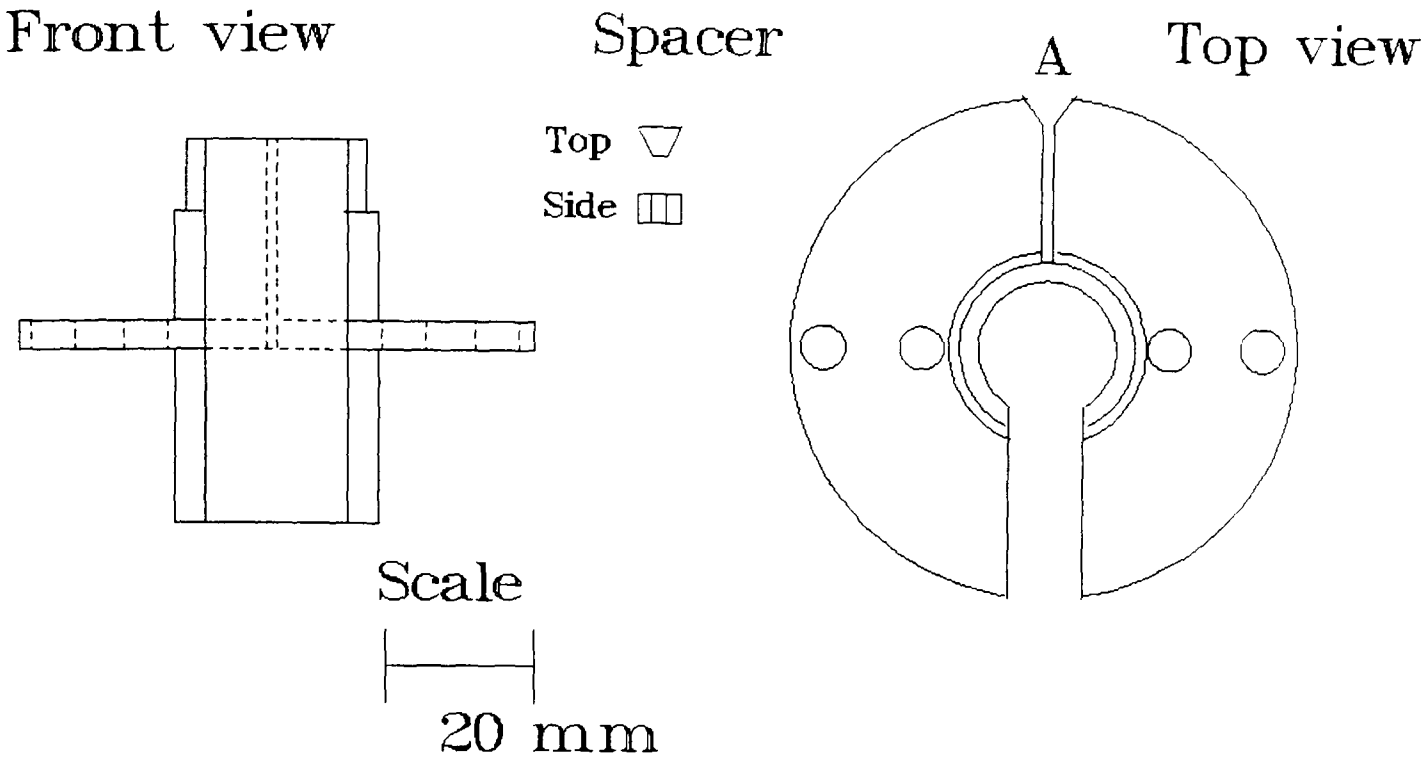

Fig. C.4. Views of the Inchworm holder

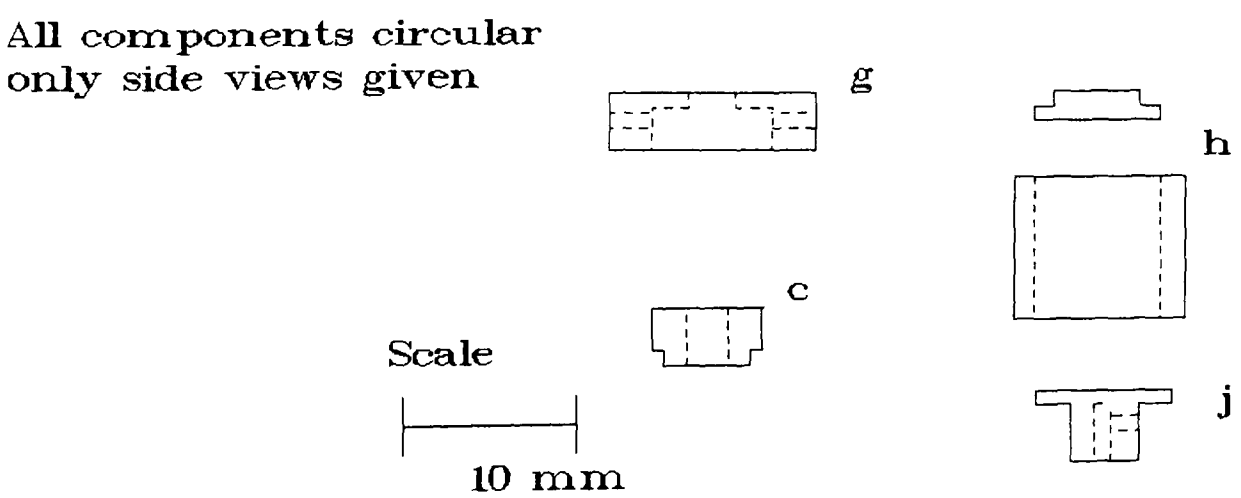

Fig. C.5. Diagram of the piezo tube/tip holder components

(Labels as in fig. 3.5 (b))